AERO-STRUCTURAL ANALYSIS OF THE MORPHING TRAILING EDGE CONTROL SURFACE OF A FULLY MORPHING UNMANNED AERIAL VEHICLE WING

A THESIS SUBMITTED TO
THE GRADUATE SCHOOL OF NATURAL AND APPLIED SCIENCES
OF
MIDDLE EAST TECHNICAL UNIVERSITY

BY

UĞUR KALKAN

IN PARTIAL FULFILLMENT OF THE REQUIREMENTS
FOR
THE DEGREE OF MASTER OF SCIENCE
IN
AEROSPACE ENGINEERING

JANUARY 2017

Approval of the thesis:

AERO-STRUCTURAL ANALYSIS OF THE MORPHING TRAILING EDGE CONTROL SURFACE OF A FULLY MORPHING UNMANNED AERIAL VEHICLE WING

submitted by **UĞUR KALKAN** in partial fulfillment of the requirements for the degree of **Master of Science in Aerospace Engineering Department, Middle East Technical University** by,

Prof. Dr. Gülbin Dural Ünver _____
Director, Graduate School of **Natural and Applied Sciences**

Prof. Dr. Ozan Tekinalp _____
Head of Department, **Aerospace Engineering**

Assoc. Prof. Dr. Melin Şahin _____
Supervisor, **Aerospace Engineering Dept., METU**

Examining Committee Members:

Prof. Dr. Yavuz Yaman _____
Aerospace Engineering Dept., METU

Assoc. Prof. Dr. Melin Şahin _____
Aerospace Engineering Dept., METU

Prof. Dr. Serkan Özgen _____
Aerospace Engineering Dept., METU

Assist. Prof. Dr. Ercan Gürses _____
Aerospace Engineering Dept., METU

Assoc. Prof. Dr. Erdem Acar _____
Mechanical Engineering Dept., TOBB-ETU

Date: 26.01.2017

I hereby declare that all the information in this document has been obtained and presented in accordance with academic rules and ethical conduct. I also declare that, as required by these rules and conduct, I have fully cited and referenced all material and results that are not original to this work.

Name, Last Name :

Signature :

ABSTRACT

AERO-STRUCTURAL ANALYSIS OF THE MORPHING TRAILING EDGE CONTROL SURFACE OF A FULLY MORPHING UNMANNED AERIAL VEHICLE WING

Kalkan, Uğur

M.S., Department of Aerospace Engineering

Supervisor : Assoc. Prof. Dr. Melin Şahin

January 2017, 177 pages

This thesis investigates the aero-structural analysis of the morphing trailing edge control surface of a fully morphing unmanned aerial vehicle wing for some camber morphing missions. Designed control surface was structurally analyzed with Finite Element Method using ANSYS Workbench v14.0 Static Structural module. Open Cell, Closed Cell designs with some material and thickness changes were studied in order to find the optimum design in terms of minimum weight and structural relevance. Analyses were both performed in-vacuo and under aerodynamic loads. Initially in-vacuo analyses were performed and it was seen that Closed Cell-Neoprene rubber is the best design in terms of stresses, loads and morphing capabilities. Therefore, for Closed Cell-Neoprene rubber design analyses were performed under aerodynamic loads. Aerodynamic pressure distribution over the wing is obtained by Computational Fluid Dynamics analyses. Pointwise v17.2R2 was used to generate aerodynamic mesh and Stanford University Unstructured v3.2.03 was used as a solver. Aerodynamic load on the control surface was obtained by the interpolation method using the Tecplot 360 2013R1 package programme. Results of the analyses showed that designed control surface is capable of performing all the morphing conditions. However 3g and 4g aerodynamic load

created bump at the compliant part which is not desired. Considering the weight of control surface Closed Cell – Neoprene rubber design with 1.0 [mm] composite thickness was selected as the best design.

Keywords: Morphing Control Surfaces, Morphing Wing, Structural Analysis, Finite Element Method, Aerodynamic Analysis, Computational Fluid Dynamics, Aero-Structural Analysis

ÖZ

BÜYÜK ORANDA ŞEKİL DEĞİŞTİREBİLEN BİR İNSANSIZ HAVA ARACI KANADININ HİBRİT FİRAR KENARI KONTROL YÜZEYİNİN VAKUM ve AERODİNAMİK YÜKLER ALTINDA YAPISAL ANALİZİ

Kalkan, Uğur

Yüksek Lisans, Havacılık ve Uzay Mühendisliği Bölümü

Tez Yöneticisi : Assoc. Prof. Dr. Melin Şahin

Ocak 2017, 177 sayfa

Bu çalışmada, büyük oranda şekil değiştirebilen bir insansız hava aracı kanadının hibrit firar kenarı kontrol yüzeyinin vakum ve aerodinamik yükler altında yapısal analizi incelenmiştir. Tasarlanmış kontrol yüzeyi Sonlu Elemanlar Yöntemi kullanılarak ANSYS Workbench v14.0 programının Static Structural modülü ile yapısal olarak incelenmiştir. Minimum ağırlık ve yapısal uygunluk açısından optimum tasarımın bulunması için Açık Hücre, Kapalı Hücre tasarımları bazı malzeme ve kalınlık değişiklikleri ile incelenmiştir. Analizler hem vakum ortamında hem de aerodinamik yükler altında gerçekleştirilmiştir. İlk olarak analizler vakum ortamında yapılmıştır ve Kapalı Hücre – Neopren kauçuk tasarımının gerilmeler, yükler ve şekil değiştirme özellikleri açısından en iyi tasarım olduğu görülmüştür. Bu nedenle, Kapalı Hücre – Neopren kauçuk tasarımı aerodinamik yükler altında tekrar analiz edilmiştir. Kanat üzerindeki aerodinamik basınç dağılımı Hesaplamalı Akışkanlar Dinamiği analizleri ile elde edilmiştir. Aerodinamik çözüm ağı için Pointwise v17.2R2, çözücü için ise Stanford University Unstructured v3.2.03 yazılımı kullanılmıştır. Kontrol yüzeyindeki aerodinamik yük, Tecplot 360 2013R1 paket programı kullanılarak interpolasyon yöntemi ile elde edilmiştir. Analiz sonuçları, tasarlanan kontrol yüzeyinin tüm şekil değiştirme koşullarını yerine

getirebildiğini göstermektedir fakat 3g ve 4g aerodinamik yükler Neopren kauçuk malzemesinde yumrulara neden olmuştur. Ağırlık göz önüne alındığında 1.0 [mm] kompozit kalınlığındaki Kapalı Hücre – Neopren kauçuk tasarımı en iyi tasarım olarak seçilmiştir.

Anahtar Kelimeler: Şekil Değiştirebilen Kontrol Yüzeyleri, Şekil Değiştirebilen Kanat, Yapısal Analiz, Sonlu Elemanlar Yöntemi, Aerodinamik Analiz, Hesaplamaı Akışkanlar Dinamiği, Aerodinamik Yükler Altında Yapısal Analiz

To:

My Love Gülçin

ACKNOWLEDGEMENTS

I would like to express my gratitude to my supervisor Assoc. Prof. Dr. Melin Şahin, for giving me an opportunity to work with him, allowing me to benefit from his invaluable comments and experiences and his endless patience throughout my study.

I am also indebted to my superiors within the CHANGE project, Prof. Dr. Yavuz Yaman, Assist. Prof. Dr. Ercan Gürses, and Prof. Dr. Serkan Özgen for their supports during the studies.

I must also express my gratitude to my colleagues Pınar Arslan, Harun Tıraş, İlhan Ozan Tunçöz and Yosheph Yang. Without their help and patience, this study would not finish. Harun and Pınar always argued with me to find the best solution to the problems in the thesis. Ozan always answered my questions calmly. Yosheph tried to finish the CFD analyses from Korea within all his hard working. Additionally, I must also thank to my co-workers in the laboratory Nima Pedramasl and Onur Akın for their supports. In addition I must thank Fatih Mutlu Karadal and Seyhan Gül for their helpfulness and comments on my presentation.

I also would like to express my thanks to Derya Gürak, for her endless support and encouragement. Without her understanding and help this study would not finish in time.

Also, I would like to thank Alcan, Kalkan, Çakır, Aktaş families, Behiye-Mustafa İnal for their supports. I also thank baby Azra and Damla.

I must also express my gratitude to my friend Emre Asarcıklı, Eren Parladıroğlı and Utku Şahin. They always encouraged me.

The greatest thanks goes to my mother Rebiye, my father Hakkı, sister Aydan and my grandmother Terlan supported and encouraged me throughout my life. It would never and ever be possible without their help.

The work presented herein has been partially funded by the European Community's Seventh Framework Programme (FP7) under the Grant

Agreement 314139. The CHANGE project ("Combined morphing assessment software using flight envelope data and mission based morphing prototype wing development") is a L1 project funded under the topic AAT.2012.1.1-2 involving nine partners.

TABLE OF CONTENTS

LIST OF TABLES

TABLES

LIST OF FIGURES

FIGURES

LIST OF ABBREVIATIONS

CFD	Computational Fluid Dynamics
CHANGE	Combined morphing assessment software using flight envelope data and mission based morphing wing prototype development
FEA	Finite Element Analysis
FEM	Finite Element Model
LaRC	Langley Research Center
L/D	Lift to Drag Ratio
METU	Middle East Technical University
NASA	National Aeronautics and Space Administration
SU2	Stanford University Unstructured
TAI	Turkish Aerospace Industries
TUBİTAK	The Scientific and Technological Research Council of Turkey
UAV	Unmanned Aerial Vehicle

CHAPTER 1

INTRODUCTION

1.1 Objective of the Study

When designing the aircraft there are two main parameters that are taken into account. First one is to perform the mission successively. All the conventional aircraft are designed for a specific mission such as transportation, combat or cargo. Second critical parameter of design is the efficiency. Aircraft are designed in order to complete its mission with the highest efficiency. Today's conventional aircraft are designed in order to complete a single mission. However, if a single aircraft can perform multiple missions, there is no need to design different types of aircraft. A single aircraft can perform multi missions. There are lots of studies about this issue under the 'Morphing Wing' concept.

In this study, morphing trailing edge control surface is introduced. The control surface changes the camber from mission to mission and there is no hinge/gap between the control surface and wing. This increases aerodynamic efficiency and eliminates noise due to gap.

The study is conducted within the scope of research and development project named CHANGE (**C**ombined morp**H**ing **A**ssessment software usi**NG** flight **E**nvelope data and mission based morphing prototype wing development) which is a project of 7th Framework Programme of European Commission.

1.2 Layout of Thesis

Chapter 1 introduces the objectives of the study by also providing the main assumptions and limitations.

Chapter 2 gives literature survey about the morphing wing aircraft. Relation between the aircraft and birds is presented and source of morphing concept is illustrated. Then, some morphing studies in Turkey are presented.

In Chapter 3, the designed hybrid trailing edge control surface in CHANGE Project is illustrated. First, brief information about the control surface and the wing is given. Then dimensions and materials used in the control surface design are presented together with the servo actuators used. Finally, two different hybrid trailing edge control surface designs namely “Open Cell design” and “Closed Cell design” are illustrated.

Chapter 4 is devoted to the static structural analysis of control surface in-vacuo condition. Initially, FEM of Open Cell and Closed Cell designs are presented. Then, decamber capabilities of control surfaces are shown.

In Chapter 5, initially, aerodynamic analyses of the morphing wing for all morphing missions are presented briefly. Then, interpolation of the pressure from wing to the FEM of hybrid trailing edge control surface is described.

Chapter 6 is dedicated to the static structural analysis of hybrid trailing edge control surface under aerodynamic loads. Aerodynamic loads varying from 1g to 4g are applied to the control surface and all the morphing mission are achieved.

Chapter 7 concludes the work with general conclusions drawn and the recommendations for the future work are also presented.

1.3 Limitations of the Thesis

The main limitations of the study can be listed as follows:

- In this thesis, 1g aerodynamic loadings are performed for each morphing flight mission profiles. Higher load factors such as 2g, 3g

and 4g are obtained by scaling the dynamic pressure of 1g condition. Dynamic pressure scaling is performed by increasing the velocity. Angle of attack variation is not considered to increase the aerodynamic load factor.

- Loads on the control surface due to maneuvers such as pullup, pushover, yawing maneuvers together with gust condition are not considered in this thesis.
- Structural analysis of the connection apparatus such as screws, nuts and bolts are not considered.
- Connections are defined by coupling the rotations and displacements of nodes. No glue or connection material is considered.

CHAPTER 2

LITERATURE REVIEW

2.1 Introduction

In this chapter, first, the relation between the aircraft and birds are explained. After that the reason why morphing is essential is illustrated and the definition of the morphing is described. Then, morphing concept is explained by giving the examples from the types of morphing. Finally, the information about the morphing studies in Turkey is provided.

2.2 Aircraft and Birds

Since the ancient time, mankind has been investigating the birds and there has always been a desire of flight. By inventing the first successful airplane in 1903, Wright brothers made the mankind's flight dream real. They designed the first controlled, powered and sustained heavier than air flying machine. After that developments in aviation has increased sharply. These developments have always been in the light of birds' nature because of the fact that birds' nature is much more efficient than the engineers' aircraft as in the all engineer-nature comparisons. Today, there are some establishments such as National Aeronautics and Space Administration's (NASA) Langley Research Center (LaRC) that are investigating birds to understand how they maneuver and try to apply to the aircraft[1]. In consequence of these researches, aircraft are designed and there are many common properties between aircraft and birds. For example, Wandering Albatross in Figure 1 (a) and ANKA aircraft in Figure 1 (b) has some similar wing properties. They both have high aspect ratio wing and they are expert gliders, capable of remaining in the

air for several hours at a time. On the other hand, Peregrine Falcon in Figure 2 (a) and F-22 Raptor aircraft in Figure 2 (b) have delta wings and they are fast to catch their prey.

(a) Wandering Albatross [2]

(b) ANKA [3]

Figure 1: High Endurance Bird and Aircraft

(a) Peregrine Falcon [4]

(b) F-22 Raptor [5]

Figure 2: High Speed Bird and Aircraft

For the fixed wing aircraft aerodynamic performance is optimum at a specific design condition, e.g. cruise for long range commercial passenger aircraft or high speed short range flight for fighter aircraft. This means that if the aircraft is not flying at the design point, aerodynamic performance will decrease. Although many fixed wing aircraft are designed to perform a single mission efficiently, investigating the birds also revealed performing efficiently the wide ranges of flight segments such

as take-off, loiter, strike and landing is possible. Birds are able to achieve such a wide dynamic range missions through large shape changes of their wings. To illustrate, from loiter to strike flight mission, dihedral and sweep angles of the wings are changed as shown in Figure 3 [6]. Therefore, to achieve multi flight missions efficiently with a single aircraft, wing shapes should change accordingly and the morphing concept is raised.

(a) Dihedral Angle Change

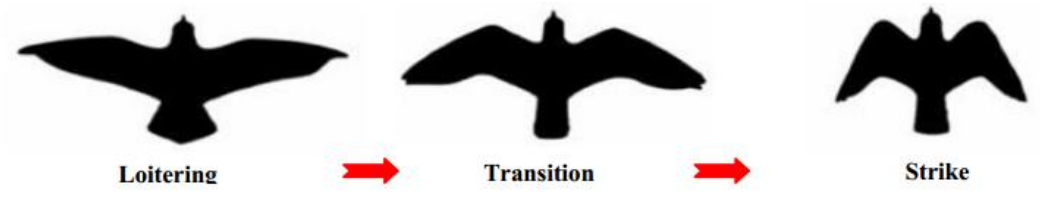

(b) Sweep Angle Change

Figure 3: Wing Shape Changes from Loiter to Strike [6]

2.3 Definition of Morphing

Silvestro et al. stated that there is neither an exact definition nor an agreement between the researchers about the type or the extent of the geometrical changes necessary to qualify an aircraft for the title ‘shape morphing’ [7]. Different definitions for morphing in literature confirm this idea. For example, Manoranjan et al. says that Wright Brothers utilized morphing concept at the first flight in 1903 by using a series of cables and pulleys that twisted the wing to change directions and control the airplane [8].On the other hand, Brian et al defines the morphing as the shape change of the wing during flight to perform in highly dissimilar flight conditions for maximum performance[9]. Although there is mismatch between the

researches about the morphing concept, today in most recent applications the use of unconventional structural designs and materials appears to be the most common point [10].

2.4 Morphing Concept

The concept of morphing is a fairly broad-ranging area[11] because an aircraft can be morphed in several ways. Barbarino et al. states that geometrical parameters that can be affected by morphing can be categorized into planform, out of plane transformation and airfoil adjustment[7].

Wing planform is affected by the three parameters which are span, sweep and chord. These parameters influence the wing aspect ratio and change in wing aspect ratio also changes range and endurance[12]. Wings with high aspect ratio have the advantage of long range and high fuel efficiency but have disadvantage of low cruise speed and less maneuverability [7]. On the other hand; aircraft with low aspect ratio wings are faster and high maneuverable but low in aerodynamic performance[13]. Therefore, planform morphing takes the advantage of both designs where necessary. Since the bending moment at the wing root will increase with the increase of span length, both aerodynamic and aeroelastic characteristics should be investigated. The MAK-10 is the first aircraft which has the telescoping wing flew in 1931 [7]. Span length of MAK-10 increased up to 62% and wing area is increased about 57% [14].

Out of plane transformation is affected by twist, dihedral/gull and span-wise bending. Changing the twist of the wing is accepted as the oldest form of morphing. To illustrate, Wright Brothers employed wing warping technique to provide roll control for their first flying machine [7]. With the help of dihedral/gull and span-wise one can reduce induced drag by changing the vorticity distribution and improve stall characteristics. Therefore, dihedral/gull and span-wise bending of aircraft wing helped to optimize the performance of winglets[7]. In addition to winglets, morphing in dihedral/gull have other benefits on an aircraft. For example, Cuji and Garcia studied the dynamics of aircraft turning for symmetric and asymmetric V-shaped

wings and they found that wings with asymmetric dihedral perform better in terms of bank angle, load factor and rolling moment coefficient [7]. Therefore, asymmetric dihedral increase the turning performance of an aircraft.

Airfoil adjustment mainly achieved by chamber and thickness variation. However, researches in airfoil morphing showed that camber morphing concept is preferred much more than the airfoil thickness change [7]. Many methods can be applied to change the camber of an aircraft airfoil. Leading or trailing edges of wing can be morphed to change the chamber or entire wing can act as a unique control surface by changing the entire camber of the wing. One benefit of camber change is that lift to drag ratio (L/D) of the wing can be improved which affects the efficiency of the aircraft [7]. Camber actuation systems can be categorized according to the size of the aircraft. Conventional actuators are used in all aircrafts except sub-MAV scale, shape memory alloys are used in unmanned aerial vehicle wings and rotorcraft blades, piezoelectric actuators are used in small UAVs and MAVs [7]. Gano and Renaud represented a concept to increase the efficiency of aircraft by changing the airfoil thickness [15]. They suggested decreasing the volume of wing fuel tanks as the fuel is consumed and thus decrease the drag.

In order to achieve all types of the morphing concept described, material used has a very important role since it limits the design process as in the all engineering solutions. When the subject is morphing aircraft the importance of the material becomes much more significant. The reason is that the shape of the wing at each design phase is different in morphing aircraft. Therefore, the structure should be capable of withstanding the loads but also able to change its shape at each flight phase. Recent developments in smart materials overcome the limitations and enhance the benefits from existing design solutions[7]. With the help of smart materials both the actuation forces of servo actuators and the weight is decreased. In addition, developments in actuation mechanisms have also important role in morphing concept. Piezoelectric actuators, electric motor, hydraulic/pneumatic mechanisms, servo actuators, ultrasonic motors and dc motors are some of the actuation mechanisms used in the morphing concept.

Focusing on the trailing edge control surface, in Middle East Technical University (METU) Aerospace Engineering Department, a tactical unmanned aerial vehicle (UAV) having mission adaptive wing was indigenously designed within the scope of TÜBİTAK (The Scientific and Technological Research Council of Turkey) 107M103 Project with the name of 'Aeroservoelastic Analysis of the Effects of Camber and Twist on Tactical UAV Mission-adaptive Wings'[16]. In this project, an UAV with hingeless control surface as shown in Figure 4 was designed by METU and manufactured in Turkish Aerospace Industries (TAI). Since the hingeless control surface removes the gap at the line where control surface and the wing joins, air flows smoothly from wing to control surface. Therefore, aerodynamic performance is increased and the noise due to this gap is eliminated. Also, the designed control surfaces have the ability to change the camber and twist. Camber change increases the lift and the twist change improves the control ability of the aircraft.

Figure 4: METU's Indigenously Designed UAV with Hingeless Control Surfaces [16]

Another morphing study in METU is the design and development of a morphing trailing edge control surface concept of an UAV. This study is being developed within the framework of CHANGE (Combined morphing Assessment software usiNG flight Envelope data and mission based morphing prototype wing

development) Project financed under the 7th Framework Programme of the European Commission [17]. Designed trailing edge control surface should maintain NACA6510 profile for loiter mission. Since most of the flight time is thought to be spend in loiter phase, baseline wing is selected as NACA 6510. In the take-off and high-speed configurations wing could morph to NACA3510 and NACA2510, respectively. Flight phases and corresponding NACA profiles are shown in Figure 5 and the desired morphing capability of the wing is shown in Figure 6. Initially, there was pre-twist along the wing span and both aero and structural analyses are performed [18], [19], [20]. Then, it was decided to use wing without pre-twist because the wing with pre-twist is not operational for telescoping morphing. In addition, structural and aerodynamic analyses are performed for several different designs of the morphing trailing edge control surface for the morphing missions described [21], [22], [23], [24], [25].

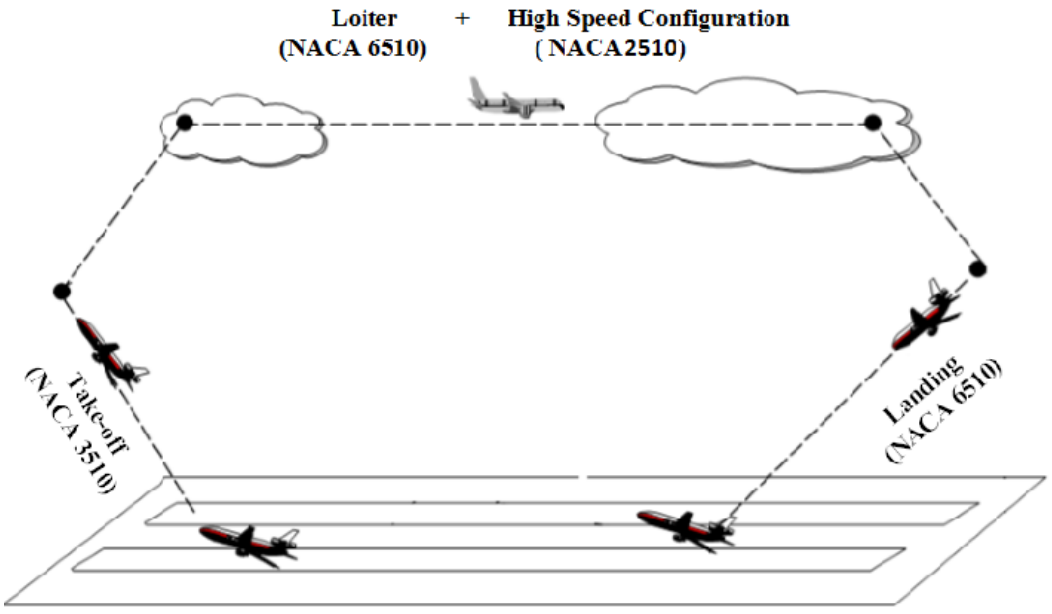

Figure 5: Flight Phases and Corresponding NACA Profiles for CHANGE Project

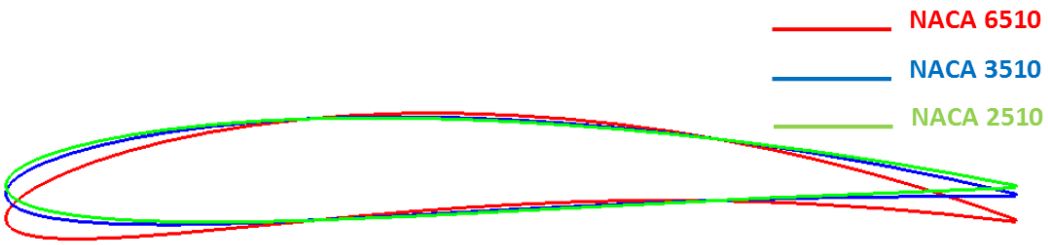

Figure 6: Morphing Capability of CHANGE Wing

In his Ph. D. thesis, Körpe dealed with the aerodynamic optimization of morphing wings under performance and geometric constraints[26]. Fixed wing optimization was performed for three cases which are only airfoil shape change, only planform change and combination of airfoil and planform shape change. He concluded that the planform change is the most effective way of drag reduction in morphing wings[26]. In addition to Körpe's studies on morphing, Ünlüsoy provided a broad view for the effects of morphing especially on the linear aeroelastic behavior of the UAV wings[27]. He concluded that at any phase of the morphing aircraft design, aeroelastic behavior of the structure should be considered with great attention; otherwise, the design should have a variation of flutter speeds[27]. Also, Oktay et al. studied to improve autonomous flight performance of load carrying UAV through active wing and horizontal tail active morphing [28]. He showed that morphing gives increases the performance and gives confidence/easy utility to UAV users.

CHAPTER 3

DESIGNED HYBRID TRAILING EDGE CONTROL SURFACE

3.1 Introduction

In this chapter, brief information about the wing and hybrid trailing edge control surface is given. Then, dimensions of the control surface are stated in detail. After that, servo actuators used in the control surface design are shown together with its properties. Material properties used in the control surface design are also given. Finally, types of control surfaces which will be used for the static structural analysis are stated.

3.2 Brief Information about the Designed Control Surface and the Wing

Designed hybrid trailing edge control surface is a part of a UAV wing which is designed with NACA 6510 airfoil and has several morphing capabilities. Span and chord lengths of the wing are 2000 [mm] and 600 [mm] respectively. Designed morphing wing has no pre-twist along its span and has no incidence angle. Top view of the morphing wing is shown in Figure 7. Morphing wing has also morphing leading edge control surface in the leading edge portion. In addition, it is capable of telescoping morphing. Actuation mechanism of the telescoping morphing is embedded into the torque box.

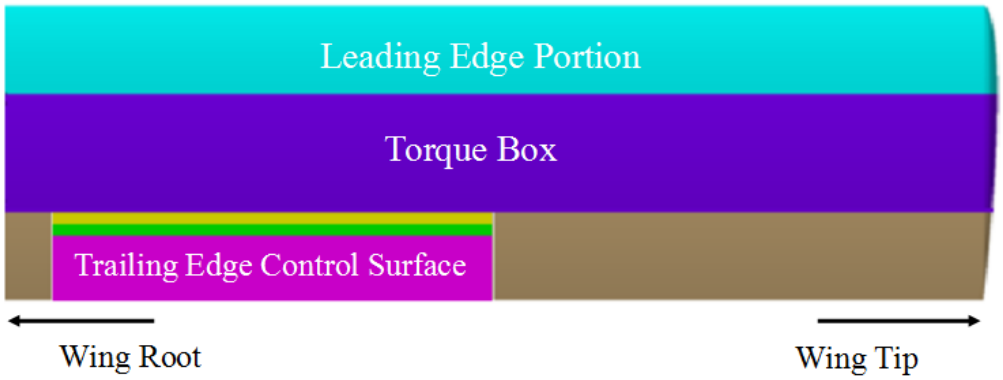

Figure 7: Top View of the Morphing Wing

Designed hybrid control surface consists of three parts as shown in Figure 8. Aluminum C Part has three parts which are C bar, upper shell and lower shell. The Aluminum C Part is attached to the main wing with no gap and no hinge. In the conventional control surfaces, there exist hinge to flap control surface up or down but hinge creates gap between control surface and wing as shown in Figure 9.

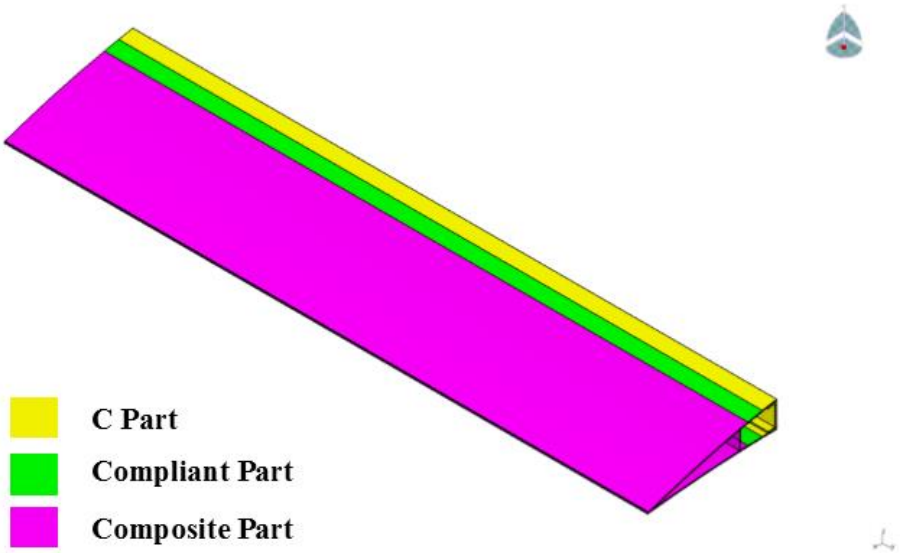

Figure 8: Hybrid Control Surface

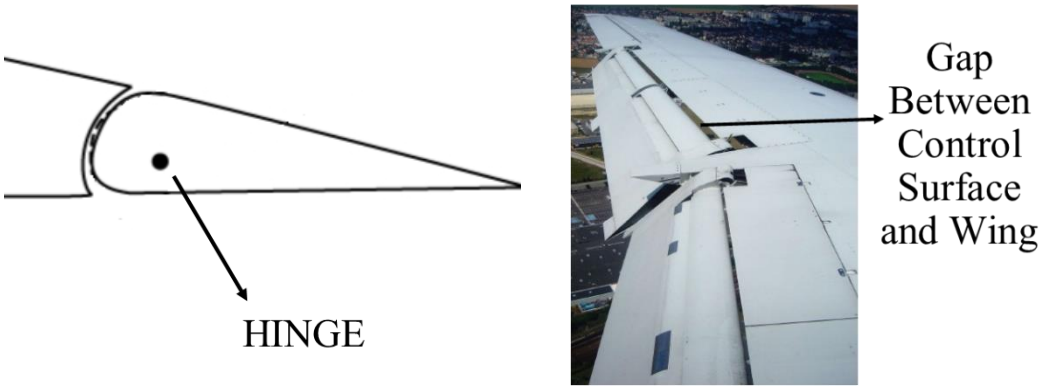

Figure 9: Hinge and Gap in the Conventional Control Surface

By using Aluminum C Part, gap between the control surface and wing is eliminated. Therefore, aerodynamic efficiency of the hybrid trailing edge control surface is increased and aerodynamic noise is eliminated when compared to conventional control surfaces. Between the composite and aluminum a very flexible compliant material is used. Because of the flexibility of the compliant material, stress is decreased and as a result servo loads are decreased. In addition, due to the stiffness difference between composite part and compliant part, composite part makes rigid body motion. Two different types of compliant materials are used in the analyses which are Neoprene rubber and Silicone. Silicone material is provided by CHANGE project partner Invent [29] and Neoprene Rubber is taken from ANSYS material library [30].

Trailing edge control surface has 900 [mm] span and 180 [mm] chord length as shown in Figure 10. 180 [mm] chord length is %30 of the wing chord length. In addition, it has 36.7 [mm] thickness at the location where control surface connects to the wing. Chord length of both Aluminum and compliant part is 20 [mm] whereas composite has 140 [mm] chord length. Dimensions described are shown on the control surface and given in Figure 10.

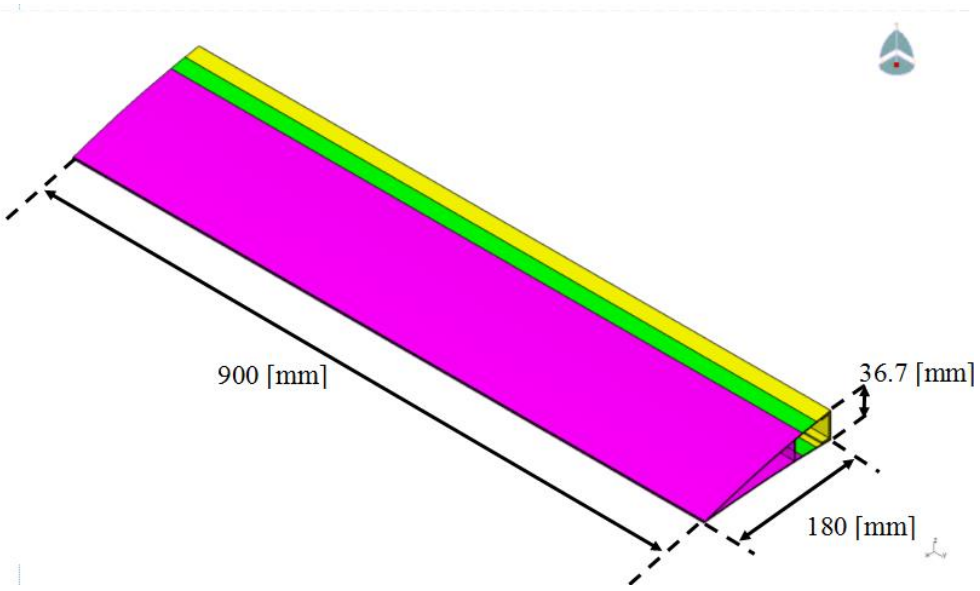

Figure 10: Span and Chord Length of the Hybrid Trailing Edge Control Surface

3.3 Servo Actuators Used

The mechanisms and the servos of the telescoping morphing are placed inside the torque box so there is not enough space to place the servo actuators of the trailing edge control surface inside the torque box. Therefore; servo actuators are placed inside the trailing edge control surface so as to deflect the trailing edge control surface. As it is not possible to place the trailing edge servo actuators inside the torque box, there is a very limited volume at the trailing edge control surface to place servos. This brings the problem of appropriate servo actuator selection to deflect the trailing edge control surface into the desired shape. The reason is that as the servo actuator dimension gets smaller maximum available torque decreases. Volz DA 13-05-60 servo actuator [31] which has the highest torque with the appropriate dimensions that can be put inside the trailing edge control surface is selected. Moment arm and push rod are used in order to deflect the control surface by using the torque of servo actuator. CAD drawing of the selected servo with the moment

arm and push rod is shown in Figure 11. Some properties of the servo Volz DA 13-05-60 servo actuator can be seen from Table 1 [31].

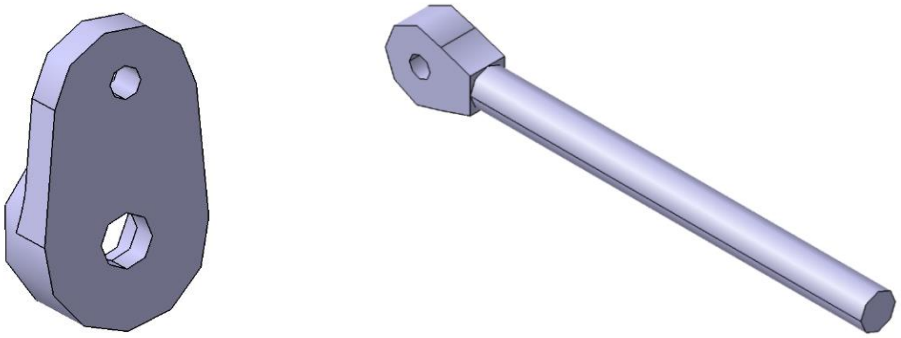

(a) Moment Arm

(b) Push Rod

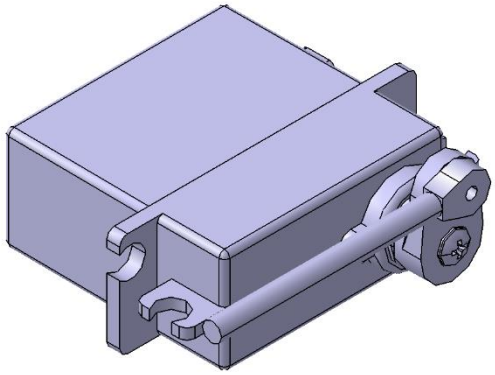

(c) Full Assembly of Servo with Moment Arm and Push Rod

Figure 11: Volz DA 13-05-60 Servo Actuator with Moment Arm and Push Rod

Table 1: Properties of the Volz DA 13-05-60 Servo Actuator [31]

Dimensions:	28.5 x 28.5 x 13 [mm x mm x mm]
Weight:	19 [g]
Gear Set:	Hardened Steel
Peak Stall Torque:	600 [N-mm] at 5 [V]
Operating Voltage:	4.8-5 [V]

Connection between the servo and the Aluminum C Part is achieved via L-Shaped connection which is also made by Aluminum. L-Shaped fastener is locked to the female guide which is on the C Part by super glue. L-Shaped fastener is shown in Figure 12 and female guide is shown in Figure 13.

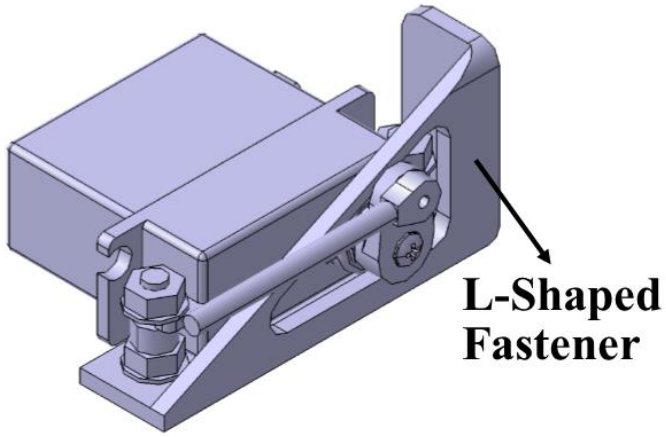

Figure 12: L-Shaped Fastener

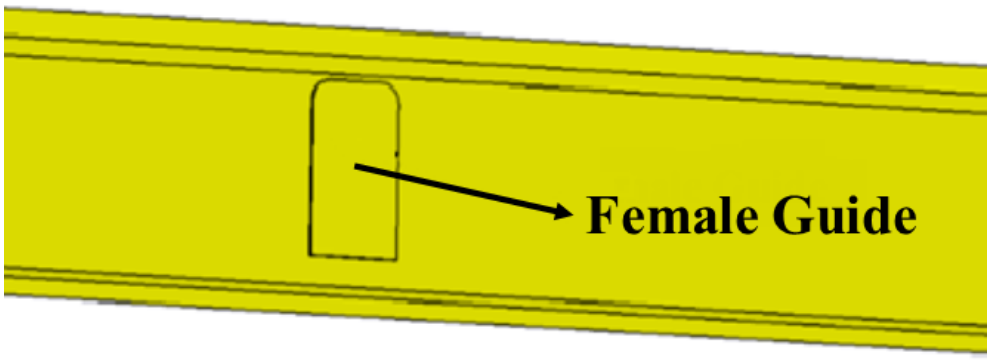

Figure 13: Female Guide at C Bar where L-Shaped Fastener is Attached

3.4 Material Properties Used in the Control Surface Design

Aluminum is used for the C Part, servo moment arm and push rod. Material properties of the Aluminum are shown at Table 2. As composite material Glass-Fibre Prepreg EHG250-68-37 [29] is used and material properties are shown in Table 3.

Table 2: Aluminum Material Properties [30]

Density, ρ:	2770 [kg/m^3]
Young's Modulus, E:	71 [GPa]
Poisson's Ratio, ν:	0.33
Tensile Yield Strength:	280 [MPa]
Compressive Yield Strength	280 [MPa]
Tensile Ultimate Strength:	310 [MPa]

Table 3: Glass-Fibre Prepreg EHG250-68-37 Composite Material Properties [29]

Density, ρ:	1900 [kg/m^3]
Young's Modulus, E_{11}:	24.5 [GPa]
Young's Modulus, E_{22}:	23.8 [GPa]
Poisson's Ratio, ν_{12}:	0.11
Shear Modulus, G_{12}:	4.7 [GPa]
Shear Modulus, G_{23}:	2.6 [GPa]
Shear Modulus, G_{13}:	3.6 [GPa]
Ply Thickness:	0.25 [mm]

For the compliant material, both Neoprene Rubber and Silicone are used. Properties of the Neoprene Rubber are obtained from ANSYS Workbench v14.0 material library. On the other hand, uniaxial test is performed in METU Aerospace Engineering laboratory for the silicone material obtained from CHANGE Project Partner Invent [29]. Material properties of the Neoprene Rubber and Silicone are shown in Figure 14 and Figure 15, respectively. Both density of the Neoprene Rubber [32] and Silicone [29] is 1250 [kg/m^3].

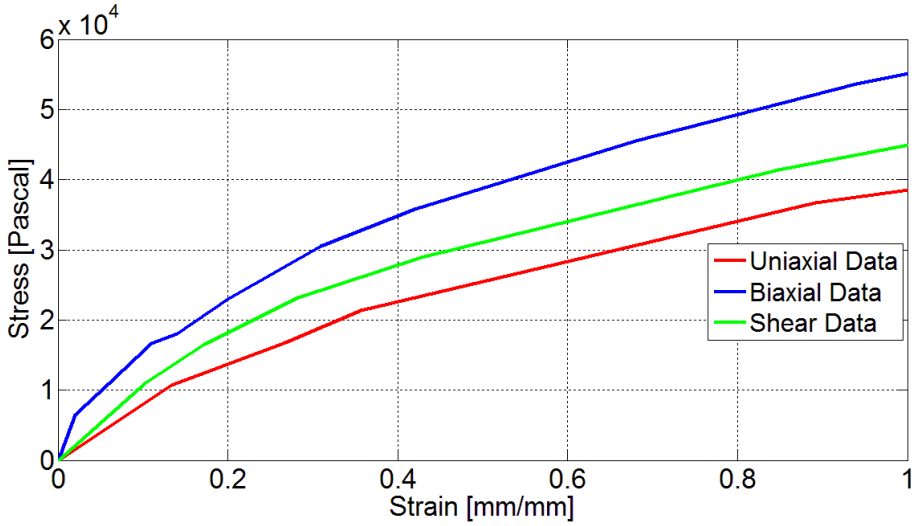

Figure 14: Experimental Data of Neoprene Rubber [30]

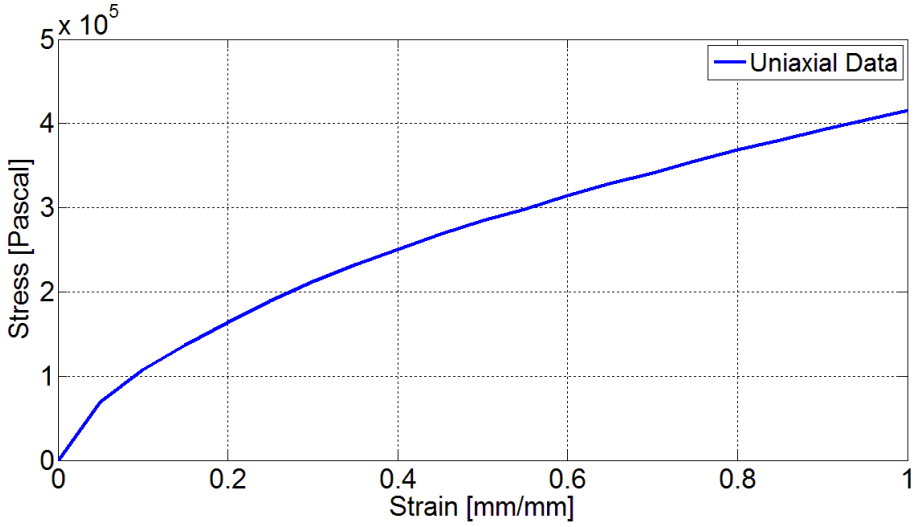

Figure 15: Experimental Data of Silicone Obtained in METU [33]

Silicone is also a hyperelastic material as Neoprene Rubber. When modelling a hyperelastic material in ANSYS, there is a need of biaxial, uniaxial and shear data. In order to obtain the biaxial and shear data Neo-Hookean material model under the hyperelastic module is used. Neo-Hookean material model is used to predict the biaxial and shear stress-strain behavior of silicone. Neo-Hookean obtains the shear, uniaxial and biaxial data of a material with the strain energy density function [34]. Biaxial, uniaxial and shear data of Silicone is shown in Figure 16.

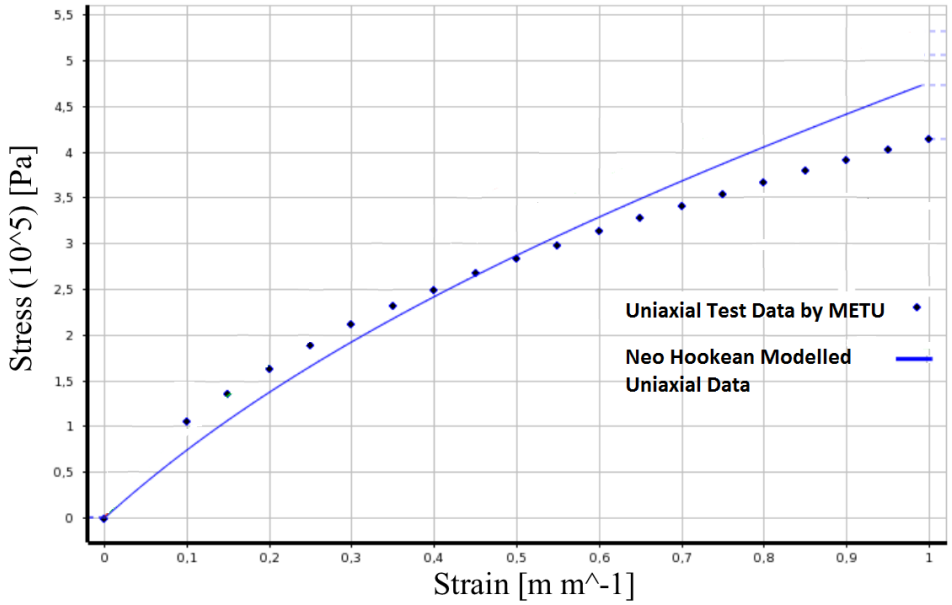

Figure 16: Silicone Material Modelled with Neo-Hookean in ANSYS

It is seen from the Figure 14 and Figure 16 that stress level of the silicone has higher than the Neoprene rubber. This means that the silicone is stiffer than the Neoprene rubber.

3.5 Types of Control Surfaces

There are two types of control surfaces that will be analyzed. First one is the Open Cell design. In this design, there is a little gap at the transmission part of the composite. Second one is the Closed Cell design and there is no gap at the transmission part of composite material. Stiffness of the transmission part for these two designs are different from each other. Therefore, effect of transmission part stiffness change will be observed in the analyses. Open Cell and Closed Cell designs are shown in Figure 17 and Figure 18 respectively.

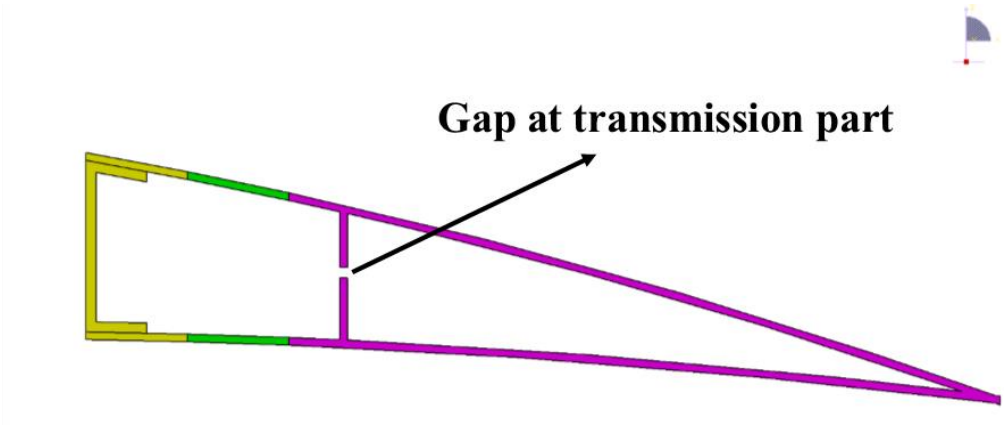

Figure 17: Hybrid Trailing Edge Control Surface Open Cell Design

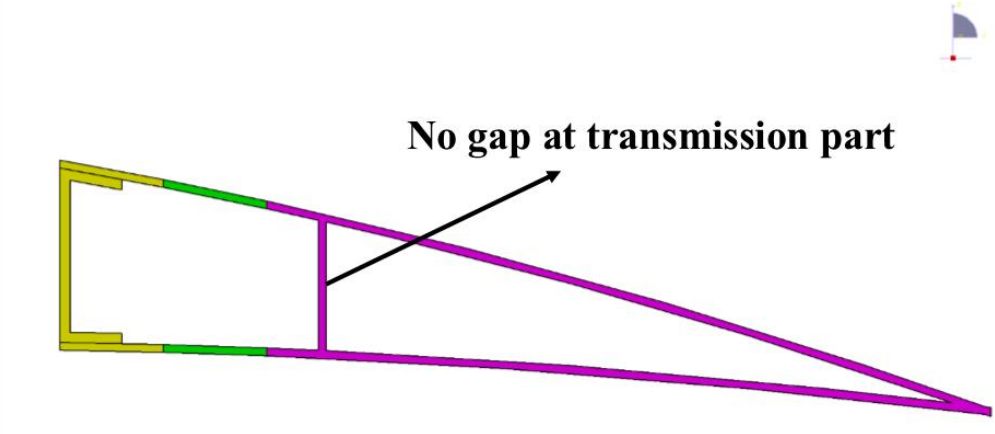

Figure 18: Hybrid Trailing Edge Control Surface Closed Cell Design

3.6 Location of Servo Actuators and Material Thicknesses

In this study, five servo actuators are placed inside the control surface as shown in Figure 19 [35]. Tunçöz [35] showed that three servo actuating the lower part and two servos actuating the upper part of the control surface is best for the design in terms of weight of control surface, loads and stresses on the control surface and servo actuators for the thicknesses given in Figure 20. Shell thickness of C bar is 2 [mm] where upper and lower shell have thickness of 1.5 [mm]. C Part could be designed as a single part but maintenance of control surface is thought to be done when upper and lower shell is detached. On the other hand, Neoprene Rubber and Silicone has

1.5 [mm] shell thicknesses. For the composite part, various thicknesses are considered in this study which are 1.0 [mm], 1.5 [mm] and 2.0 [mm].

Tunçöz also studied spanwise variation of servo locations in order to achieve the optimum design [35]. Figure 19 shows the optimum locations of servo actuators for designed control surface.

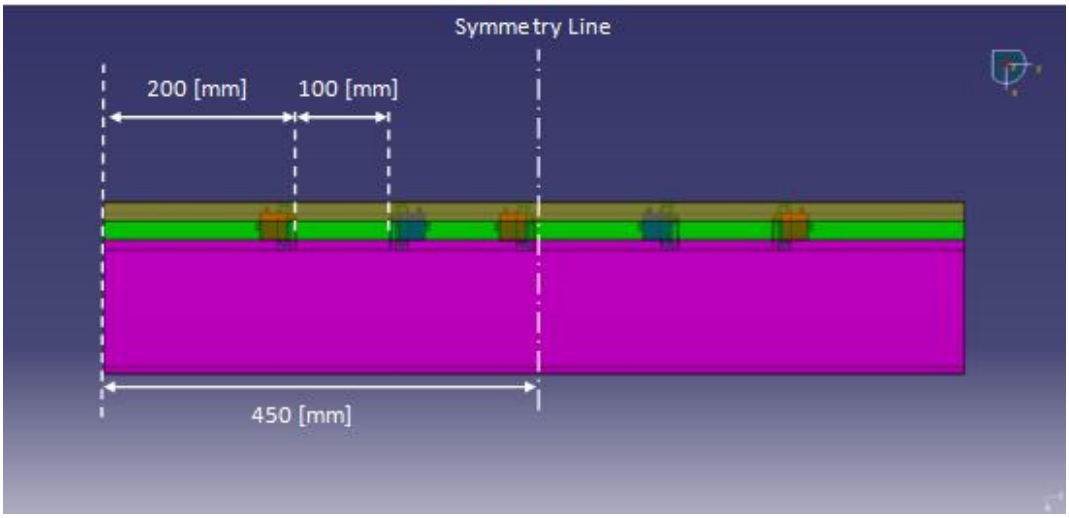

Figure 19: Top View of Control Surface with Full Assembly [35]

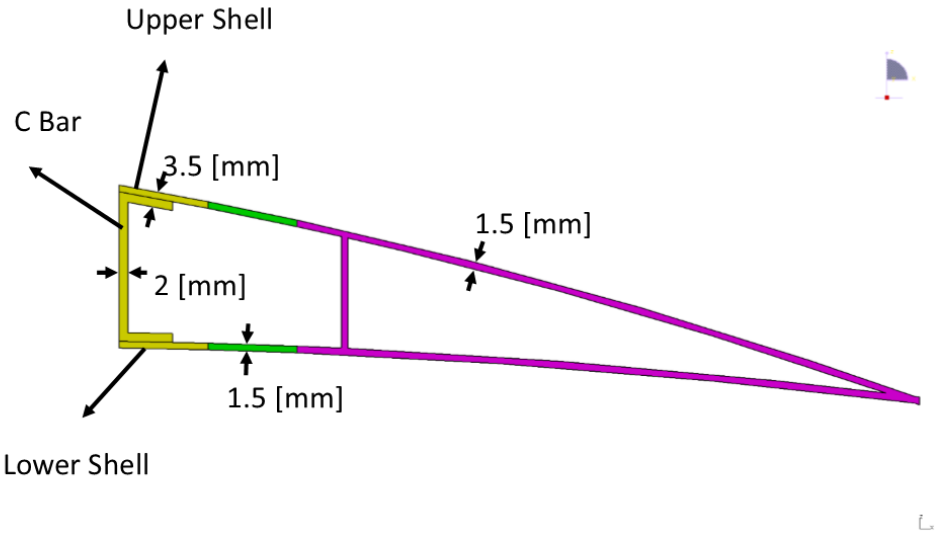

Figure 20: Thicknesses of the Control Surface Parts [35]

3.7 Weight of Designed Control Surface

Weight of the control surface described is given in Table 4. It is valid both for Neoprene rubber and Silicone design since material densities are same as given in Section 3.4. In addition, there is a negligible weight difference between Open Cell and Closed Cell designs. Weight difference is due the gap at the transmission part. Therefore, there is no distinct weight information for Open and Closed Cell designs.

Table 4: Weight of the Hybrid Trailing Edge Control Surface

Composite Thickness [mm]	Rigid Part (Composite Part) [kg]	Compliant Part [kg]	C Part [kg]	Servos (Including Equipments) [kg]	Total [kg]
2.0	1.0721	0.0682	0.4224	0.1550	1.7177
1.5	0.8040	0.0682	0.4224	0.1550	1.4496
1.0	0.5360	0.0682	0.4224	0.1550	1.1816

CHAPTER 4

STATIC STRUCTURAL ANALYSIS OF HYBRID TRAILING EDGE CONTROL SURFACE IN-VACUO CONDITION

4.1 Introduction

In this chapter, morphing wing hybrid trailing control surface is structurally analyzed. There is no pressure on the control surface which is called as in-vacuo condition. Static Structural module of ANSYS Workbench v14.0 is used in the analyses. In the FEM part of this chapter, both Open Cell and Closed Cell designs are established and then structural analysis is performed. Analyses performed in this Chapter are summarized in Figure 21. For each design, structural analysis is performed for:

- Maintaining the NACA 6510 profile,
- Morphing from NACA 6510 to NACA 3510 profile,
- Morphing from NACA 6510 to NACA 2510 profile.

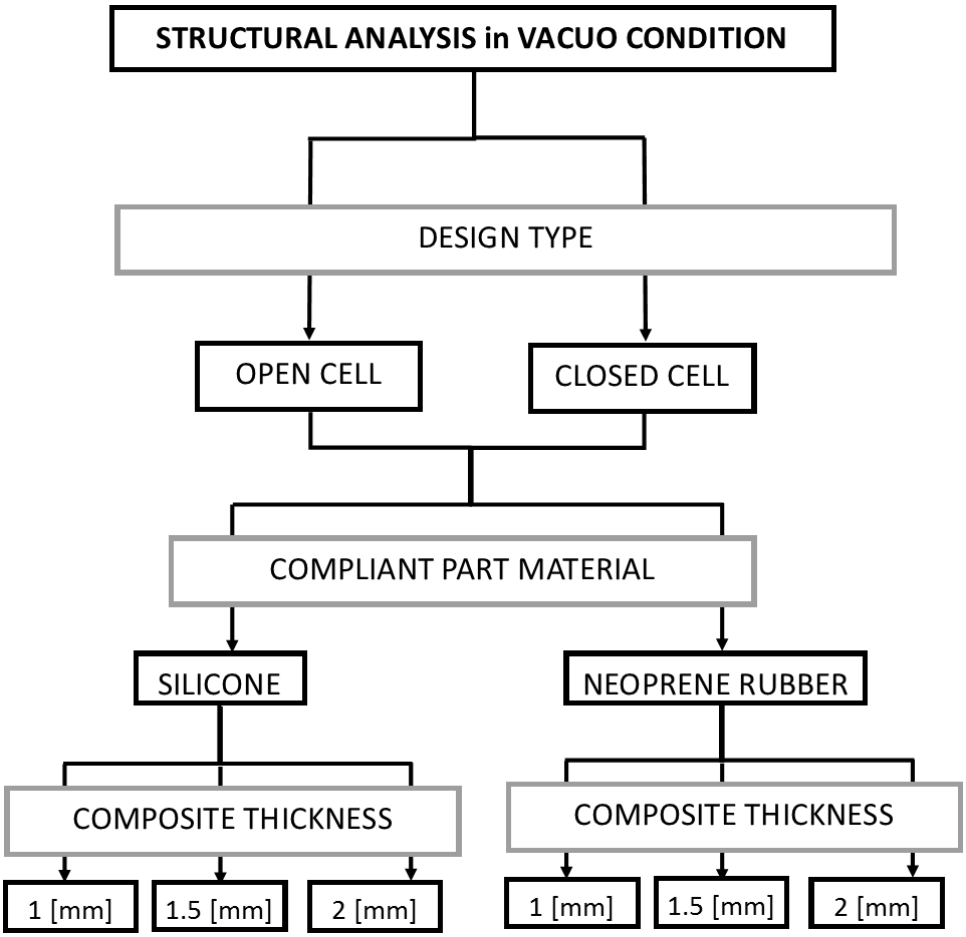

Figure 21. Static Structural Analyses Performed for Hybrid Trailing Edge Control Surface in-Vacuo Condition

4.2 Finite Element Model of Closed Cell Hybrid Trailing Edge Control Surface

The FEM geometry of the Open Cell control surface, servo actuator moment arms and actuation rods are generated by using CATIA V5-6R2012 package software. The generated geometry is then imported to the ANSYS Workbench Static Structural module as shown in Figure 22 and Figure 23.

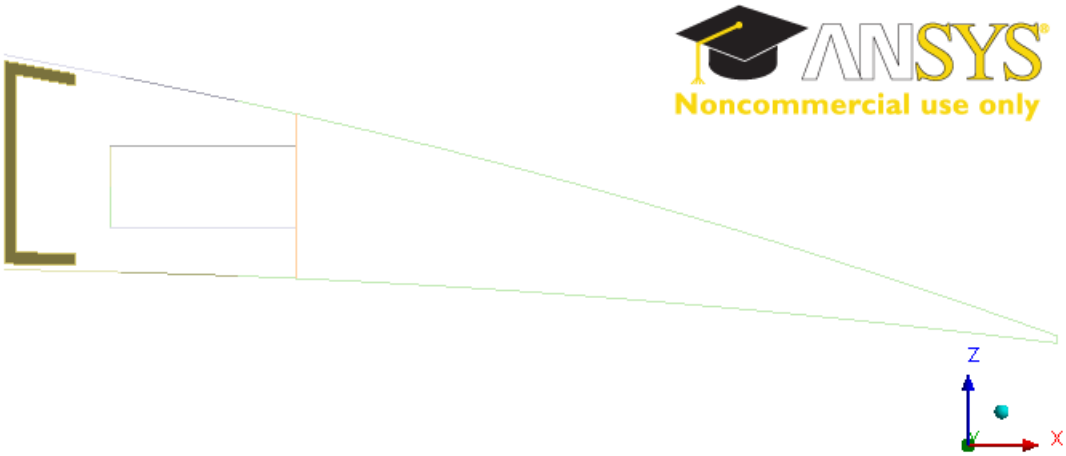

Figure 22: Side View of the Closed Cell - Hybrid Trailing Edge Control Surface for Finite Element Analysis

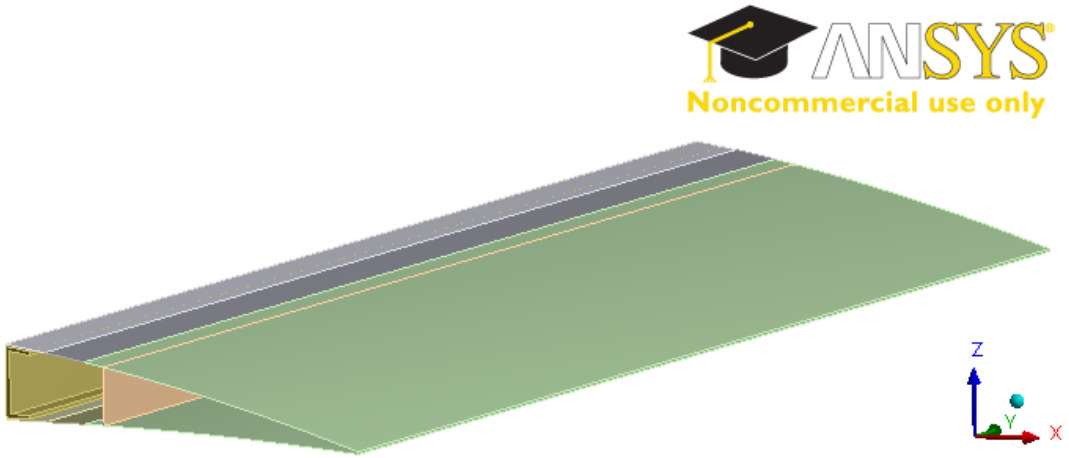

Figure 23: Isometric View of the Closed Cell - Hybrid Trailing Edge Control Surface for Finite Element Analysis

In the FEM, servo actuators are assumed to be rigid; therefore, they are not modelled. In addition, servo actuator moment arms and actuation rods are modelled as straight lines (i.e. line bodies). After that, circular cross section with 1.25 [mm] radius is defined for actuation rods and rectangular cross section with 7.5 [mm] width and 1.9 [mm] height is defined for moment arms. As a result, moment arm and actuation rods are modelled as beam elements. Moment arm and actuation rods with their cross sections can be seen from Figure 24. BEAM188 element is used for these

parts which is a two-node beam element and has six degrees of freedom at each node: translation in the x, y and z directions, and rotations about the x, y and z axes. The element is well-suited for large rotation, and/or large strain nonlinear applications [34]. As explained before, servo actuators are thought to be rigid; therefore, x, y and z displacements of the moment arm connection point to the servos is set zero. Also, servo actuators have the ability to rotate the moment arm only in y axes. As a result, rotations about x and z axes are also set zero for moment arm connection point to the servos. Moment arm connection point to the servo actuator is shown in Figure 24. In the analyses, rotations of servo moment arms about the y axes in order to deform or maintain the each NACA profile are defined such that they are always pushing the control surface. To illustrate, servos actuating the lower part of control surface has negative degree of rotation about the y axes whereas servos actuating the upper part has positive degree of rotation about the y axes according to the axis shown in Figure 25. None of the servo actuator moment arm is pulled because no compression is desired at the compliant part. If there is compression at this part, geometry buckles and flow separates. This is not desired phenomenon because aerodynamic efficiency decreases. Therefore, smoothness of the surface is maintained by pushing the control surface.

In the FEM, the required connection between the moment arm and actuation rod was achieved by coupling the x, y and z displacement degrees of freedom and rotational degrees of freedom about x and z axes of the nodes connecting the moment arm and actuation rod. Figure 26 shows coupled nodes of moment arm and actuation rods.

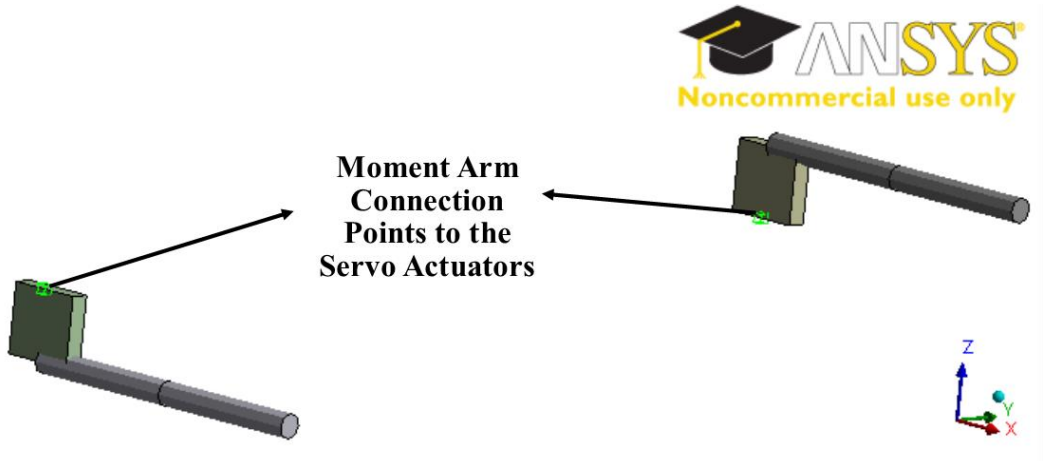

Figure 24: Moment Arm Connection Points to the Servo Actuators

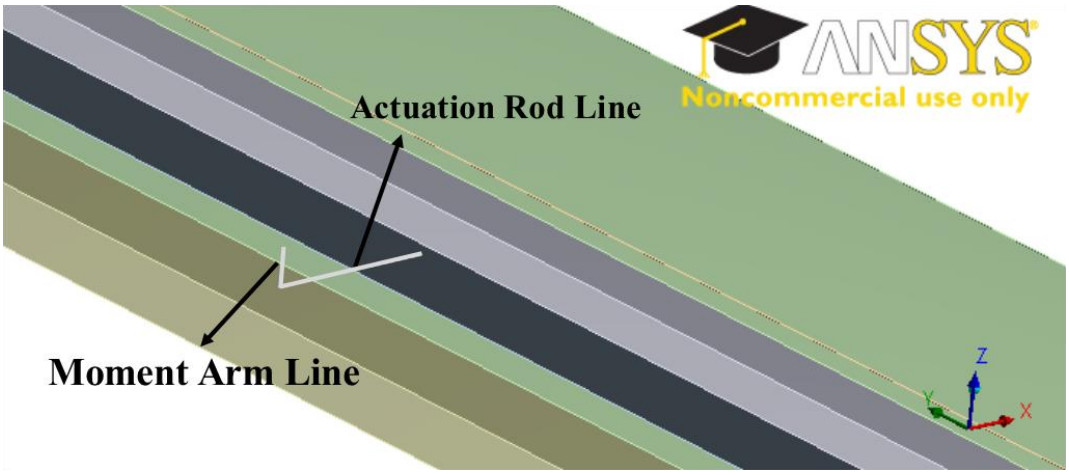

Figure 25: Actuation Rod Line and Moment Arm Line

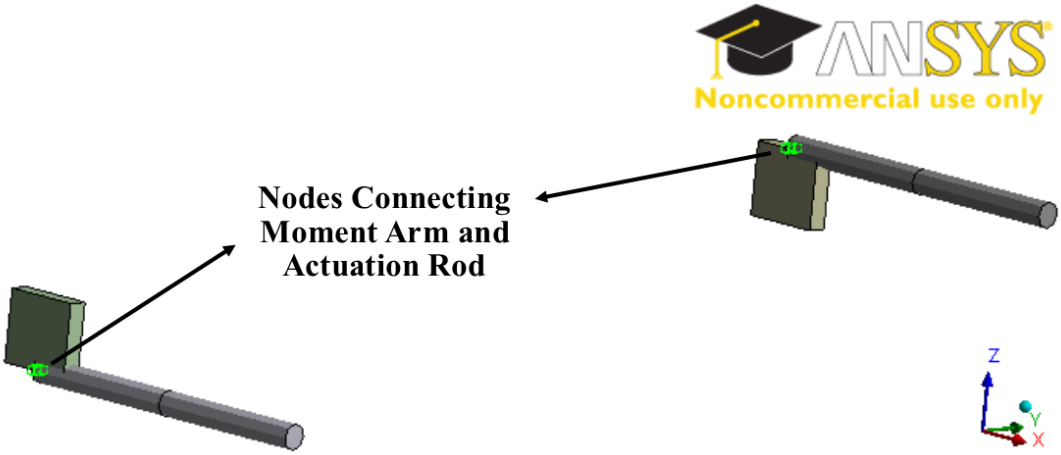

Figure 26: Coupled Nodes of Moment Arm and Actuation Rod

Rigid part, compliant part and upper-lower shells of C Part are modelled with surface bodies as shell elements. SHELL181 element is used for these parts. It is a four-node element with six degrees of freedom at each node: translation in the x, y and z directions, and rotations about the x, y and z axes. SHELL181 is well-suited for large rotation and/or large strain nonlinear applications [34].

Element sizes of rigid part and compliant part are performed in a study based on a mesh convergence study [18]. According to this study, rigid part's skin is modelled with 30 [mm] element size while upper-lower shells of C Part and Compliant Parts are modelled with 10 [mm] element size.

C bar is modelled as a solid body. SOLID185 is used for this part. It is an eight-node, 3D structural solid element. 5 [mm] element size is used for this part. Side view and isometric view of meshed hybrid trailing edge closed cell control surface are given in Figure 27 and Figure 28, respectively.

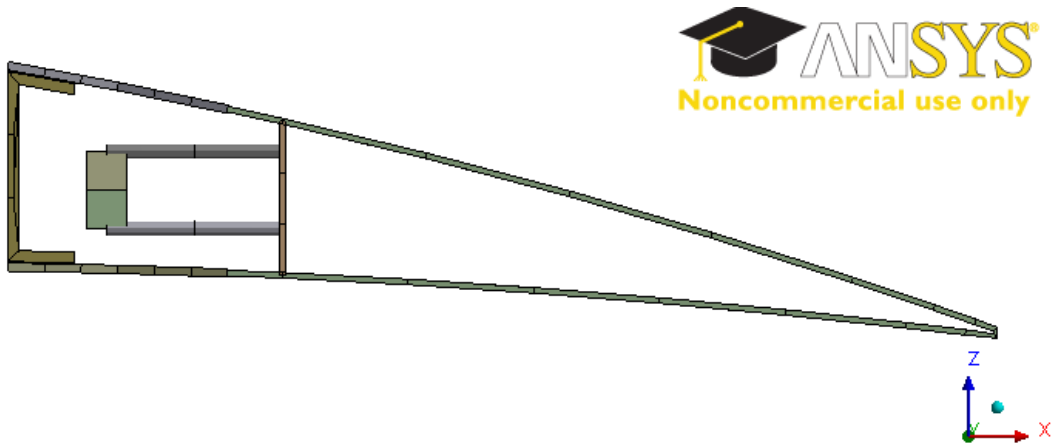

Figure 27: Side View of Meshed Hybrid Trailing Edge Closed Cell Control Surface

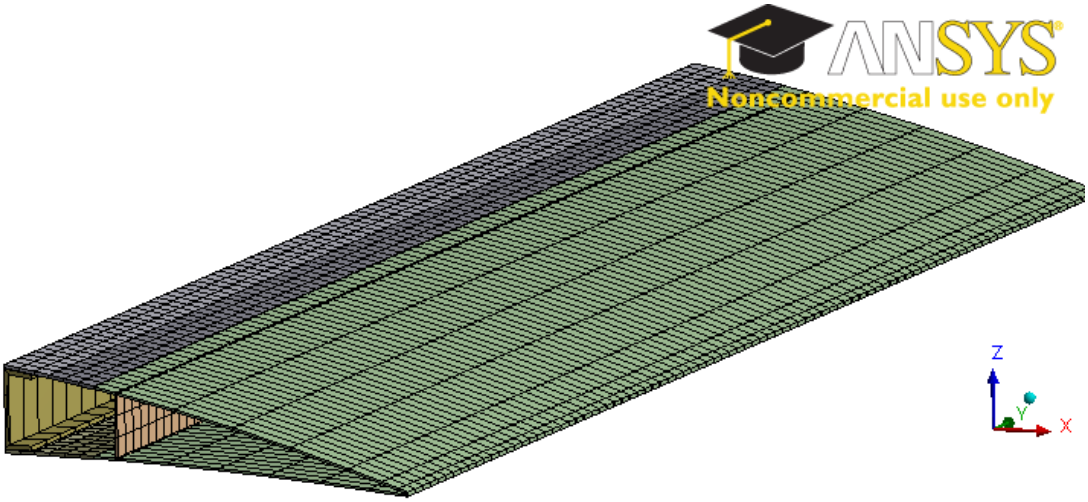

Figure 28: Isometric View of Meshed Hybrid Trailing Edge Closed Cell Control Surface

As described before, hybrid trailing edge control surface consists of three parts which are C Part, Compliant Part and Rigid Part. Connections between these parts should be described in FEM. In addition, servo actuators connection to the transmission should be defined. The connections are performed by Contact Tool of ANSYS Workbench Static Structural module. Bonded Contact is selected as a contact type. Therefore, there is no sliding or separation between the contact edges or faces. Connection between upper-lower shells of C part to the C bar is shown in Figure 29. Compliant Part, on the other hand, is connected to the composite part and upper – lower shells of C Part. Edge to edge connection is established. The connection described is shown in Figure 30.

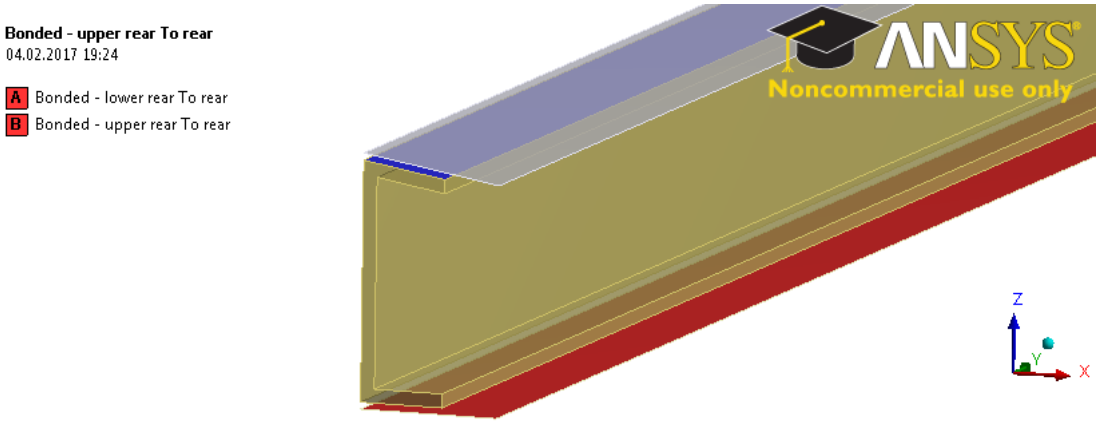

Figure 29: Connection between Upper and Lower Shells of C Part to the C Bar

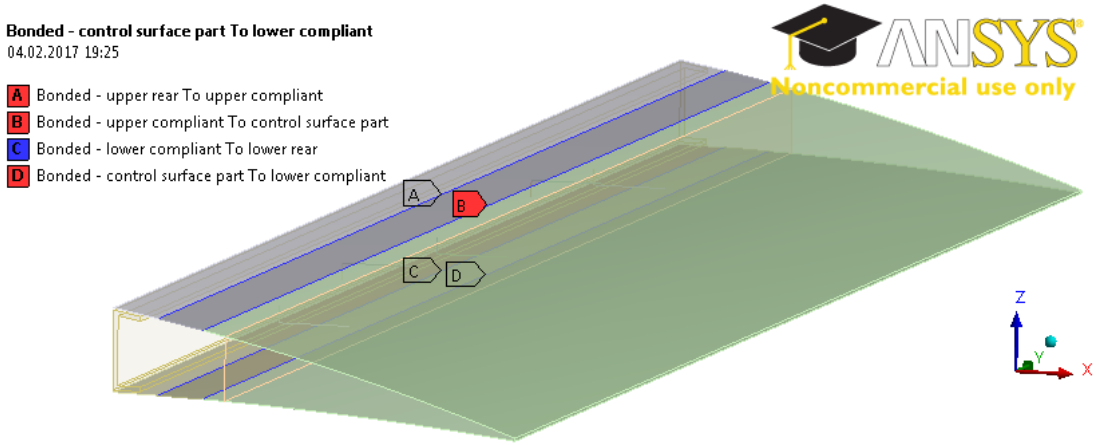

Figure 30: Connection between Compliant Part-Rigid Part and Compliant Part-Upper, Lower Shells of C Part

Connection between the push rod and transmission part is an edge to surface connection. Connection is performed by selecting the surfaces of transmission part and edges of the push rods where push rod touches the transmission part. This connection is shown in Figure 31.

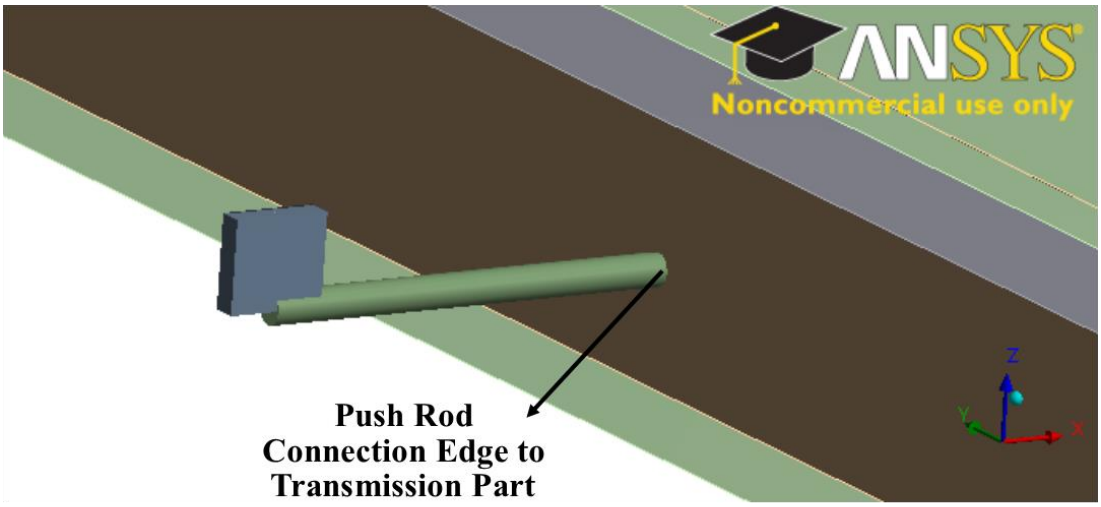

Figure 31: Connection Push Rod and Transmission Part

It is assumed that there will be no deformations on the wing due to loads on the trailing edge control surface. Therefore, surface of the C Part touching the wing is fixed. There is no rotational and translational deformation at that surface. Boundary condition described is shown in Figure 32.

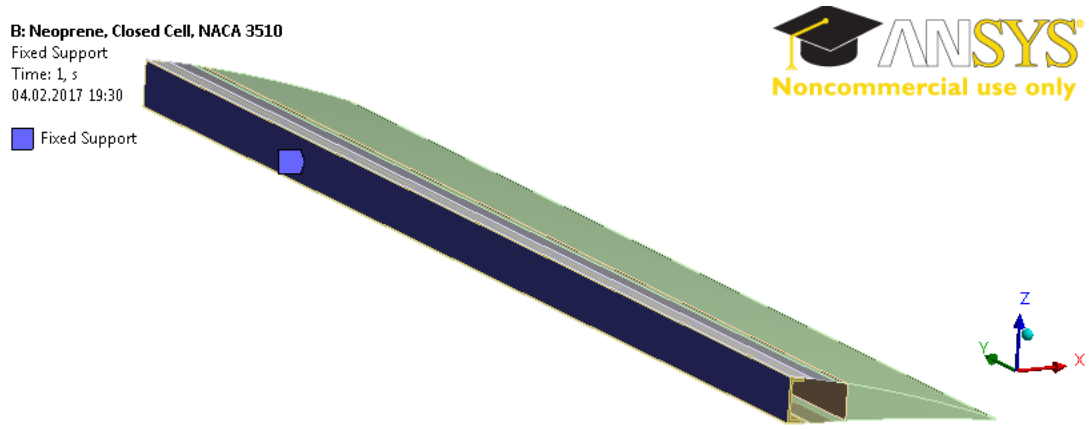

Figure 32: Fixed Boundary Condition of C Bar

4.3 Finite Element Model of Open Cell Hybrid Trailing Edge Control Surface

Open Cell hybrid trailing edge control surface FEM is constructed with the same element sizes, connections and boundary conditions of Closed Cell design as

described in Section 4.2. Side view and isometric view of meshed hybrid trailing edge closed cell control surface are given in Figure 33 and Figure 34 respectively.

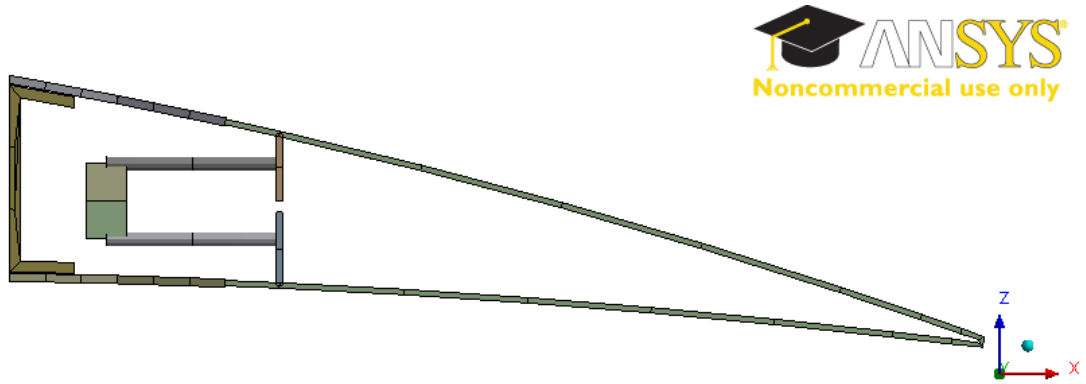

Figure 33: Side View of Meshed Hybrid Trailing Edge Open Cell Control Surface

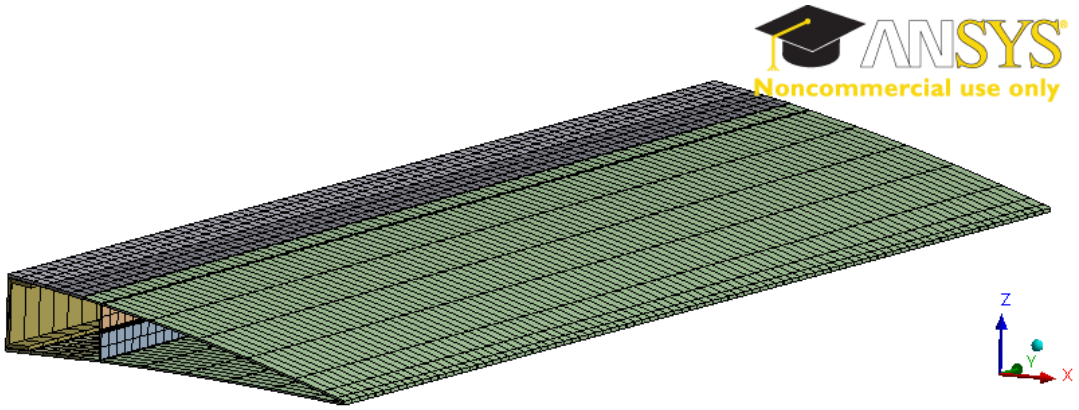

Figure 34: Isometric View of Meshed Hybrid Trailing Edge Open Cell Control Surface

4.4 Finite Element Analysis

In the Finite Element Analysis (FEA), hybrid trailing edge control surface is structurally analyzed. Nonlinear analyses are performed which include both geometric and material nonlinearities. For the compliant part, Neoprene Rubber and Silicone are used. Different composite thicknesses are investigated for both designs.

In order to deflect from NACA 6510 to NACA 3510, 20.2 [mm] trailing edge displacement in upward direction should be obtained. Also, to deflect from NACA 6510 to NACA 2510 15.2 [mm] trailing edge displacement in upward direction should be obtained. Structural analyses are performed in order to displace the tip of the trailing edge approximately 15.2 [mm] and 20.2 [mm]. In addition, composite thicknesses of 1.0 [mm], 1.5 [mm] and 2.0 [mm] are used in the analysis. In all of the composite thickness variations, mirror with respect to midline is aimed for symmetry. For example, 1.0 [mm] case has the ply orientation of 0/90/90/0, 1.5 [mm] case has ply orientation of 90/0/0/0/0/90, 2.0 [mm] case has ply orientation of 90/0/90/0/0/90/0/90. Here, 0^0 means that the orientation is in the chord-wise direction and 90^0 means that the one is in the span-wise direction.

4.5 Finite Element Analysis of Open Cell Hybrid Trailing Edge Control Surface

4.5.1 Neoprene Rubber Design with Different Composite Thicknesses

In this part, analysis results of Open Cell – Neoprene Rubber design with 2.0 [mm], 1.5 [mm] and 1.0 [mm] composite thickness are presented.

According to Table 5 given, Open Cell – Neoprene Rubber design with 2.0 [mm] composite thickness designs deflections are achieved by pushing the all servo actuators. Axis system is the same as in Figure 34; therefore, y axis rotation of the servo actuator moment arm results in z displacement of control surface.

Displacement in z direction, beam combined stress, equivalent elastic strain contours are given from Figure 35 to Figure 37 for maintaining the NACA 6510 profile. As seen from Figure 36, maximum beam combined stress is 106 [MPa] which is below the tensile yield strength of 280 [MPa] of Aluminium material. It can be concluded from Figure 37 that there is almost no strain on the control surface except the compliant part. This was the expected result because hyperelastic material is used for this part which is a very soft. From the analysis, reaction torque for the

servos actuating upper side of transmission part is 219 [Nmm] and reaction torque for the servos actuating lower side of transmission part is 162 [Nmm]. Selected servo actuators are capable of supporting this torques.

Table 5: Rotations of the Servo Moment Arms to Obtain the Desired NACA Profiles (Open Cell-Neoprene Rubber Design with 2.0 [mm] composite thickness)

Morphing/Maintaining NACA Profile	y-Axis Rotation of Moment Arm Actuating the Upper Part [deg]	y-Axis Rotation of Moment Arm Actuating the Lower Part [deg]
NACA 6510	1.0	-3.0
NACA 3510	12.0	-26.0
NACA 2510	12.0	-29.9

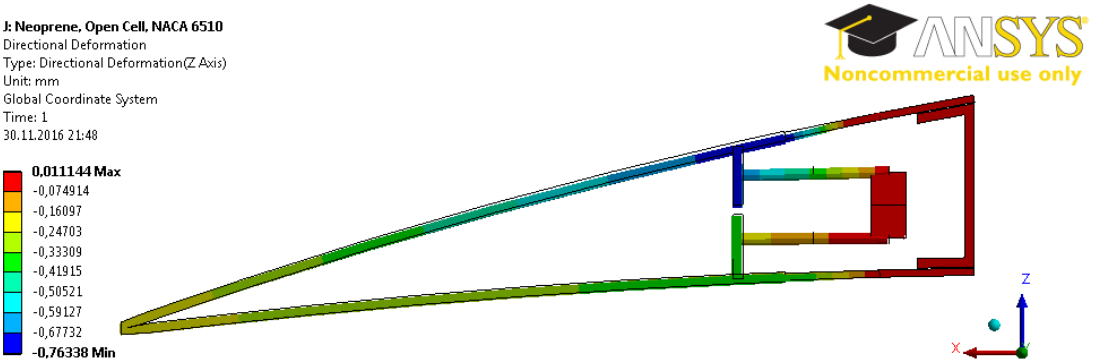

Figure 35: Displacement in z Direction Contour - Maintaining the NACA 6510 Profile (Max 0.01 [mm], Open Cell-Neoprene Rubber with 2.0 [mm] composite thickness)

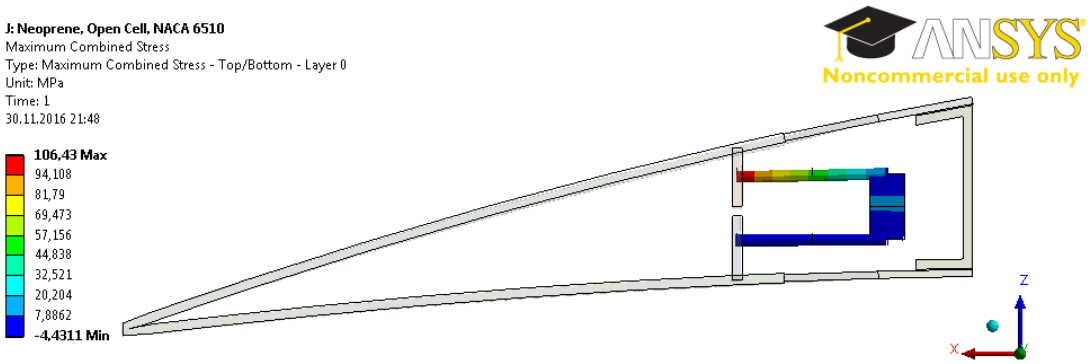

Figure 36: Maximum Beam Combined Stress Contour - Maintaining the NACA 6510 Profile (Max 106.43 [MPa], Open Cell-Neoprene Rubber Design with 2.0 [mm] composite thickness)

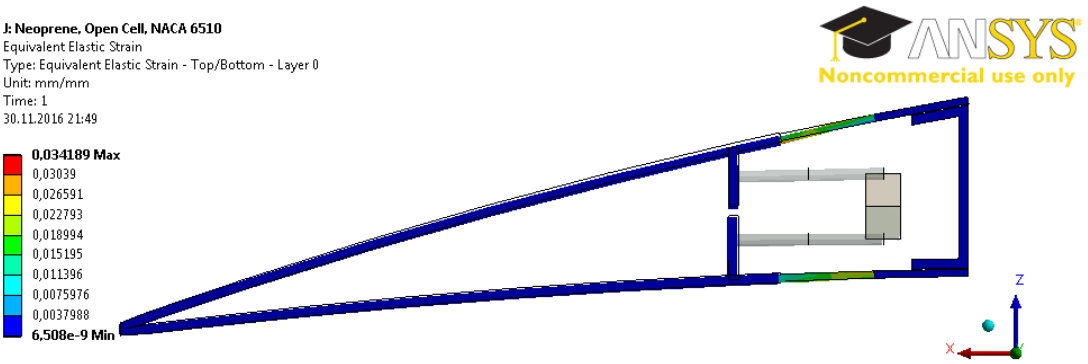

Figure 37: Equivalent Elastic Strain (von-Mises) Contour - Maintaining the NACA 6510 Profile (Max 0.03 [mm/mm], Open Cell-Neoprene Rubber Design with 2.0 [mm] composite thickness)

Displacement in z direction, beam combined stress, equivalent elastic strain contours are given from Figure 38 to Figure 40 for morphing from NACA6510 to NACA 3510 profile. As seen from Figure 40, maximum beam combined stress is 108 [MPa] which is below the tensile yield strength of 280 [MPa] of Aluminium material. Also, it can be seen from Figure 40 that the composite part makes a rigid body motion. From the analysis, reaction torque for the servos actuating upper side of transmission part is 271 [Nmm] and reaction torque for the servos actuating lower side of transmission part is 248 [Nmm]. Selected servo actuators are capable of supporting this torques.

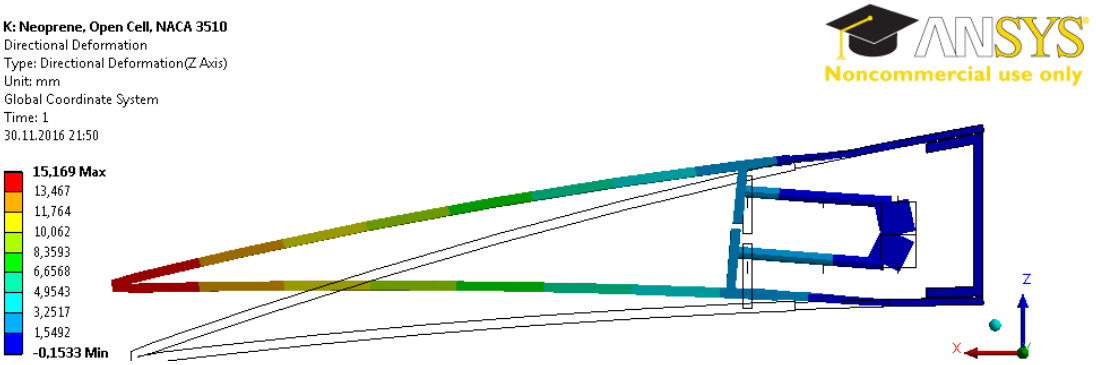

Figure 38: Displacement in z Direction Contour – Morphing from NACA 6510 to NACA 3510 Profile (Max 15.17 [mm], Open Cell-Neoprene Rubber Design with 2.0 [mm] composite thickness)

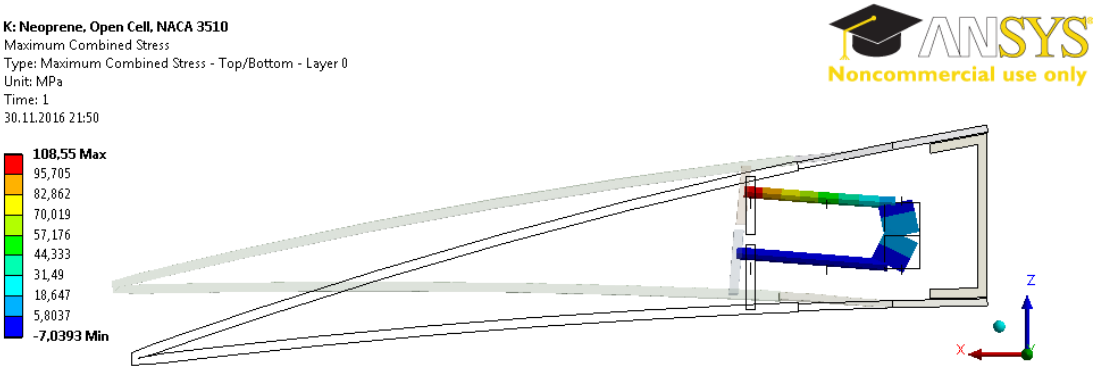

Figure 39: Maximum Beam Combined Stress Contour - Morphing from NACA 6510 to NACA 3510 Profile (Max 108.55 [MPa], Open Cell-Neoprene Rubber Design with 2.0 [mm] composite thickness)

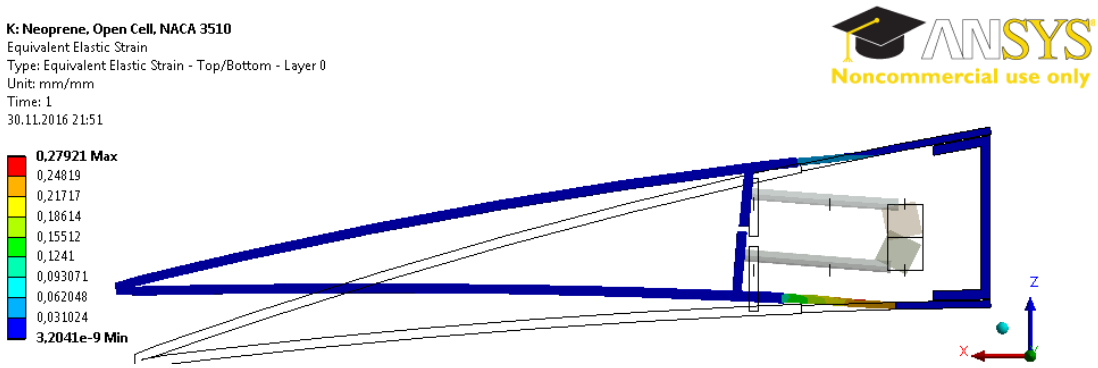

Figure 40: Equivalent Elastic Strain (von-Mises) Contour - Morphing from NACA 6510 to NACA 3510 Profile (Max 0.28 [mm/mm], Open Cell-Neoprene Rubber Design with 2.0 [mm] composite thickness)

Displacement in z direction, beam combined stress, equivalent elastic strain contours are given from Figure 41 to Figure 43 for morphing from NACA6510 to NACA 2510 profile. As seen from Figure 42, maximum beam combined stress is 114 [Mpa] which is below the tensile yield strength of 280 [Mpa] of Aluminium material. From the analysis, reaction torque for the servos actuating upper side of transmission part is 301 [Nmm] and reaction torque for the servos actuating lower side of transmission part is 267 [Nmm]. Selected servo actuators are capable of supporting this torques.

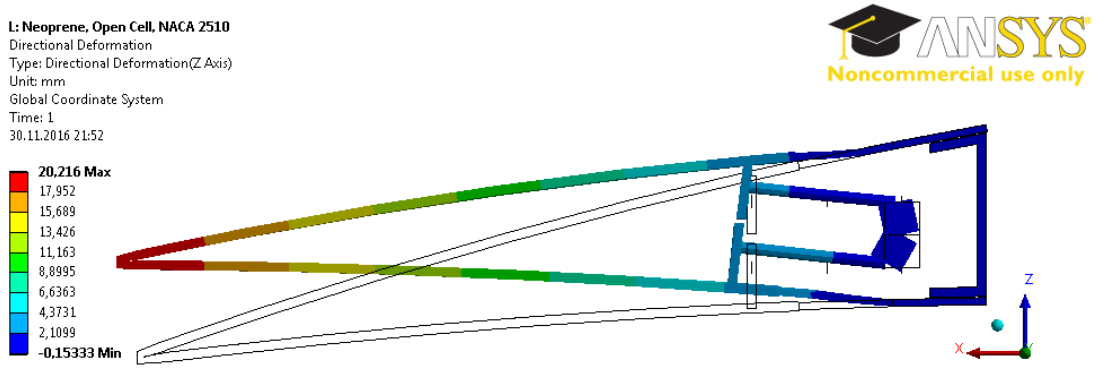

Figure 41: Displacement in z Direction Contour – Morphing from NACA 6510 to NACA 2510 Profile (Max 20.22 [mm], Open Cell-Neoprene Rubber Design with 2.0 [mm] composite thickness)

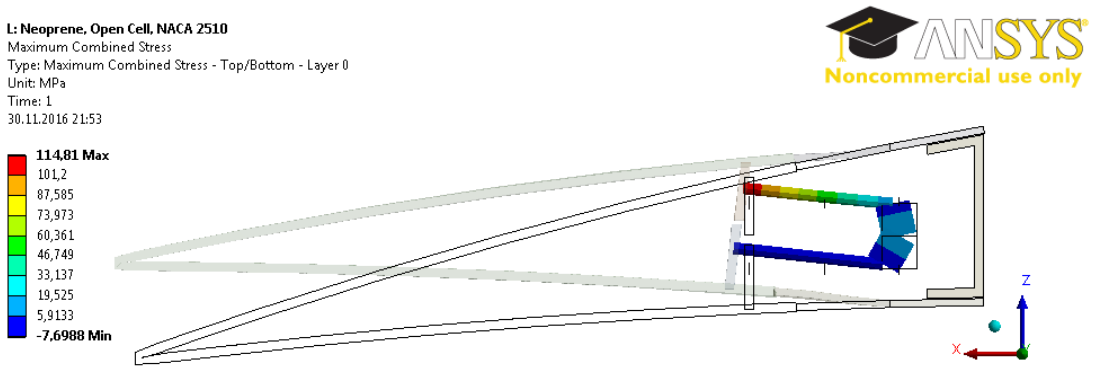

Figure 42: Maximum Beam Combined Stress Contour - Morphing from NACA 6510 to NACA 2510 Profile (Max 114.81 [MPa], Open Cell-Neoprene Rubber Design with 2.0 [mm] composite thickness)

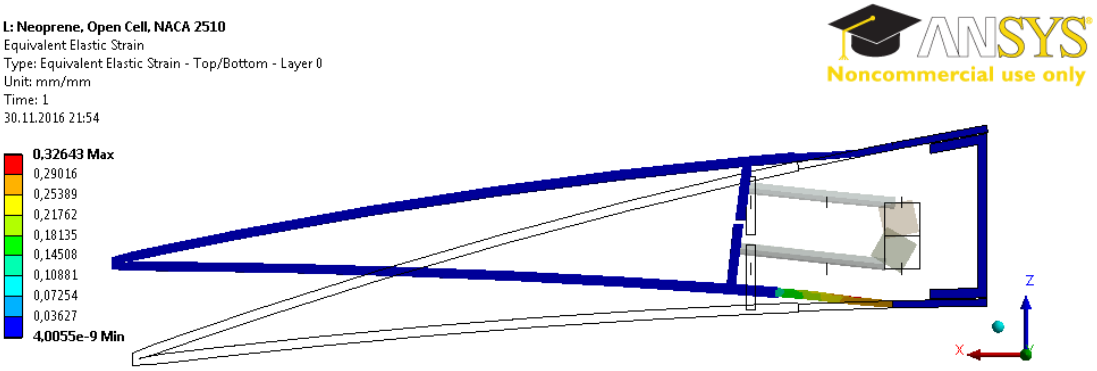

Figure 43: Equivalent Elastic Strain (von-Mises) Contour - Morphing from NACA 6510 to NACA 2510 Profile (Max 0.33 [mm/mm], Open Cell-Neoprene Rubber Design with 2.0 [mm] composite thickness)

It is seen from the analysis that Open Cell, Neoprene Rubber with 2.0 [mm] composite thickness design is capable of morphing to all desired NACA profiles in-vacuo condition in terms of both material strength and servo actuators capability.

From this point, the rest of the Figures of the results will be given in Appendices in order to have a better readability. Rotation of servo actuator moment arms which is input to the system and results/outputs such as displacement in z-axis, maximum beam combined stress, equivalent elastic strain (von-Mises) and reaction torques of servo actuators results will be given in tables with their maximum values. Rotations of servo moment arms in order to deform or maintain the each NACA profile are given in Table 6 for Open Cell – Neoprene Rubber design with 1.5 [mm]

and 1.0 [mm]. It is seen from the analyses that 1.0 [mm] composite thickness design deflection is not capable of morphing from NACA 6510 to NACA 3510 profile and NACA 6510 to NACA 2510 profile. This is because of the fact that transmission part is not stiff enough to transfer rotation of moment arms to the displacement.

Table 6: Rotations of the Servo Moment Arms to Obtain the Desired NACA Profiles (Open Cell-Neoprene Rubber Design with 1.5 [mm] and 1.0 [mm] composite thickness)

Thickness of Composite Part	Morphing/Maintaining NACA Profile	y-Axis Rotation of Moment Arm Actuating the Upper Part [deg]	y-Axis Rotation of Moment Arm Actuating the Lower Part [deg]
1.5 [mm]	NACA 6510	1.0	-4.0
	NACA 3510	12.0	-27.6
	NACA 2510	12.0	-31.7
1.0 [mm]	NACA 6510	1.0	-5.0
	NACA 3510	N/A	N/A
	NACA 2510	N/A	N/A

Resultant displacement in z-axis, maximum beam combined stress and equivalent elastic strain (von-Mises) results for Open Cell – Neoprene Rubber design with 1.5 [mm] and 1.0 [mm] composite thicknesses are given in Table 7 and figures can be obtained from Appendix A1 from Figure 72 to Figure 83. It is seen that maximum beam combined stress values for moment arm and push rod are below the tensile yield strength of 280 [MPa] of Aluminium material. In addition, there is no compression in the compliant part because there is no negative strain in the results.

Table 7: Analysis Results to Obtain the Desired NACA Profiles (Open Cell-Neoprene Rubber Design with 1.5 [mm] and 1.0 [mm] composite thickness)

Thickness of Composite Part	Morphing/Maintaining NACA Profile	Maximum Displacement in z Direction [mm]	Maximum Beam Combined Stress [MPa]	Maximum Equivalent Elastic Strain (von-Mises) [mm/mm]
1.5 [mm]	NACA 6510	0.02	83.30	0.04
	NACA 3510	15.23	95.56	0.29
	NACA 2510	20.19	103.52	0.33
1.0 [mm]	NACA 6510	0.03	47.46	0.07
	NACA 3510	N/A	N/A	N/A
	NACA 2510	N/A	N/A	N/A

For the Open Cell-Neoprene Rubber Design with 1.5 [mm] and 1.0 [mm] composite thickness design, reaction torques for different morphing/maintaining NACA profiles are given in Table 8. Selected servo actuators are capable of supporting this torques.

Table 8: Reaction Torques of Servo Actuators to Obtain the Desired NACA Profiles (Open Cell-Neoprene Rubber Design with 1.5 [mm] and 1.0 [mm] composite thickness)

Thickness of Composite Part	Morphing/Maintaining NACA Profile	Reaction Torque for the Servos Actuating Upper Side of Transmission Part [Nmm]	Reaction Torque for the Servos Actuating Lower Side of Transmission Part [Nmm]
1.5 [mm]	NACA 6510	160	123
	NACA 3510	210	201
	NACA 2510	239	218
1.0 [mm]	NACA 6510	88	79
	NACA 3510	N/A	N/A
	NACA 2510	N/A	N/A

4.5.2 Silicone Design with Different Composite Thicknesses

In this part, analysis results of Open Cell – Silicone design with 2.0 [mm], 1.5 [mm] and 1.0 [mm] composite thickness analyses are presented. Rotations of servo moment arms in order to deform or maintain the each NACA profile are given in Table 9 for Open Cell – Silicone design with 2.0 [mm], 1.5 [mm] and 1.0 [mm]. It is seen from the analyses that 1.0 [mm] composite thickness design deflection is not capable of morphing from NACA 6510 to NACA 3510 profile and NACA 6510 to NACA 2510 profile. This is because of the fact that transmission part is not stiff enough to transfer rotation of moment arms to the displacement.

Table 9: Rotations of the Servo Moment Arms to Obtain the Desired NACA Profiles (Open Cell-Silicone Design with 2.0 [mm], 1.5 [mm] and 1.0 [mm] composite thickness)

Thickness of Composite Part	Morphing/Maintaining NACA Profile	y-Axis Rotation of Moment Arm Actuating the Upper Part [deg]	y-Axis Rotation of Moment Arm Actuating the Lower Part [deg]
2.0 [mm]	NACA 6510	0.5	-2.0
	NACA 3510	2.0	-20.4
	NACA 2510	2.0	-25.6
1.5 [mm]	NACA 6510	0.5	-2.0
	NACA 3510	2.0	-25.0
	NACA 2510	2.0	-31.8
1.0 [mm]	NACA 6510	0.5	-2.0
	NACA 3510	N/A	N/A
	NACA 2510	N/A	N/A

Resultant displacement in z-axis, maximum beam combined stress and equivalent elastic strain (von-Mises) results for Open Cell – Silicone design with 2.0 [mm], 1.5 [mm] and 1.0 [mm] composite thicknesses are given in Table 10 and figures can be obtained from Appendix A2 from Figure 84 to Figure 104. It is seen from the results that 2.0 [mm] composite thickness configuration cannot perform morphing to NACA 2510 profile because the stress is higher than the tensile yield strength of Aluminum which is 280 [MPa]. However for the other conditions given in Table 10, maximum beam combined stress values for moment arm and push rod

are below the tensile yield strength of Aluminium. In addition, there is no compression in the compliant part because there is no negative strain in the results.

Table 10: Analysis Results to Obtain the Desired NACA Profiles (Open Cell-Silicone Design with 2.0 [mm], 1.5 [mm] and 1.0 [mm] composite thickness)

Thickness of Composite Part	Morphing/Maintaining NACA Profile	Maximum Displacement in z Direction [mm]	Maximum Beam Combined Stress [MPa]	Maximum Equivalent Elastic Strain (von-Mises) [mm/mm]
2.0 [mm]	NACA 6510	0.01	78.09	0.02
	NACA 3510	15.21	295.68	0.23
	NACA 2510	20.19	355.50	0.28
1.5 [mm]	NACA 6510	0.01	48.26	0.03
	NACA 3510	15.23	226.96	0.24
	NACA 2510	20.24	268.84	0.30
1.0 [mm]	NACA 6510	0.01	18.88	0.03
	NACA 3510	N/A	N/A	N/A
	NACA 2510	N/A	N/A	N/A

For the Open Cell-Silicone Design with 2.0 [mm], 1.5 [mm] and 1.0 [mm] composite thickness designs, reaction torques for morphing/maintaining NACA profiles are given in Table 11. Selected servo actuators are just capable of

maintaining the NACA 6510 profile. Morphing to NACA 3510 and NACA 2510 cannot be achieved because of the torque limit of servo actuator.

Table 11: Reaction Torques of Servo Actuators to Obtain the Desired NACA Profiles (Open Cell-Silicone Design with 2.0 [mm], 1.5 [mm] and 1.0 [mm] composite thickness)

Thickness of Composite Part	Morphing/Maintaining NACA Profile	Reaction Torque for the Servos Actuating Upper Side of Transmission Part [Nmm]	Reaction Torque for the Servos Actuating Lower Side of Transmission Part [Nmm]
2.0 [mm]	NACA 6510	140	181
	NACA 3510	892	1002
	NACA 2510	1149	1191
1.5 [mm]	NACA 6510	64	126
	NACA 3510	701	931
	NACA 2510	929	1090
1.0 [mm]	NACA 6510	4	75
	NACA 3510	N/A	N/A
	NACA 2510	N/A	N/A

4.6 Finite Element Analysis of Closed Cell Hybrid Trailing Edge Control Surface

4.6.1 Neoprene Rubber Design with Different Composite Thicknesses

In this part, analysis results of Closed Cell – Neoprene Rubber design with 2.0 [mm], 1.5 [mm] and 1.0 [mm] composite thickness analyses are presented.

Rotations of servo moment arms in order to deform or maintain the each NACA profile are given in Table 12 for Closed Cell – Neoprene Rubber design with 2.0 [mm], 1.5 [mm] and 1.0 [mm].

Resultant displacement in z-axis, maximum beam combined stress and equivalent elastic strain (von-Mises) results for Closed Cell – Neoprene design with 2.0 [mm], 1.5 [mm] and 1.0 [mm] composite thicknesses are given in Table 13 and figures can be obtained from Appendix A3 from Figure 105 to Figure 131. It is seen that maximum beam combined stress values for moment arm and push rod are below the tensile yield strength of 280 [MPa] of Aluminium material. In addition, there is no compression in the compliant part because there is no negative strain in the results.

For the Closed Cell-Neoprene Rubber Design with 2.0 [mm], 1.5 [mm] and 1.0 [mm] composite thickness design, reaction torques for different morphing/maintaining NACA profiles are given in Table 14. Selected servo actuators are capable of supporting this torques.

Table 12: Rotations of the Servo Moment Arms to Obtain the Desired NACA Profiles (Closed Cell-Neoprene Rubber Design with 2.0 [mm], 1.5 [mm] and 1.0 [mm] composite thickness)

Thickness of Composite Part	Morphing/Maintaining NACA Profile	y-Axis Rotation of Moment Arm Actuating the Upper Part [deg]	y-Axis Rotation of Moment Arm Actuating the Lower Part [deg]
2.0 [mm]	NACA 6510	1.0	-1.5
	NACA 3510	12.0	-23.1
	NACA 2510	12.0	-26.6
1.5 [mm]	NACA 6510	1.0	-1.5
	NACA 3510	12.0	-23.2
	NACA 2510	12.0	-26.8
1.0 [mm]	NACA 6510	1.0	-1.5
	NACA 3510	12.0	-23.8
	NACA 2510	12.0	-27.5

Table 13: Analysis Results to Obtain the Desired NACA Profiles (Closed Cell-Neoprene Rubber Design with 2.0 [mm], 1.5 [mm] and 1.0 [mm] composite thickness)

Thickness of Composite Part	Morphing/Maintaining NACA Profile	Maximum Displacement in z Direction [mm]	Maximum Beam Combined Stress [MPa]	Maximum Equivalent Elastic Strain (von-Mises) [mm/mm]
2.0 [mm]	NACA 6510	0.11	51.73	0.02
	NACA 3510	15.20	95.89	0.26
	NACA 2510	20.20	111.01	0.30
1.5 [mm]	NACA 6510	0.03	39.27	0.02
	NACA 3510	15.22	79.11	0.26
	NACA 2510	20.26	93.10	0.31
1.0 [mm]	NACA 6510	0.07	27.21	0.02
	NACA 3510	15.20	53.61	0.26
	NACA 2510	20.28	65.23	0.31

Table 14: Reaction Torques of Servo Actuators to Obtain the Desired NACA Profiles (Closed Cell-Neoprene Rubber Design with 2.0 [mm], 1.5 [mm] and 1.0 [mm] composite thickness)

Thickness of Composite Part	Morphing/Maintaining NACA Profile	Reaction Torque for the Servos Actuating Upper Side of Transmission Part [Nmm]	Reaction Torque for the Servos Actuating Lower Side of Transmission Part [Nmm]
2.0 [mm]	NACA 6510	155	226
	NACA 3510	247	260
	NACA 2510	267	283
1.5 [mm]	NACA 6510	168	117
	NACA 3510	201	208
	NACA 2510	225	228
1.0 [mm]	NACA 6510	110	81
	NACA 3510	144	168
	NACA 2510	169	188

4.6.2 Silicone Design with Different Composite Thicknesses

In this part, analysis results of Closed Cell – Silicone design with 2.0 [mm], 1.5 [mm] and 1.0 [mm] composite thickness analyses are presented. Analyses include displacement from NACA 6510 to NACA 2510, NACA 6510 to NACA 3510 and maintaining the NACA 6510 profiles in-vacuo condition.

Rotations of servo moment arms in order to deform or maintain the each NACA profile are given in Table 15 for Closed Cell – Silicone design with 2.0 [mm], 1.5 [mm] and 1.0 [mm] composite thicknesses.

Resultant displacement in z-axis, maximum beam combined stress and equivalent elastic strain (von-Mises) results for Closed Cell – Neoprene design with 2.0 [mm], 1.5 [mm] and 1.0 [mm] composite thicknesses are given in Table 16 and figures can be obtained from Appendix A4 from Figure 132 to Figure 158. It is seen that maximum beam combined stress values for moment arm and push rod are below the tensile yield strength of 280 [MPa] of Aluminium material. In addition, there is no compression in the compliant part because there is no negative strain in the results.

For the Closed Cell-Silicone Design with 2.0 [mm], 1.5 [mm] and 1.0 [mm] composite thickness design, reaction torques for different morphing/maintaining NACA profiles are given in Table 17. Selected servo actuators are just capable of maintaining the NACA 6510 profile. Morphing to NACA 3510 and NACA 2510 cannot be achieved because of the torque limit of servo actuator exceeds.

Table 15: Rotations of the Servo Moment Arms to Obtain the Desired NACA Profiles (Closed Cell- Silicone Design with 2.0 [mm], 1.5 [mm] and 1.0 [mm] composite thickness)

Thickness of Composite Part	Morphing/Maintaining NACA Profile	y-Axis Rotation of Moment Arm Actuating the Upper Part [deg]	y-Axis Rotation of Moment Arm Actuating the Lower Part [deg]
2.0 [mm]	NACA 6510	1.0	-1.5
	NACA 3510	12.0	-23.8
	NACA 2510	12.0	-27.8
1.5 [mm]	NACA 6510	1.0	-1.5
	NACA 3510	12.0	-24.6
	NACA 2510	12.0	-28.8
1.0 [mm]	NACA 6510	1.0	-1.5
	NACA 3510	12.0	-27.4
	NACA 2510	12.0	-32.7

Table 16: Analysis Results to Obtain the Desired NACA Profiles (Closed Cell- Silicone Design with 2.0 [mm], 1.5 [mm] and 1.0 [mm] composite thickness)

Thickness of Composite Part	Morphing/Maintaining NACA Profile	Maximum Displacement in z Direction [mm]	Maximum Beam Combined Stress [MPa]	Maximum Equivalent Elastic Strain (von-Mises) [mm/mm]
2.0 [mm]	NACA 6510	0.19	37.30	0.02
	NACA 3510	15.16	55.66	0.26
	NACA 2510	20.28	88.07	0.31
1.5 [mm]	NACA 6510	0.13	26.06	0.02
	NACA 3510	15.27	53.14	0.26
	NACA 2510	20.27	62.57	0.31
1.0 [mm]	NACA 6510	0.01	15.94	0.01
	NACA 3510	15.26	49.16	0.27
	NACA 2510	20.26	57.12	0.32

Table 17: Reaction Torques of Servo Actuators to Obtain the Desired NACA Profiles (Closed Cell-Silicone Design with 2.0 [mm], 1.5 [mm] and 1.0 [mm] composite thickness)

Thickness of Composite Part	Morphing/Maintaining NACA Profile	Reaction Torque for the Servos Actuating Upper Side of Transmission Part [Nmm]	Reaction Torque for the Servos Actuating Lower Side of Transmission Part [Nmm]
2.0 [mm]	NACA 6510	180	192
	NACA 3510	525	1029
	NACA 2510	788	1210
1.5 [mm]	NACA 6510	119	150
	NACA 3510	470	987
	NACA 2510	725	1163
1.0 [mm]	NACA 6510	49	100
	NACA 3510	401	929
	NACA 2510	652	1097

4.7 Discussion and Conclusion

In this chapter, Open Cell and Closed Cell designs are structurally analyzed in-vacuo conditions in order to perform the desired morphing capabilities.

It could be concluded from the results that thickness of the composite part and the required torque to deflect the control surface into the desired NACA profiles is directly proportional as can be seen from Figure 44 and Figure 45. The reason is that standard earth gravity is included in the calculations and thicker/heavier composite design needs more torque for the deflection. The same is true for beam combined stress. Heavier design creates more stress on the moment arm and push rod beams. Also, strain values of the designs are close to each other for same morphing motion as can be seen from Figure 46. This is excepted because 15.2 [mm] tip deflection for NACA 6510 to NACA 3510 morphing and 20.2 [mm] tip deflection for NACA 6510 to NACA 2510 morphing is achieved in the analyses as shown in Figure 47. Material, design and composite thickness does not affect the strain values.

Open Cell design with 2.0 [mm], 1.5 [mm] and 1.0 [mm] composite thickness is performed with Neoprene rubber and silicone materials used for compliant part. It was shown that Open Cell design can perform desired morphing motions only for 2.0 [mm] and 1.5 [mm] composite thickness. It is not capable to morph into desired NACA profiles for 1.0 [mm] composite thickness. The reason is explained as follows. It is seen from the results that as the composite thickness get thicker rotation of servo moment arms gets smaller. This is because of the fact that transmission part is stiffer when the thickness is increased and stiffer structure transfers rotation of moment arms to the displacement better. The reason why open cell 1.0 [mm] composite thickness design is not capable of morphing is because of this fact. Also, Open Cell with silicone design is not capable of morphing to NACA 2510 because the maximum combined stress on the push rod and moment arm part is higher than the tensile yield strength of Aluminum as shown in Figure 48.

Closed Cell design with 2.0 [mm], 1.5 [mm] and 1.0 [mm] composite thickness is performed with Neoprene rubber and silicone materials used for

compliant part. It is seen from the results that Closed Cell design is much stiffer than the Open Cell design because it can perform desired morphing motions for 1 [mm] composite thickness design. Closed form of transmission part of the control surface is stiffer than the open form. As a result, Closed Cell design is better than the Open Cell design. In addition, silicone design exceeds the torque limits of the selected servo actuators. Therefore, Closed Cell Neoprene rubber design with different composite thicknesses will be analyzed under the aerodynamic loads.

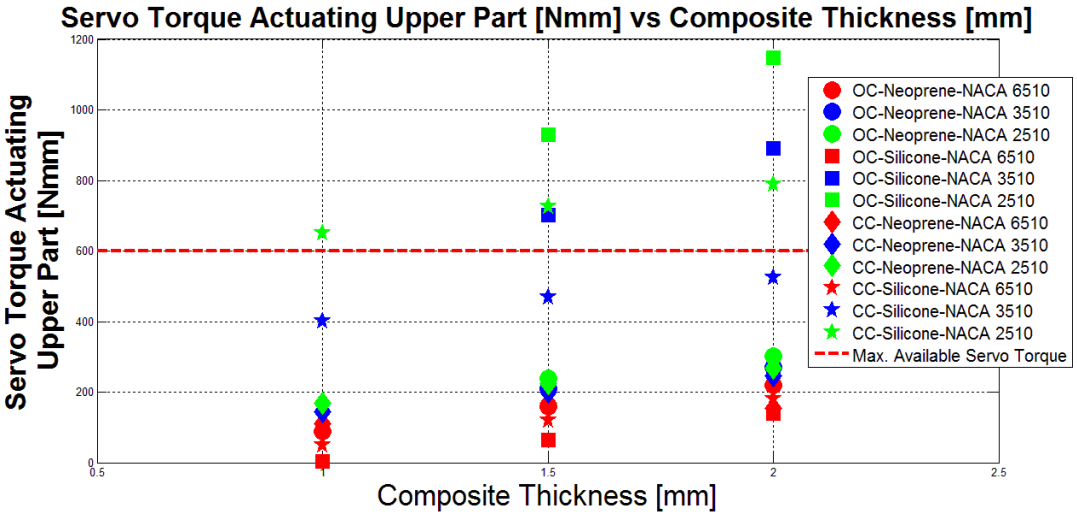

Figure 44: Servo Torque Actuating Upper Part for Open Cell (OC) and Closed Cell (CC) Designs

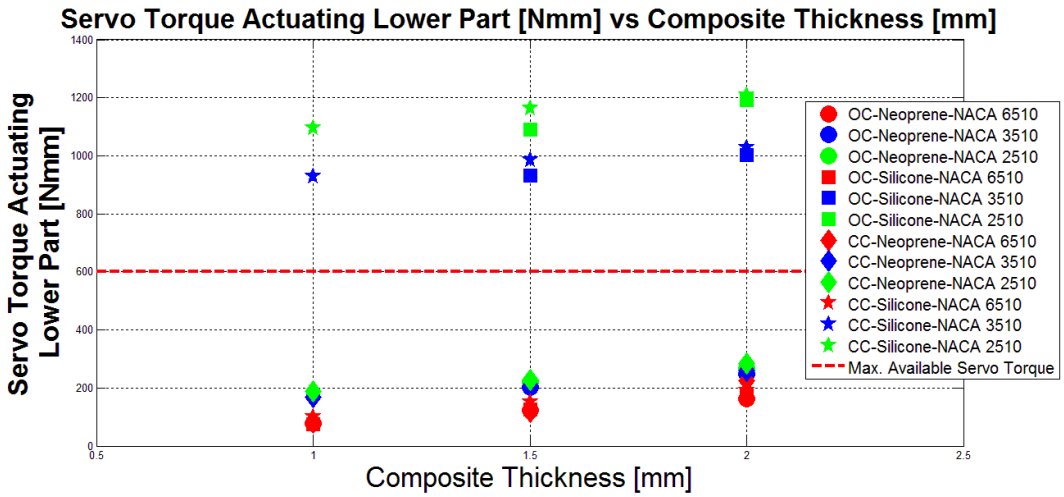

Figure 45: Servo Torque Actuating Lower Part for Open Cell (OC) and Closed Cell (CC) Designs for all Morphing Missions

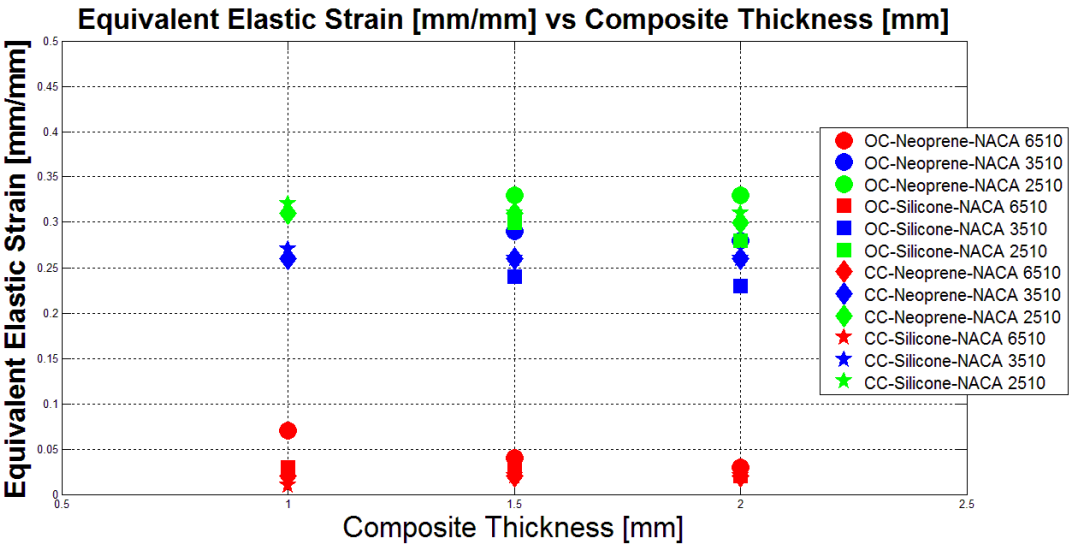

Figure 46: Equivalent Elastic Strain (von-Mises) of Control Surface for Open Cell (OC) and Closed Cell (CC) Designs

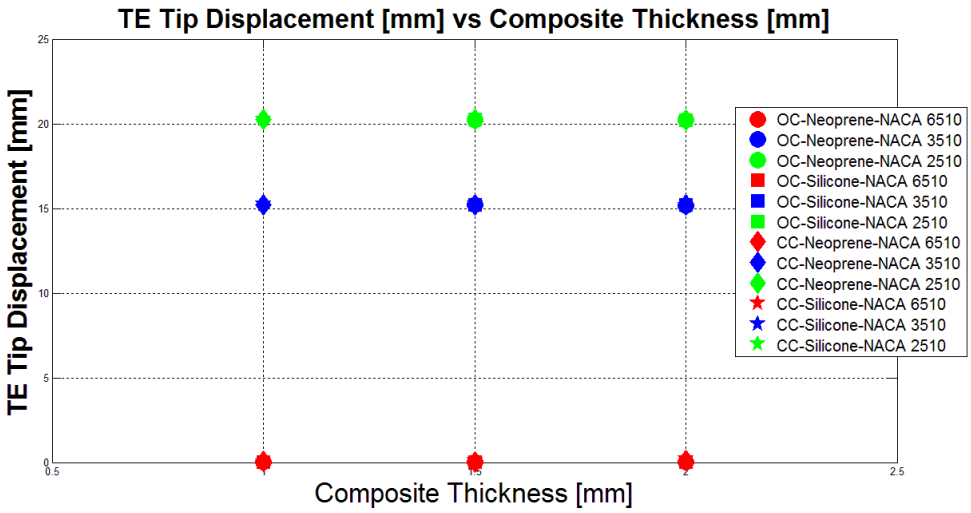

Figure 47: Trailing Edge Tip Displacement of Control Surface for Open Cell (OC) and Closed Cell (CC) Designs

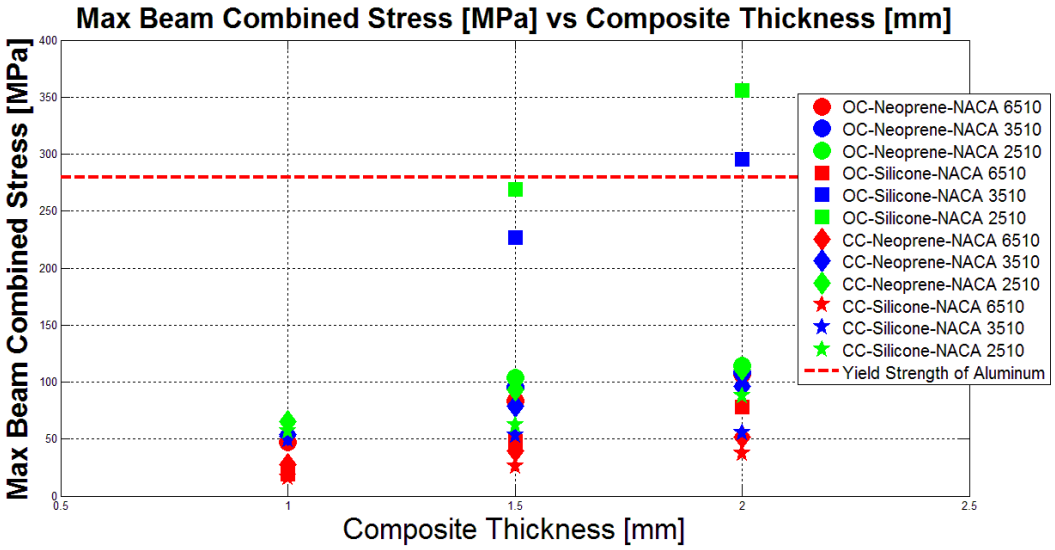

Figure 48: Max Beam Combined Stresses of Push Rod/Moment Arm for Open Cell (OC) and Closed Cell (CC) Designs

CHAPTER 5

AERODYNAMIC LOADS

5.1 Introduction

In this chapter, calculation of aerodynamic loads on the hybrid trailing edge control surface is described. Aerodynamic load is calculated by Computational Fluid Dynamics (CFD) analysis. First, brief information about the aerodynamic mesh generated and CFD analysis performed are given. Generated mesh over the wing, flow field mesh and total lifting force of the wing obtained with a script are given together with the non-dimensional pressure coefficient (Cp) contours. Then, to obtain the aerodynamic loads on FEM, interpolation method is described and interpolated Cp contours on the hybrid trailing edge control surface are given. Finally, methodology of script developed to obtain the total pressure force is described.

5.2 Brief Information about the Aerodynamic Analysis

In order to analyze the control surface structurally under the pressure loading due to flight conditions, CFD analysis is performed for each morphing missions given in Table 18 [36]. CFD analyses are performed within the CHANGE project.

For the Aerodynamic analysis, the flow field mesh is required. The mesh is created base on the wing geometry with Pointwise V17.2R2 package program. Type of the generated mesh is triangular and element size is 8 [mm]. There exists refining near leading and trailing edges because flow starts from leading edge and leaves from leading edge. In addition, there is high surface curvature at the leading edge and trailing edges. During the meshing, y+ is also considered for the turbulence modelling. Generated mesh over the wing and mesh of the outer domain can be seen

from Figure 50 and Figure 50 respectively. Stanford University Unstructured (SU2) v3.2.03 is chosen as the flow solver and the incompressible flow is chosen as the flow regime since the Mach number is very small. The turbulence is modelled by using Spallart-Allmaras turbulence modelling.

Table 18: Flight Conditions and Parameters Used in CFD

	Loiter	**Take-off Phase**	**Cruise or High Speed Dash Phase**
Mission	Maintaining 6510 Profile	Morphing to 3510 Profile	Morphing to 2510 Profile
Flight Speed [m/s]	13.24	21.15	30.55
Angle of Attack [deg]	6.62	1.71	1.05
Density [kg/m^3]	1.189	1.225	1.189
Altitude [m]	304.8 (~1000 [ft])	0	304.8 (~1000 [ft])
Mach Number	0.039	0.063	0.090

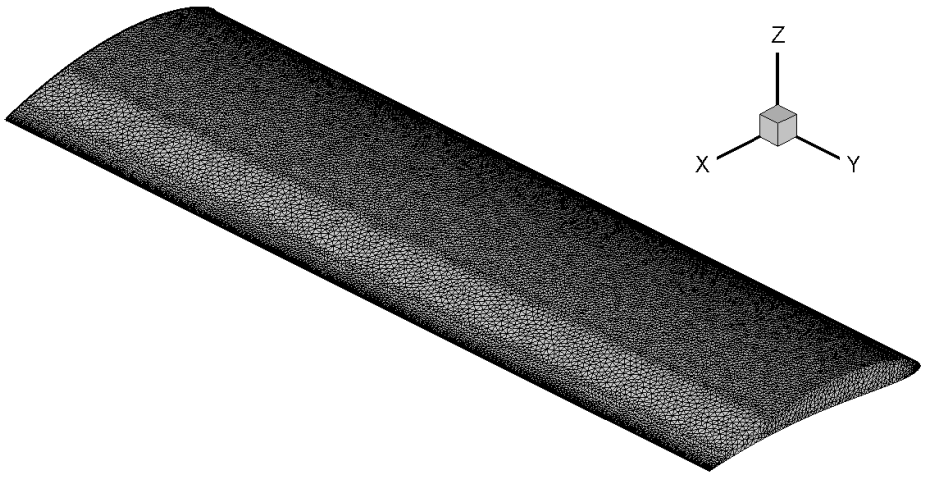

Figure 49. Generated Mesh Over the Wing for CFD Analysis [36]

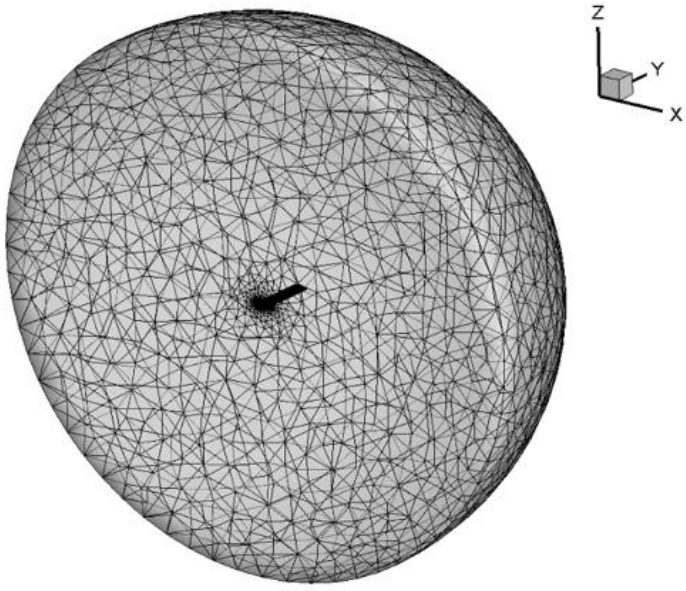

Figure 50. Generated Mesh of the Outer Domain for CFD Analysis [36]

In addition to the aerodynamic loads due to the flight condition given in Table 18, it is checked whether the control surface can perform the missions under higher aerodynamic loads which are 2g, 3g and 4g. From the formula given in (1) and (2) it is seen that aerodynamic load is proportional to the square root of velocity. In

addition, (3) shows that force and load factor are directly proportional to each other. Therefore for 2g, 3g and 4g aerodynamic loads V*$\sqrt{2}$, V*$\sqrt{3}$ and 2*V is used.

$$F = q * S * Cf \quad (1)$$

$$q = \frac{1}{2} * \rho_{\infty} * V_{\infty}^2 \quad (2)$$

where

- q is the dynamic pressure
- S is the reference area
- Cf is the force coefficient
- F is the total force

In addition, load factor n is defined as given in (3).

$$n = \frac{F}{W} \quad (3)$$

where

- F is the total force
- W is the weight

Pressure distribution over the wing is taken from SU2 as Cp distribution. Therefore, formula (4) is used in order to get the gauge pressure.

$$C_p = \frac{P_{gauge}}{\frac{1}{2}\rho_{\infty} V_{\infty}} \quad (4)$$

For 1g, 2g, 3g and 4g aerodynamic load of loiter mission CFD analysis is performed and pressure coefficient contours are given in Figure 51, Figure 52, Figure 53 and Figure 54. Since the Mach numbers for each configuration are considerably

small, the contours of pressure coefficient for higher load factors are almost similar to the one for 1g load factor condition. It is also seen that the Cp contour levels are same for different loads factors in loiter mission. In addition, total force of the wing due to pressure is calculated by a script written in Fortran language and verified with SU2 output. Methodology used in the script is described in Chapter 5.4. According to the results given in Table 19, there is a linear relation between the aerodynamic load factor and lifting force of the wing. Therefore, for take-off phase (i.e. NACA 3510 configuration) and cruise/high speed dash phase (i.e. NACA 2510 configuration) CFD run is performed only for 1g condition. Higher aerodynamic load cases are obtained from 1g Cp distribution multiplying by 2g, 3g and 4g dynamic pressure.

Table 19: Total Lifting Force of the Wing (Loiter Mission)

Mission	**Aerodynamic Load Factor**	**Script Ouput Wing Lifting Force - Fz [N]**	**SU2 Output Wing Lifting Force - Fz [N]**
Loiter (NACA 6510)	1g	121.59	121.68
	2g	244.30	244.47
	3g	360.47	360.72
	4g	492.76	493.10

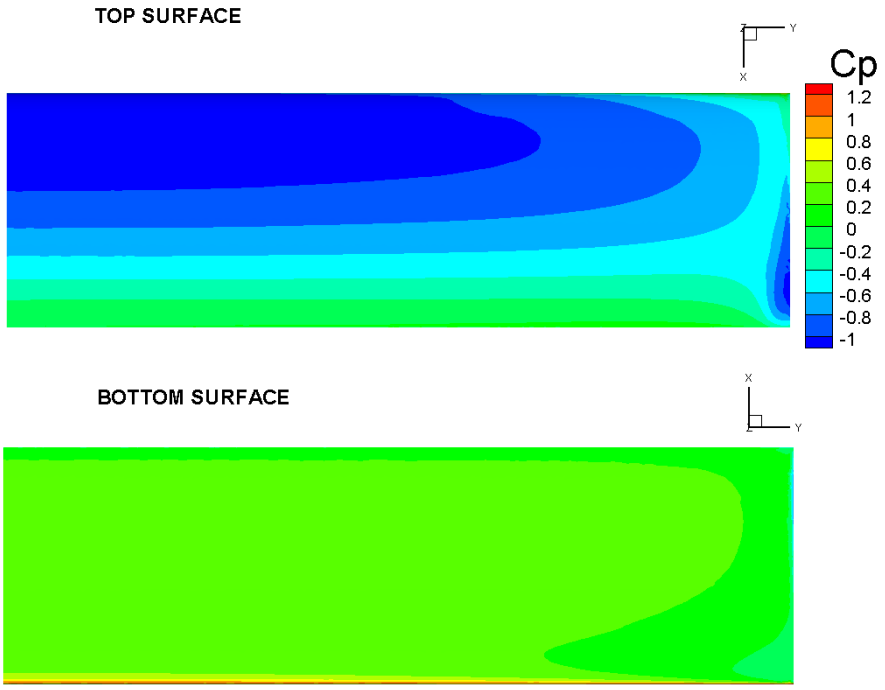

Figure 51. Cp Contour for Loiter Mission (NACA 6510) 1g Aerodynamic Load

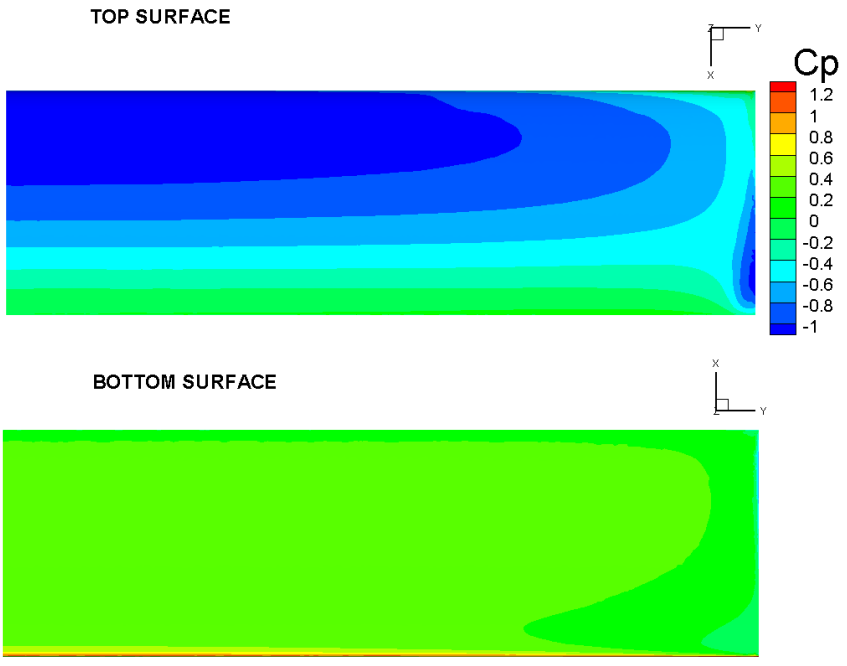

Figure 52. Cp Contour for Loiter Mission (NACA 6510) 2g Aerodynamic Load

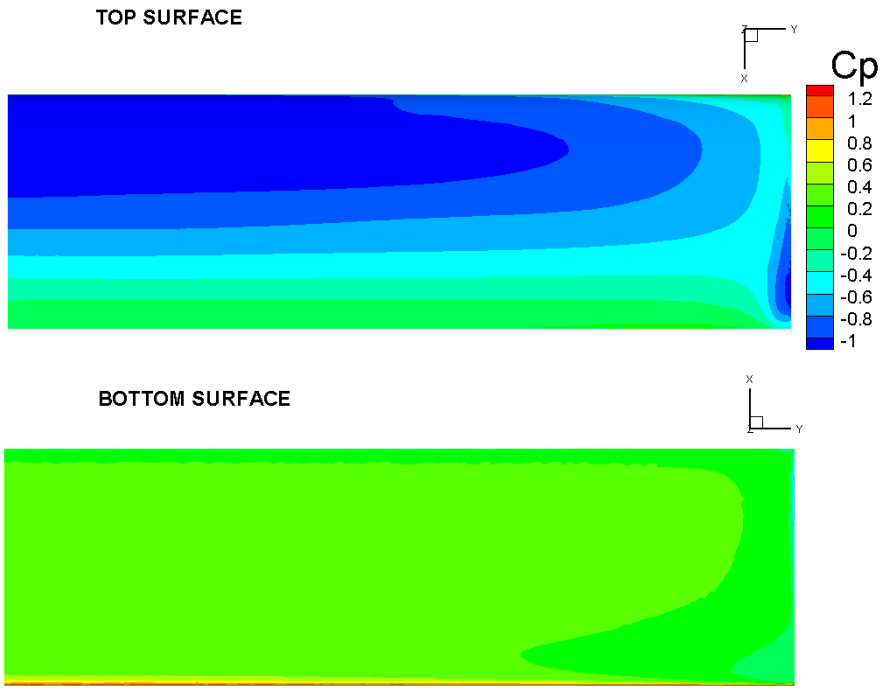

Figure 53. Cp Contour for Loiter Mission (NACA 6510) 3g Aerodynamic Load

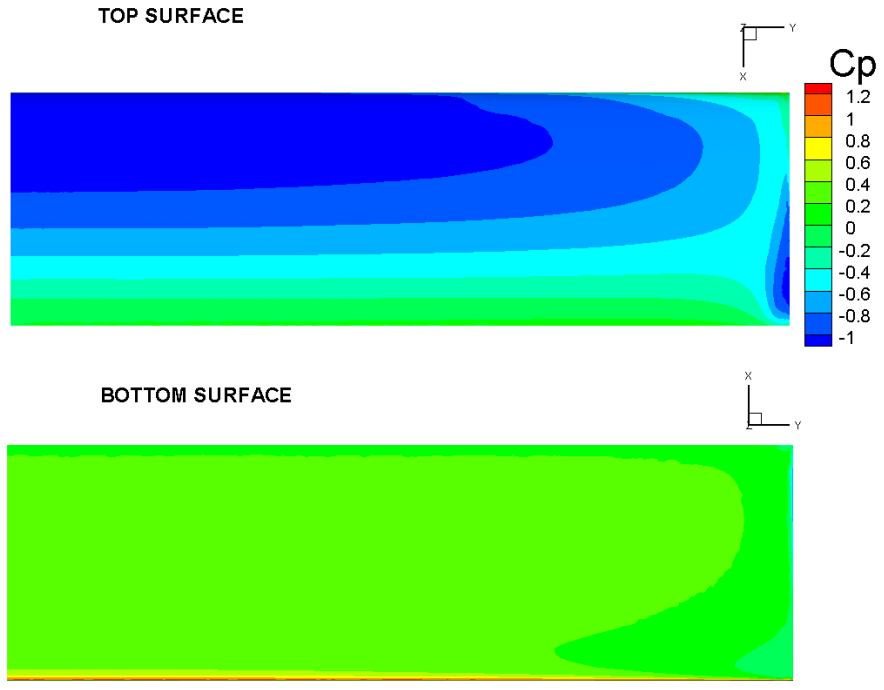

Figure 54. Cp Contour for Loiter Mission (NACA 6510) 4g Aerodynamic Load

1g aerodynamic pressure coefficient contours for takeoff and cruise/high speed dash phase are given in Figure 55 and Figure 56. Aerodynamic pressure loads for 2g, 3g and 4g are obtained by scaling the 1g pressure contour with corresponding dynamic pressure. At the cruise/high speed dash phase span of the wing is 1.6 [m] which is smaller than the other phases. Table 20 shows the total lifting force of the wing obtained by in-house developed code for take-off and cruise/high speed dash missions.

Table 20: Total Lifting Force of the Wing (Take-off and Cruise/High Speed Dash Missions)

Mission	**Aerodynamic Load Factor**	**Wing Lifting Force - Fz [N]**	**SU2 Output Wing Lifting Force - Fz [N]**
Take-off (NACA 3510)	1g	127.80	127.52
	2g	255.60	N/A
	3g	383.40	N/A
	4g	511.20	N/A
Cruise or High Speed Dash (NACA 2510)	1g	127.29	126.94
	2g	254.58	N/A
	3g	381.87	N/A
	4g	509.16	N/A

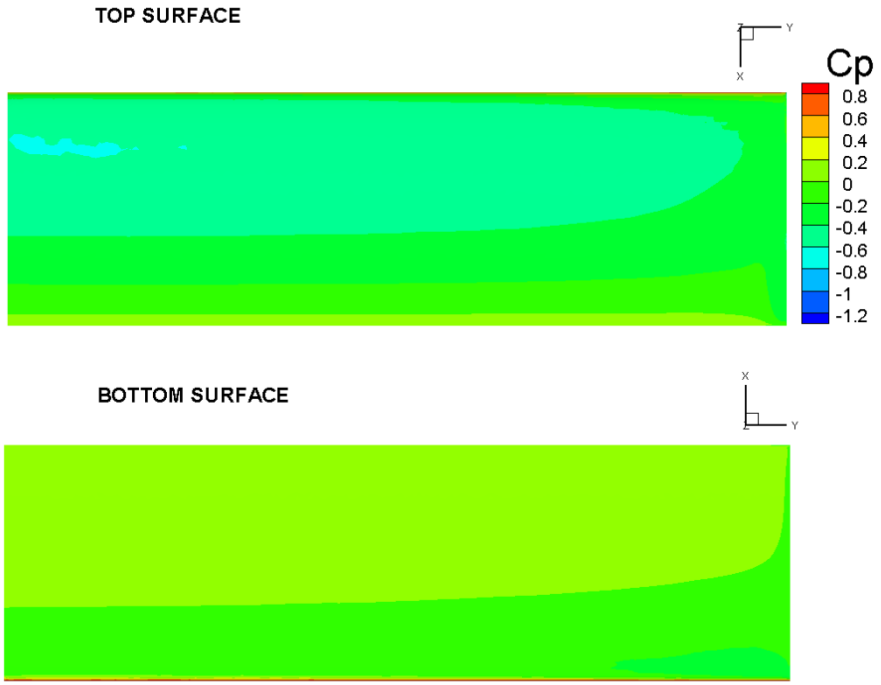

Figure 55. Cp Contour for Takeoff Phase (NACA 3510) 1g Aerodynamic Load

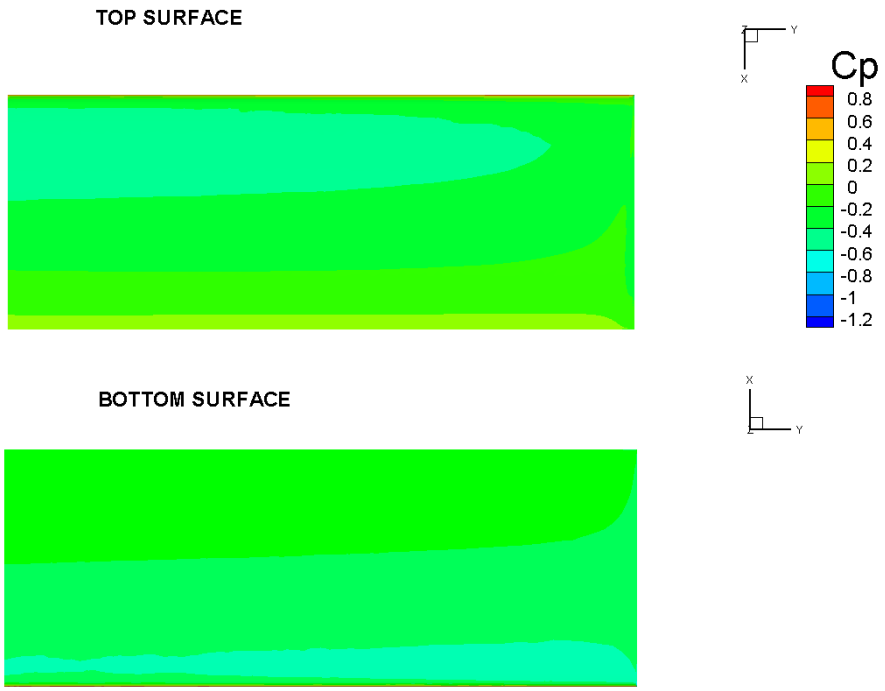

Figure 56. Cp Contour for Cruise/High Speed Dash (NACA 2510) 1g Aerodynamic Load

5.3 Interpolation of Aerodynamic Loads on the Hybrid Trailing Edge Control Surface

Aerodynamic pressure distribution on the control surface is obtained by interpolation method. Pressures on the aerodynamic mesh nodes are interpolated to the structural mesh nodes by Tecplot 360 2013R1 package programme. FEM mesh is exported from ANSYS Static Structural module. FEM data contains node id, x, y and z location of each node. FEM of undeformed control surface is then imported to the Tecplot together with the aerodynamic pressure data. Inverse-distance interpolation method is chosen while interpolating the pressure to FEM mesh. Inverse-distance averages the values at the data points from the source zone to the data points in destination zone [37]. Overall wing having the pressure distribution is taken as the source zone and hybrid trailing edge control surface is the destination zone. The average is weighted by a function of the distance between each source data point to the destination data point. The closer a source data point to the destination data point, the greater its value is weighted. The closest two aerodynamic node is weighted and interpolated to the destination FEM node. Two node is selected because upper and lower surfaces of trailing edge of the control surface is very close. If higher node number is selected for source node, pressure distribution at the trailing edge is not realistic. For example, upper side of the trailing edge of control surface interpolates pressure from the lower side of the trailing edge of the control surface. Interpolated pressures are given from Figure 57 to Figure 62. Lifting force of the control surface for each morphing missions is given in Table 22.

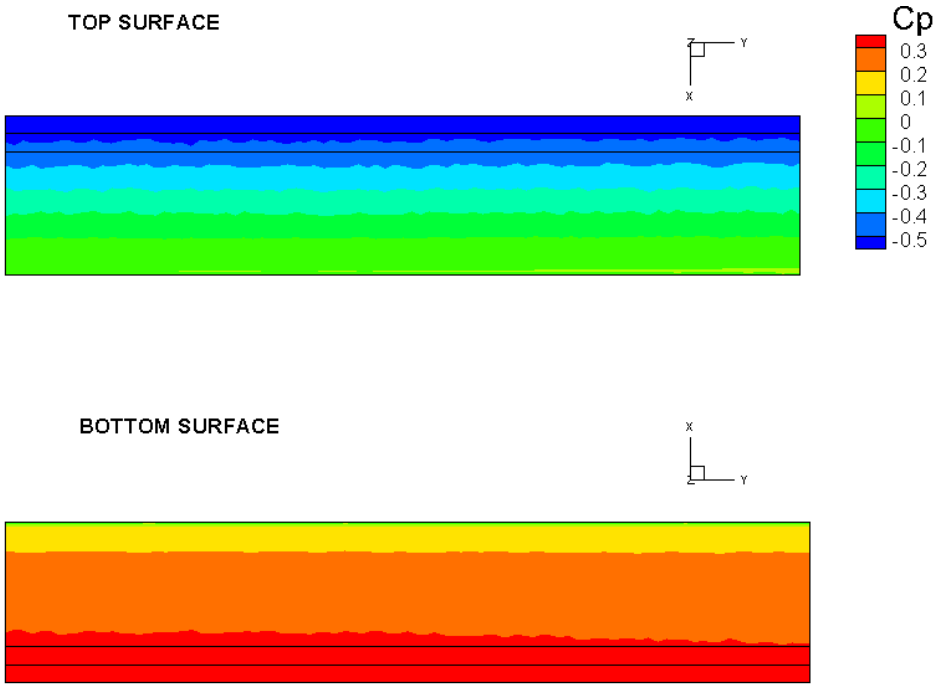

Figure 57. Cp Contour for Loiter Mission 1g Aerodynamic Load Interpolated on Hybrid Trailing Edge Control Surface

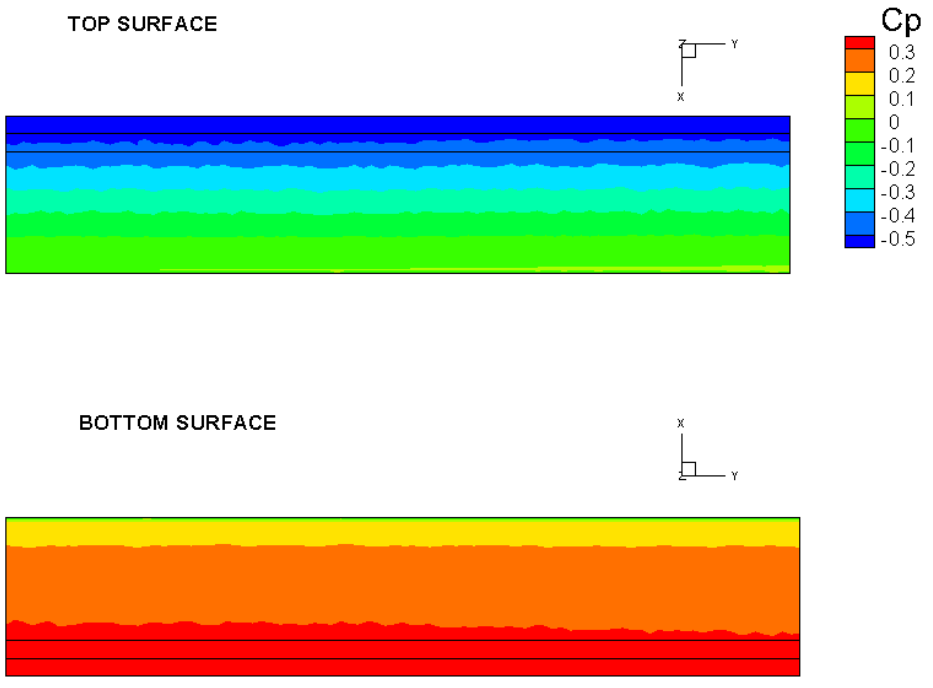

Figure 58. Cp Contour for Loiter Mission 2g Aerodynamic Load Interpolated on Hybrid Trailing Edge Control Surface

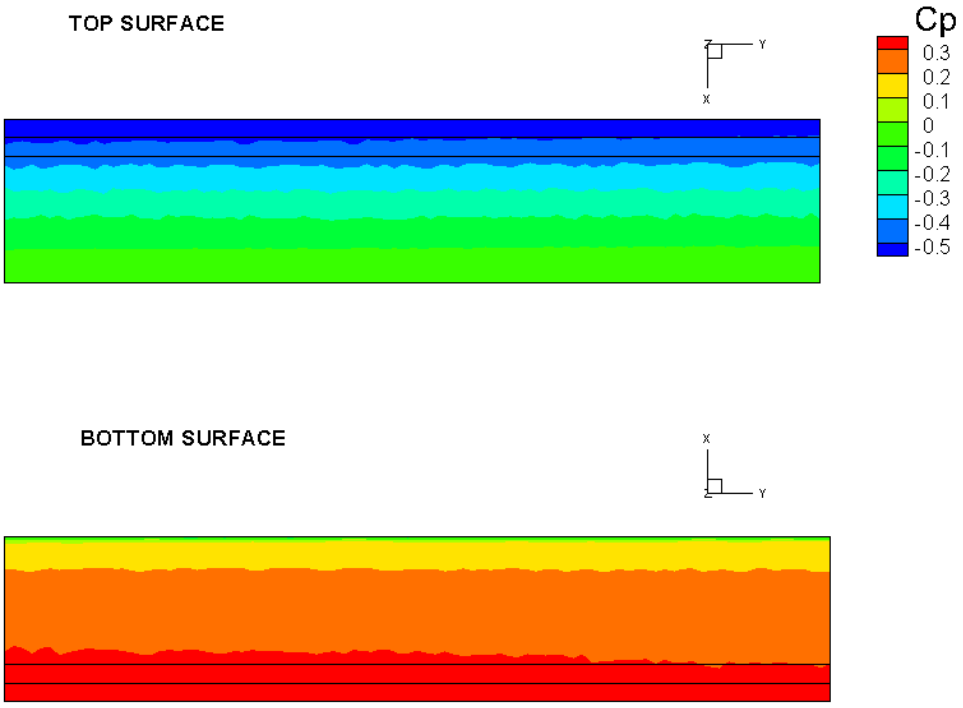

Figure 59. Cp Contour for Loiter Mission 3g Aerodynamic Load Interpolated on Hybrid Trailing Edge Control Surface

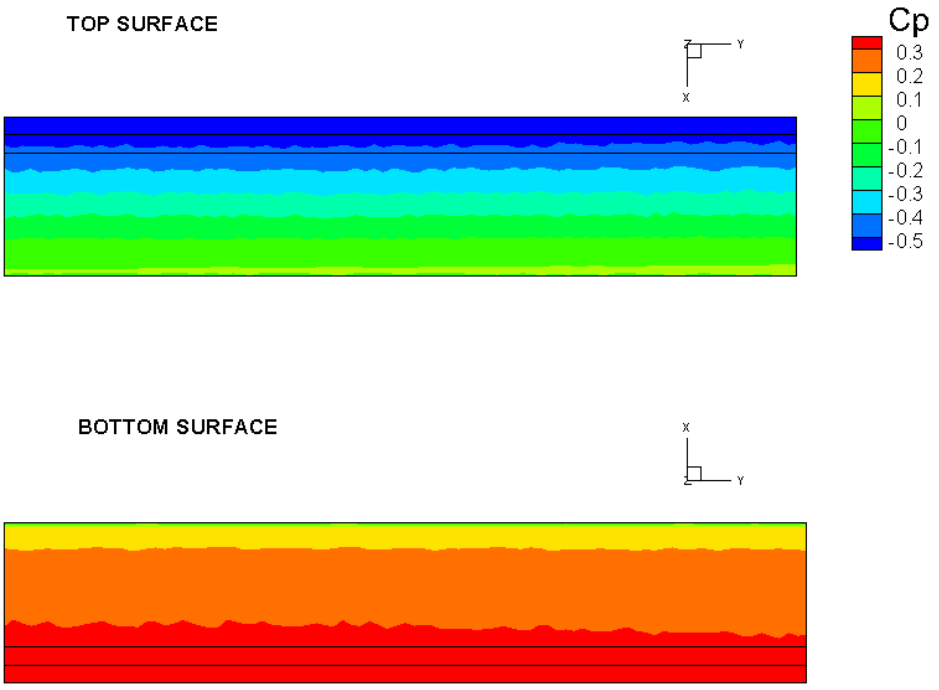

Figure 60. Cp Contour for Loiter Mission 4g Aerodynamic Load Interpolated on Hybrid Trailing Edge Control Surface

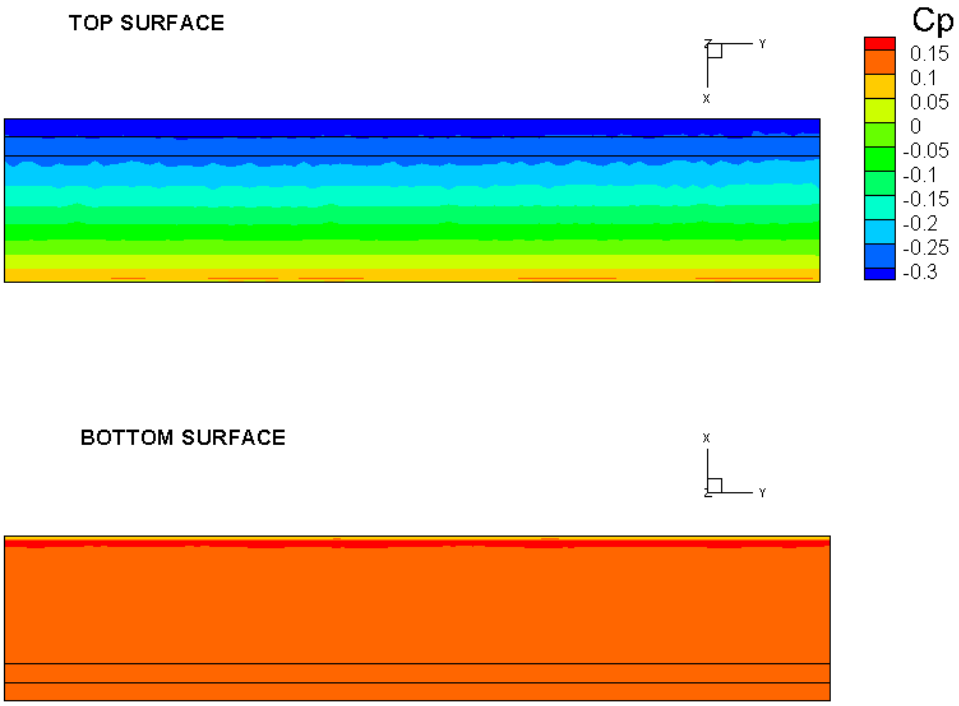

Figure 61. Cp Contour for Takeoff Phase 1g Aerodynamic Load Interpolated on Hybrid Trailing Edge Control Surface

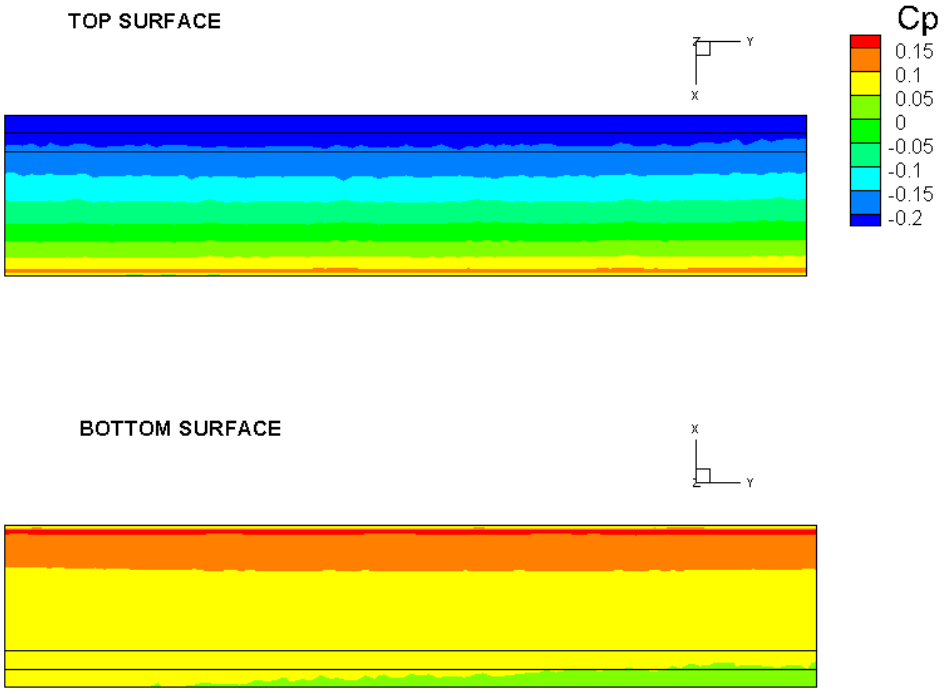

Figure 62. Cp Contour for Cruise/High Speed Dash 1g Aerodynamic Load Interpolated on Hybrid Trailing Edge Control Surface

Table 21: Total Lifting Force of the Control Surface Obtained by Script

Mission	Aerodynamic Load Factor	Control Surface Lifting Force - Fz [N]
Loiter (NACA 6510)	1g	8.97
	2g	18.08
	3g	26.42
	4g	36.68
Take-off (NACA 3510)	1g	12.19
	2g	24.37
	3g	36.56
	4g	48.74
Cruise or High Speed Dash (NACA 2510)	1g	16.17
	2g	32.34
	3g	48.51
	4g	64.68

5.4 Script Methodology for the Calculation of Total Aerodynamic Load

This script is developed in FORTRAN language for the calculation of total force due to pressure. It is a post processing tool which reads the output file of SU2 and from the pressure values at each nodes it calculates the total pressure load. Method, code input/outputs together with its format are presented as follows.

Input mesh file format for the code is the ASCII, Point format as shown in Figure 63. Unit of the node location should be in meters and pressure should be in Pascal. After the node x, y, z and pressure, element node connectivity information is

given in the input mesh file as shown in Figure 64. If the element is triangular, three nodes are written in the element connectivity information.

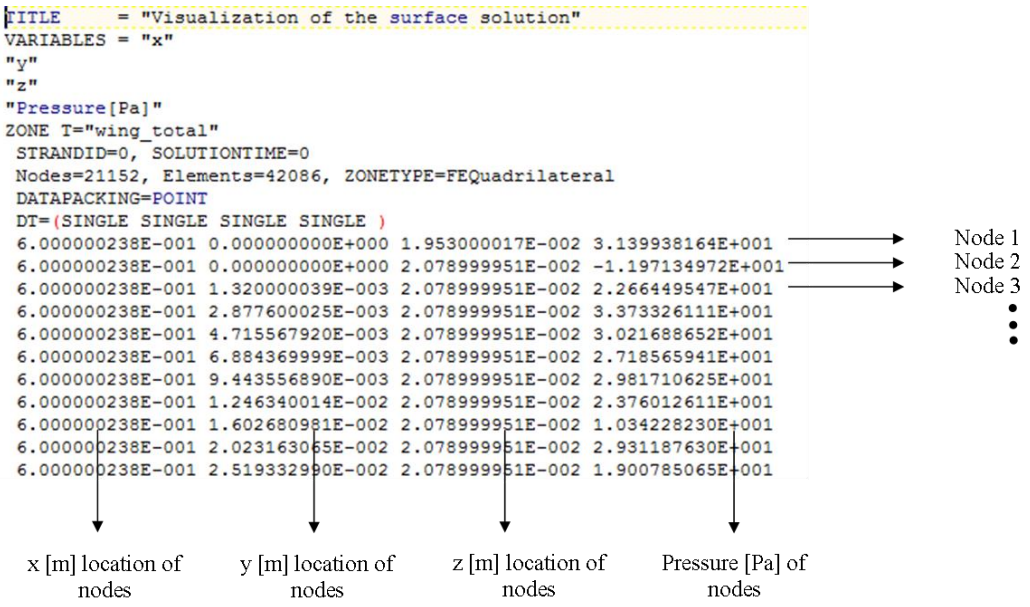

Figure 63. Mesh Input File Format Node Locations and Pressures

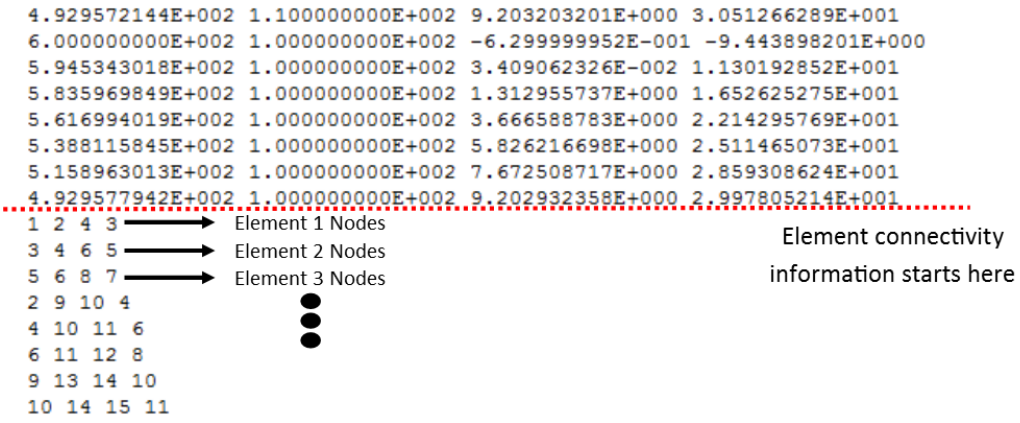

Figure 64. Mesh Input File Format Element Node Connectivity Information

After reading the mesh input file, code generates the element properties such as area, unit normal and center of gravity. Area is calculated as given in (5). If the element is triangular (6) is used for the element area.

$$Area\ of\ Quad\ Element = \left|\overrightarrow{AB} x \overrightarrow{AC}\right| \qquad (5)$$

$$Area\ of\ Triangle = \frac{\left|\overrightarrow{AB} x \overrightarrow{AC}\right|}{2} \qquad (6)$$

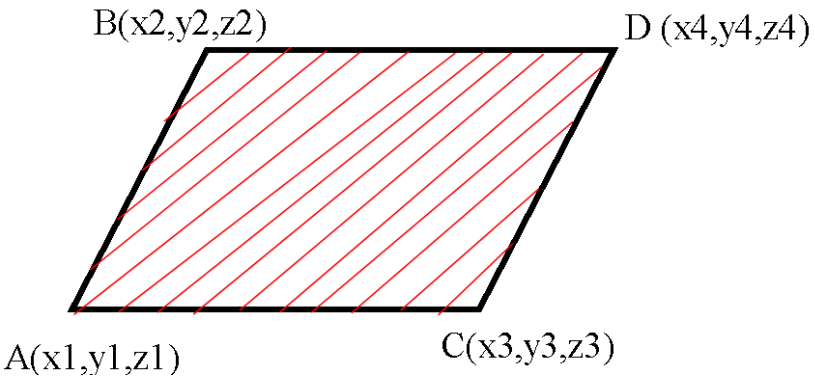

Figure 65. Area of a Quad Element

Unit normal of an element is calculated as given in (7). All the unit normal of the elements should be to the out of surface.

$$Unit\ Normal = \frac{\overrightarrow{AC} x \overrightarrow{AB}}{\left|\overrightarrow{AC} x \overrightarrow{AB}\right|} \qquad (7)$$

After that pressure is averaged from the nodes of an element. Then averaged pressure is multiplied with the element area. Therefore, force of an element is obtained. Force in x, y and z direction is obtained by using the unit normal of element.

CHAPTER 6

STATIC STRUCTURAL ANALYSIS OF HYBRID TRAILING EDGE CONTROL SURFACE UNDER AERODYNAMIC LOADS

6.1 Introduction

In this chapter, morphing wing hybrid trailing control surface is structurally analyzed under aerodynamic loads. Static Structural module of ANSYS Workbench v14.0 is used in the analysis. Closed cell hybrid trailing edge control surface with Neoprene rubber material for different composite thicknesses is analyzed. FEM described in Chapter 4.2 is used in the analyses. Analyses performed in this chapter are summarized in Figure 58. For each design, structural analysis is performed for:

- Maintaining the NACA 6510 profile,
- Morphing from NACA 6510 to NACA 3510 profile,
- Morphing from NACA 6510 to NACA 2510 profile.

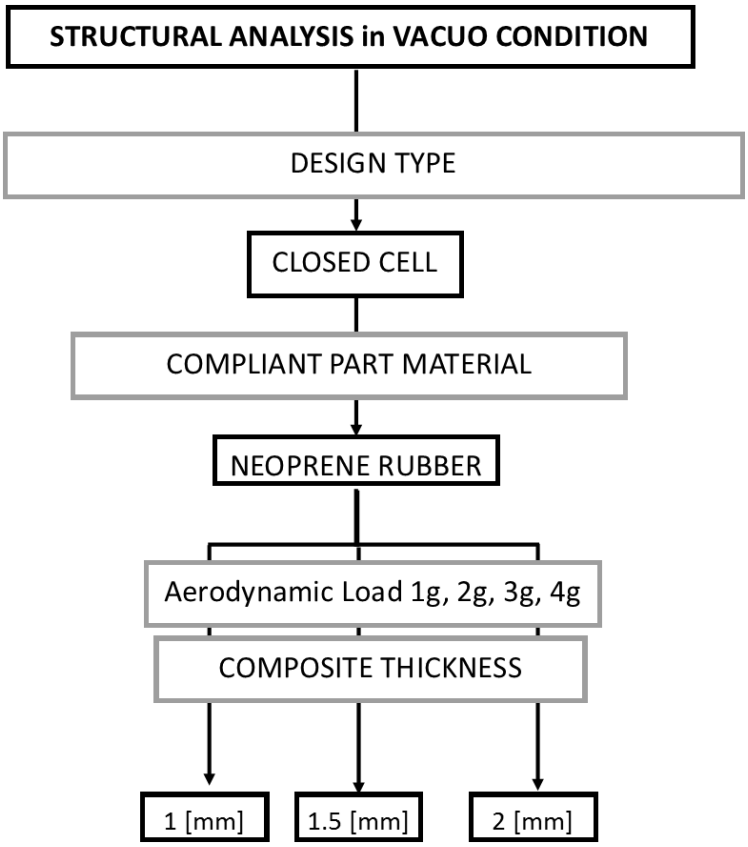

Figure 66. Static Structural Analyses Performed for Hybrid Trailing Edge Control Surface under Aerodynamic Loads

6.2 Finite Element Analysis of Closed Cell Hybrid Trailing Edge Control Surface with Neoprene Rubber Design

In this part, analysis results of Closed Cell – Neoprene Rubber design with 2.0 [mm], 1.5 [mm] and 1.0 [mm] composite thickness analyses are presented. Analyses include displacement from NACA 6510 to NACA 2510, NACA 6510 to NACA 3510 and maintaining the NACA 6510 profiles under aerodynamic loads described in CHAPTER 5. Analyses are performed in two steps. In the first step, there is no pressure acting on the system. Rotations described in Chapter 4.6.1 are given to the servo actuators. Therefore, hybrid trailing edge control surface is morphed or maintained the desired NACA profiles in-vacuo condition. In the second step, aerodynamic load is applied to the deformed control surface and rotations of servo

actuators are adjusted in order to achieve the desired NACA profiles under aerodynamic loads. Since aerodynamic load applied to the control surface is in upward direction, it helps servo actuators while deforming the control surface.

6.2.1 Composite Thicknesses of 2.0 [mm] Design

Rotations of servo moment arms under aerodynamic loads in order to deform or maintain the each NACA profile are given in Table 22 for Closed Cell – Neoprene Rubber design with 2.0 [mm] composite thickness design.

Resultant displacement in z-axis, maximum beam combined stress and equivalent elastic strain (von-Mises) results for Closed Cell – Neoprene design with 2.0 [mm] composite thicknesses are given in Table 23. Figures of the results given can be obtained from Appendix B1 between the Figure 159 and Figure 194. It is seen that maximum beam combined stress values for moment arm and push rod are below the tensile yield strength of 280 [MPa] of Aluminium material. In addition, there exist bump at the compliant part for morping to NACA 2510 profile under 3g and 4g aerodynamic loading as seen from Figure 189 and Figure 192. Therefore, 3g and 4g aerodynamic loading is not operational because control surface is not smooth anymore and hence flow separates. As a result, aerodynamic efficiency decreases which is not a desired.

For the Closed Cell-Neoprene Rubber Design with 2.0 [mm] composite thickness, reaction torques for different morphing/maintaining NACA profiles under aerodynamic loading is given in Table 24. Selected servo actuators are capable of supporting this torques. It is seen from the results that up to 2g aerodynamic loading torque of servo actuators decrease. After that reaction torques increase for 3g and 4g aerodynamic loading. This is because of the magnitude of aerodynamic load. 3g and 4g aerodynamic loading is so high that servo actuators resist instead of creating torque.

Table 22: Rotations of the Servo Moment Arms to Obtain the Desired NACA Profiles under Aerodynamic Loads (Closed Cell-Neoprene Rubber Design with 2.0 [mm] composite thickness)

Aerodynamic Load	Morphing/Maintaining NACA Profile	y-Axis Rotation of Moment Arm Actuating the Upper Part [deg]	y-Axis Rotation of Moment Arm Actuating the Lower Part [deg]
1g	NACA 6510	1.0	-1.2
	NACA 3510	12.0	-22.8
	NACA 2510	12.0	-26.2
2g	NACA 6510	1.0	-1.0
	NACA 3510	12.0	-22.5
	NACA 2510	12.0	-25.8
3g	NACA 6510	1.0	-1.0
	NACA 3510	12.0	-22.3
	NACA 2510	12.0	-25.3
4g	NACA 6510	1.0	-0.8
	NACA 3510	12.0	-21.7
	NACA 2510	12.0	-24.9

Table 23: Analysis Results to Obtain the Desired NACA Profiles under Aerodynamic Loads (Closed Cell-Neoprene Rubber Design with 2.0 [mm] composite thickness)

Aerodynamic Load	Morphing/Maintaining NACA Profile	Maximum Displacement in z Direction [mm]	Maximum Beam Combined Stress [MPa]	Maximum Equivalent Elastic Strain (von-Mises) [mm/mm]
1g	NACA 6510	0.01	26.34	0.01
	NACA 3510	15.18	69.27	0.26
	NACA 2510	20.21	93.49	0.30
2g	NACA 6510	0.12	4.54	0.01
	NACA 3510	15.17	99.76	0.26
	NACA 2510	20.21	134.45	0.30
3g	NACA 6510	0.25	23.47	0.02
	NACA 3510	15.23	130.06	0.26
	NACA 2510	20.21	162.27	0.31
4g	NACA 6510	0.41	51.20	0.02
	NACA 3510	15.16	186.81	0.26
	NACA 2510	20.24	200.78	0.31

Table 24: Reaction Torques of Servo Actuators to Obtain the Desired NACA Profiles under Aerodynamic Load (Closed Cell-Neoprene Rubber Design with 2.0 [mm] composite thickness)

Aerodynamic Load	Morphing/Maintaining NACA Profile	Reaction Torque for the Servos Actuating Upper Side of Transmission Part [Nmm]	Reaction Torque for the Servos Actuating Lower Side of Transmission Part [Nmm]
1g	NACA 6510	151	111
	NACA 3510	151	181
	NACA 2510	139	178
2g	NACA 6510	76	58
	NACA 3510	43	103
	NACA 2510	7	75
3g	NACA 6510	13	13
	NACA 3510	65	26
	NACA 2510	146	26
4g	NACA 6510	75	57
	NACA 3510	228	87
	NACA 2510	288	128

6.2.2 Composite Thicknesses of 1.5 [mm] Design

Rotations of servo moment arms under aerodynamic loads in order to deform or maintain the each NACA profile are given in Table 25 for Closed Cell – Neoprene Rubber design with 1.5 [mm] composite thickness design.

Resultant displacement in z-axis, maximum beam combined stress and equivalent elastic strain (von-Mises) results for Closed Cell – Neoprene design with 1.5 [mm] composite thicknesses are given in Table 26. Figures of the results given can be obtained from Appendix B2 between the Figure 195 and Figure 230. It is seen that maximum beam combined stress values for moment arm and push rod are below the tensile yield strength of 280 [MPa] of Aluminium material. In addition, there exist bump at the compliant part for morphing to NACA 2510 profile under 3g and 4g aerodynamic loading as seen from Figure 225 and Figure 228. Therefore, 3g and 4g aerodynamic loading is not operational because control surface is not smooth anymore and flow separates and as a result, aerodynamic efficiency decreases which is not a desired phenomenon.

For the Closed Cell-Neoprene Rubber Design with 1.5 [mm] composite thickness, reaction torques for different morphing/maintaining NACA profiles under aerodynamic loading is given in Table 27. Selected servo actuators are capable of supporting this torques. It is seen from the results that up to 2g aerodynamic loading torque of servo actuators decrease. After that reaction torques increase for 3g and 4g aerodynamic loading. This is because of the magnitude of aerodynamic load. 3g and 4g aerodynamic loading is so high that servo actuators resist instead of creating torque.

Table 25: Rotations of the Servo Moment Arms to Obtain the Desired NACA Profiles under Aerodynamic Loads (Closed Cell-Neoprene Rubber Design with 1.5 [mm] composite thickness)

Aerodynamic Load	Morphing/Maintaining NACA Profile	y-Axis Rotation of Moment Arm Actuating the Upper Part [deg]	y-Axis Rotation of Moment Arm Actuating the Lower Part [deg]
1g	NACA 6510	1.0	-1.1
	NACA 3510	12.0	-22.8
	NACA 2510	12.0	-26.2
2g	NACA 6510	1.0	-1.0
	NACA 3510	12.0	-22.5
	NACA 2510	12.0	-25.6
3g	NACA 6510	1.0	-0.9
	NACA 3510	12.0	-22.0
	NACA 2510	12.0	-24.8
4g	NACA 6510	1.0	-0.5
	NACA 3510	12.0	-21.6
	NACA 2510	12.0	-24.0

Table 26: Analysis Results to Obtain the Desired NACA Profiles under Aerodynamic Loads (Closed Cell-Neoprene Rubber Design with 1.5 [mm] composite thickness)

Aerodynamic Load	Morphing/Maintaining NACA Profile	Maximum Displacement in z Direction [mm]	Maximum Beam Combined Stress [MPa]	Maximum Equivalent Elastic Strain (von-Mises) [mm/mm]
1g	NACA 6510	0.01	13.49	0.01
	NACA 3510	15.17	71.79	0.26
	NACA 2510	20.23	94.96	0.30
2g	NACA 6510	0.16	14.42	0.01
	NACA 3510	15.28	105.48	0.26
	NACA 2510	20.20	135.96	0.30
3g	NACA 6510	0.30	33.74	0.02
	NACA 3510	15.24	132.85	0.26
	NACA 2510	20.27	155.49	0.31
4g	NACA 6510	0.48	62.02	0.03
	NACA 3510	15.26	162.83	0.26
	NACA 2510	20.18	192.51	0.31

Table 27: Reaction Torques of Servo Actuators to Obtain the Desired NACA Profiles under Aerodynamic Load (Closed Cell-Neoprene Rubber Design with 1.5 [mm] composite thickness)

Aerodynamic Load	Morphing/Maintaining NACA Profile	Reaction Torque for the Servos Actuating Upper Side of Transmission Part [Nmm]	Reaction Torque for the Servos Actuating Lower Side of Transmission Part [Nmm]
1g	NACA 6510	93	69
	NACA 3510	93	137
	NACA 2510	82	133
2g	NACA 6510	19	17
	NACA 3510	69	105
	NACA 2510	63	31
3g	NACA 6510	44	31
	NACA 3510	122	17
	NACA 2510	200	69
4g	NACA 6510	135	95
	NACA 3510	229	94
	NACA 2510	342	173

6.2.3 Composite Thicknesses of 1.0 [mm] Design

Rotations of servo moment arms under aerodynamic loads in order to deform or maintain the each NACA profile are given in Table 28 for Closed Cell – Neoprene Rubber design with 1.0 [mm] composite thickness design.

Resultant displacement in z-axis, maximum beam combined stress and equivalent elastic strain (von-Mises) results for Closed Cell – Neoprene design with 1.0 [mm] composite thicknesses are given in Table 29. Figures of the results given can be obtained from Appendix B3 between the Figure 231 and Figure 266. It is seen that maximum beam combined stress values for moment arm and push rod are below the tensile yield strength of 280 [MPa] of Aluminium material. In addition, there exist bump at the compliant part for morphing to NACA 2510/3510 profile under 3g and morphing to NACA 2510 profile under 4g aerodynamic loading as seen from Figure 252, Figure 261 and Figure 264. Therefore, 3g and 4g aerodynamic loading is not operational because control surface is not smooth anymore and flow separates which results in decrease in aerodynamic efficiency.

For the Closed Cell-Neoprene Rubber Design with 1.0 [mm] composite thickness, reaction torques for different morphing/maintaining NACA profiles under aerodynamic loading is given in Table 30. Selected servo actuators are capable of supporting this torques. It is seen from the results that for 2g and higher aerodynamic loading torque of servo actuators increase. This is because of the magnitude of aerodynamic load. 2g, 3g and 4g aerodynamic loading is so high that servo actuators again resist instead of creating required torque.

Table 28: Rotations of the Servo Moment Arms to Obtain the Desired NACA Profiles under Aerodynamic Loads (Closed Cell-Neoprene Rubber Design with 1.0 [mm] composite thickness)

Aerodynamic Load	Morphing/Maintaining NACA Profile	y-Axis Rotation of Moment Arm Actuating the Upper Part [deg]	y-Axis Rotation of Moment Arm Actuating the Lower Part [deg]
1g	NACA 6510	1.0	-1.1
	NACA 3510	12.0	-22.9
	NACA 2510	12.0	-26.2
2g	NACA 6510	1.0	-0.7
	NACA 3510	12.0	-21.9
	NACA 2510	12.0	-24.9
3g	NACA 6510	1.0	-0.2
	NACA 3510	12.0	-21.1
	NACA 2510	12.0	-22.8
4g	NACA 6510	1.0	0.0
	NACA 3510	12.0	-19.2
	NACA 2510	12.0	-21.1

Table 29: Analysis Results to Obtain the Desired NACA Profiles under Aerodynamic Loads (Closed Cell-Neoprene Rubber Design with 1.0 [mm] composite thickness)

Aerodynamic Load	Morphing/Maintaining NACA Profile	Maximum Displacement in z Direction [mm]	Maximum Beam Combined Stress [MPa]	Maximum Equivalent Elastic Strain (von-Mises) [mm/mm]
1g	NACA 6510	0.03	2.1	0.01
	NACA 3510	15.20	62.25	0.26
	NACA 2510	20.29	82.24	0.30
2g	NACA 6510	0.24	25.19	0.01
	NACA 3510	15.11	92.99	0.26
	NACA 2510	20.17	123.56	0.30
3g	NACA 6510	0.41	45.55	0.02
	NACA 3510	15.26	123.91	0.25
	NACA 2510	20.26	129.70	0.31
4g	NACA 6510	0.85	72.63	0.03
	NACA 3510	15.21	122.24	0.26
	NACA 2510	20.19	162.52	0.31

Table 30: Reaction Torques of Servo Actuators to Obtain the Desired NACA Profiles under Aerodynamic Load (Closed Cell-Neoprene Rubber Design with 1.0 [mm] composite thickness)

Aerodynamic Load	Morphing/Maintaining NACA Profile	Reaction Torque for the Servos Actuating Upper Side of Transmission Part [Nmm]	Reaction Torque for the Servos Actuating Lower Side of Transmission Part [Nmm]
1g	NACA 6510	36	28
	NACA 3510	37	93
	NACA 2510	26	88
2g	NACA 6510	36	24
	NACA 3510	70	17
	NACA 2510	117	13
3g	NACA 6510	100	70
	NACA 3510	175	60
	NACA 2510	250	116
4g	NACA 6510	186	130
	NACA 3510	271	137
	NACA 2510	389	220

6.3 Discussion and Conclusion

In this chapter, Closed Cell – Neoprene rubber design with different composite thicknesses are structurally analyzed under aerodynamic loads in order to perform the desired morphing capabilities.

As given in Table 21, aerodynamic pressure distributions apply a force to the control surface in upward/decamber direction. As a result, torque values of the servo actuators decrease. However, results of analyses showed that for higher aerodynamic loads servo actuators are resisting aerodynamic loads to maintain the desired NACA profiles. For 2.0 [mm] and 1.5 [mm] composite thickness, 1g and 2g aerodynamic load helps servo actuators to decamber but 3g and 4g aerodynamic load requires servo actuator resistance in order to morph into desired NACA profiles. For 1.0 [mm] composite thickness, servo actuators are resisting to keep the control surface in the desired NACA profiles under aerodynamic loads higher than 1g. Summary of the servo actuator torques are given in Figure 67 and Figure 68.

It could be concluded from the results of the analyses that Closed Cell – Neoprene rubber design with 2.0 [mm], 1.5 [mm] and 1.0 [mm] composite thicknesses are capable of performing all the missions even if under higher aerodynamic loads up to 4g. However, 3g and 4g aerodynamic loads create bump at the compliant part. This is not a desired phenomenon because control surface is not smooth anymore and as a result, aerodynamic efficiency decreases. Strain and trailing edge tip displacement for the analyses under aerodynamic loads is given in Figure 69 and Figure 70. It is seen that 15.2 [mm] and 20.2 [mm] tip displacement while morphing to NACA 3510 and NACA 2510 is successfully achieved. Also, stress values of push rod and moment arm are below the yield strength of Aluminum as shown in Figure 71.

Considering the weight of the control surface, 1 [mm] composite thickness design is 0.268 [kg] and 0.536 [kg] lighter than 1.5 [mm] and 2.0 [mm] composite thickness designs respectively. As a result, Closed Cell – Neoprene rubber design with 1.0 [mm] composite thickness turns out to be the best design.

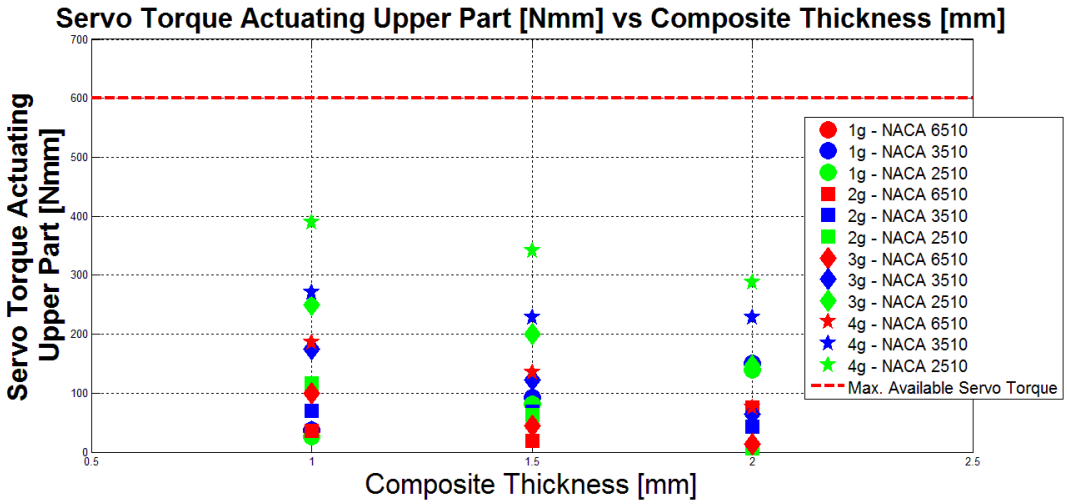

Figure 67: Servo Torque Actuating Upper Part for Closed Cell-Neoprene Design under Aerodynamic Loads

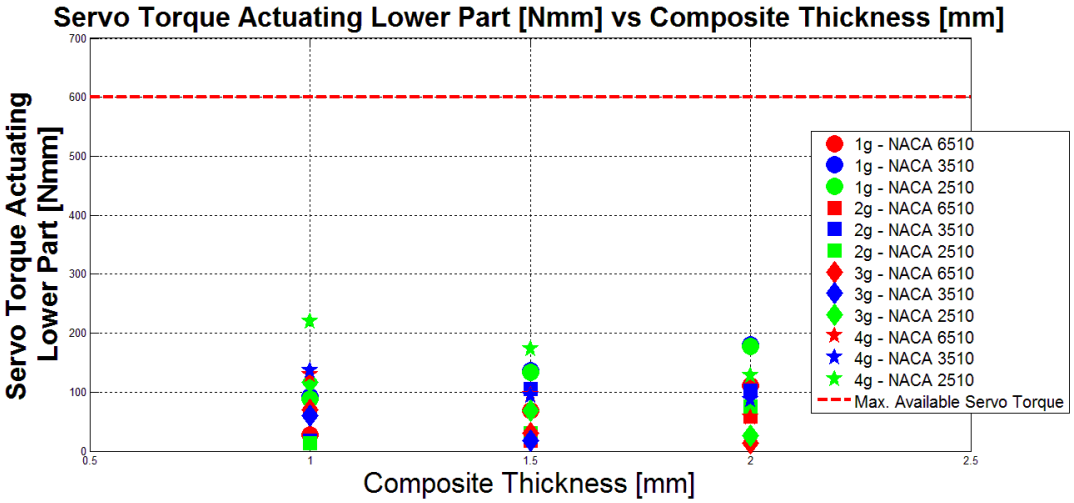

Figure 68: Servo Torque Actuating Lower Part for Closed Cell-Neoprene Design under Aerodynamic Loads

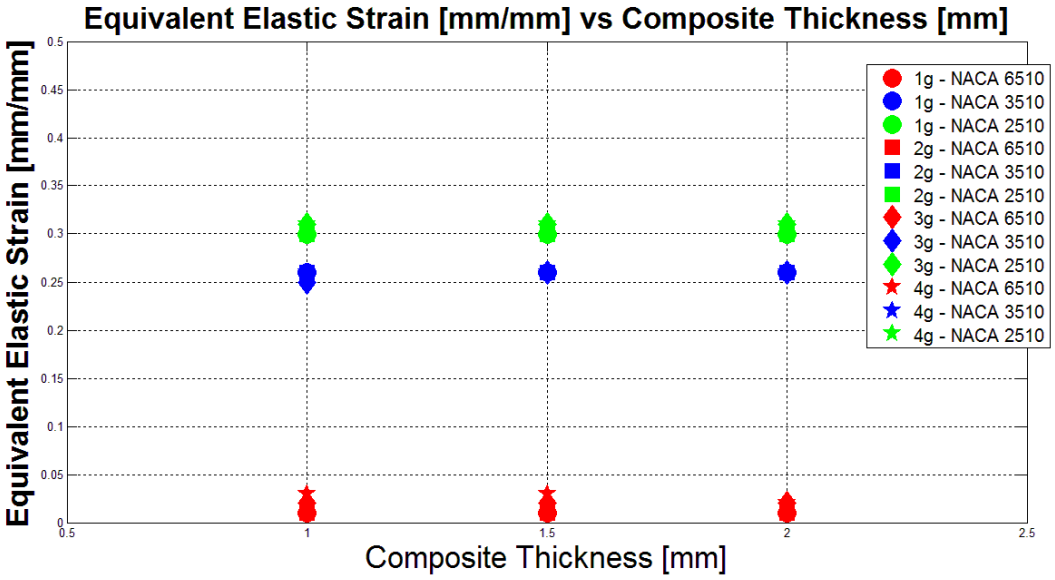

Figure 69: Equivalent Elastic Strain (von-Mises) of Control Surface for Closed Cell-Neoprene Design under Aerodynamic Loads

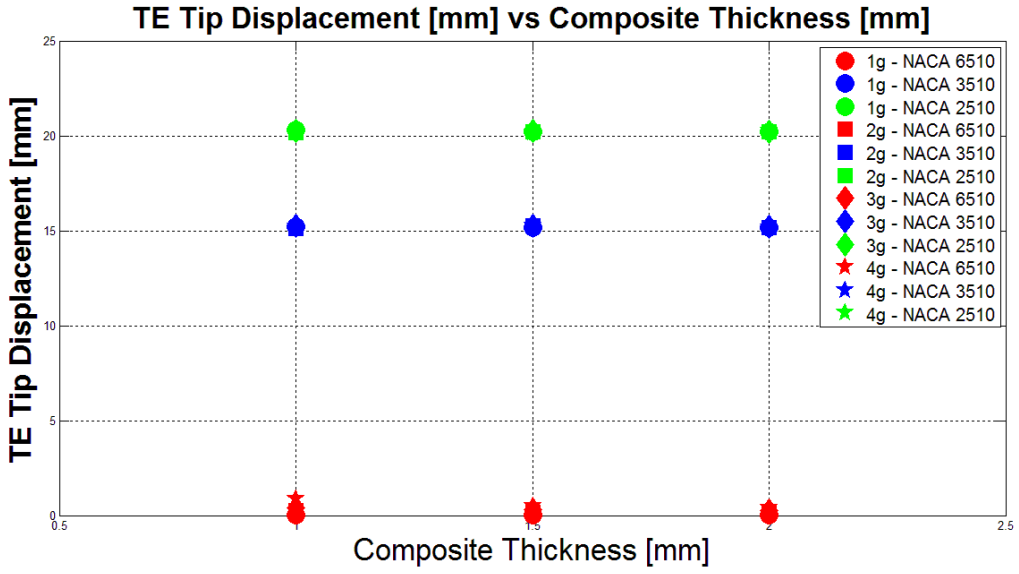

Figure 70: Trailing Edge Tip Displacement of Control Surface for Closed Cell-Neoprene Design under Aerodynamic Loads

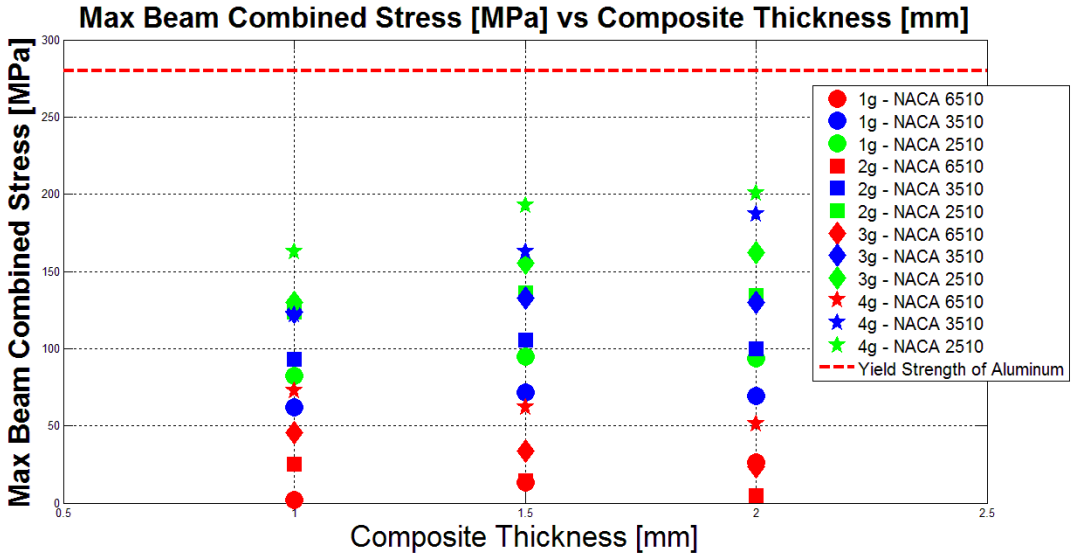

Figure 71: Max Beam Combined Stresses of Push Rod/Moment Arm for Closed Cell-Neoprene Design under Aerodynamic Loads

CHAPTER 7

CONCLUSION

7.1 General Conclusions

This thesis study aims to present the design and structural analysis of hingeless, unconventional hybrid trailing edge control surface of a fully morphing unmanned aerial vehicle wing. Control surface was designed with CATIA V5-6R2012 software and analyzed with ANSYS Static Structural software.

The first part of the thesis was dedicated to the design and analysis of the hybrid trailing edge control surface in-vacuo condition. Neoprene and silicone material for compliant part, Open and Closed Cell designs for composite part, thickness of composite part variations were investigated. It was shown that as composite structure gets thicker, torque of servo actuators increased due to earth gravity. In addition, heavier design created more stress on the moment arm and push rod beams. Also, it was shown that Open Cell design was not able to perform desired morphing missions for 1 [mm] composite thickness because it was not rigid/stiff enough to transmit the rotation of moment arm to the control surface. Open Cell with silicone design was not capable of morphing to NACA 2510 because the maximum combined stress on the push rod and moment arm part is higher than the tensile yield strength of Aluminum which is 280 [MPa]. It was seen from the results that closed cell design is much stiffer than the open cell design because it performed desired morphing motions for 1 [mm] composite thickness design. However, Closed Cell with silicone material exceeded the torque limits of the selected servo actuators. Therefore, structural analysis under aerodynamic loads only performed for Closed Cell design with Neoprene rubber material.

The second part of the thesis focused on the aerodynamic loads on the control surface. CFD analyses of morphed wings were performed. It was shown that the pressure distribution over the wing for loiter mission is similar for 1g, 2g, 3g and 4g aerodynamic loading. In addition, total lifting force increased linearly with increasing aerodynamic load. Therefore, it was assumed that cruise/high speed dash and takeoff 2g, 3g and 4g aerodynamic loads can be obtained by scaling the 1g pressure distribution with the corresponding dynamic pressure. After that, aerodynamic loads on the control surface were obtained by interpolation method. Pressure distribution over the wing was interpolated to the Finite Element Model of control surface. Total lifting force over the wing and control surface was calculated with in-house developed code for each morphing missions.

In the third part of the thesis, control surface was structurally analyzed under the aerodynamic loads due to morphing missions. 1g, 2g, 3g and 4g aerodynamic loads were applied to the control surface. It was shown in Table 21 that resultant aerodynamic loads on the control surface are in upward/decamber direction. Therefore, torque values of the servo actuators decreased. Results of analyses also showed that for higher aerodynamic loads servo actuators are resisting aerodynamic loads to maintain the desired NACA profiles. It was shown that control surface is capable of performing all the morphing missions for all aerodynamic loads. However, 3g and 4g aerodynamic loads created bump at the compliant part which is not desired. Considering the weight of the control surface, Closed Cell – Neoprene rubber design with 1.0 [mm] composite thickness was selected as the best design. 1 [mm] composite thickness design saved 0.268 [kg] and 0.536 [kg] for 1.5 [mm] and 2.0 [mm] composite thickness designs respectively for one wing.

7.2 Recommendations for Further Studies

Different type, thicknesses, lengths of compliant material can be studied in order to reduce the servo actuator torques.

C part can be redesigned with different materials and different thicknesses considering the servo actuator connections.

Composite material properties can be varied and the effects of this change can be investigated.

By setting the thickness of the transmission part at a particular value which is stiff enough to carry the pushrod /moment arm load, parametric structural analyses regarding the thickness change in the composite part can be performed.

Angle of attack change can be considered for the 2g, 3g and 4g aerodynamic loads instead of just increasing the flight velocity.

Fatigue analysis for the compliant and transmission part can be performed.

Aeroelastic characteristic of the control surface can be conducted.

Shape memory alloys can be used in the control surface design.

REFERENCES

[1] M. T. Kikuta, “Mechanical Properties of Candidate Materials for Morphing Wings,” Virginia Polythenic Institute and State University, 2003.

[2] D. Gimesy, “Wandering Albatross.” [Online]. Available: http://yourshot.nationalgeographic.com/photos/5542388/?source=gallery. [Accessed: 05-Feb-2017].

[3] “ANKA.” [Online]. Available: https://www.tai.com.tr/tr/proje/anka. [Accessed: 05-Feb-2017].

[4] R. Ettlinger, “Peregrine Falcon.” [Online]. Available: http://www.richardettlinger.com/. [Accessed: 05-Feb-2017].

[5] “F-22 Raptor.” [Online]. Available: http://lockheedmartin.com/us/products/f22.html. [Accessed: 05-Feb-2017].

[6] W. Akl, S. Poh, and a. Baz, “Wireless and distributed sensing of the shape of morphing structures,” *Sensors Actuators, A Phys.*, vol. 140, no. 1, pp. 94–102, 2007.

[7] S. Barbarino, O. Bilgen, R. M. Ajaj, M. I. Friswell, and D. J. Inman, “A Review of Morphing Aircraft,” *J. Intell. Mater. Syst. Struct.*, vol. 22, no. 9, pp. 823–877, 2011.

[8] C. Thill, J. Etches, I. Bond, K. Potter, and P. Weaver, “Morphing skins,” *Aeronaut. J.*, vol. 112, no. 1129, pp. 117–139, 2008.

[9] B. D. Roth and W. a Crossley, “Application of Optimization Techniques in the Conceptual Design of Morphing Aircraft,” *Am. Inst. Aeronaut. Astronaut.*, no. November, pp. 1–11, 2003.

[10] L. Ünlüsoy, “Structural Design and Analysis of the Mission Adaptive Wings of an Unmanned Aerial Vehicle,” Middle East Technical University, 2010.

[11] M. Abdulrahim, H. Garcia, G. F. Ivey, and R. Lind, “Flight Testing A Micro Air Vehicle Using Morphing For Aeroservoelastic Control,” *J. Aircr.*, vol. 42, N^{o} 1, no. January-February, pp. 1–17, 2005.

[12] J. D. Anderson, *Introduction to Flight*, 4th ed. New York: McGraw Hill Book Company, 2000.

[13] B. W. McCormic, *Aeronautics and Flight Mechanics*, 2nd ed. New York, 1995.

[14] T. Weisshaar, “Morphing aircraft technology-new shapes for aircraft design,” *Multifunct. Struct. / Integr. Sensors Antennas*, pp. O1-1 – O1-20, 2006.

[15] S. E. Gano and J. E. Renaud, “Optimized Unmanned Aerial Vehicle with Wing Morphing for Extended Range and Endurance,” *AIAA*, vol. 9, 2002.

[16] Y. Yaman, S. Özgen, M. Şahin, G. Seber, E. Sakarya, L. Ünlüsoy, and E. T. İnsuyu, "Aeroservoelastic Analysis of the Effects of Camber and Twist on Tactical UAV Mission-adaptive Wings," 2011. [Online]. Available: http://ae.metu.edu.tr/~yyaman/. [Accessed: 20-May-2015].

[17] "CHANGE FP7 Project." [Online]. Available: http://change.tekever.com/. [Accessed: 25-May-2015].

[18] P. Arslan, U. Kalkan, H. Tıraş, İ. O. Tunçöz, E. Gürses, Ş. Melin, S. Özgen, Y. Yaman, and İ. O. Tunçöz, "Structural Analysis of an Unconventional Hybrid Control Surface of a Morphing Wing," in *ICAST 2014: 25nd International Conference on Adaptive Structures and Technologies*, 2014, pp. 1–12.

[19] P. Arslan, U. Kalkan, H. Tıraş, İ. O. Tunçöz, Y. Yang, E. Gürses, M. Şahin, S. Özgen, and Y. Yaman, "A Hybrid Trailing Edge Control Surface Concept," in *Design, Modelling and Experiments of Advanced Structures and Systems*, 2014.

[20] P. Arslan, U. Kalkan, Y. Yang, S. Özgen, M. Şahin, E. Gürses, and Y. Yaman, "Büyük Oranda Şekil Değiştirebilen Kanat Yüzeylerinin Aerodinamik Yükler Altındaki Davranışları," in *II. Ulusal Havacılık Teknolojisi ve Uygulamaları Kongresi*, 2013.

[21] P. Arslan, U. Kalkan, H. Tıraş, İ. O. Tunçöz, Y. Yang, E. Gürses, M. Şahin, S. Özgen, and Y. Yaman, "Bir İnsansız Hava Aracının Konvansiyonel Olmayan Esnek Kontrol Yüzeylerinin Yapısal Analizi ve İç Yapısının Tasarımı," in *3. Ulusal Havacılıkta İleri Teknolojiler Konferansı*, 2014.

[22] P. Arslan, U. Kalkan, H. Tıraş, İ. O. Tunçöz, Y. Yang, E. Gürses, M. Şahin, S. Özgen, and Y. Yaman, "Konvansiyonel ve Konvansiyonel Olmayan Kontrol Yüzeylerine Sahip İnsansız Hava Aracı Kanatlarının Ağırlıklarının İncelenmesi," in *Savunma Teknolojileri Kongresi*, 2014, pp. 90–97.

[23] P. Arslan, U. Kalkan, H. Tıraş, İ. O. Tunçöz, Y. Yang, E. Gürses, M. Şahin, S. Özgen, and Y. Yaman, "Konvansiyonel Olmayan İki Farklı Kontrol Yüzeyinin Yapısal Özelliklerinin Değerlendirilmesi ve Karşılaştırılması," in *V. Ulusal Havacılık ve Uzay Konferansı*, 2014.

[24] P. Arslan, U. Kalkan, H. Tıraş, İ. O. Tunçöz, Y. Yang, E. Gürses, M. Şahin, S. Özgen, and Y. Yaman, "Bir Hibrit Firar Kenarı Kontrol Yüzeyinin Tasarımı ve Analizi," in *TMMOB Makina Mühendisleri Odası VIII. Ulusal Uçak, Havacılık ve Uzay Mühendisliği Kurultayı*, 2015.

[25] P. Arslan, U. Kalkan, H. Tıraş, İ. O. Tunçöz, Y. Yang, S. Özgen, E. Gürses, M. Şahin, and Y. Yaman, "Hibrit Bir Kontrol Yüzeyinin Hesaplamalı Akışkanlar Dinamiği Destekli Yapısal Analizi," in *Uluslararası Katılımlı 17. Makina Teorisi Sempozyumu*, 2015.

[26] D. S. Körpe, "Aerodynamic Modelling and Optimization of Morphing Wings," Middle East Technical University, 2014.

[27] L. Unlusoy, “Effects of Morphing Aeroelastic Behaviour of Unmanned Aerial Vehicle,” Middle East Technical University, 2014.

[28] T. Oktay, M. Konar, M. A. Mohamed, M. Aydin, F. Sal, M. Onay, and SoylakM., “Autonomous Flight Performance Improvement of Load-Carrying Unmanned Aerial Vehicles by Active Morphing,” *Int. J. Mech. Aerospace, Ind. Mechatron. Manuf. Eng.*, vol. 10, no. 1, pp. 123–132, 2016.

[29] “Invent.” [Online]. Available: http://www.invent-gmbh.de/. [Accessed: 13-Mar-2016].

[30] “ANSYS Workbench v14.0 Material Library.” .

[31] “Volz-Servos.” [Online]. Available: http://www.volz-servos.com/English/13mmClass/. [Accessed: 13-Mar-2016].

[32] “Cambridge University Engineering Department Materials Data Book.” [Online]. Available: http://www-mdp.eng.cam.ac.uk/web/library/enginfo/cueddatabooks/materials.pdf. [Accessed: 13-Mar-2016].

[33] E. Gu rses, I. O. Tunco z, Y. Yang, P. Arslan, U. Kalkan, H. T ras, M. Sahin, S. O zgen, and Y. Yaman, “Structural and aerodynamic analyses of a hybrid trailing edge control surface of a fully morphing wing,” *J. Intell. Mater. Syst. Struct.*, p. 1045389X16641200-, 2016.

[34] “ANSYS Workbench v14.0 Help.” .

[35] O. Tunçöz, “Design and Analysis of a Hybrid Trailing Edge Control Surface of a Fully Morphing Unmanned Aerial Vehicle Wing,” Middle East Technical University, 2015.

[36] Y. Yaman, İ. O. Tunçöz, Y. Yang, P. Arslan, U. Kalkan, H. Tıraş, E. Gürses, M. Şahin, and S. Özgen, “Decamber Morphing Concept by Using a Hybrid Trailing Edge Control Surface,” *Aerospace*, vol. 2, pp. 482–504, 2015.

[37] “Tecplot 360 2013 R1 User Manual.” 2013.

APPENDICES

APPENDIX A1

Open Cell – Neoprene Rubber Design Results

In this part, in-vacuo condition Open Cell – Neoprene Rubber design results of the analysis are presented.

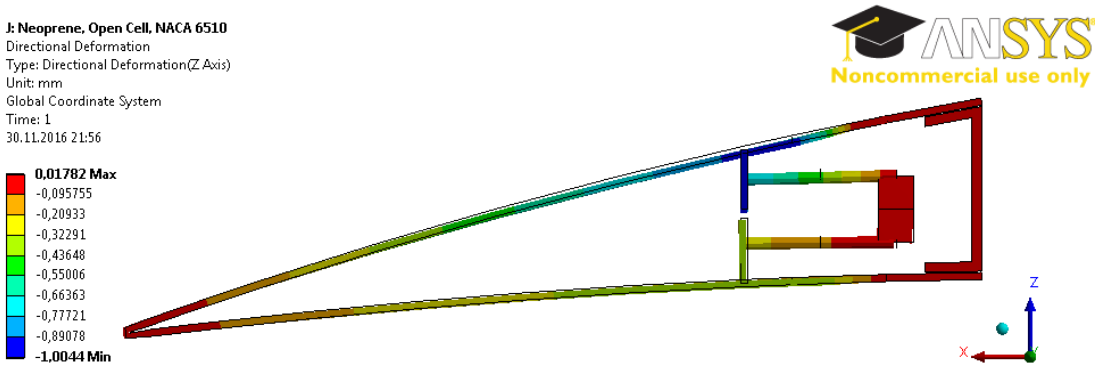

Figure 72: Displacement in z Direction Contour - Maintaining the NACA 6510 Profile (Max 0.02 [mm], Open Cell-Neoprene Rubber Design with 1.5 [mm] composite thickness)

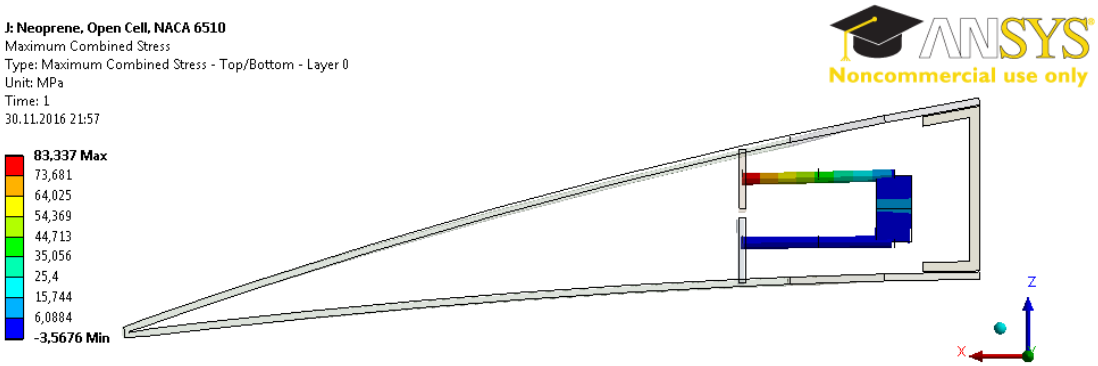

Figure 73: Maximum Beam Combined Stress Contour - Maintaining the NACA 6510 Profile (Max 83.34 [MPa], Open Cell-Neoprene Rubber Design with 1.5 [mm] composite thickness)

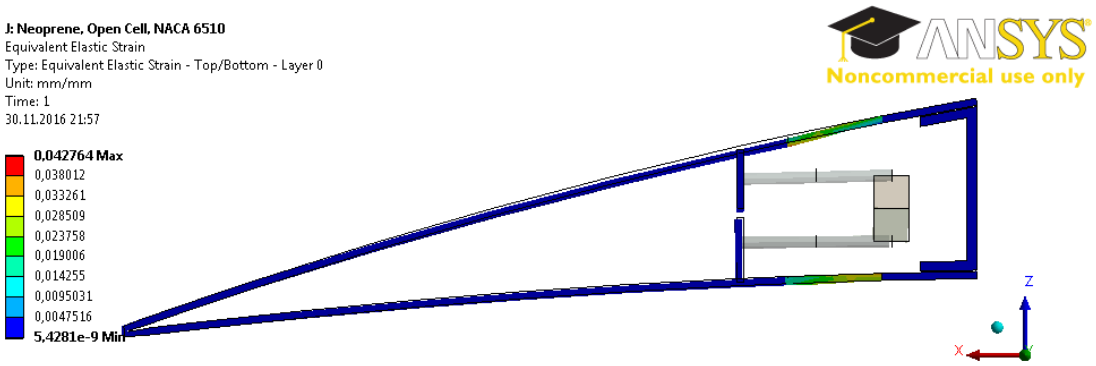

Figure 74: Equivalent Elastic Strain (von-Mises) Contour - Maintaining the NACA 6510 Profile (Max 0.04 [mm/mm], Open Cell-Neoprene Rubber Design with 1.5 [mm] composite thickness)

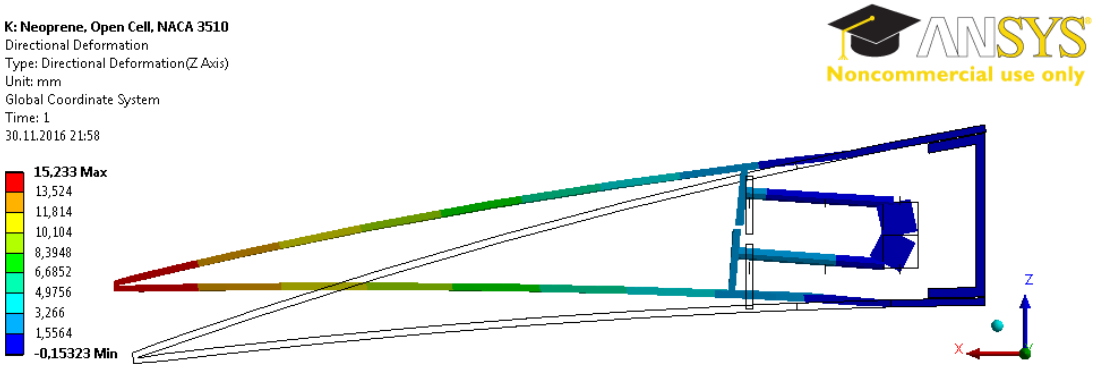

Figure 75: Displacement in z Direction Contour - Morphing from NACA 6510 to NACA 3510 Profile (Max 15.23 [mm], Open Cell-Neoprene Rubber Design with 1.5 [mm] composite thickness)

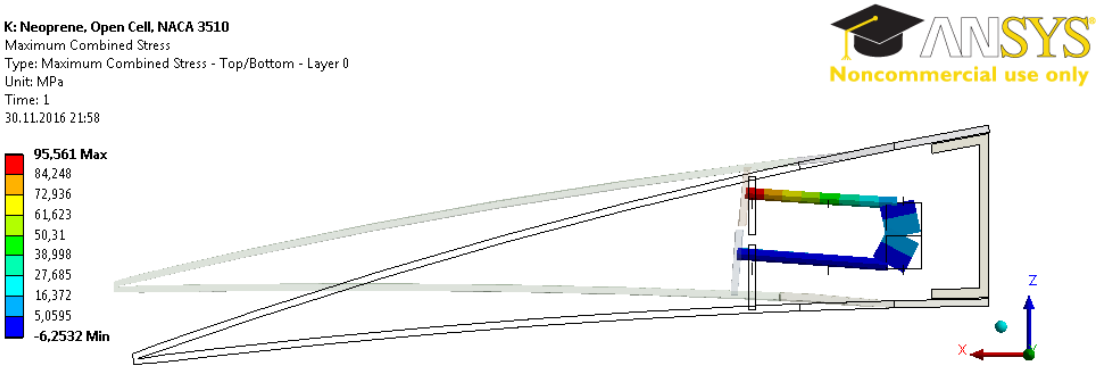

Figure 76: Maximum Beam Combined Stress Contour - Morphing from NACA 6510 to NACA 3510 Profile (Max 95.56 [MPa], Open Cell-Neoprene Rubber Design with 1.5 [mm] composite thickness)

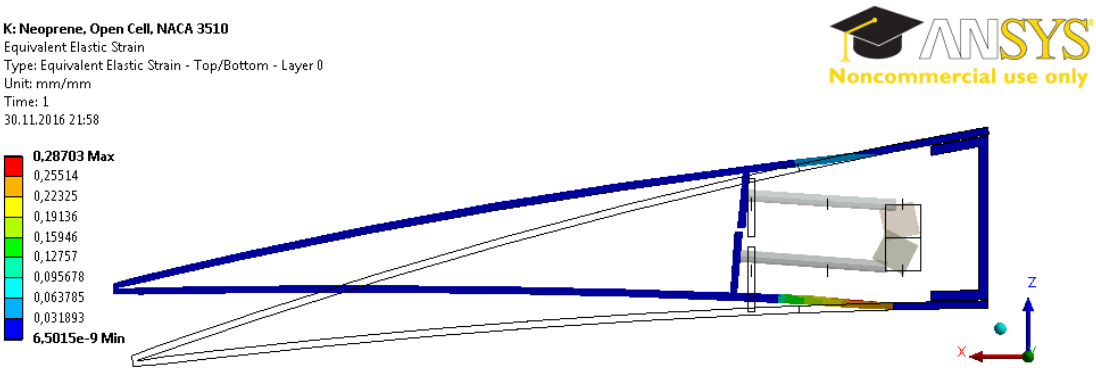

Figure 77: Equivalent Elastic Strain (von-Mises) Contour - Morphing from NACA 6510 to NACA 3510 Profile (Max 0.29 [mm/mm], Open Cell-Neoprene Rubber Design with 1.5 [mm] composite thickness)

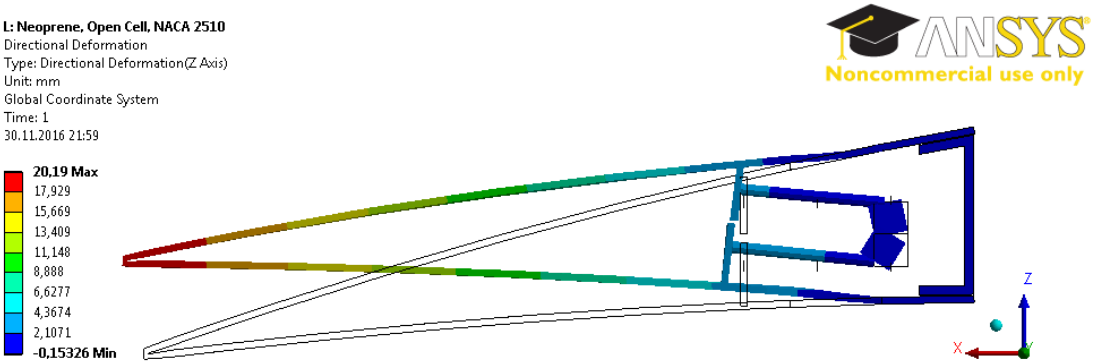

Figure 78: Displacement in z Direction Contour - Morphing from NACA 6510 to NACA 2510 Profile (Max 20.19 [mm], Open Cell-Neoprene Rubber Design with 1.5 [mm] composite thickness)

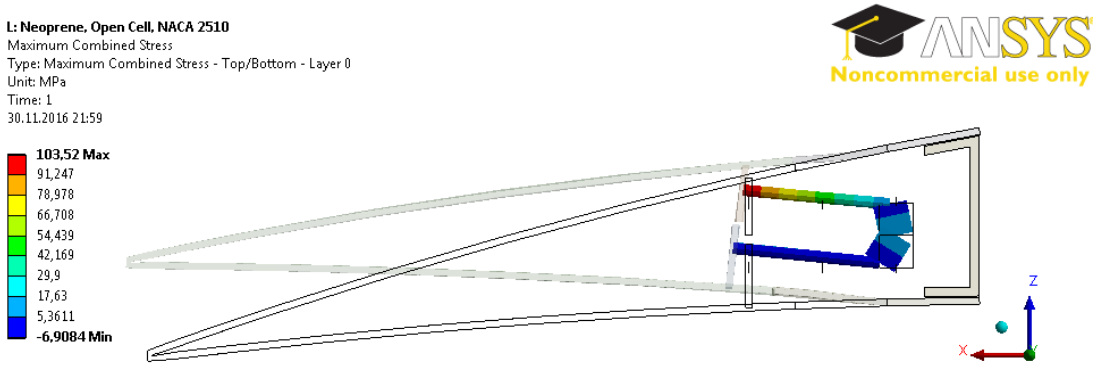

Figure 79: Maximum Beam Combined Stress Contour - Morphing from NACA 6510 to NACA 2510 Profile (Max 103.52 [MPa], Open Cell-Neoprene Rubber Design with 1.5 [mm] composite thickness)

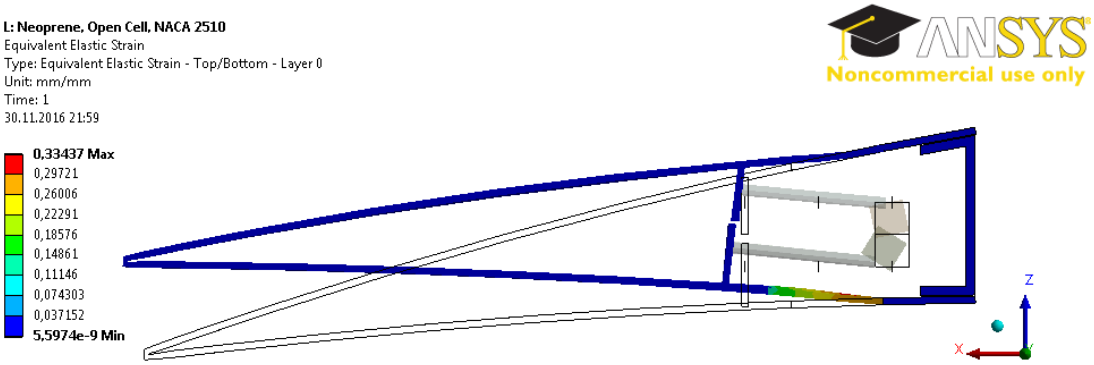

Figure 80: Equivalent Elastic Strain (von-Mises) Contour - Morphing from NACA 6510 to NACA 2510 Profile (Max 0.33 [mm/mm], Open Cell-Neoprene Rubber Design with 1.5 [mm] composite thickness)

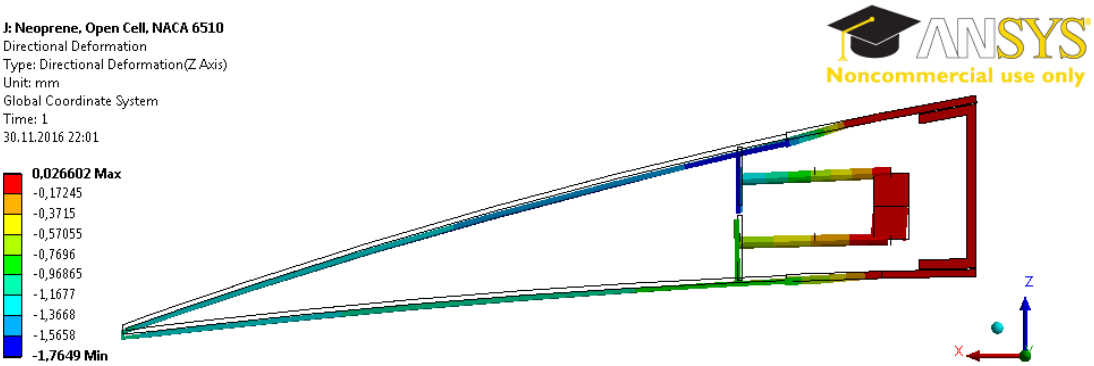

Figure 81: Displacement in z Direction Contour - Maintaining the NACA 6510 Profile (Max 0.02 [mm], Open Cell-Neoprene Rubber Design with 1.0 [mm] composite thickness)

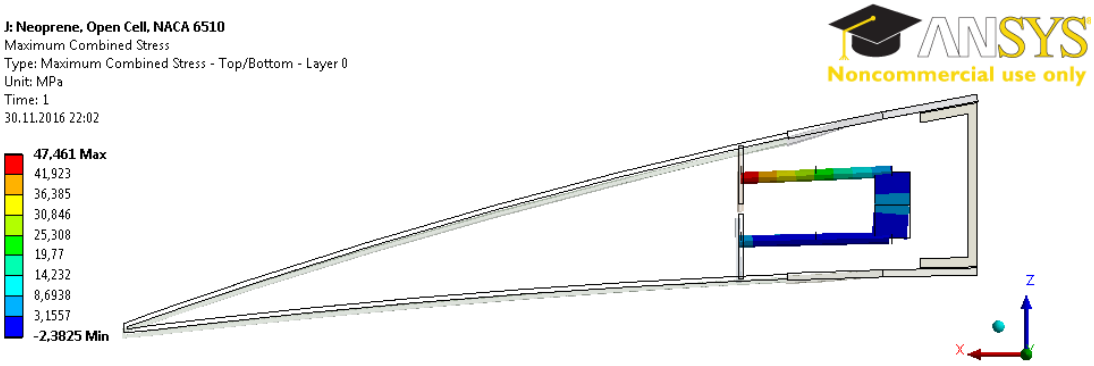

Figure 82: Maximum Beam Combined Stress Contour - Maintaining the NACA 6510 Profile (Max 47.46 [MPa], Open Cell-Neoprene Rubber Design with 1.0 [mm] composite thickness)

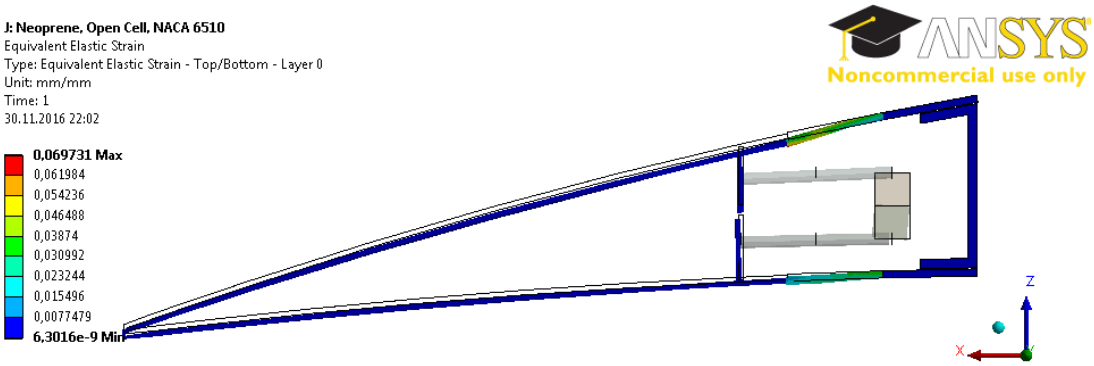

Figure 83: Equivalent Elastic Strain (von-Mises) Contour - Maintaining the NACA 6510 Profile (Max 0.07 [mm/mm], Open Cell-Neoprene Rubber Design with 1.0 [mm] composite thickness)

APPENDIX A2

Open Cell – Silicone Design Results

In this part, in-vacuo condition Open Cell – Silicone design results of the analysis are presented.

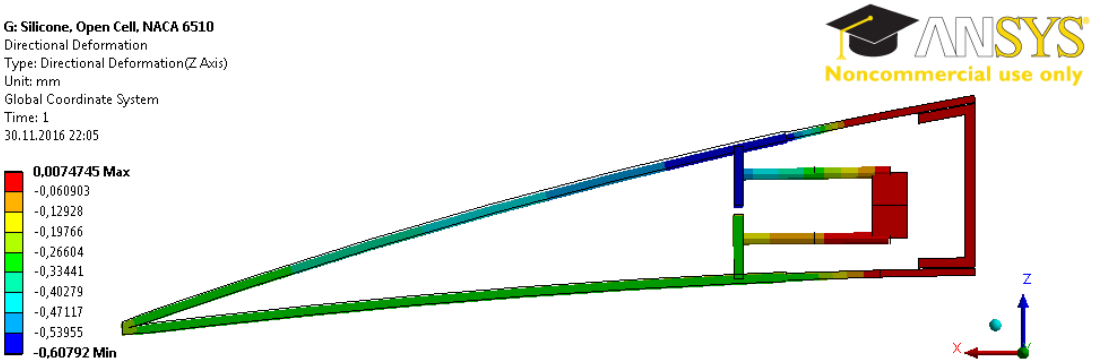

Figure 84: Displacement in z Direction Contour - Maintaining the NACA 6510 Profile (Max 0.01 [mm], Open Cell-Silicone Design with 2.0 [mm] composite thickness)

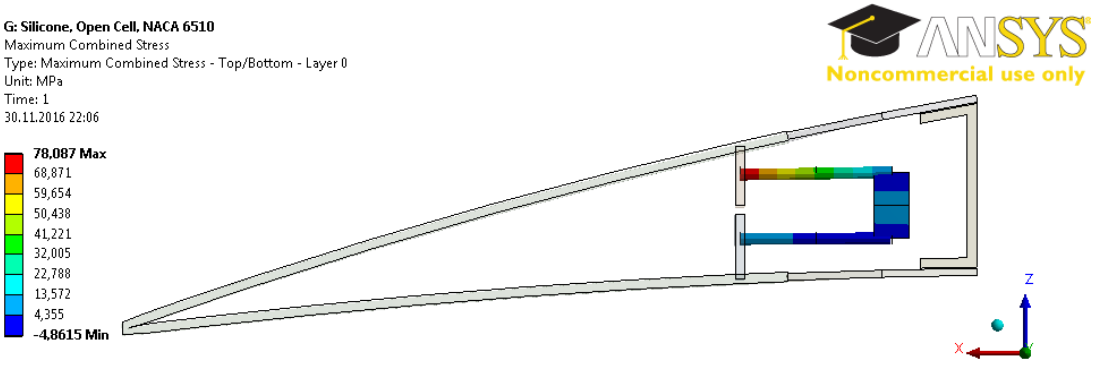

Figure 85: Maximum Beam Combined Stress Contour - Maintaining the NACA 6510 Profile (Max 78.09 [MPa], Open Cell-Silicone Design with 2.0 [mm] composite thickness)

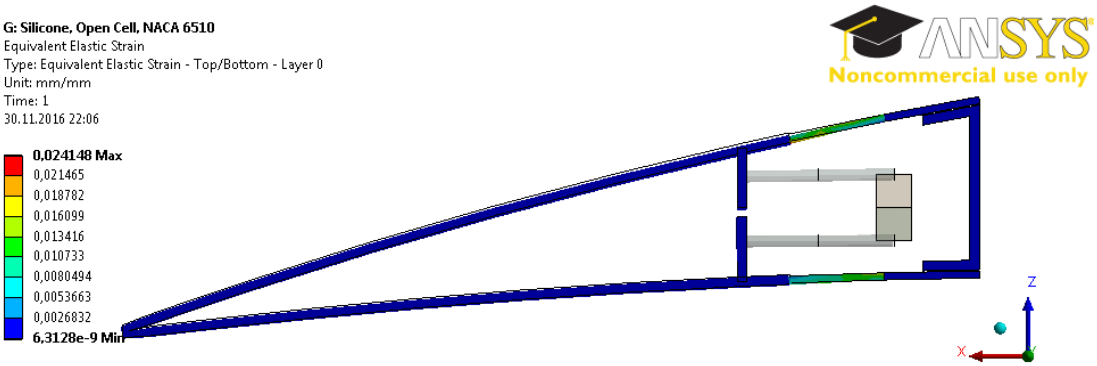

Figure 86: Equivalent Elastic Strain (von-Mises) Contour - Maintaining the NACA 6510 Profile (Max 0.02 [mm/mm], Open Cell-Silicone Design with 2.0 [mm] composite thickness)

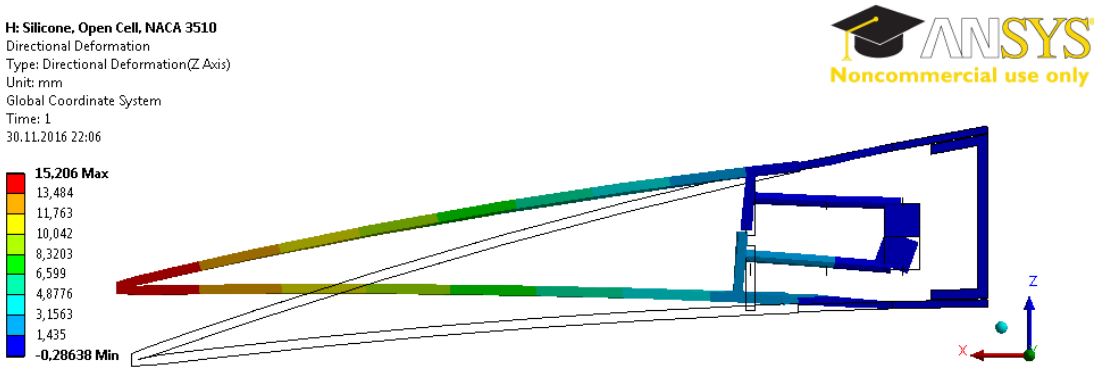

Figure 87: Displacement in z Direction Contour - Morphing from NACA 6510 to NACA 3510 Profile (Max 15.21 [mm], Open Cell-Silicone Design with 2.0 [mm] composite thickness)

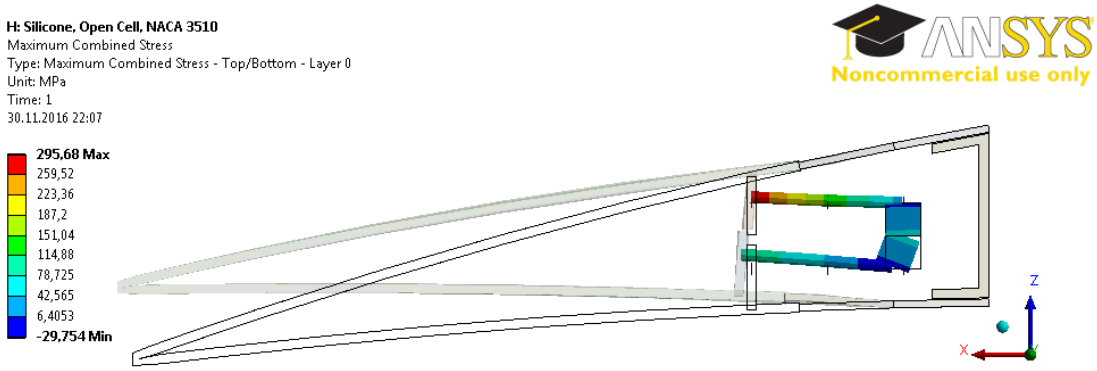

Figure 88: Maximum Beam Combined Stress Contour - Morphing from NACA 6510 to NACA 3510 Profile (Max 295.68 [MPa], Open Cell-Silicone Design with 2.0 [mm] composite thickness)

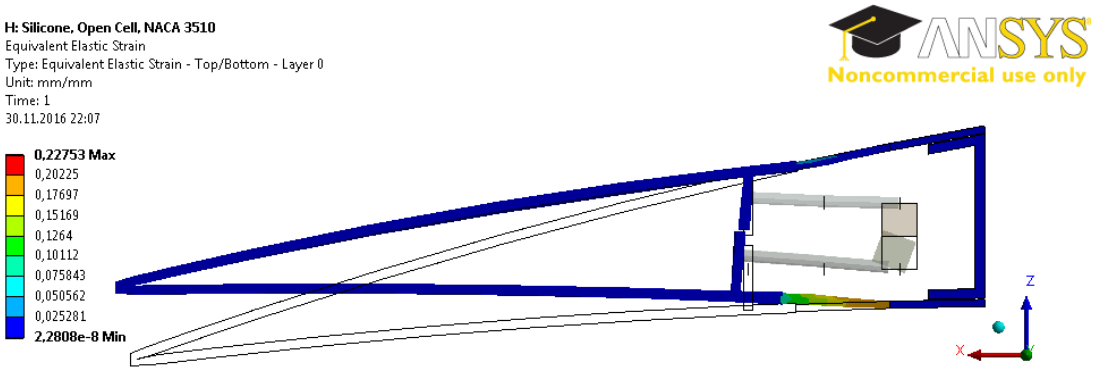

Figure 89: Equivalent Elastic Strain (von-Mises) Contour - Morphing from NACA 6510 to NACA 3510 Profile (Max 0.23 [mm/mm], Open Cell-Silicone Design with 2.0 [mm] composite thickness)

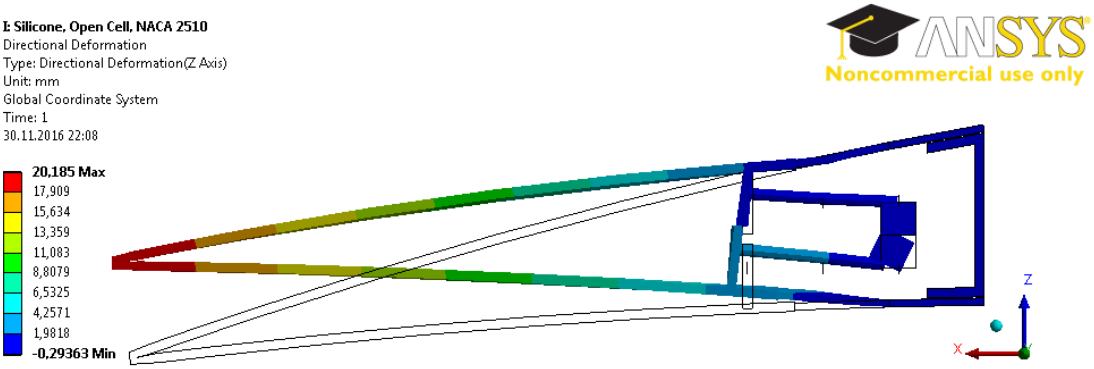

Figure 90: Displacement in z Direction Contour - Morphing from NACA 6510 to NACA 2510 Profile (Max 20.19 [mm], Open Cell-Silicone Design with 2.0 [mm] composite thickness)

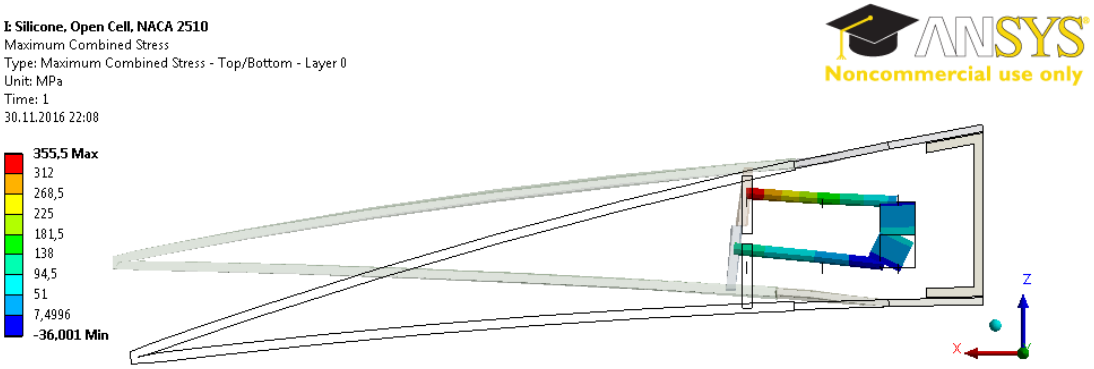

Figure 91: Maximum Beam Combined Stress Contour - Morphing from NACA 6510 to NACA 2510 Profile (Max 355.50 [MPa], Open Cell-Silicone Design with 2.0 [mm] composite thickness)

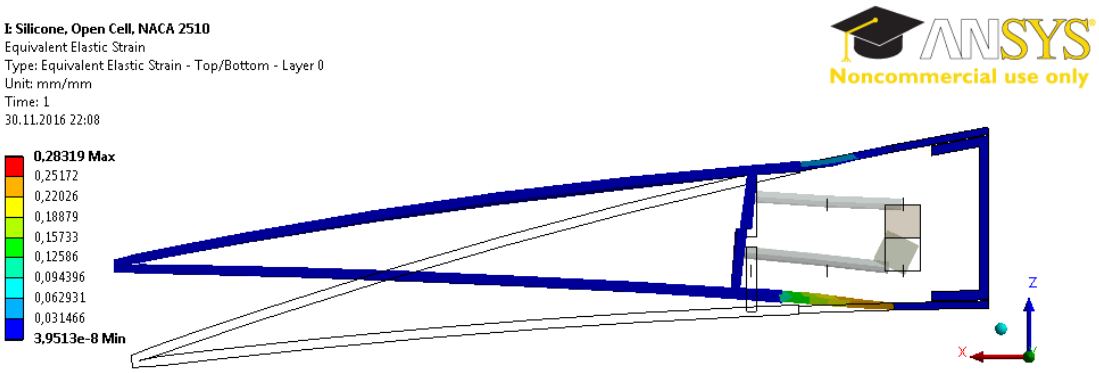

Figure 92: Equivalent Elastic Strain (von-Mises) Contour - Morphing from NACA 6510 to NACA 2510 Profile (Max 0.28 [mm/mm], Open Cell-Silicone Design with 2.0 [mm] composite thickness)

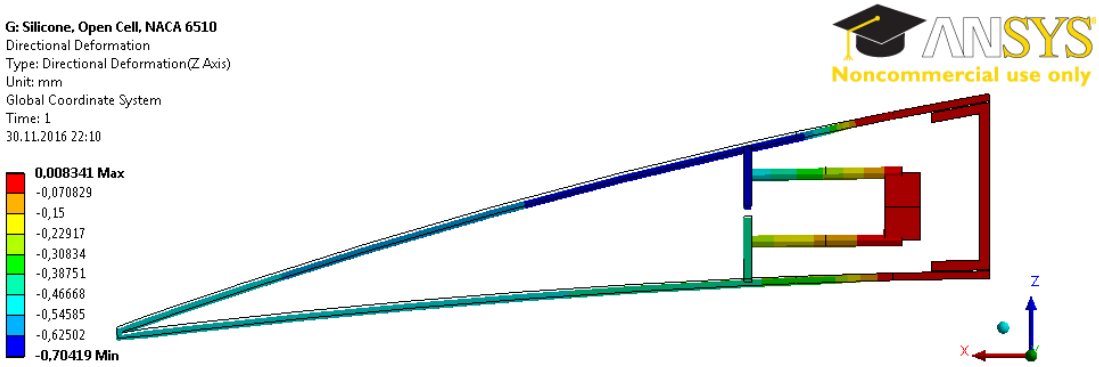

Figure 93: Displacement in z Direction Contour - Maintaining the NACA 6510 Profile (Max 0.01 [mm], Open Cell-Silicone Design with 1.5 [mm] composite thickness)

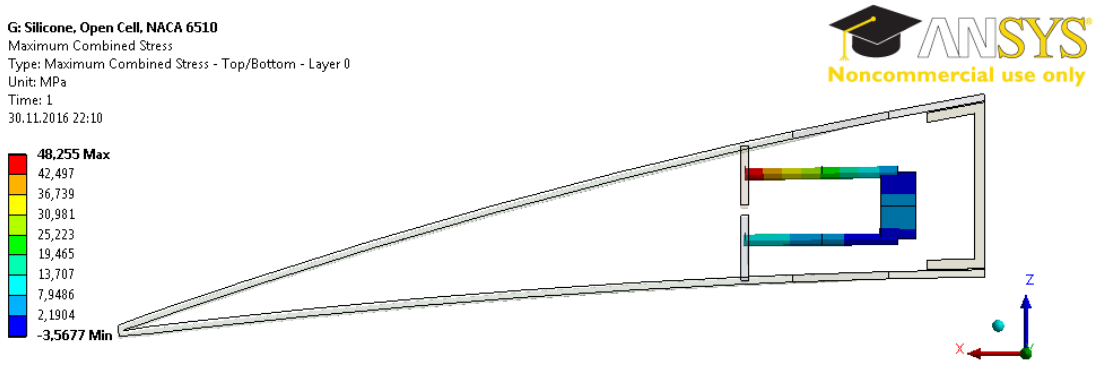

Figure 94: Maximum Beam Combined Stress Contour - Maintaining the NACA 6510 Profile (Max 48.26 [MPa], Open Cell-Silicone Design with 1.5 [mm] composite thickness)

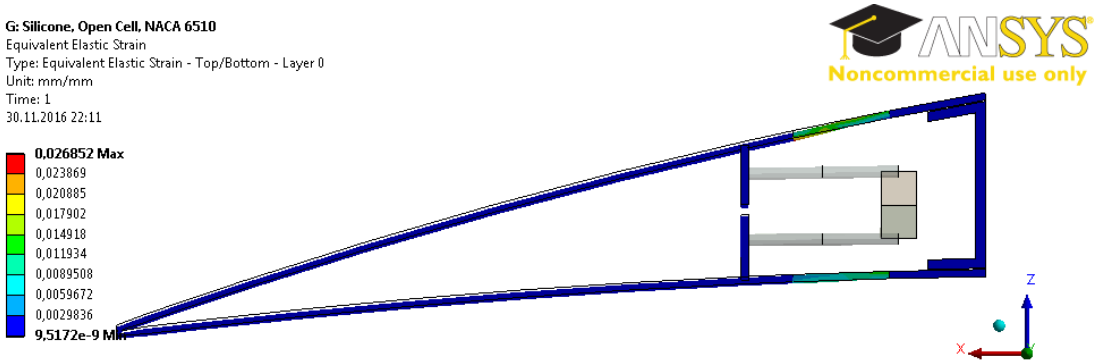

Figure 95: Equivalent Elastic Strain (von-Mises) Contour - Maintaining the NACA 6510 Profile (Max 0.03 [mm/mm], Open Cell-Silicone Design with 1.5 [mm] composite thickness)

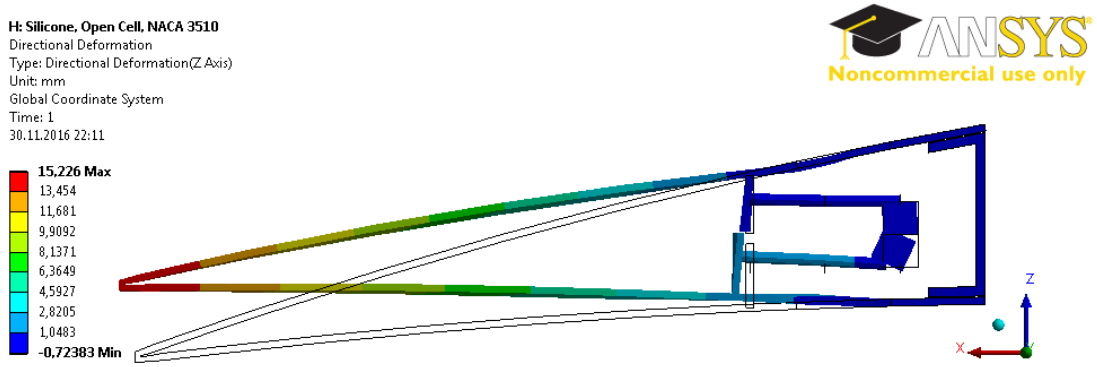

Figure 96: Displacement in z Direction Contour - Morphing from NACA 6510 to NACA 3510 Profile (Max 15.23 [mm], Open Cell-Silicone Design with 1.5 [mm] composite thickness)

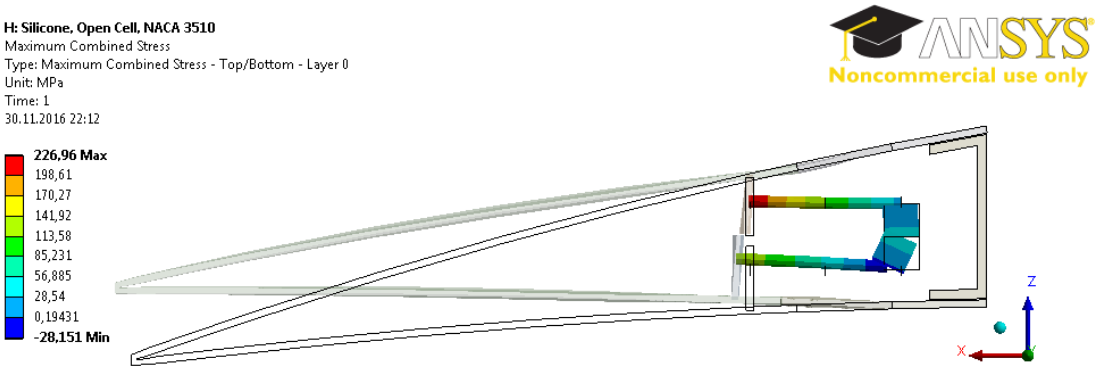

Figure 97: Maximum Beam Combined Stress Contour - Morphing from NACA 6510 to NACA 3510 Profile (Max 226.96 [MPa], Open Cell-Silicone Design with 1.5 [mm] composite thickness)

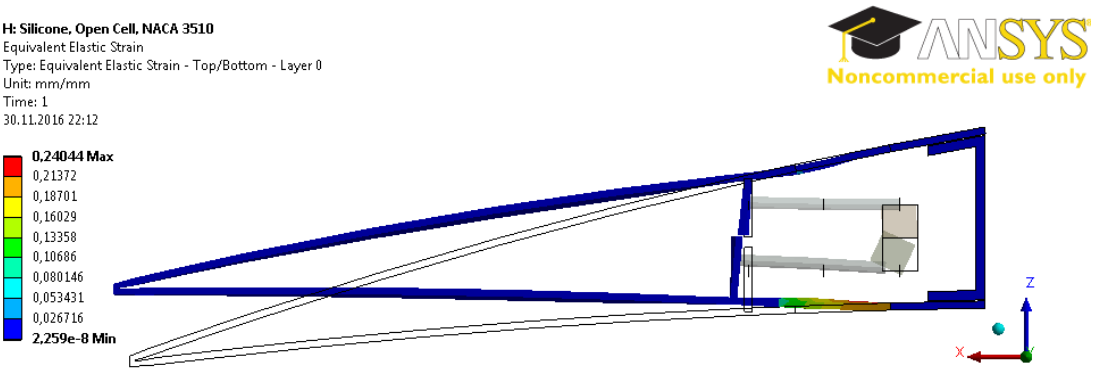

Figure 98: Equivalent Elastic Strain (von-Mises) Contour - Morphing from NACA 6510 to NACA 3510 Profile (Max 0.24 [mm/mm], Open Cell-Silicone Design with 1.5 [mm] composite thickness)

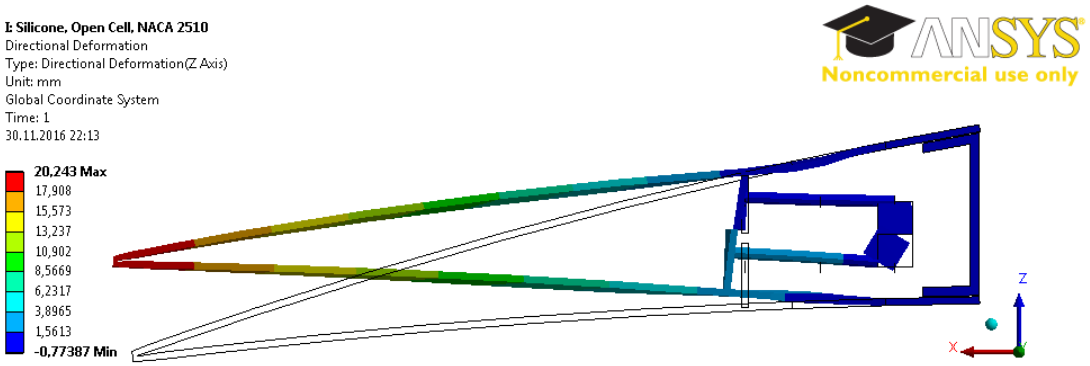

Figure 99: Displacement in z Direction Contour - Morphing from NACA 6510 to NACA 2510 Profile (Max 20.24 [mm], Open Cell-Silicone Design with 1.5 [mm] composite thickness)

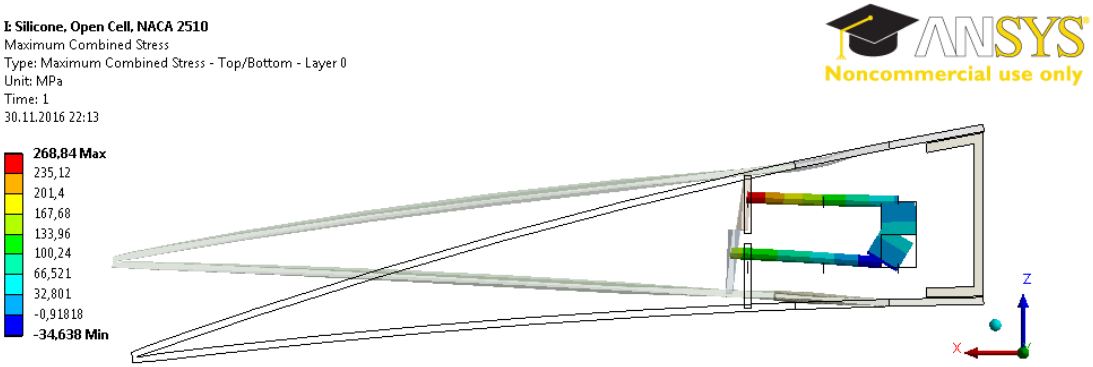

Figure 100: Maximum Beam Combined Stress Contour - Morphing from NACA 6510 to NACA 2510 Profile (Max 268.84 [MPa], Open Cell-Silicone Design with 1.5 [mm] composite thickness)

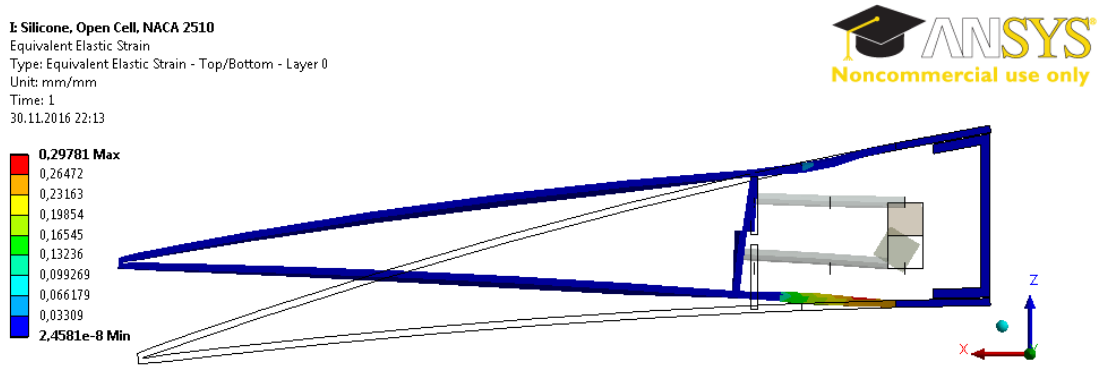

Figure 101: Equivalent Elastic Strain (von-Mises) Contour - Morphing from NACA 6510 to NACA 2510 Profile (Max 0.30 [mm/mm], Open Cell-Silicone Design with 1.5 [mm] composite thickness)

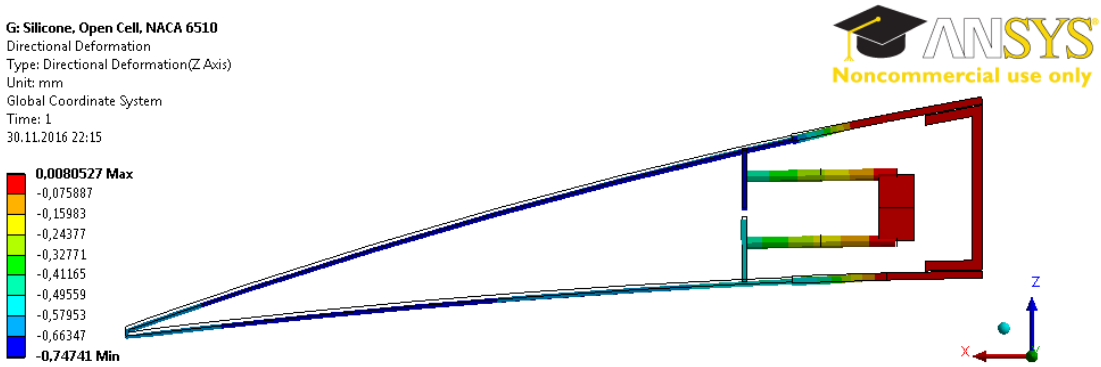

Figure 102: Displacement in z Direction Contour - Maintaining the NACA 6510 Profile (Max 0.01 [mm], Open Cell-Silicone Design with 1.0 [mm] composite thickness)

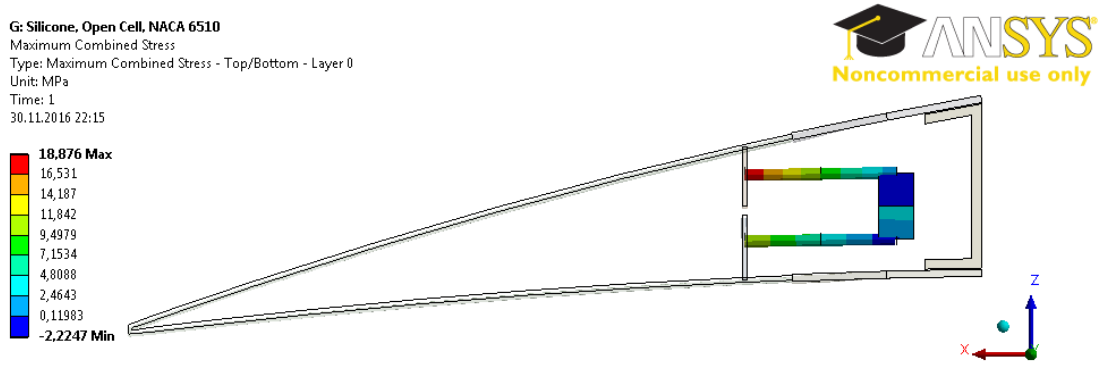

Figure 103: Maximum Beam Combined Stress Contour - Maintaining the NACA 6510 Profile (Max 18.88 [MPa], Open Cell-Silicone Design with 1.0 [mm] composite thickness)

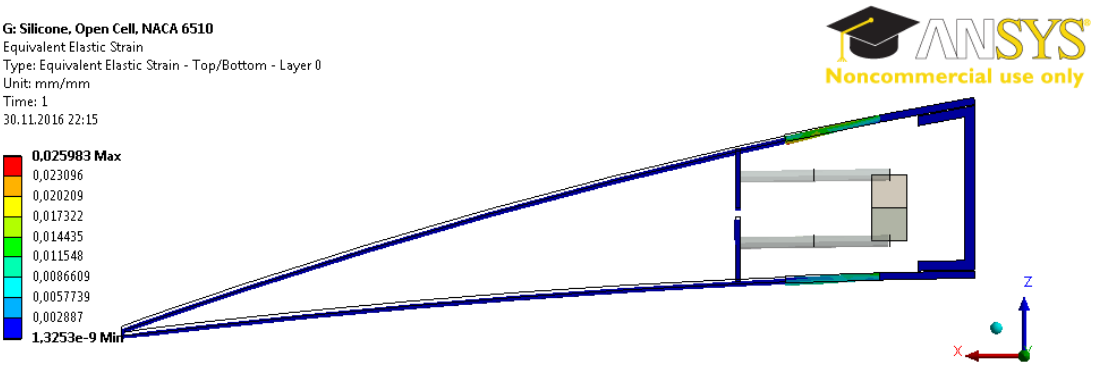

Figure 104: Equivalent Elastic Strain (von-Mises) Contour - Maintaining the NACA 6510 Profile (Max 0.03 [mm/mm], Open Cell-Silicone Design with 1.0 [mm] composite thickness)

APPENDIX A3

Closed Cell – Neoprene Rubber Design Results

In this part, in-vacuo condition Closed Cell – Neoprene Rubber design results of the analysis are presented.

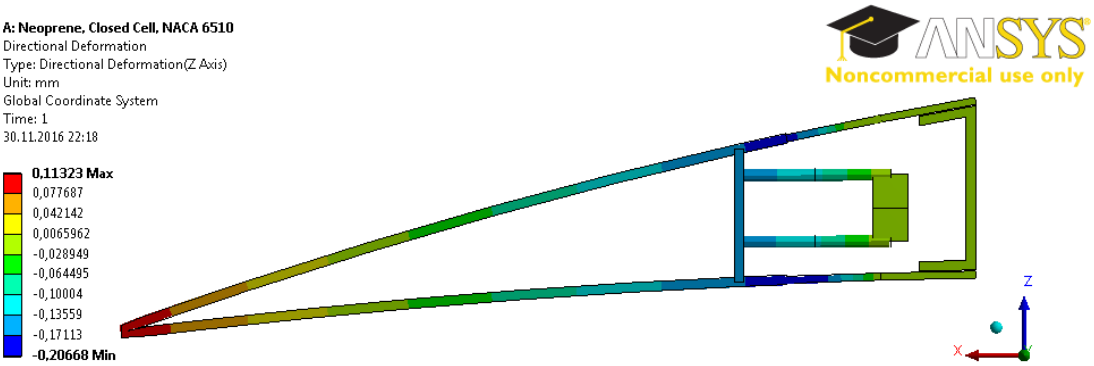

Figure 105: Displacement in z Direction Contour - Maintaining the NACA 6510 Profile (Max 0.11 [mm], Closed Cell-Neoprene Rubber Design with 2.0 [mm] composite thickness)

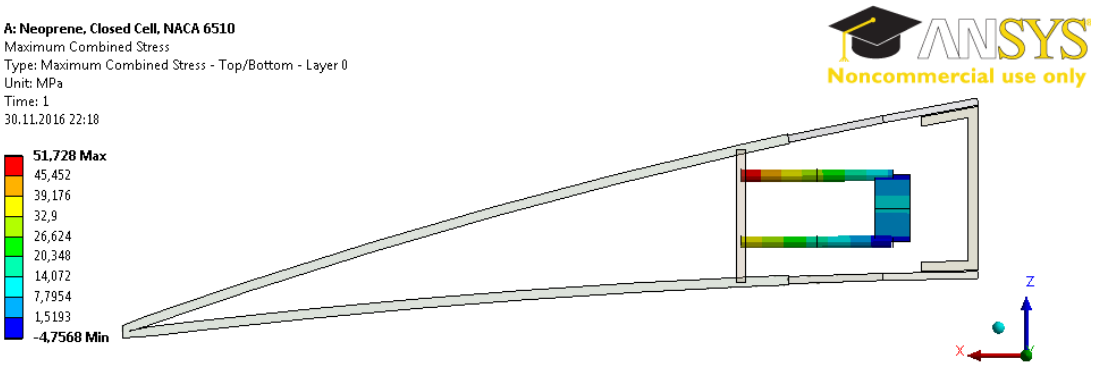

Figure 106: Maximum Beam Combined Stress Contour - Maintaining the NACA 6510 Profile (Max 51.73 [MPa], Closed Cell-Neoprene Rubber Design with 2.0 [mm] composite thickness)

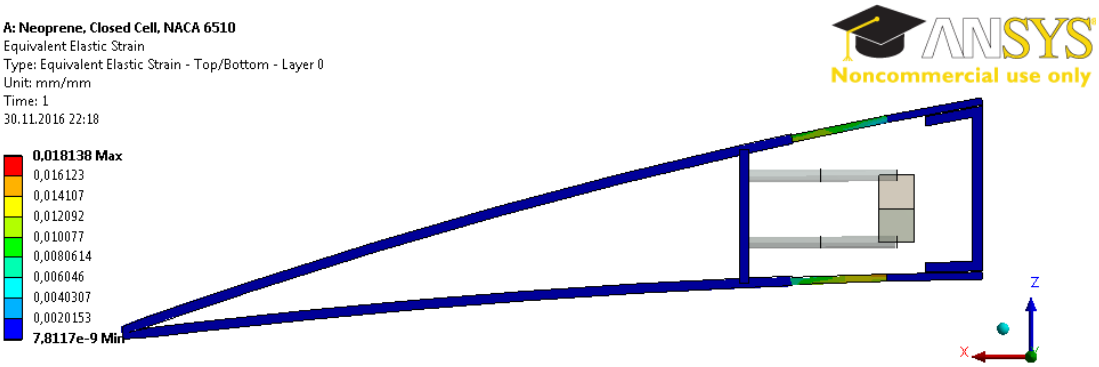

Figure 107: Equivalent Elastic Strain (von-Mises) Contour - Maintaining the NACA 6510 Profile (Max 0.03 [mm/mm], Closed Cell-Neoprene Rubber Design with 2.0 [mm] composite thickness)

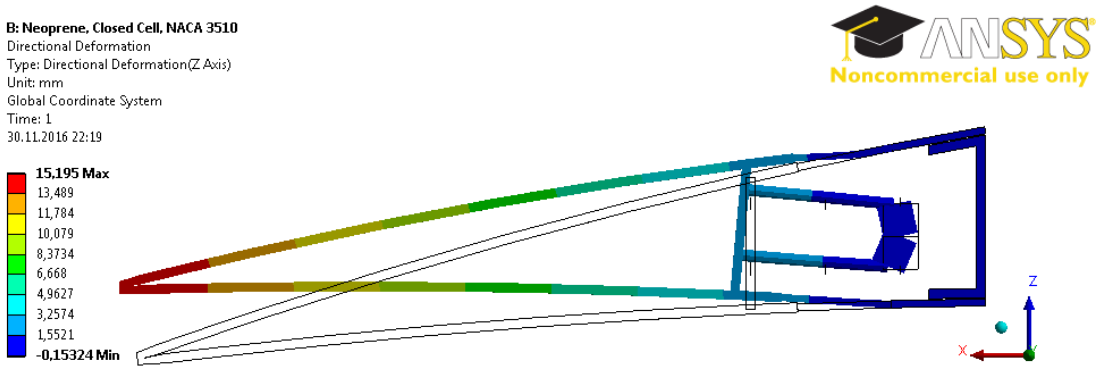

Figure 108: Displacement in z Direction Contour - Morphing from NACA 6510 to NACA 3510 Profile (Max 15.20 [mm], Closed Cell-Neoprene Rubber Design with 2.0 [mm] composite thickness)

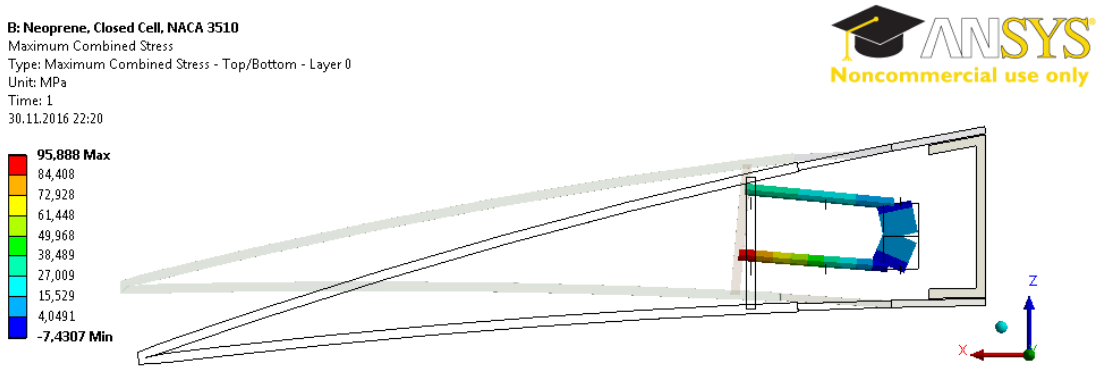

Figure 109: Maximum Beam Combined Stress Contour - Morphing from NACA 6510 to NACA 3510 Profile (Max 95.89 [MPa], Closed Cell-Neoprene Rubber Design with 2.0 [mm] composite thickness)

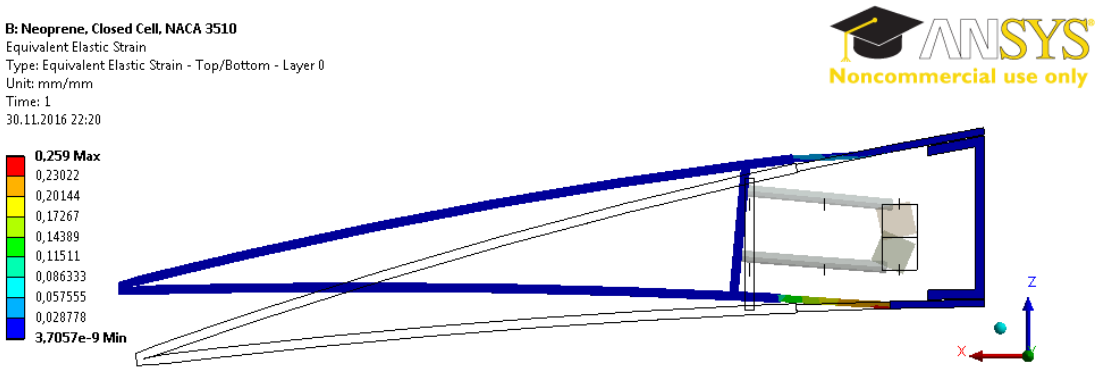

Figure 110: Equivalent Elastic Strain (von-Mises) Contour - Morphing from NACA 6510 to NACA 3510 Profile (Max 0.26 [mm/mm], Closed Cell-Neoprene Rubber Design with 2.0 [mm] composite thickness)

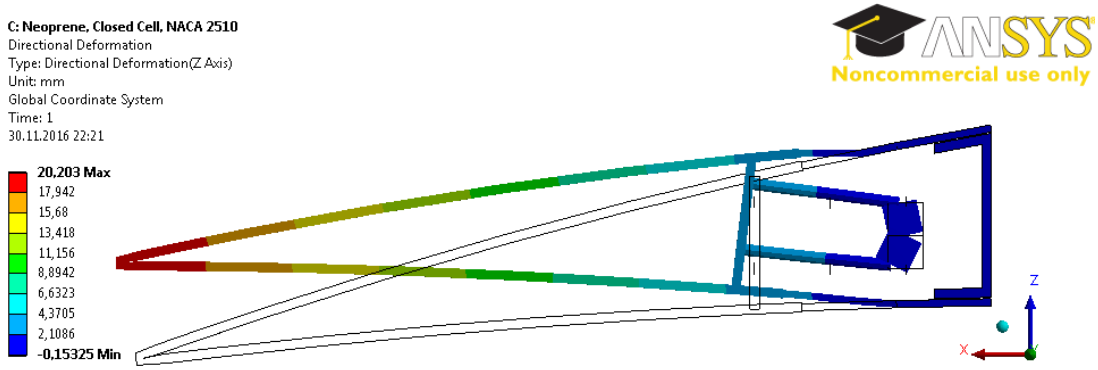

Figure 111: Displacement in z Direction Contour - Morphing from NACA 6510 to NACA 2510 Profile (Max 20.20 [mm], Closed Cell-Neoprene Rubber Design with 2.0 [mm] composite thickness)

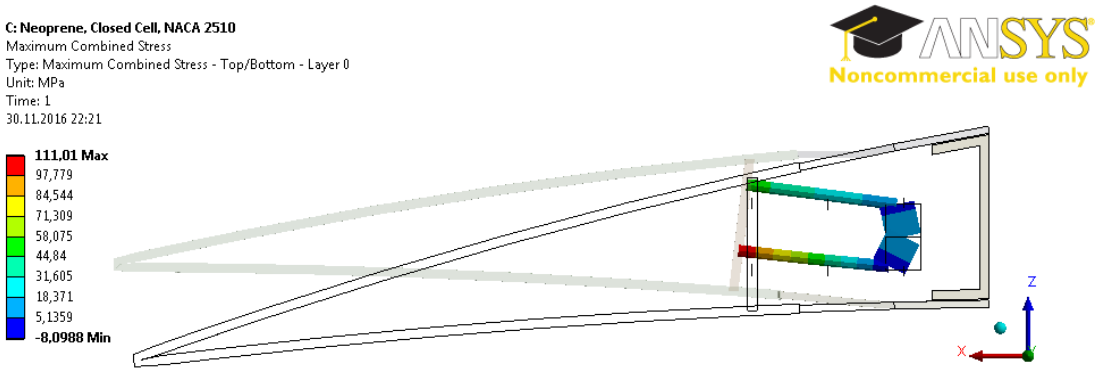

Figure 112: Maximum Beam Combined Stress Contour - Morphing from NACA 6510 to NACA 2510 Profile (Max 111.01 [MPa], Closed Cell-Neoprene Rubber Design with 2.0 [mm] composite thickness)

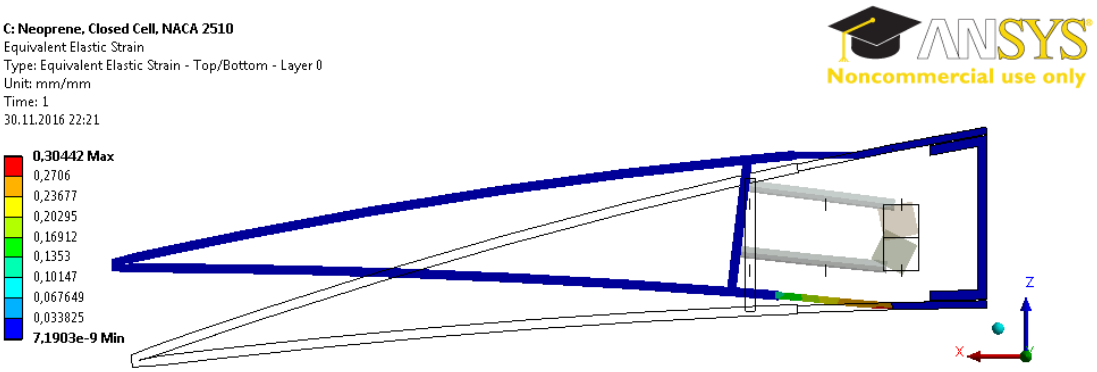

Figure 113: Equivalent Elastic Strain (von-Mises) Contour - Morphing from NACA 6510 to NACA 2510 Profile (Max 0.30 [mm/mm], Closed Cell-Neoprene Rubber Design with 2.0 [mm] composite thickness)

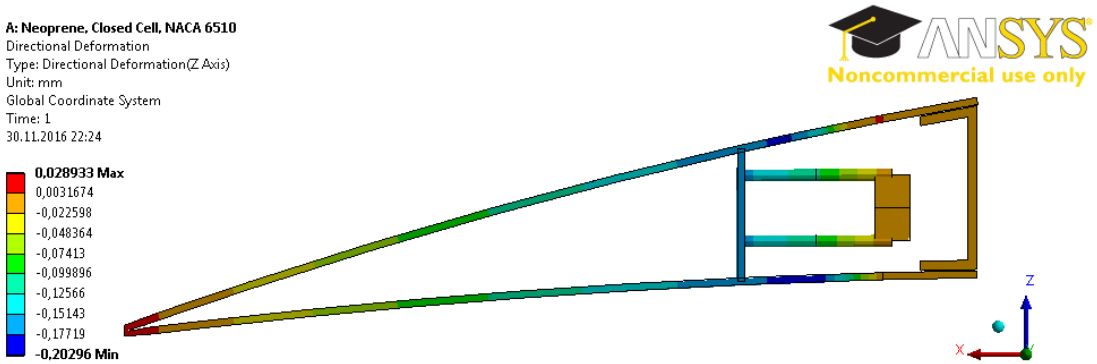

Figure 114: Displacement in z Direction Contour - Maintaining the NACA 6510 Profile (Max 0.03 [mm], Closed Cell-Neoprene Rubber Design with 1.5 [mm] composite thickness)

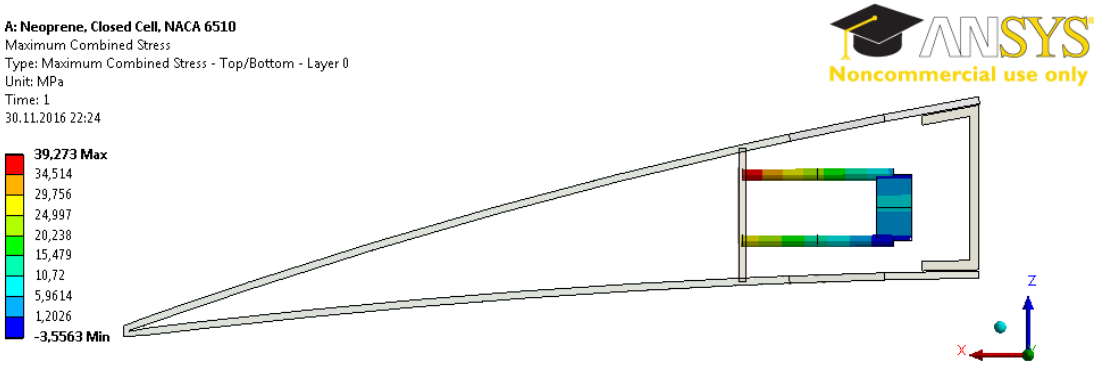

Figure 115: Maximum Beam Combined Stress Contour - Maintaining the NACA 6510 Profile (Max 39. 27[MPa], Closed Cell-Neoprene Rubber Design with 1.5 [mm] composite thickness)

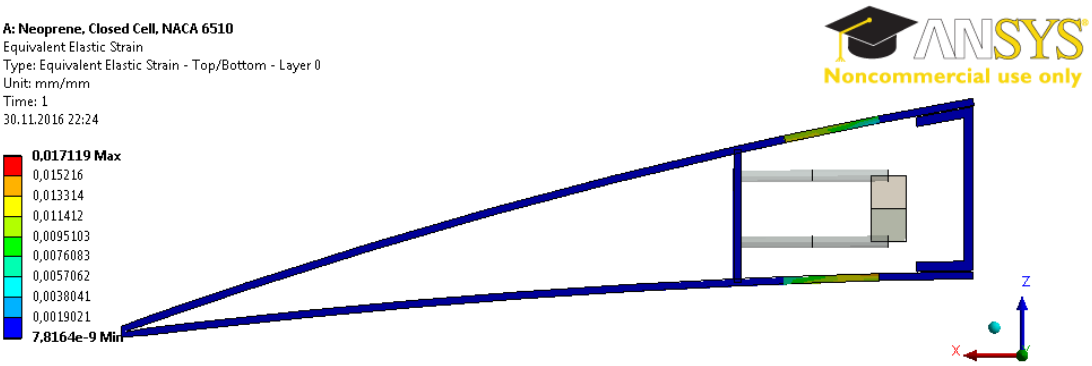

Figure 116: Equivalent Elastic Strain (von-Mises) Contour - Maintaining the NACA 6510 Profile (Max 0.02 [mm/mm], Closed Cell-Neoprene Rubber Design with 1.5 [mm] composite thickness)

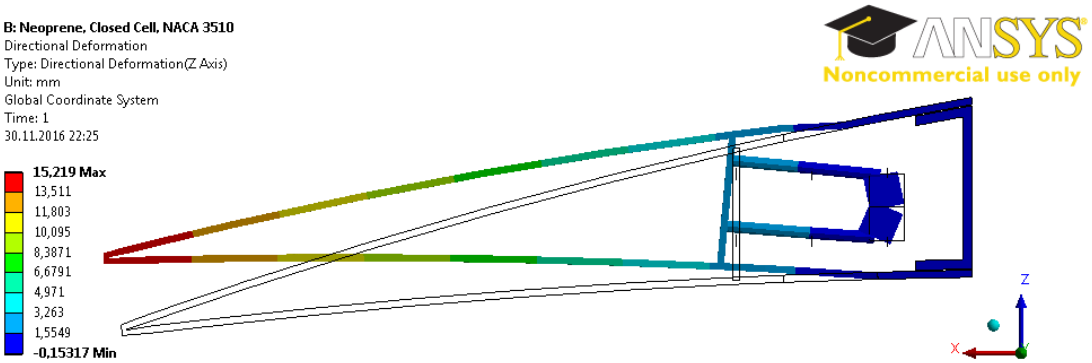

Figure 117: Displacement in z Direction Contour - Morphing from NACA 6510 to NACA 3510 Profile (Max 15.22 [mm], Closed Cell-Neoprene Rubber Design with 1.5 [mm] composite thickness)

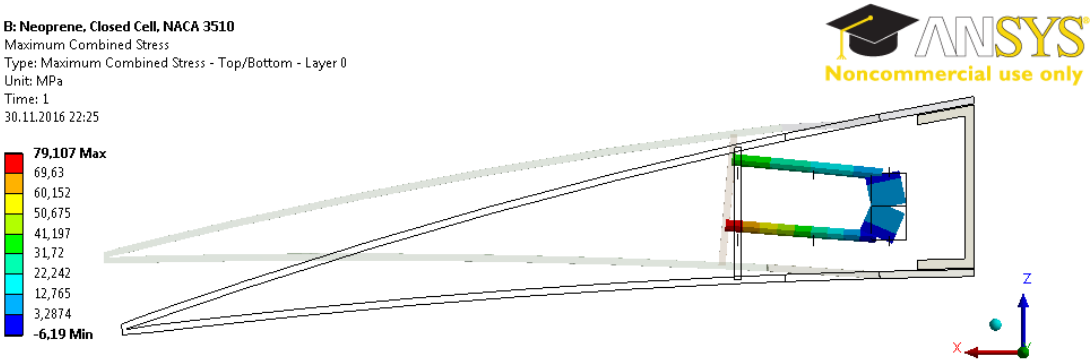

Figure 118: Maximum Beam Combined Stress Contour - Morphing from NACA 6510 to NACA 3510 Profile (Max 79.11 [MPa], Closed Cell-Neoprene Rubber Design with 1.5 [mm] composite thickness)

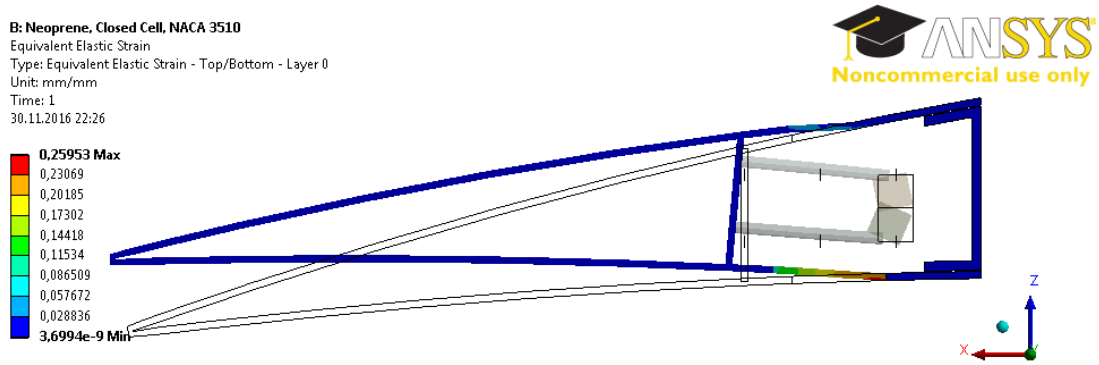

Figure 119: Equivalent Elastic Strain (von-Mises) Contour - Morphing from NACA 6510 to NACA 3510 Profile (Max 0.26 [mm/mm], Closed Cell-Neoprene Rubber Design with 1.5 [mm] composite thickness)

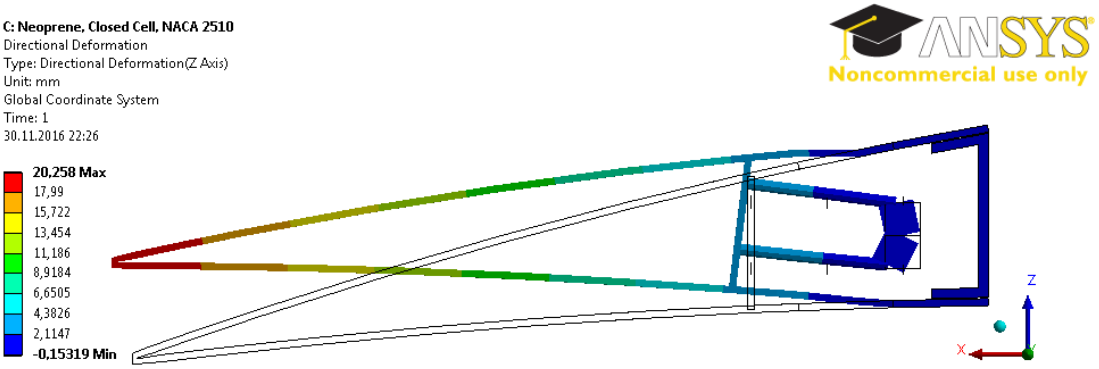

Figure 120: Displacement in z Direction Contour - Morphing from NACA 6510 to NACA 2510 Profile (Max 20.26 [mm], Closed Cell-Neoprene Rubber Design with 1.5 [mm] composite thickness)

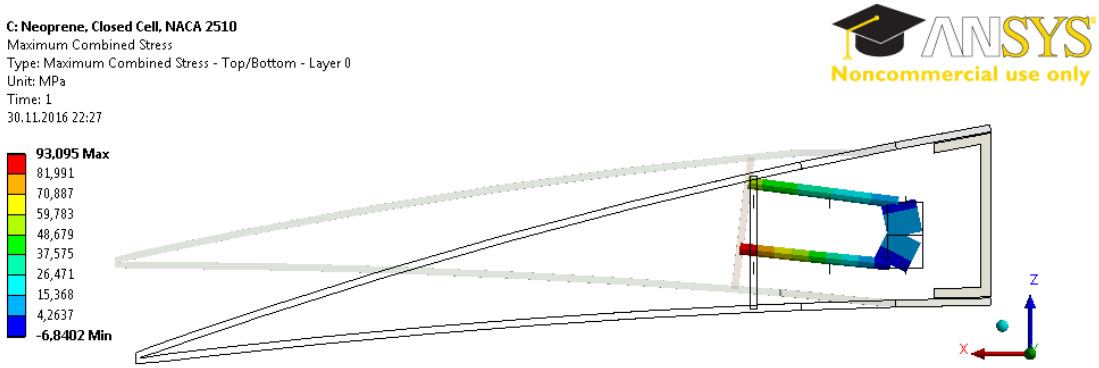

Figure 121: Maximum Beam Combined Stress Contour - Morphing from NACA 6510 to NACA 2510 Profile (Max 93.10 [MPa], Closed Cell-Neoprene Rubber Design with 1.5 [mm] composite thickness)

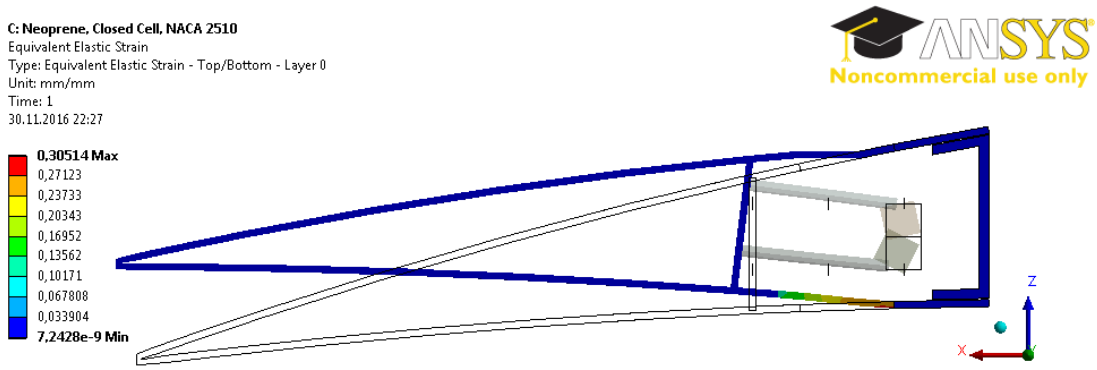

Figure 122: Equivalent Elastic Strain (von-Mises) Contour - Morphing from NACA 6510 to NACA 2510 Profile (Max 0.31 [mm/mm], Closed Cell-Neoprene Rubber Design with 1.5 [mm] composite thickness)

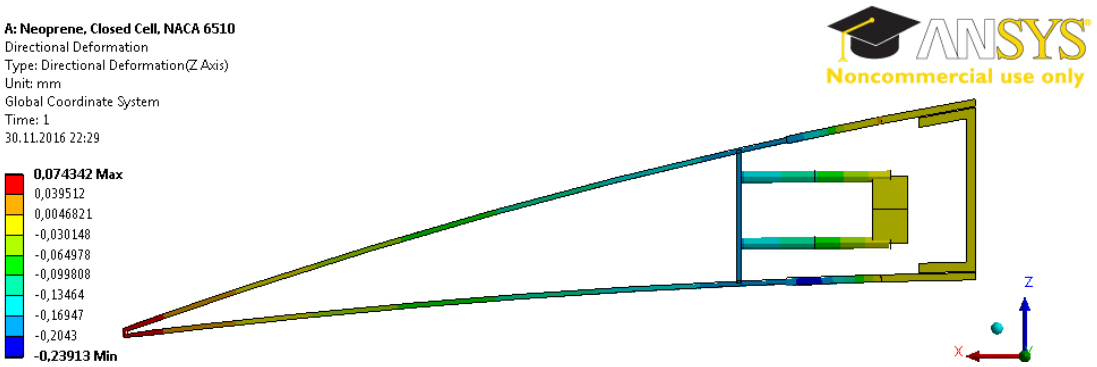

Figure 123: Displacement in z Direction Contour - Maintaining the NACA 6510 Profile (Max 0.07 [mm], Closed Cell-Neoprene Rubber Design with 1.0 [mm] composite thickness)

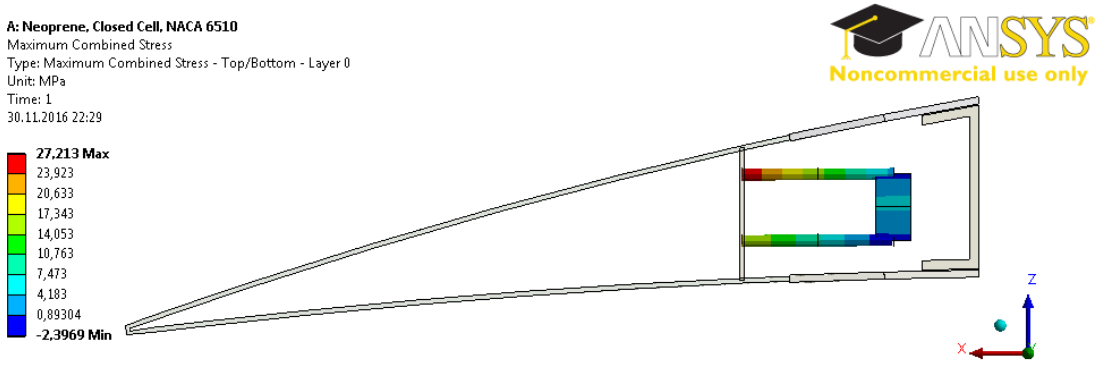

Figure 124: Maximum Beam Combined Stress Contour - Maintaining the NACA 6510 Profile (Max 27.21 [MPa], Closed Cell-Neoprene Rubber Design with 1.0 [mm] composite thickness)

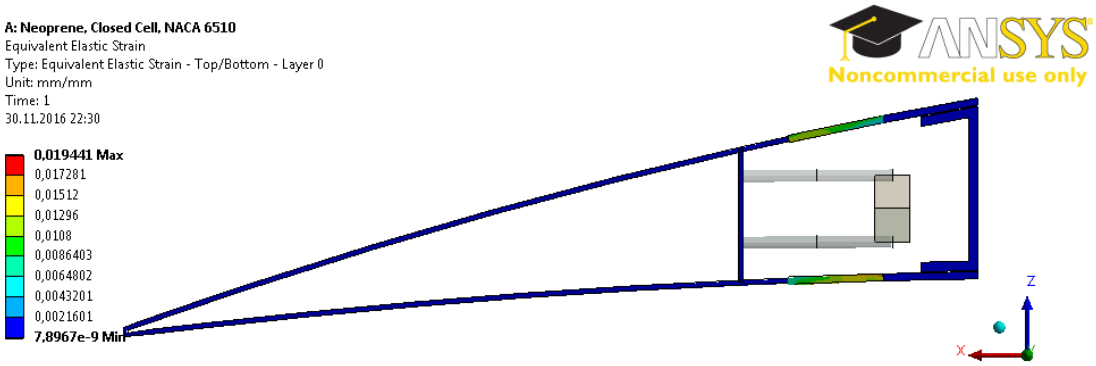

Figure 125: Equivalent Elastic Strain (von-Mises) Contour - Maintaining the NACA 6510 Profile (Max 0.02 [mm/mm], Closed Cell-Neoprene Rubber Design with 1.0 [mm] composite thickness)

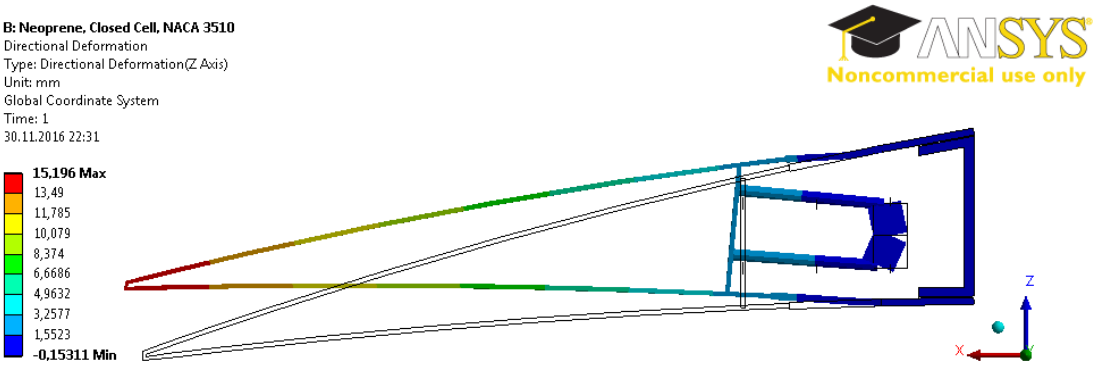

Figure 126: Displacement in z Direction Contour - Morphing from NACA 6510 to NACA 3510 Profile (Max 15.20 [mm], Closed Cell-Neoprene Rubber Design with 1.0 [mm] composite thickness)

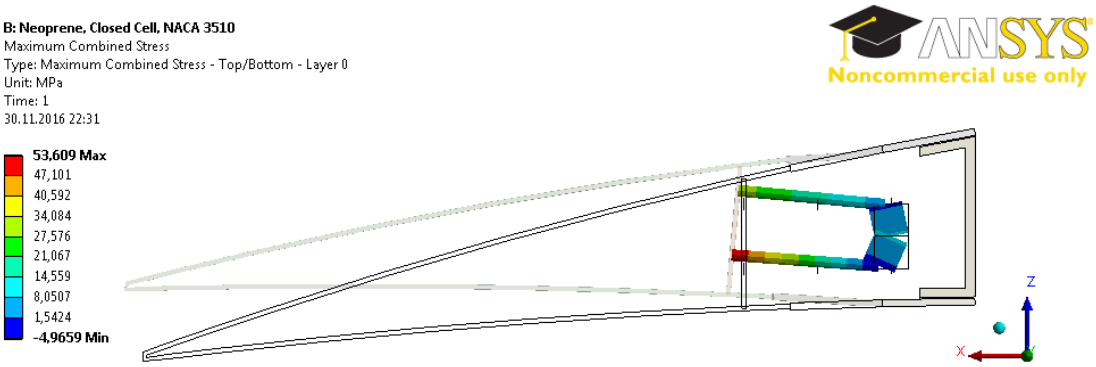

Figure 127: Maximum Beam Combined Stress Contour - Morphing from NACA 6510 to NACA 3510 Profile (Max 53.61 [MPa], Closed Cell-Neoprene Rubber Design with 1.0 [mm] composite thickness)

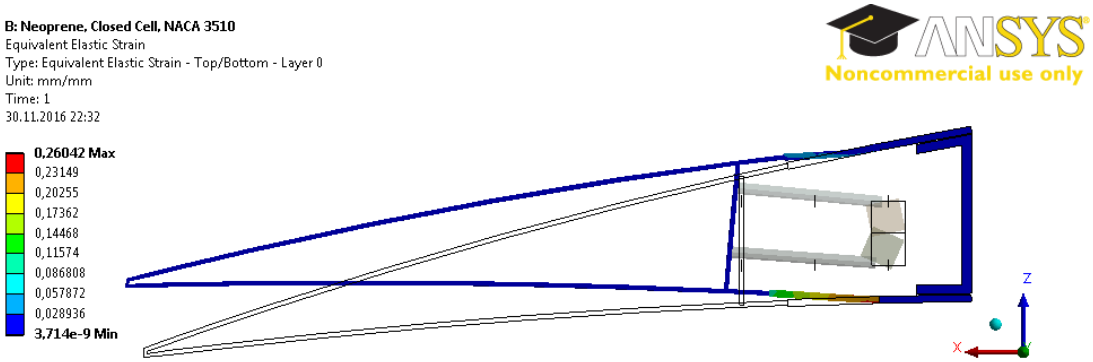

Figure 128: Equivalent Elastic Strain (von-Mises) Contour - Morphing from NACA 6510 to NACA 3510 Profile (Max 0.26 [mm/mm], Closed Cell-Neoprene Rubber Design with 1.0 [mm] composite thickness)

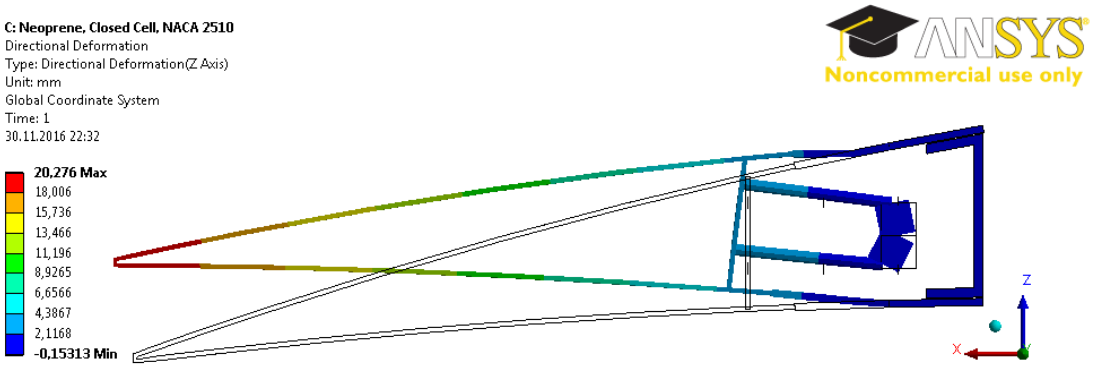

Figure 129: Displacement in z Direction Contour - Morphing from NACA 6510 to NACA 2510 Profile (Max 20.28 [mm], Closed Cell-Neoprene Rubber Design with 1.0 [mm] composite thickness)

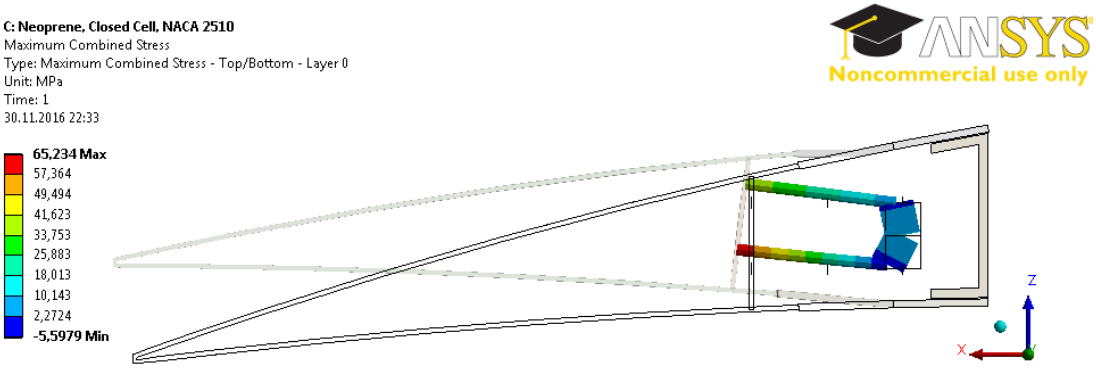

Figure 130: Maximum Beam Combined Stress Contour - Morphing from NACA 6510 to NACA 2510 Profile (Max 65.23 [MPa], Closed Cell-Neoprene Rubber Design with 1.0 [mm] composite thickness)

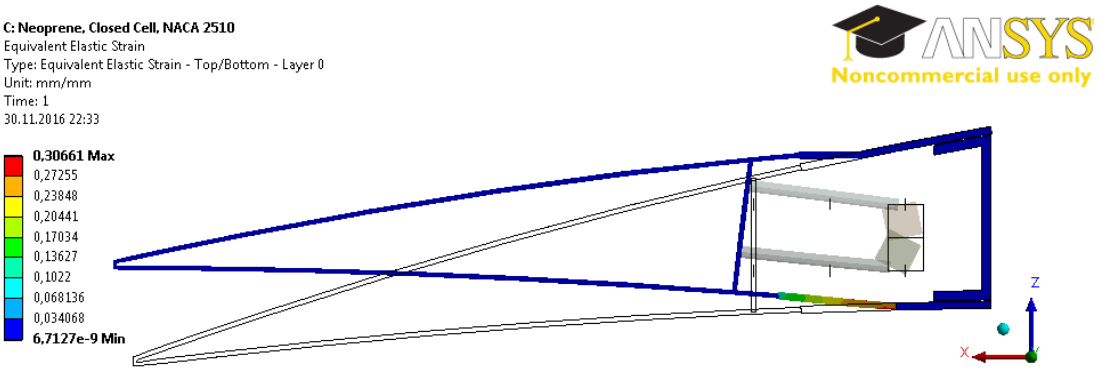

Figure 131: Equivalent Elastic Strain (von-Mises) Contour - Morphing from NACA 6510 to NACA 2510 Profile (Max 0.31 [mm/mm], Closed Cell-Neoprene Rubber Design with 1.0 [mm] composite thickness)

APPENDIX A4

Closed Cell – Silicone Design Results

In this part, in-vacuo condition Closed Cell – Silicone design results of the analysis are presented.

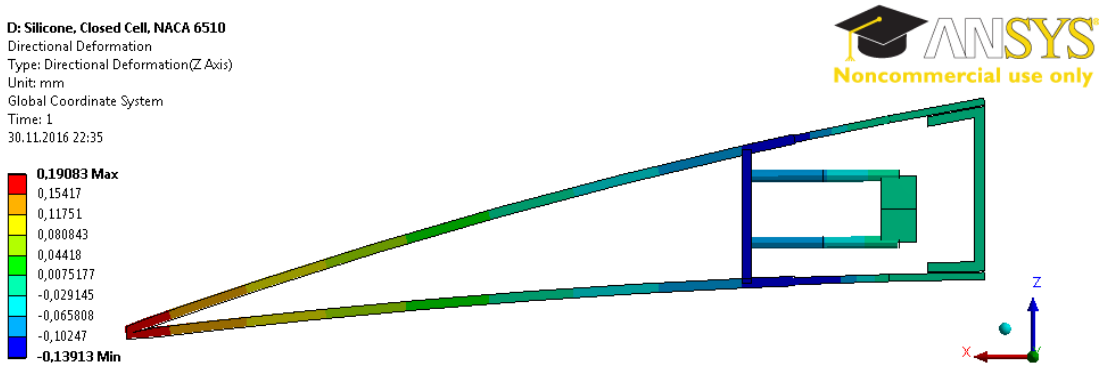

Figure 132: Displacement in z Direction Contour - Maintaining the NACA 6510 Profile (Max 0.19 [mm], Closed Cell-Silicone Design with 2.0 [mm] composite thickness)

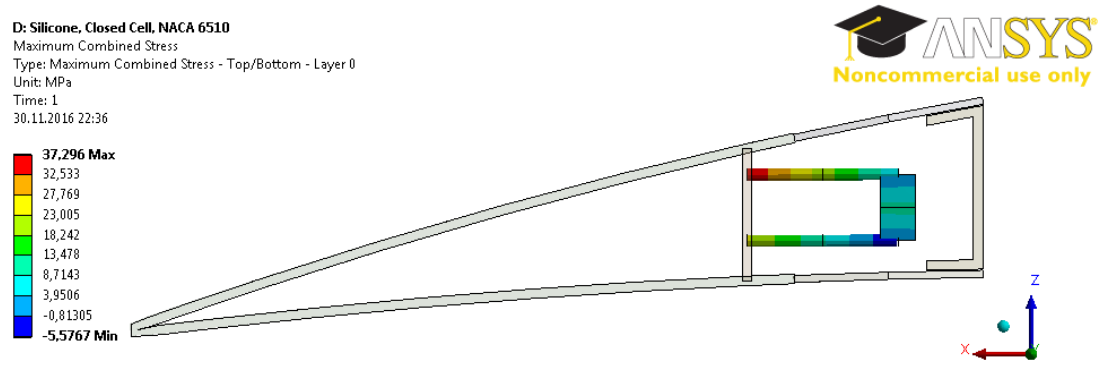

Figure 133: Maximum Beam Combined Stress Contour - Maintaining the NACA 6510 Profile (Max 37.30 [MPa], Closed Cell-Silicone Design with 2.0 [mm] composite thickness)

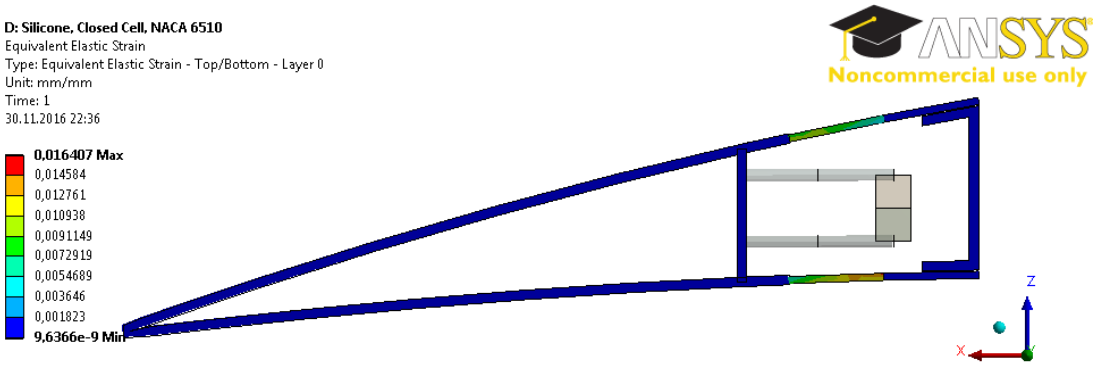

Figure 134: Equivalent Elastic Strain (von-Mises) Contour - Maintaining the NACA 6510 Profile (Max 0.02 [mm/mm], Closed Cell-Silicone Design with 2.0 [mm] composite thickness)

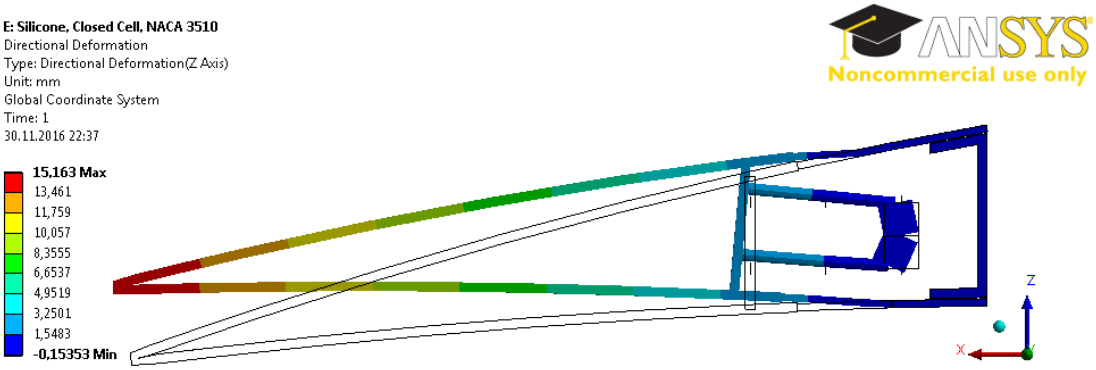

Figure 135: Displacement in z Direction Contour - Morphing from NACA 6510 to NACA 3510 Profile (Max 15.16 [mm], Closed Cell-Silicone Design with 2.0 [mm] composite thickness)

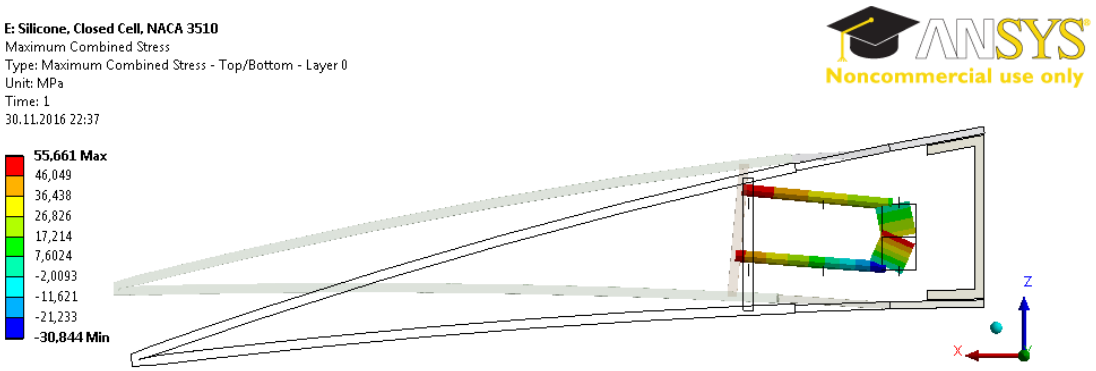

Figure 136: Maximum Beam Combined Stress Contour - Morphing from NACA 6510 to NACA 3510 Profile (Max 55.66 [MPa], Closed Cell-Silicone Design with 2.0 [mm] composite thickness)

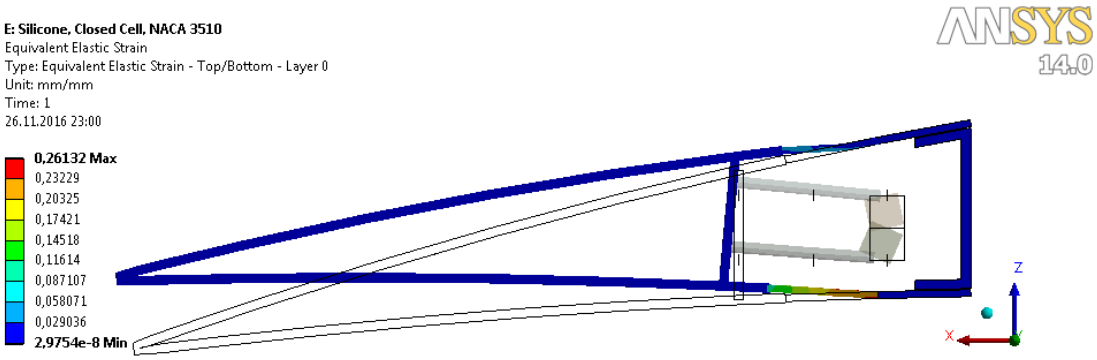

Figure 137: Equivalent Elastic Strain (von-Mises) Contour - Morphing from NACA 6510 to NACA 3510 Profile (Max 0.26 [mm/mm], Closed Cell-Silicone with 2.0 [mm] composite thickness)

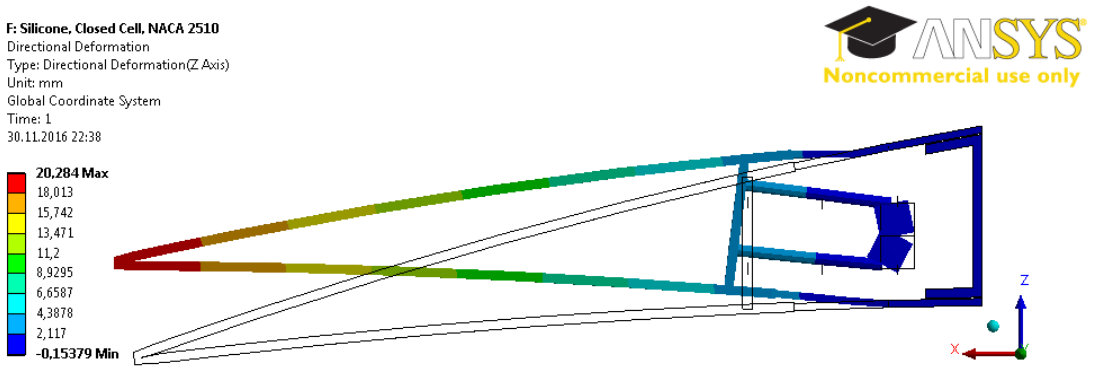

Figure 138: Displacement in z Direction Contour - Morphing from NACA 6510 to NACA 2510 Profile (Max 20.28 [mm], Closed Cell-Silicone Design with 2.0 [mm] composite thickness)

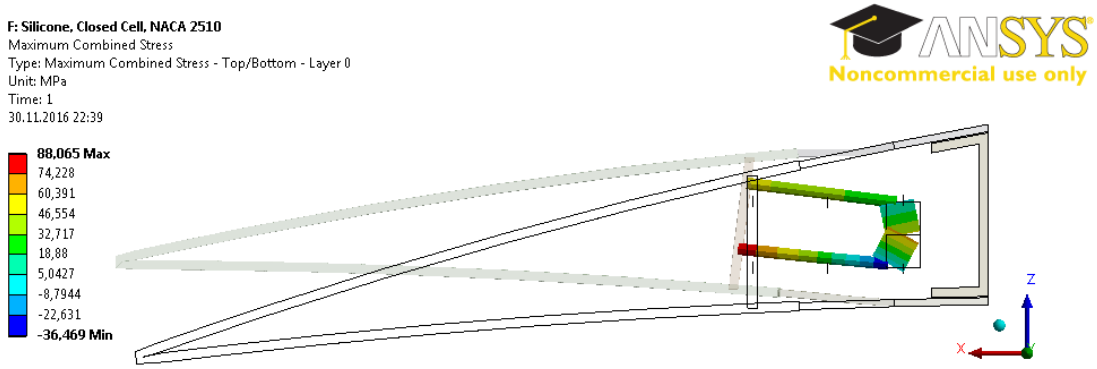

Figure 139: Maximum Beam Combined Stress Contour - Morphing from NACA 6510 to NACA 2510 Profile (Max 88.07 [MPa], Closed Cell-Silicone Design with 2.0 [mm] composite thickness)

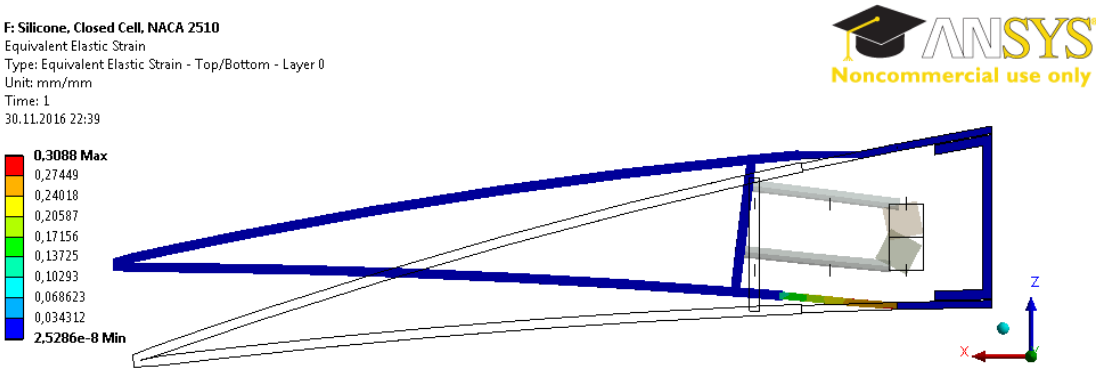

Figure 140: Equivalent Elastic Strain (von-Mises) Contour - Morphing from NACA 6510 to NACA 2510 Profile (Max 0.31 [mm/mm], Closed Cell-Silicone Design with 2.0 [mm] composite thickness)

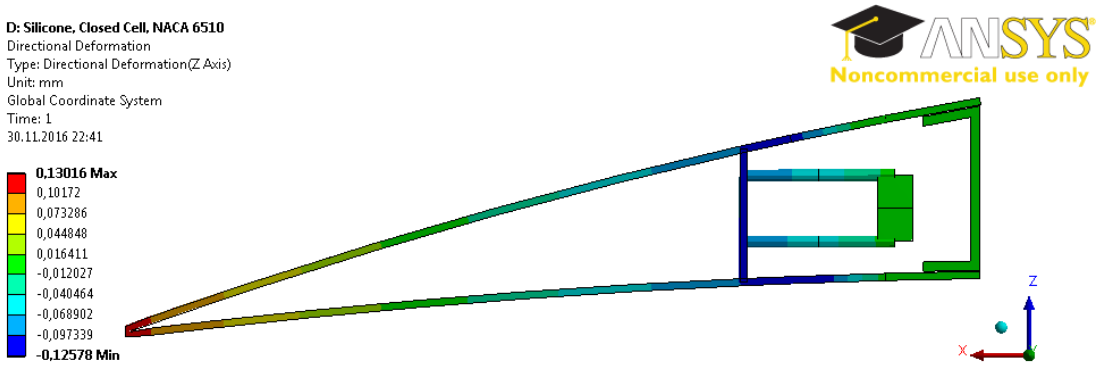

Figure 141: Displacement in z Direction Contour - Maintaining the NACA 6510 Profile (Max 0.13 [mm], Closed Cell-Silicone Design with 1.5 [mm] composite thickness)

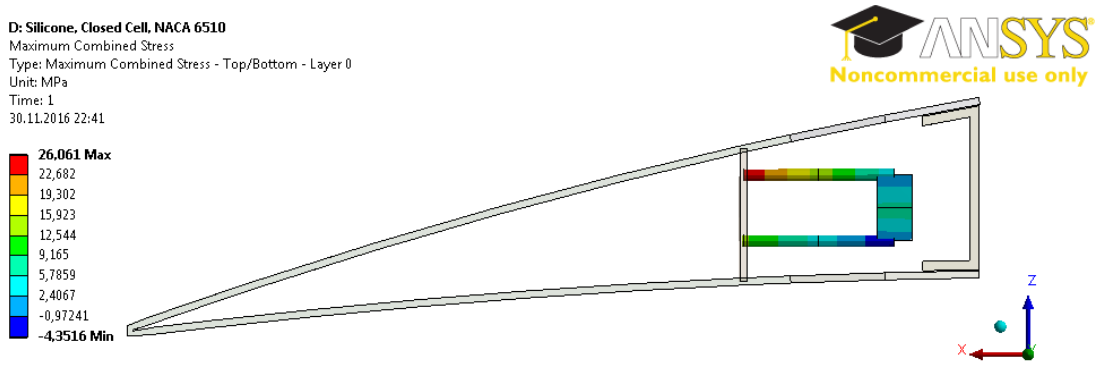

Figure 142: Maximum Beam Combined Stress Contour - Maintaining the NACA 6510 Profile (Max 26.06 [MPa], Closed Cell-Silicone Design with 1.5 [mm] composite thickness)

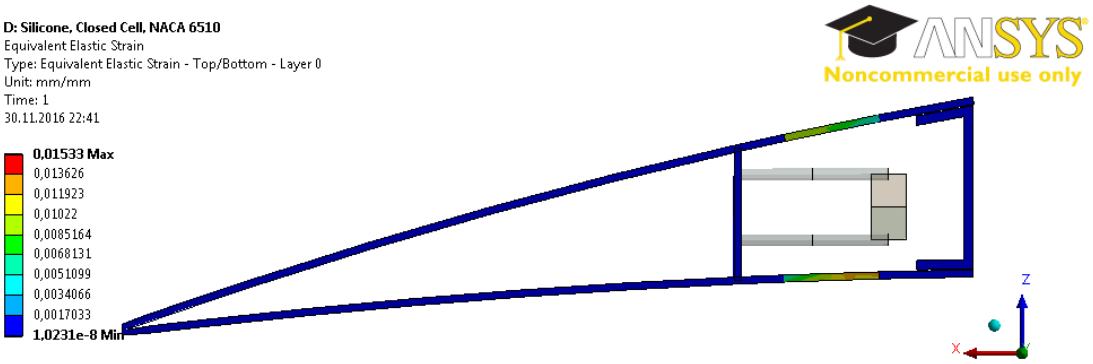

Figure 143: Equivalent Elastic Strain (von-Mises) Contour - Maintaining the NACA 6510 Profile (Max 0.02 [mm/mm], Closed Cell-Silicone Design with 1.5 [mm] composite thickness)

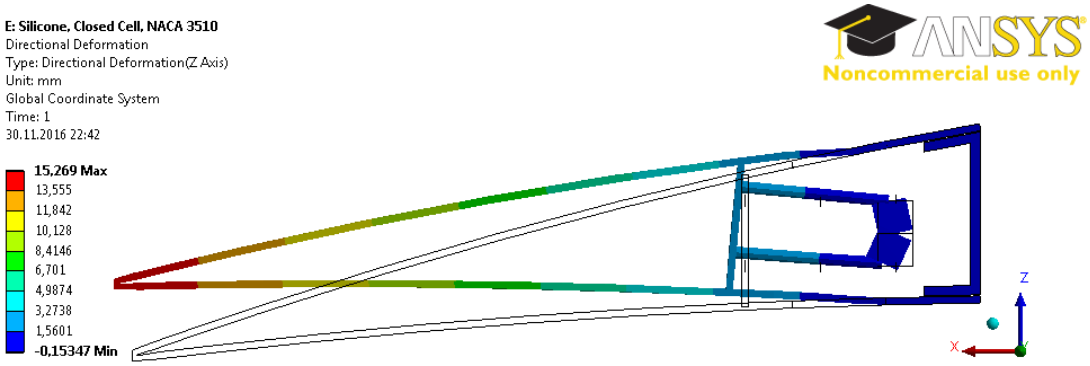

Figure 144: Displacement in z Direction Contour - Morphing from NACA 6510 to NACA 3510 Profile (Max 15.27 [mm], Closed Cell-Silicone Design with 1.5 [mm] composite thickness)

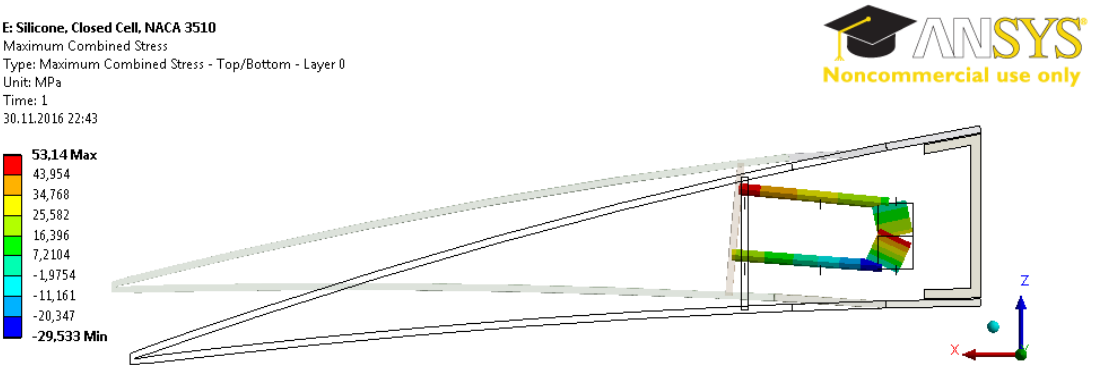

Figure 145: Maximum Beam Combined Stress Contour - Morphing from NACA 6510 to NACA 3510 Profile (Max 53.14 [MPa], Closed Cell-Silicone Design with 1.5 [mm] composite thickness)

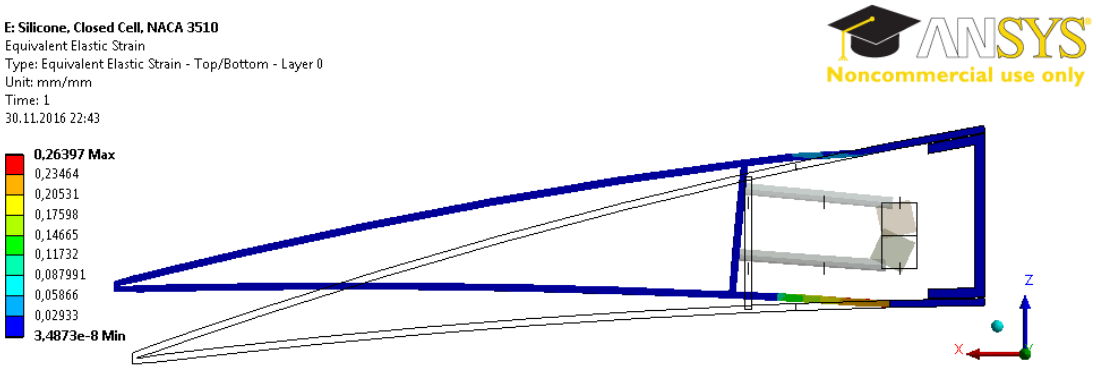

Figure 146: Equivalent Elastic Strain (von-Mises) Contour - Morphing from NACA 6510 to NACA 3510 Profile (Max 0.26 [mm/mm], Closed Cell-Silicone with 1.5 [mm] composite thickness)

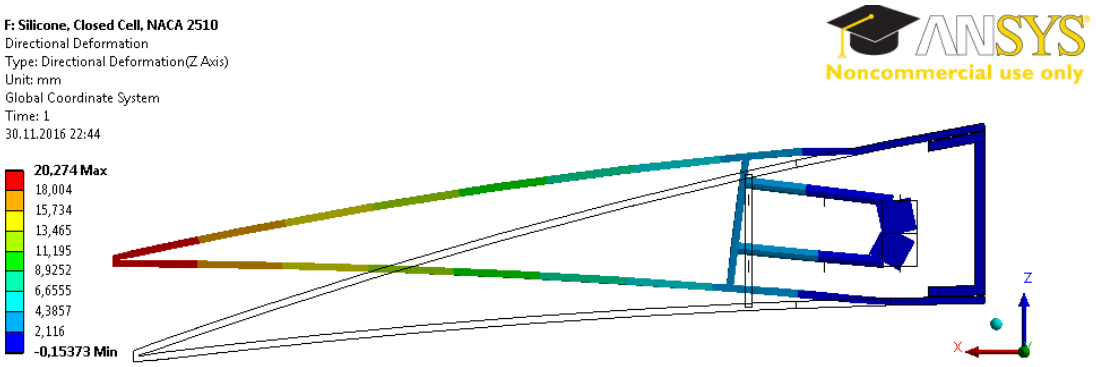

Figure 147: Displacement in z Direction Contour - Morphing from NACA 6510 to NACA 2510 Profile (Max 20.27 [mm], Closed Cell-Silicone Design with 1.5 [mm] composite thickness)

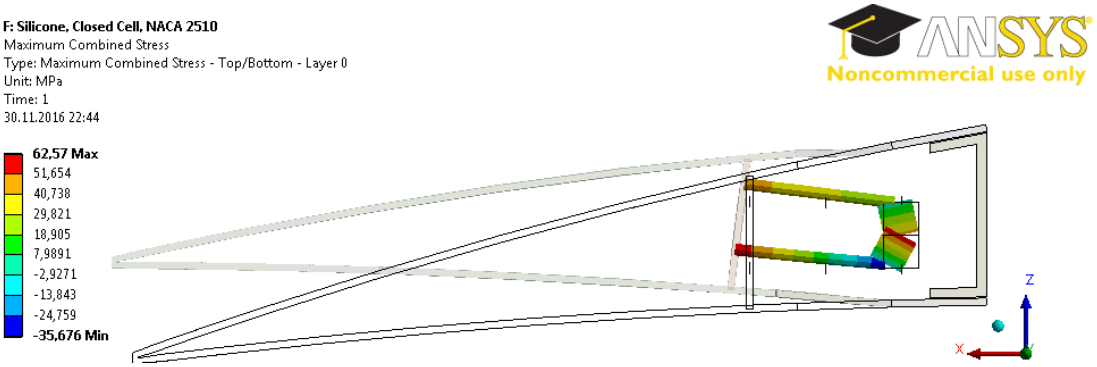

Figure 148: Maximum Beam Combined Stress Contour - Morphing from NACA 6510 to NACA 2510 Profile (Max 62.57 [MPa], Closed Cell-Silicone Design with 1.5 [mm] composite thickness)

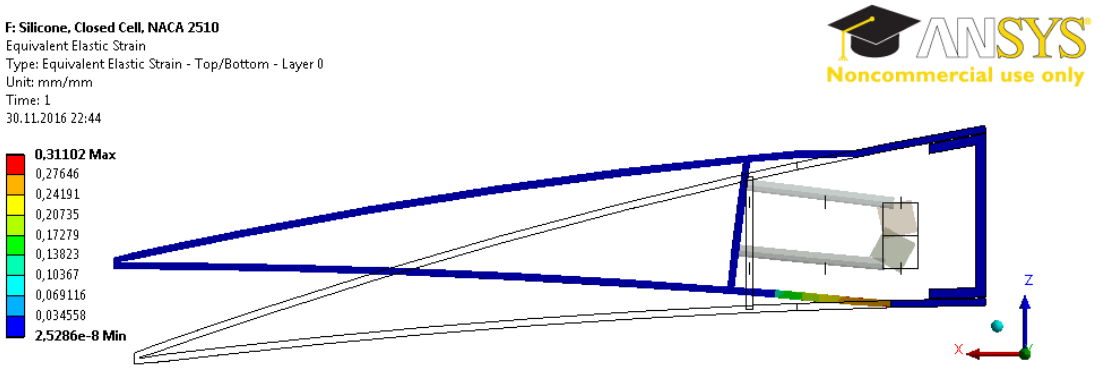

Figure 149: Equivalent Elastic Strain (von-Mises) Contour - Morphing from NACA 6510 to NACA 2510 Profile (Max 0.31 [mm/mm], Closed Cell-Silicone Design with 1.5 [mm] composite thickness)

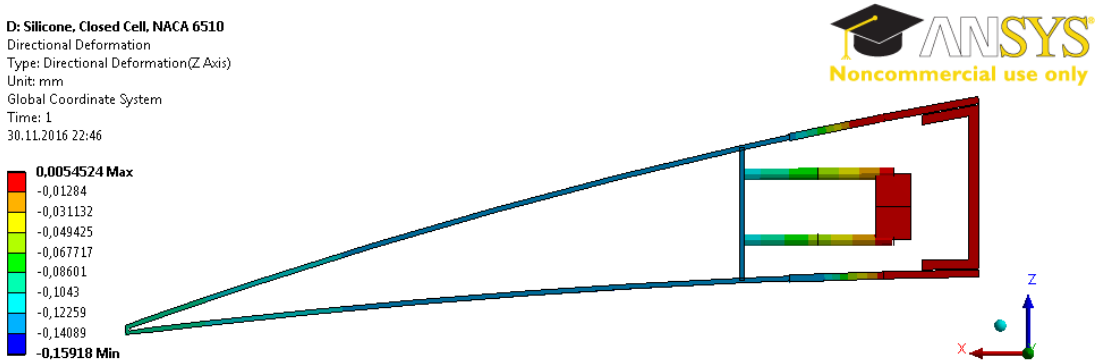

Figure 150: Displacement in z Direction Contour - Maintaining the NACA 6510 Profile (Max 0.01 [mm], Closed Cell-Silicone Design with 1.0 [mm] composite thickness)

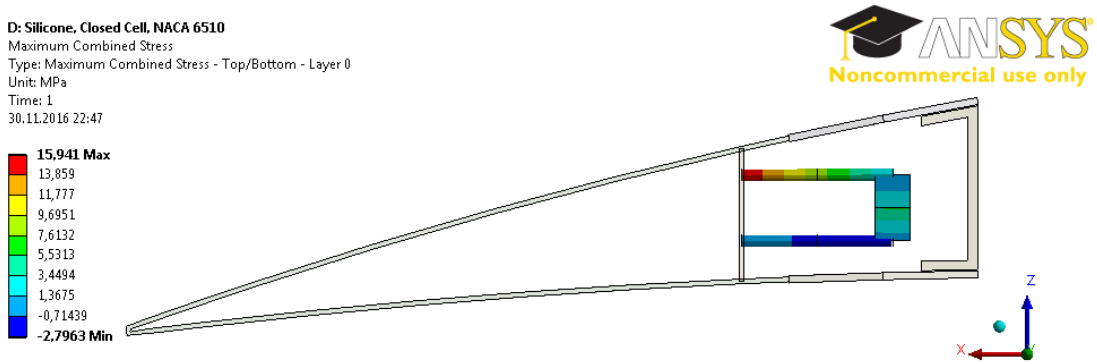

Figure 151: Maximum Beam Combined Stress Contour - Maintaining the NACA 6510 Profile (Max 15.94 [MPa], Closed Cell-Silicone Design with 1.0 [mm] composite thickness)

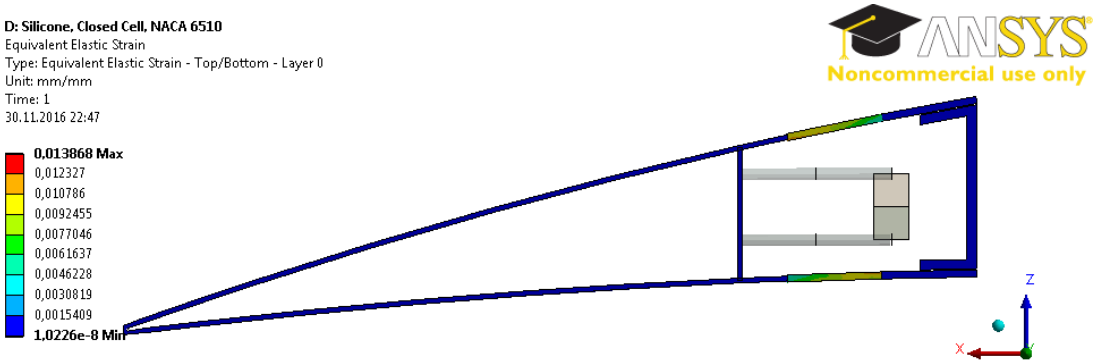

Figure 152: Equivalent Elastic Strain (von-Mises) Contour - Maintaining the NACA 6510 Profile (Max 0.01 [mm/mm], Closed Cell-Silicone Design with 1.0 [mm] composite thickness)

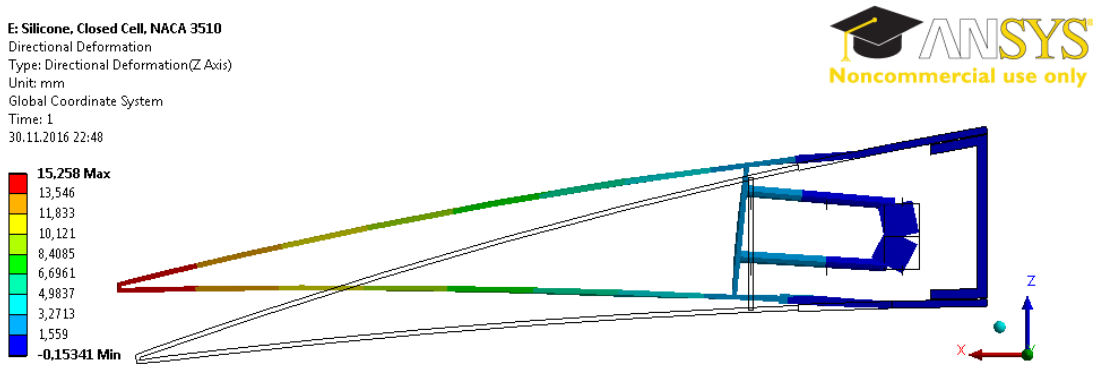

Figure 153: Displacement in z Direction Contour - Morphing from NACA 6510 to NACA 3510 Profile (Max 15.26 [mm], Closed Cell-Silicone Design with 1.0 [mm] composite thickness)

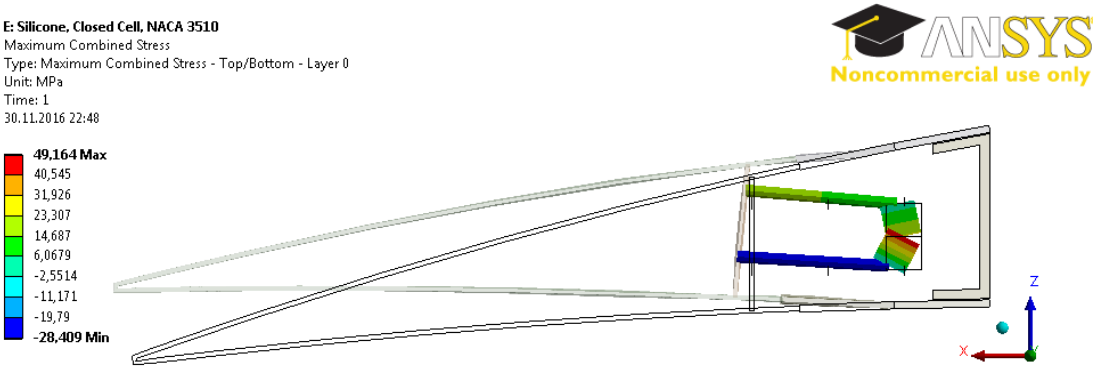

Figure 154: Maximum Beam Combined Stress Contour - Morphing from NACA 6510 to NACA 3510 Profile (Max 49.16 [MPa], Closed Cell-Silicone Design with 1.0 [mm] composite thickness)

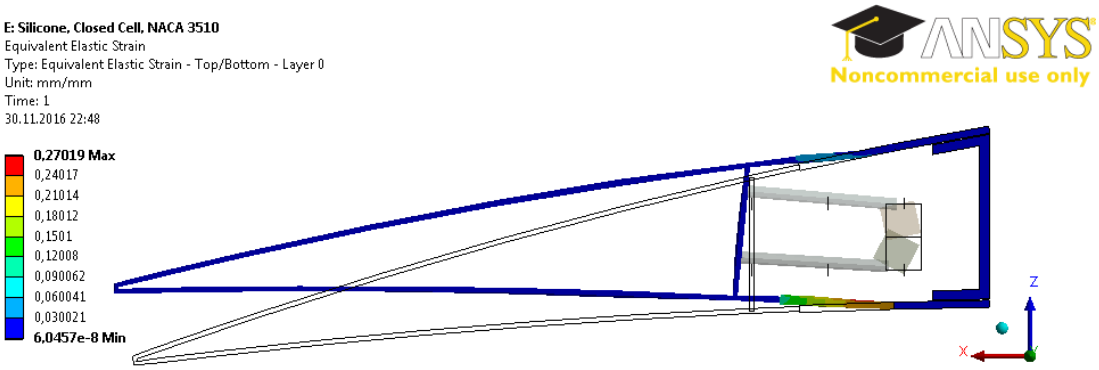

Figure 155: Equivalent Elastic Strain (von-Mises) Contour - Morphing from NACA 6510 to NACA 3510 Profile (Max 0.27 [mm/mm], Closed Cell-Silicone with 1.0 [mm] composite thickness)

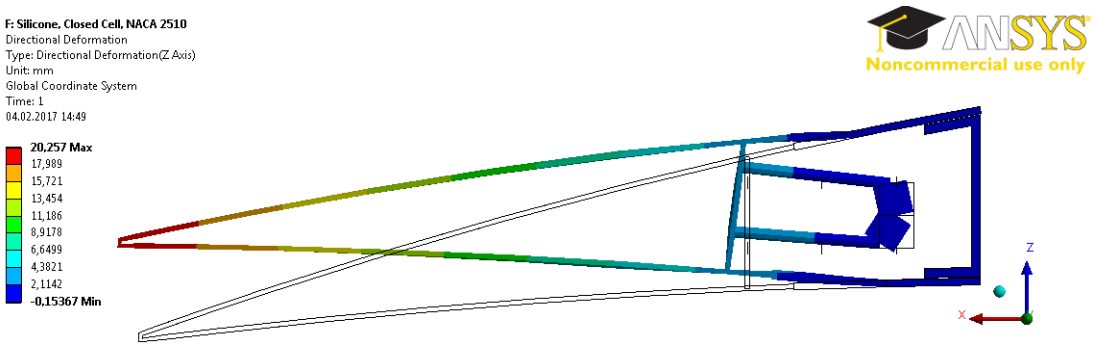

Figure 156: Displacement in z Direction Contour - Morphing from NACA 6510 to NACA 2510 Profile (Max 20.26 [mm], Closed Cell-Silicone Design with 1.0 [mm] composite thickness)

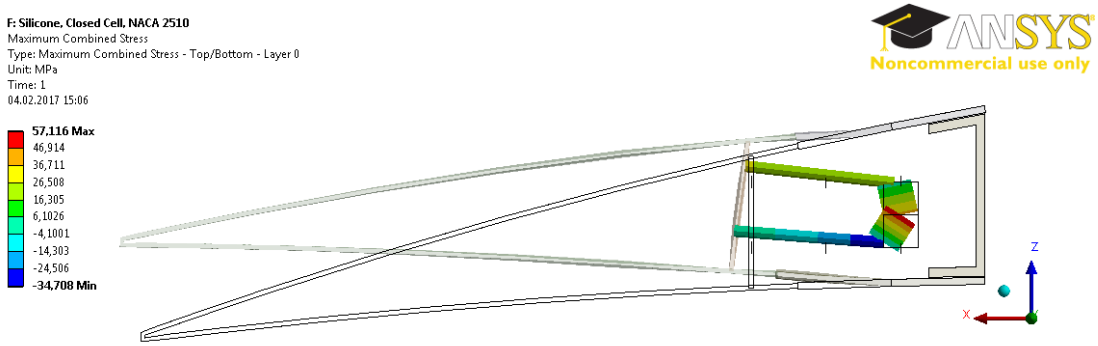

Figure 157: Maximum Beam Combined Stress Contour - Morphing from NACA 6510 to NACA 2510 Profile (Max 57.12 [MPa], Closed Cell-Silicone Design with 1.0 [mm] composite thickness)

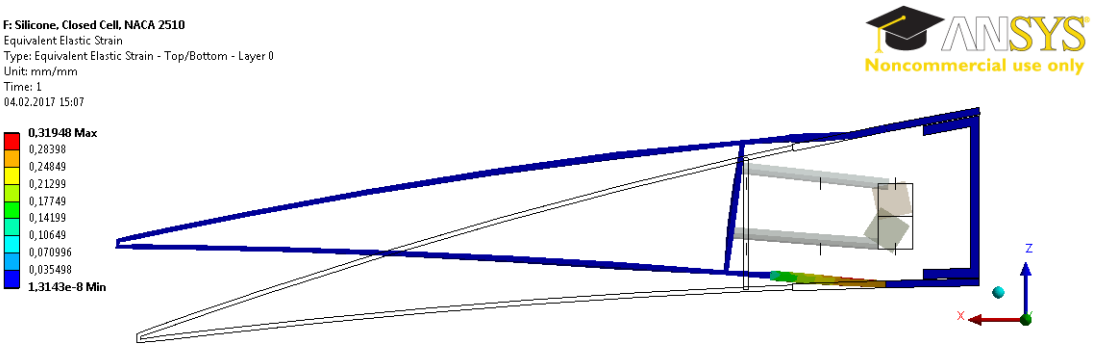

Figure 158: Equivalent Elastic Strain (von-Mises) Contour - Morphing from NACA 6510 to NACA 2510 Profile (Max 0.32 [mm/mm], Closed Cell-Silicone Design with 1.0 [mm] composite thickness)

APPENDIX B1

Closed Cell – Neoprene Rubber with 2.0 [mm] Composite Thickness Design Results

In this part, Closed Cell – Neoprene Rubber design analysis results under aerodynamic loads are presented for 2.0 [mm] composite thickness.

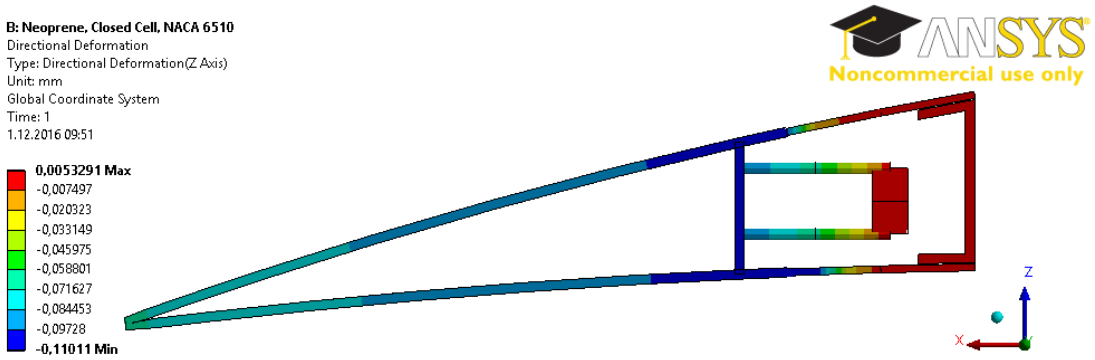

Figure 159: Displacement in z Direction Contour - Maintaining the NACA 6510 Profile under 1g Aerodynamic Loading (Max 0.01 [mm], Closed Cell- Neoprene Rubber Design with 2.0 [mm] composite thickness)

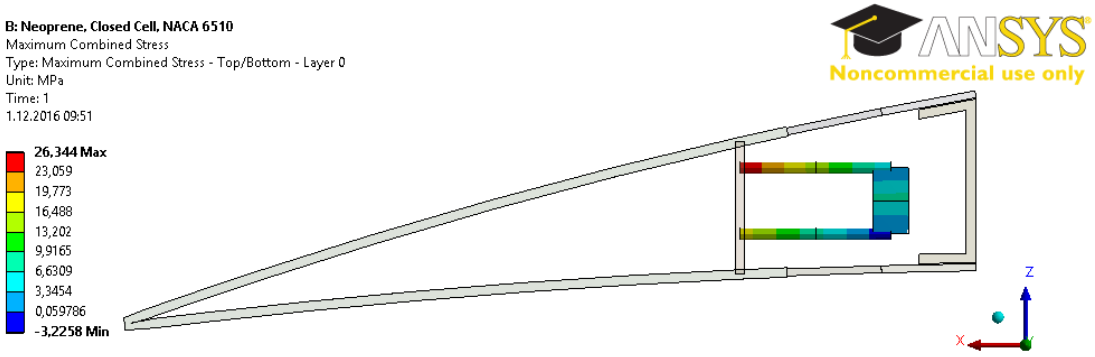

Figure 160: Maximum Beam Combined Stress Contour - Maintaining the NACA 6510 Profile under 1g Aerodynamic Loading (Max 26.34 [MPa], Closed Cell- Neoprene Rubber Design with 2.0 [mm] composite thickness)

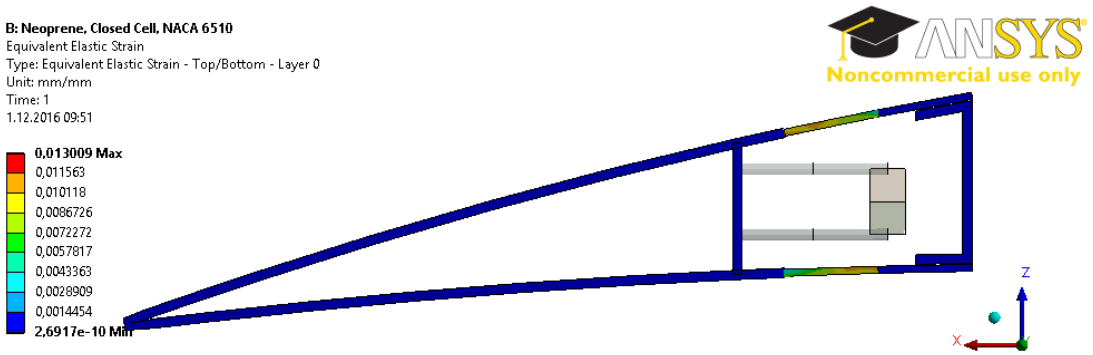

Figure 161: Equivalent Elastic Strain (von-Mises) Contour - Maintaining the NACA 6510 Profile under 1g Aerodynamic Loading (Max 0.01 [mm/mm], Closed Cell- Neoprene Rubber Design with 2.0 [mm] composite thickness)

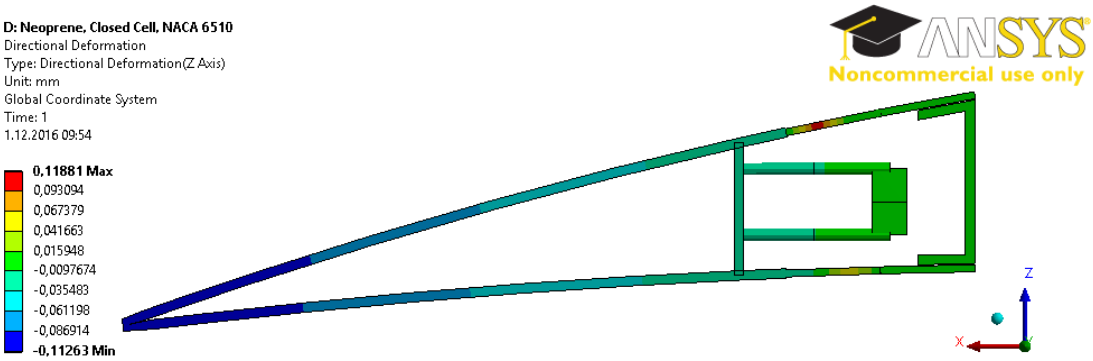

Figure 162: Displacement in z Direction Contour - Maintaining the NACA 6510 Profile under 2g Aerodynamic Loading (Max 0.12 [mm], Closed Cell- Neoprene Rubber Design with 2.0 [mm] composite thickness)

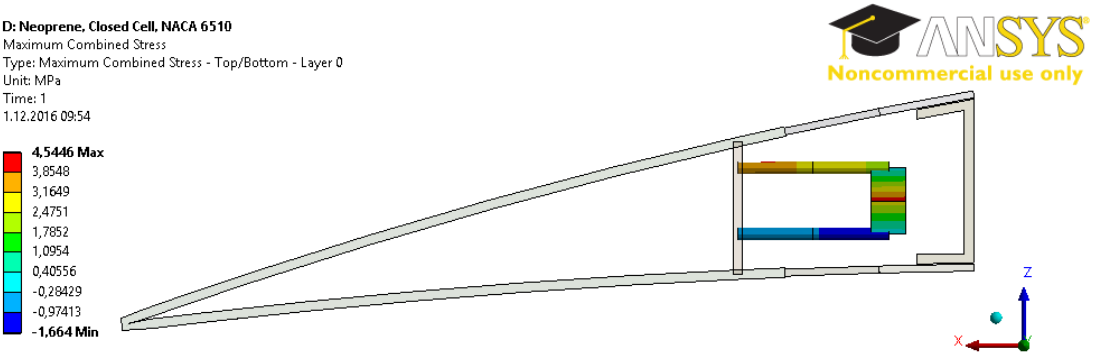

Figure 163: Maximum Beam Combined Stress Contour - Maintaining the NACA 6510 Profile under 2g Aerodynamic Loading (Max 4.54 [MPa], Closed Cell- Neoprene Rubber Design with 2.0 [mm] composite thickness)

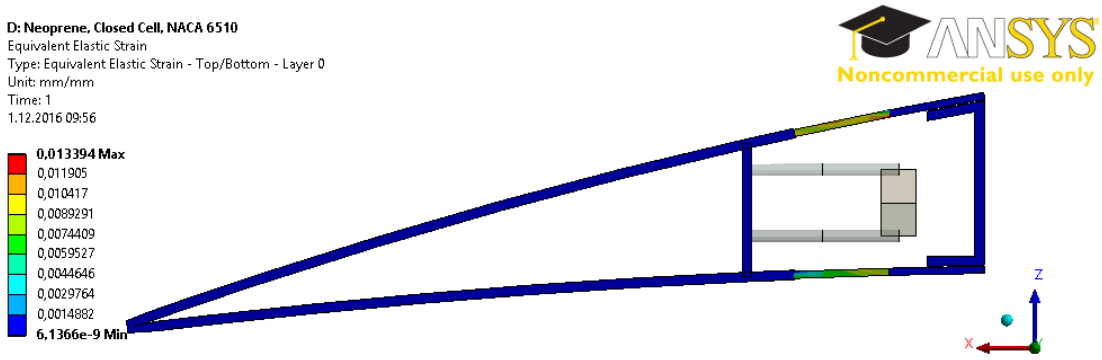

Figure 164: Equivalent Elastic Strain (von-Mises) Contour - Maintaining the NACA 6510 Profile under 2g Aerodynamic Loading (Max 0.01 [mm/mm], Closed Cell- Neoprene Rubber Design with 2.0 [mm] composite thickness)

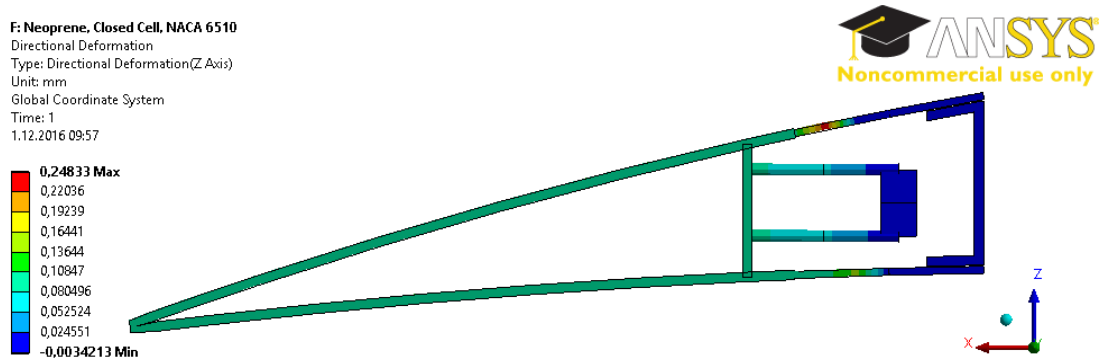

Figure 165: Displacement in z Direction Contour - Maintaining the NACA 6510 Profile under 3g Aerodynamic Loading (Max 0.25 [mm], Closed Cell- Neoprene Rubber Design with 2.0 [mm] composite thickness)

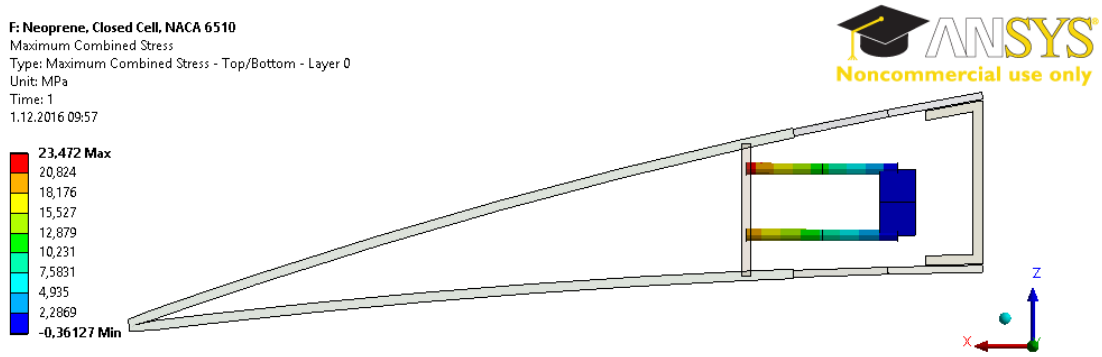

Figure 166: Maximum Beam Combined Stress Contour - Maintaining the NACA 6510 Profile under 3g Aerodynamic Loading (Max 23.47 [MPa], Closed Cell- Neoprene Rubber Design with 2.0 [mm] composite thickness)

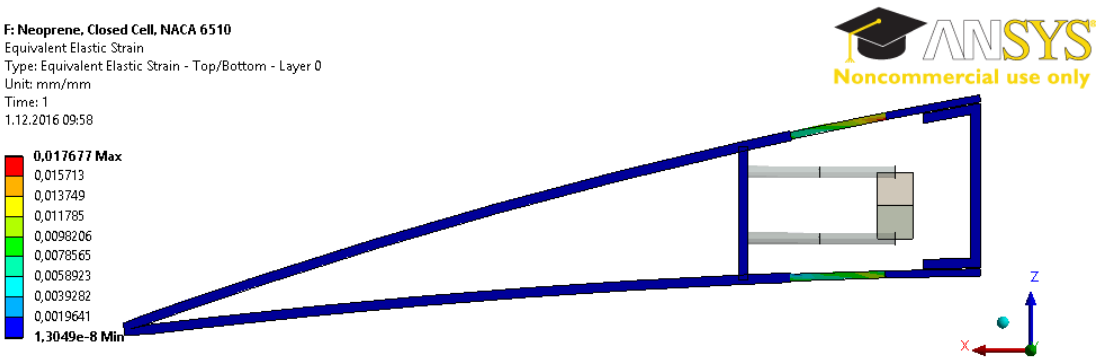

Figure 167: Equivalent Elastic Strain (von-Mises) Contour - Maintaining the NACA 6510 Profile under 3g Aerodynamic Loading (Max 0.02 [mm/mm], Closed Cell- Neoprene Rubber Design with 2.0 [mm] composite thickness)

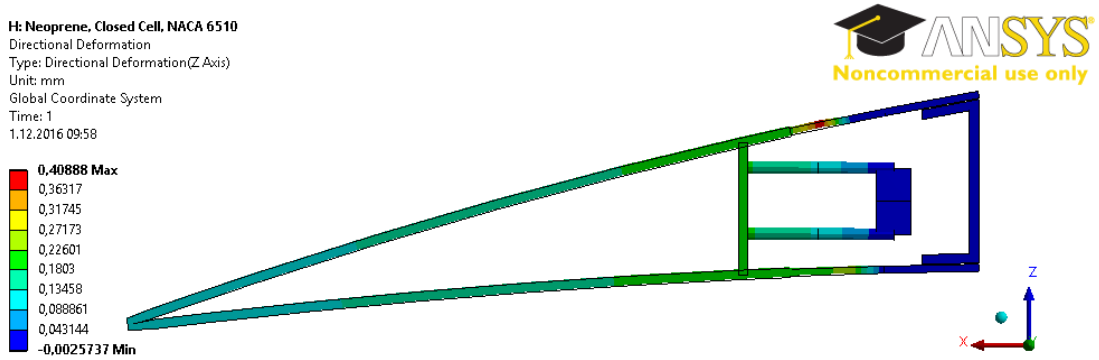

Figure 168: Displacement in z Direction Contour - Maintaining the NACA 6510 Profile under 4g Aerodynamic Loading (Max 0.41 [mm], Closed Cell- Neoprene Rubber Design with 2.0 [mm] composite thickness)

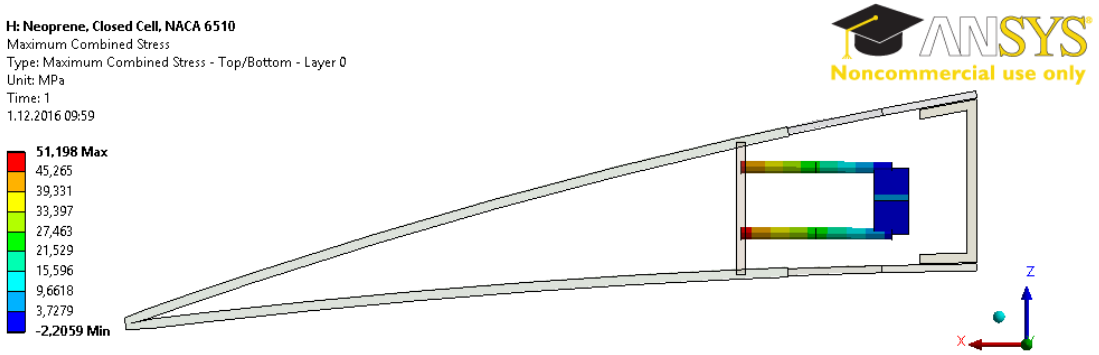

Figure 169: Maximum Beam Combined Stress Contour - Maintaining the NACA 6510 Profile under 4g Aerodynamic Loading (Max 51.20 [MPa], Closed Cell- Neoprene Rubber Design with 2.0 [mm] composite thickness)

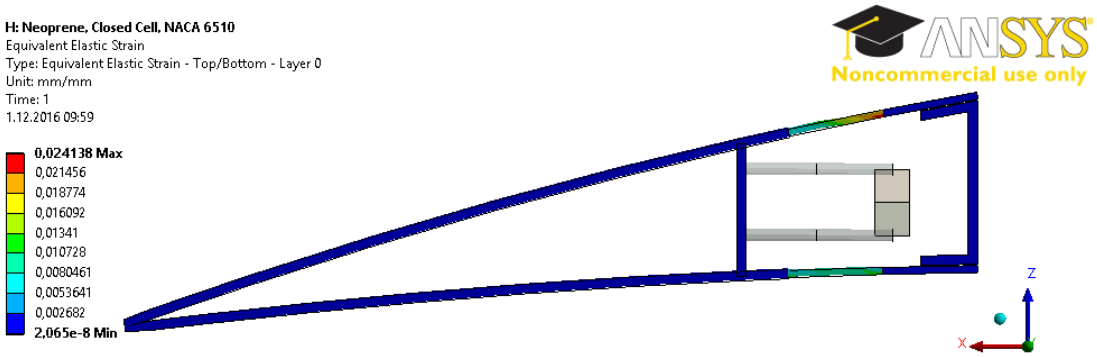

Figure 170: Equivalent Elastic Strain (von-Mises) Contour - Maintaining the NACA 6510 Profile under 4g Aerodynamic Loading (Max 0.02 [mm/mm], Closed Cell-Neoprene Rubber Design with 2.0 [mm] composite thickness)

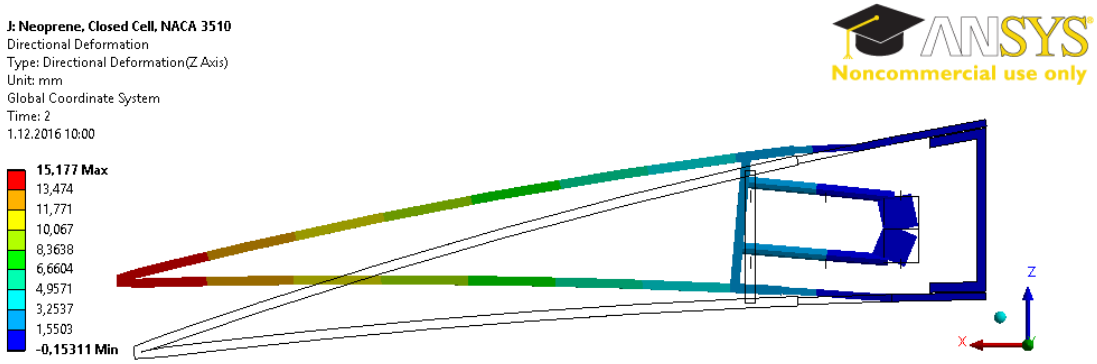

Figure 171: Displacement in z Direction Contour - Morphing from NACA 6510 to NACA 3510 Profile under 1g Aerodynamic Loading (Max 15.18 [mm], Closed Cell-Neoprene Rubber Design with 2.0 [mm] composite thickness)

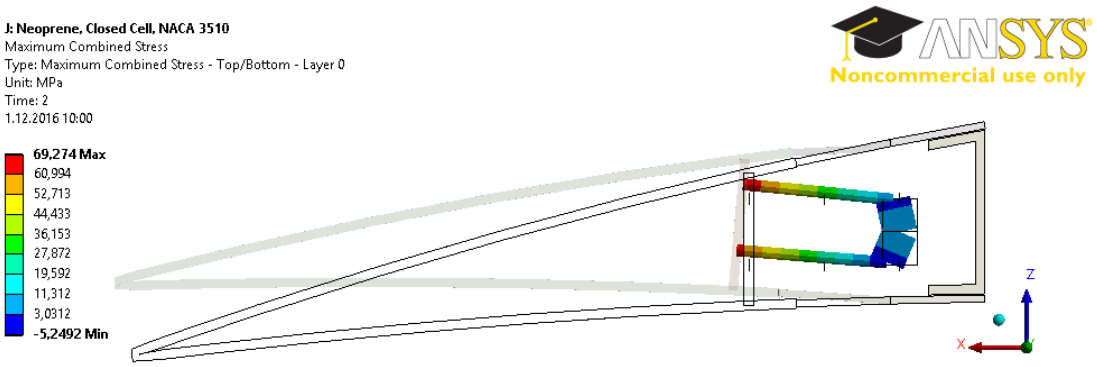

Figure 172: Maximum Beam Combined Stress Contour - Morphing from NACA 6510 to NACA 3510 Profile under 1g Aerodynamic Loading (Max 69.27 [MPa], Closed Cell-Neoprene Rubber Design with 2.0 [mm] composite thickness)

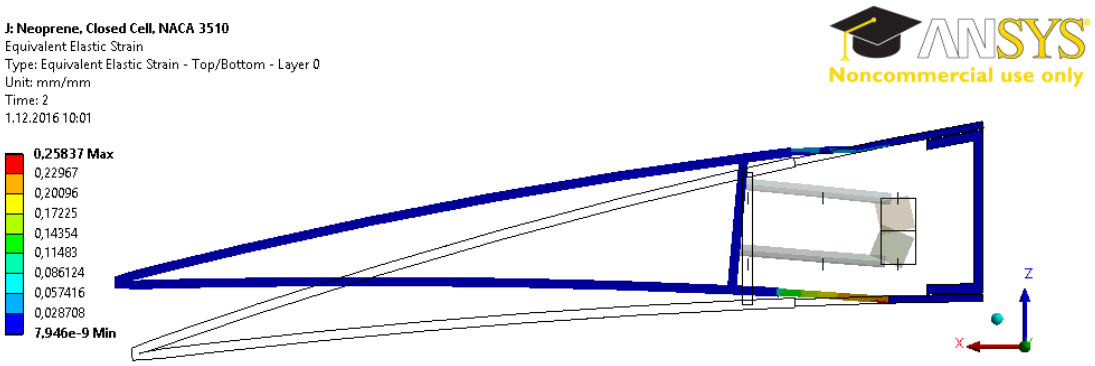

Figure 173: Equivalent Elastic Strain (von-Mises) Contour - Morphing from NACA 6510 to NACA 3510 Profile under 1g Aerodynamic Loading (Max 0.26 [mm/mm], Closed Cell-Neoprene Rubber Design with 2.0 [mm] composite thickness)

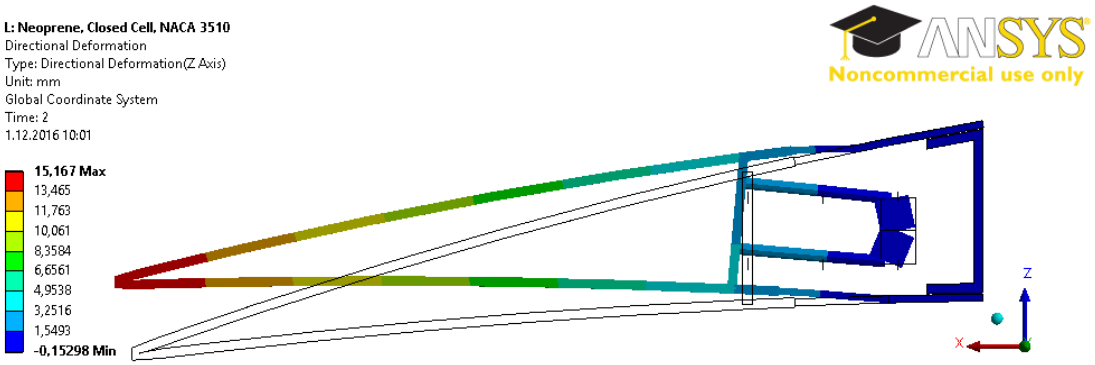

Figure 174: Displacement in z Direction Contour - Morphing from NACA 6510 to NACA 3510 Profile under 2g Aerodynamic Loading (Max 15.17 [mm], Closed Cell-Neoprene Rubber Design with 2.0 [mm] composite thickness)

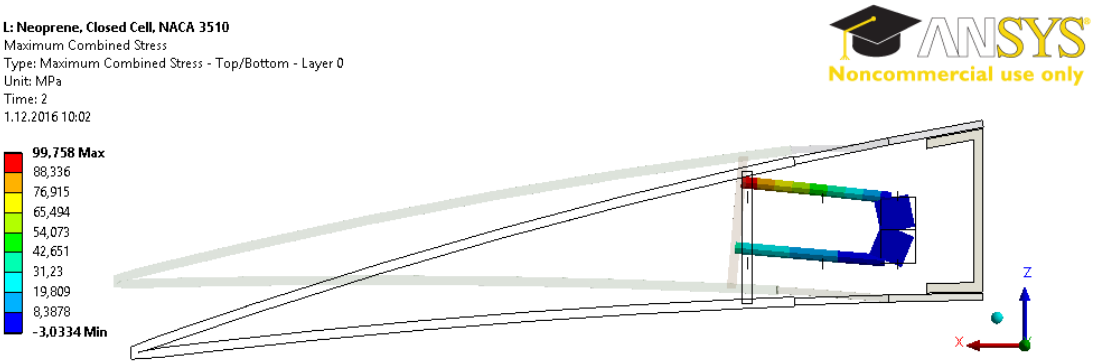

Figure 175: Maximum Beam Combined Stress Contour - Morphing from NACA 6510 to NACA 3510 Profile under 2g Aerodynamic Loading (Max 99.76 [MPa], Closed Cell-Neoprene Rubber Design with 2.0 [mm] composite thickness)

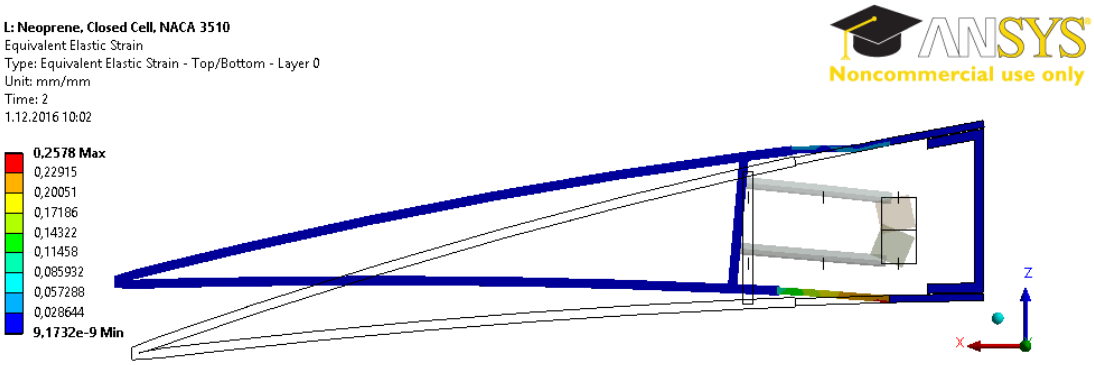

Figure 176: Equivalent Elastic Strain (von-Mises) Contour - Morphing from NACA 6510 to NACA 3510 Profile under 2g Aerodynamic Loading (Max 0.26 [mm/mm], Closed Cell-Neoprene Rubber Design with 2.0 [mm] composite thickness)

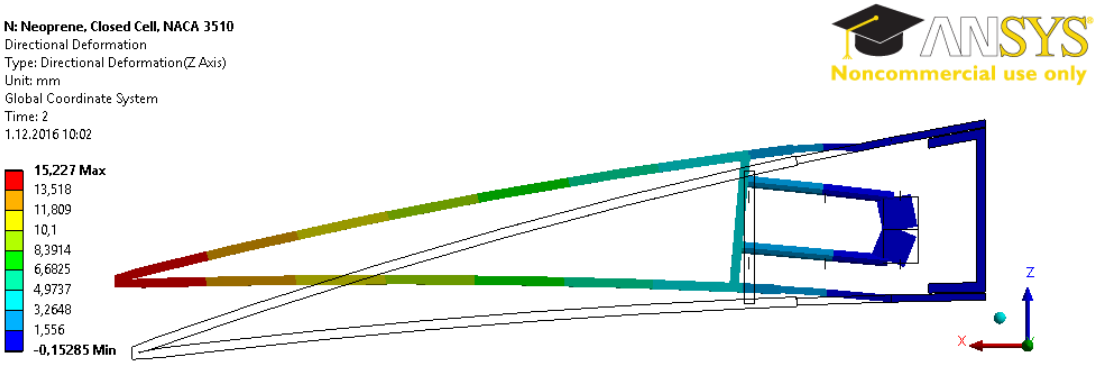

Figure 177: Displacement in z Direction Contour - Morphing from NACA 6510 to NACA 3510 Profile under 3g Aerodynamic Loading (Max 15.23 [mm], Closed Cell-Neoprene Rubber Design with 2.0 [mm] composite thickness)

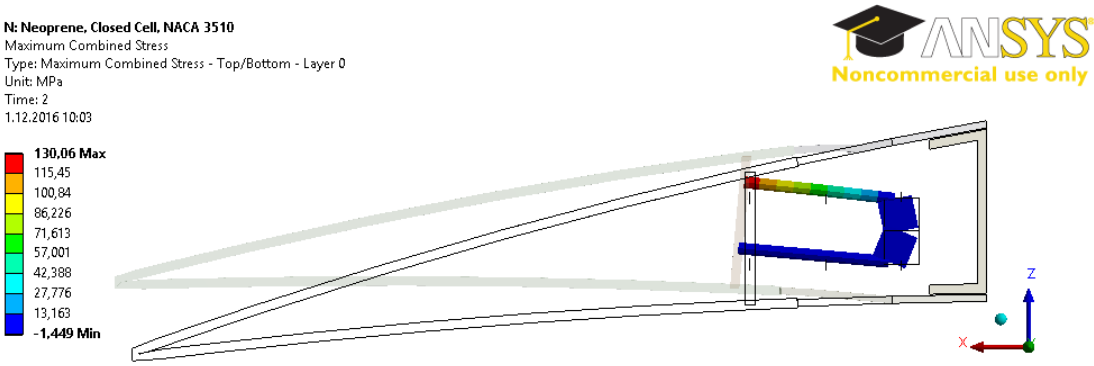

Figure 178: Maximum Beam Combined Stress Contour - Morphing from NACA 6510 to NACA 3510 Profile under 3g Aerodynamic Loading (Max 130.06 [MPa], Closed Cell-Neoprene Rubber Design with 2.0 [mm] composite thickness)

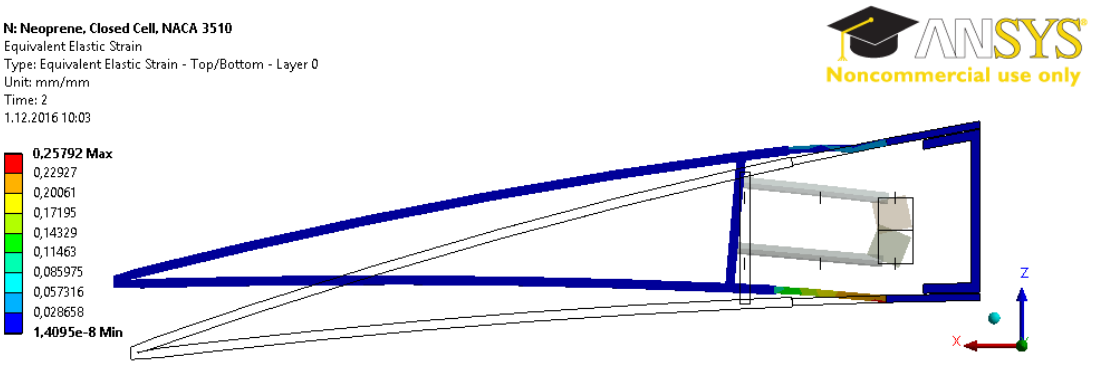

Figure 179: Equivalent Elastic Strain (von-Mises) Contour - Morphing from NACA 6510 to NACA 3510 Profile under 3g Aerodynamic Loading (Max 0.26 [mm/mm], Closed Cell-Neoprene Rubber Design with 2.0 [mm] composite thickness)

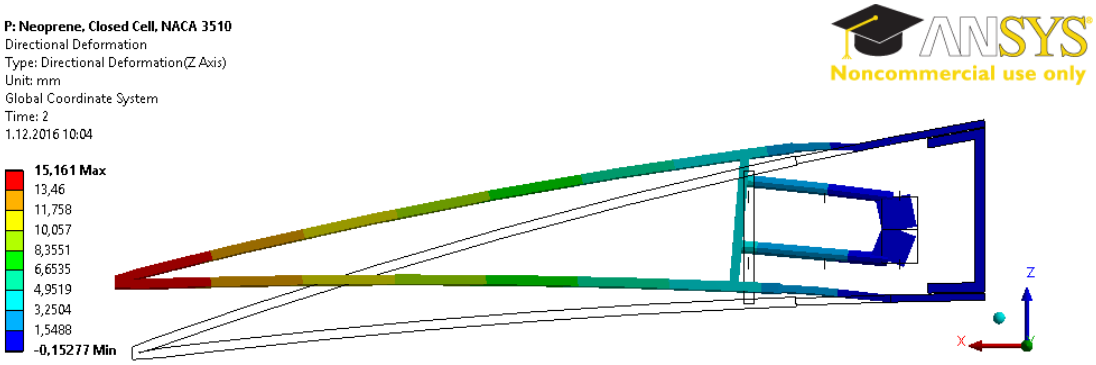

Figure 180: Displacement in z Direction Contour - Morphing from NACA 6510 to NACA 3510 Profile under 4g Aerodynamic Loading (Max 15.16 [mm], Closed Cell-Neoprene Rubber Design with 2.0 [mm] composite thickness)

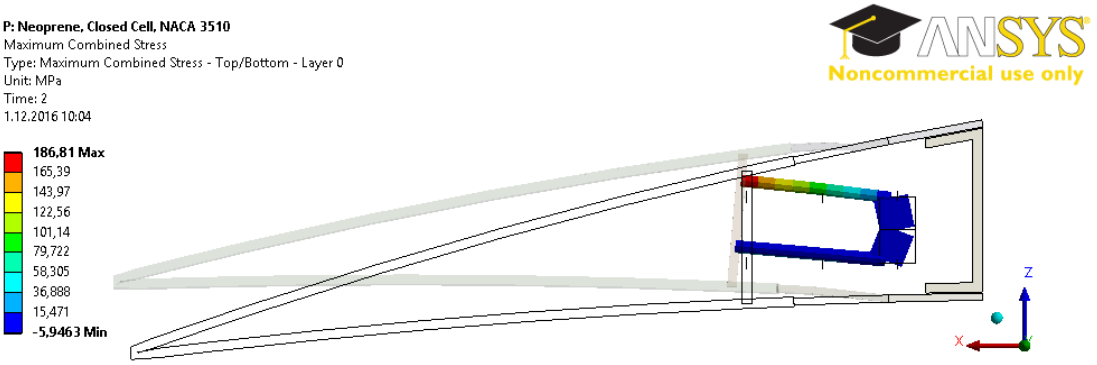

Figure 181: Maximum Beam Combined Stress Contour - Morphing from NACA 6510 to NACA 3510 Profile under 4g Aerodynamic Loading (Max 186.81 [MPa], Closed Cell-Neoprene Rubber Design with 2.0 [mm] composite thickness)

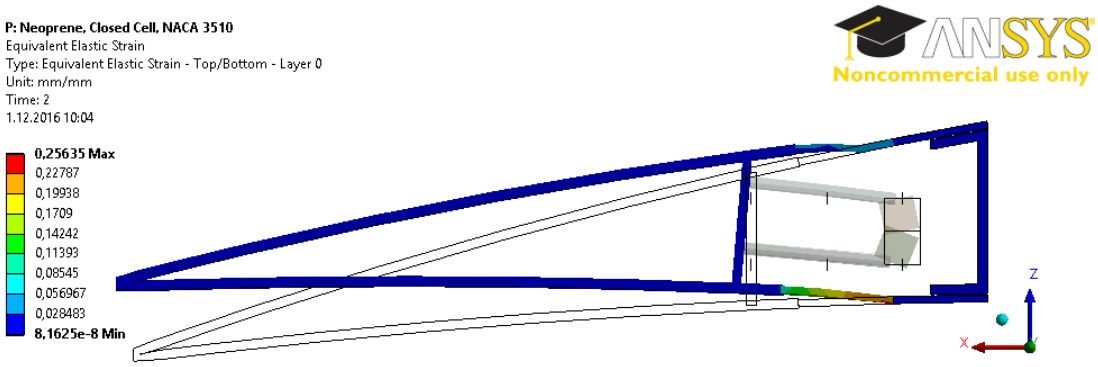

Figure 182: Equivalent Elastic Strain (von-Mises) Contour - Morphing from NACA 6510 to NACA 3510 Profile under 4g Aerodynamic Loading (Max 0.26 [mm/mm], Closed Cell-Neoprene Rubber Design with 2.0 [mm] composite thickness)

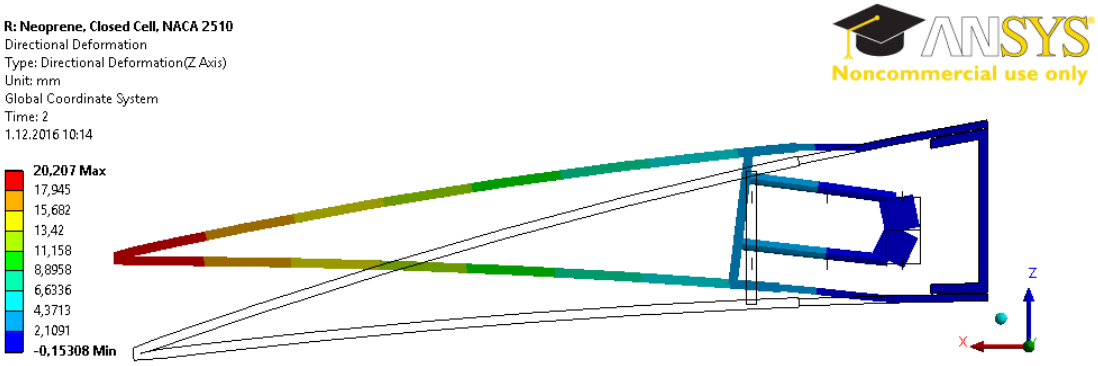

Figure 183: Displacement in z Direction Contour - Morphing from NACA 6510 to NACA 2510 Profile under 1g Aerodynamic Loading (Max 20.21 [mm], Closed Cell-Neoprene Rubber Design with 2.0 [mm] composite thickness)

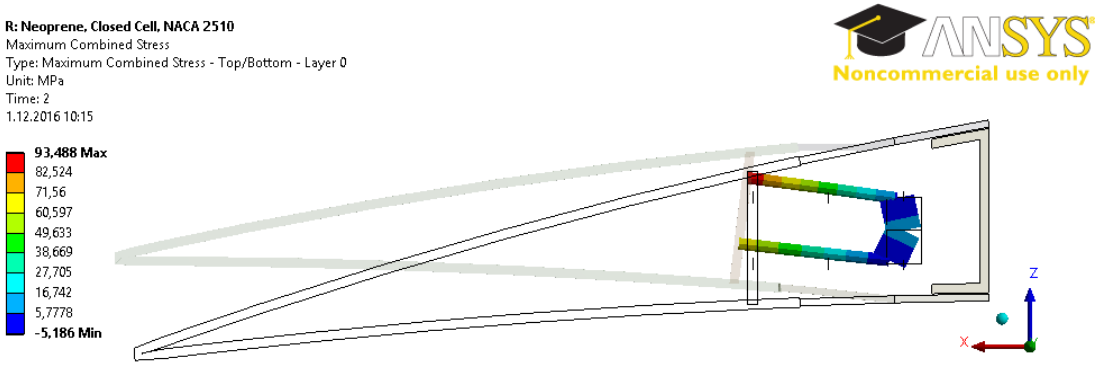

Figure 184: Maximum Beam Combined Stress Contour - Morphing from NACA 6510 to NACA 2510 Profile under 1g Aerodynamic Loading (Max 93.49 [MPa], Closed Cell-Neoprene Rubber Design with 2.0 [mm] composite thickness)

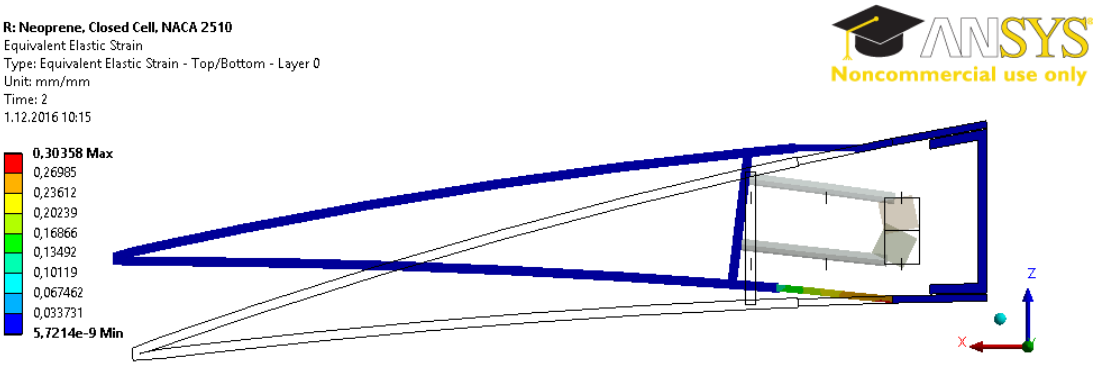

Figure 185: Equivalent Elastic Strain (von-Mises) Contour - Morphing from NACA 6510 to NACA 2510 Profile under 1g Aerodynamic Loading (Max 0.30 [mm/mm], Closed Cell-Neoprene Rubber Design with 2.0 [mm] composite thickness)

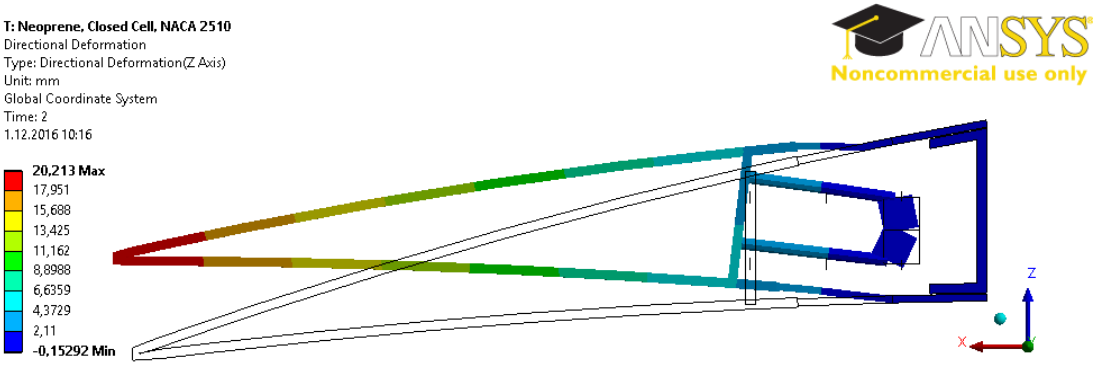

Figure 186: Displacement in z Direction Contour - Morphing from NACA 6510 to NACA 2510 Profile under 2g Aerodynamic Loading (Max 20.21 [mm], Closed Cell-Neoprene Rubber Design with 2.0 [mm] composite thickness)

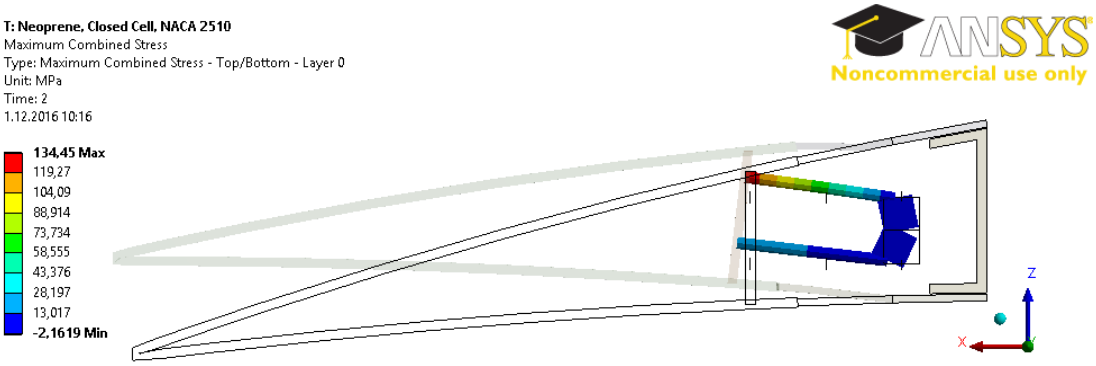

Figure 187: Maximum Beam Combined Stress Contour - Morphing from NACA 6510 to NACA 2510 Profile under 2g Aerodynamic Loading (Max 134.45 [MPa], Closed Cell-Neoprene Rubber Design with 2.0 [mm] composite thickness)

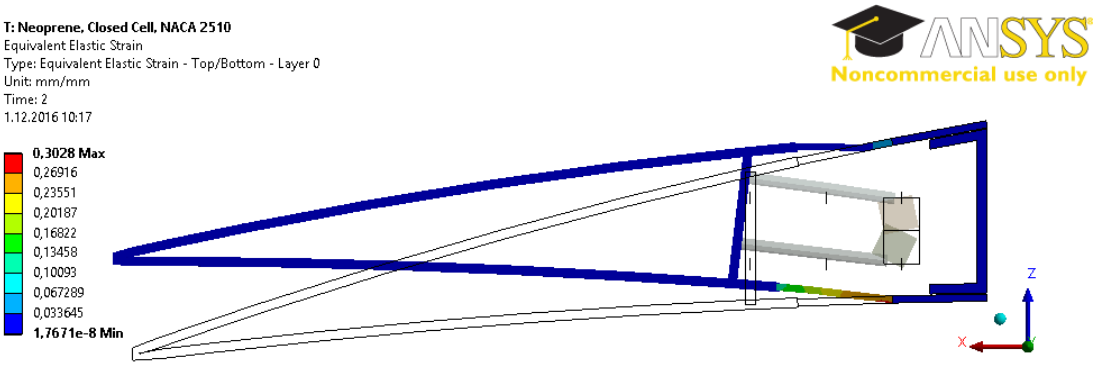

Figure 188: Equivalent Elastic Strain (von-Mises) Contour - Morphing from NACA 6510 to NACA 2510 Profile under 2g Aerodynamic Loading (Max 0.30 [mm/mm], Closed Cell-Neoprene Rubber Design with 2.0 [mm] composite thickness)

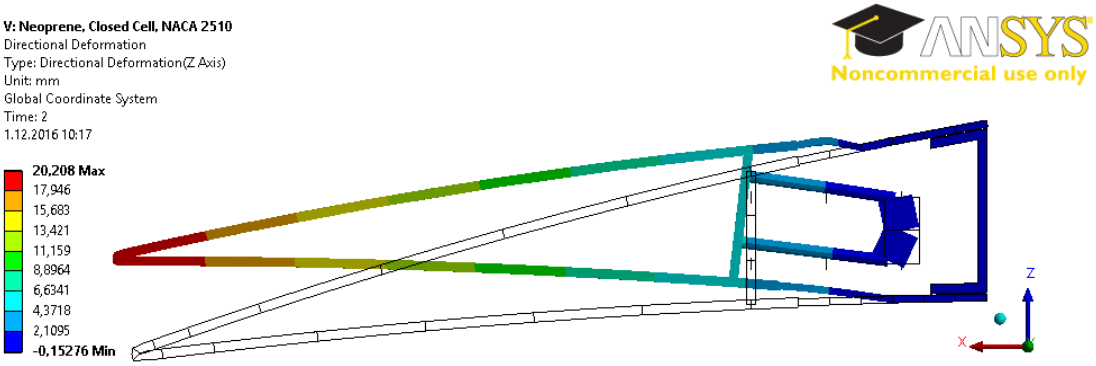

Figure 189: Displacement in z Direction Contour - Morphing from NACA 6510 to NACA 2510 Profile under 3g Aerodynamic Loading (Max 20.21 [mm], Closed Cell-Neoprene Rubber Design with 2.0 [mm] composite thickness)

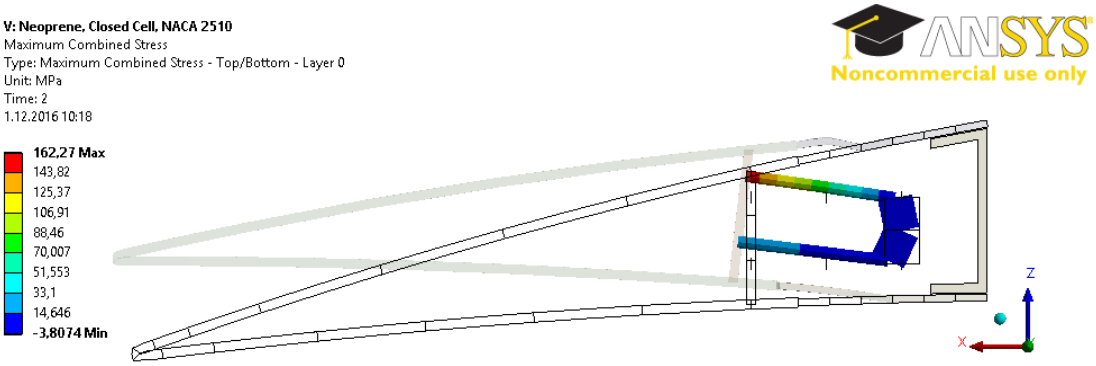

Figure 190: Maximum Beam Combined Stress Contour - Morphing from NACA 6510 to NACA 2510 Profile under 3g Aerodynamic Loading (Max 162.27 [MPa], Closed Cell-Neoprene Rubber Design with 2.0 [mm] composite thickness)

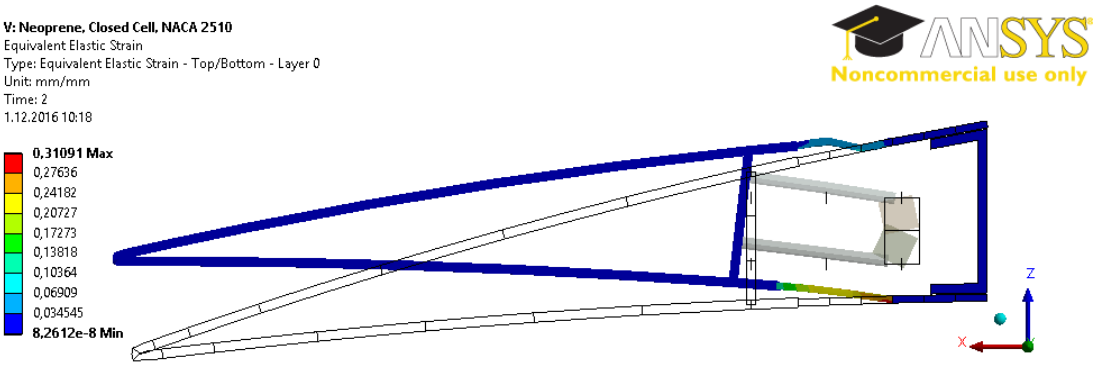

Figure 191: Equivalent Elastic Strain (von-Mises) Contour - Morphing from NACA 6510 to NACA 2510 Profile under 3g Aerodynamic Loading (Max 0.31 [mm/mm], Closed Cell-Neoprene Rubber Design with 2.0 [mm] composite thickness)

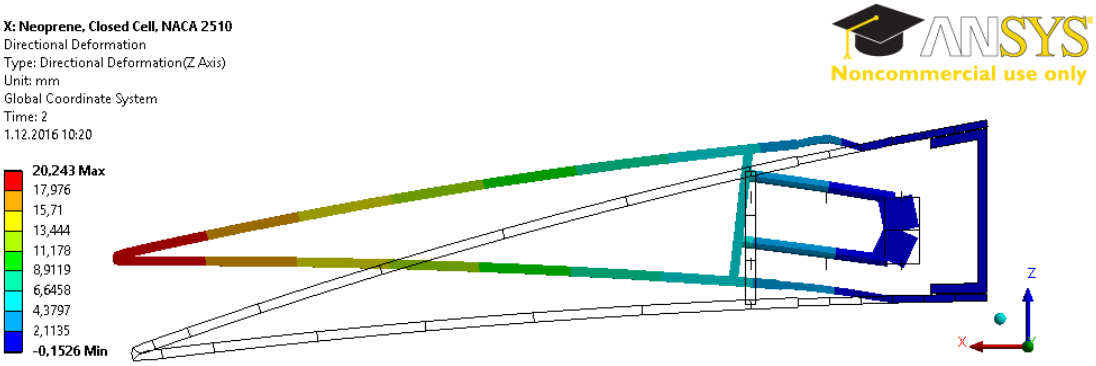

Figure 192: Displacement in z Direction Contour - Morphing from NACA 6510 to NACA 2510 Profile under 4g Aerodynamic Loading (Max 20.24 [mm], Closed Cell-Neoprene Rubber Design with 2.0 [mm] composite thickness)

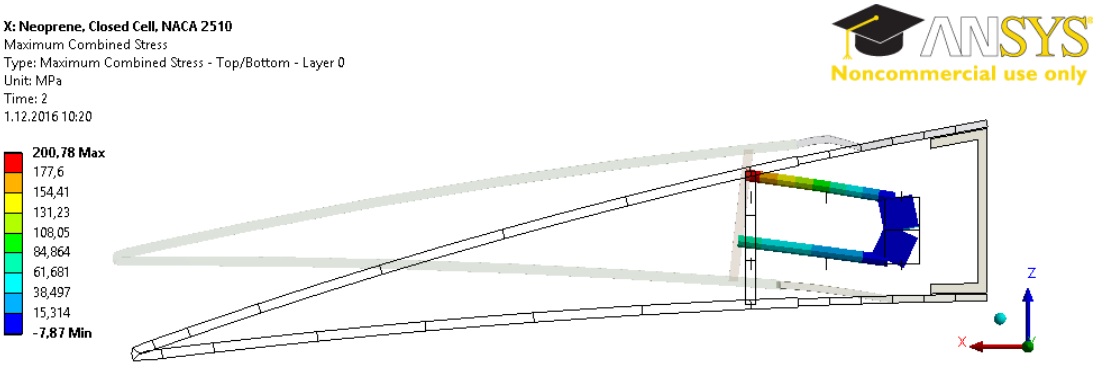

Figure 193: Maximum Beam Combined Stress Contour - Morphing from NACA 6510 to NACA 2510 Profile under 4g Aerodynamic Loading (Max 200.78 [MPa], Closed Cell-Neoprene Rubber Design with 2.0 [mm] composite thickness)

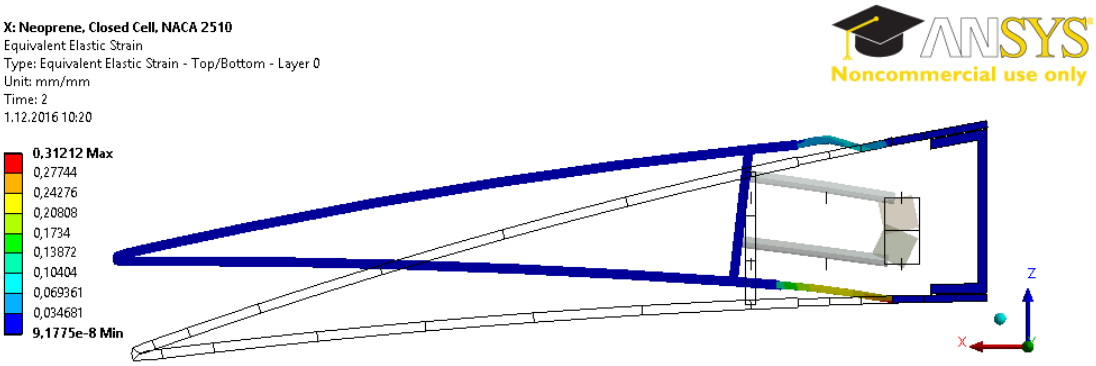

Figure 194: Equivalent Elastic Strain (von-Mises) Contour - Morphing from NACA 6510 to NACA 2510 Profile under 4g Aerodynamic Loading (Max 0.31 [mm/mm], Closed Cell-Neoprene Rubber Design with 2.0 [mm] composite thickness)

APPENDIX B2

Closed Cell – Neoprene Rubber with 1.5 [mm] Composite Thickness Design Results

In this part, Closed Cell – Neoprene Rubber design analysis results under aerodynamic loads are presented for 1.5 [mm] composite thickness.

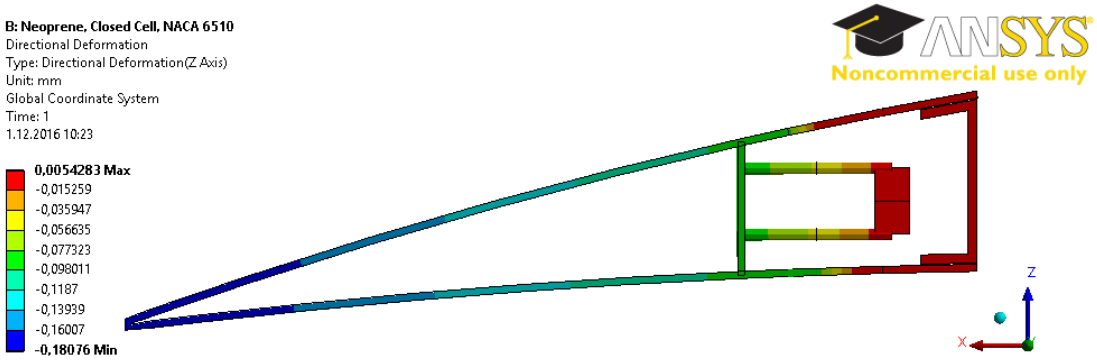

Figure 195: Displacement in z Direction Contour - Maintaining the NACA 6510 Profile under 1g Aerodynamic Loading (Max 0.01 [mm], Closed Cell- Neoprene Rubber Design with 1.5 [mm] composite thickness)

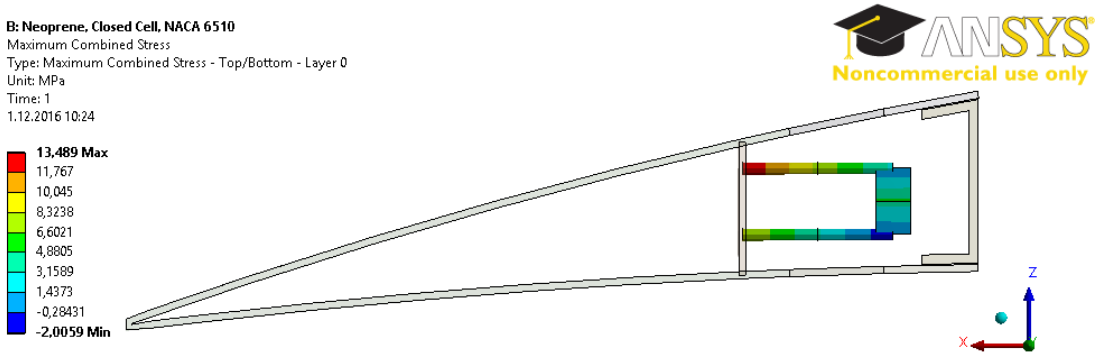

Figure 196: Maximum Beam Combined Stress Contour - Maintaining the NACA 6510 Profile under 1g Aerodynamic Loading (Max 13.49 [MPa], Closed Cell- Neoprene Rubber Design with 1.5 [mm] composite thickness)

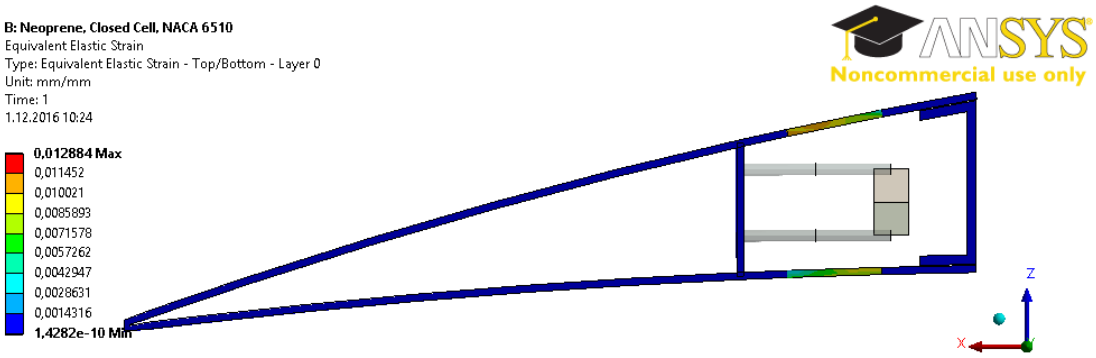

Figure 197: Equivalent Elastic Strain (von-Mises) Contour - Maintaining the NACA 6510 Profile under 1g Aerodynamic Loading (Max 0.01 [mm/mm], Closed Cell- Neoprene Rubber Design with 1.5 [mm] composite thickness)

Figure 198: Displacement in z Direction Contour - Maintaining the NACA 6510 Profile under 2g Aerodynamic Loading (Max 0.16 [mm], Closed Cell- Neoprene Rubber Design with 1.5 [mm] composite thickness)

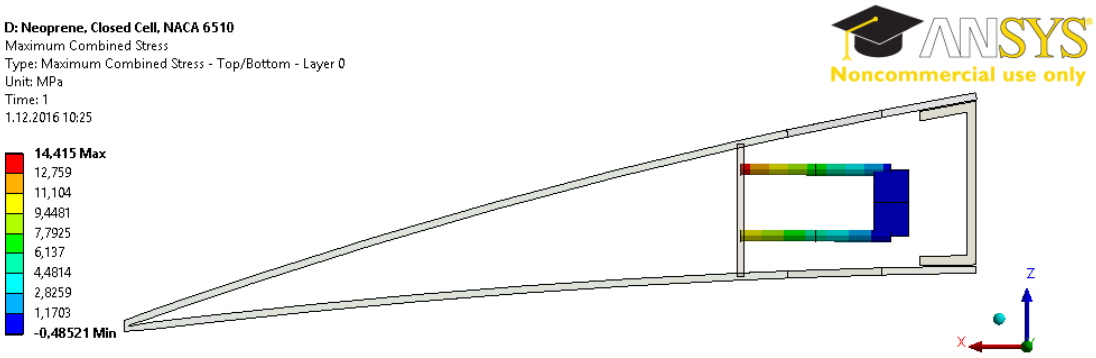

Figure 199: Maximum Beam Combined Stress Contour - Maintaining the NACA 6510 Profile under 2g Aerodynamic Loading (Max 14.42 [MPa], Closed Cell- Neoprene Rubber Design with 1.5 [mm] composite thickness)

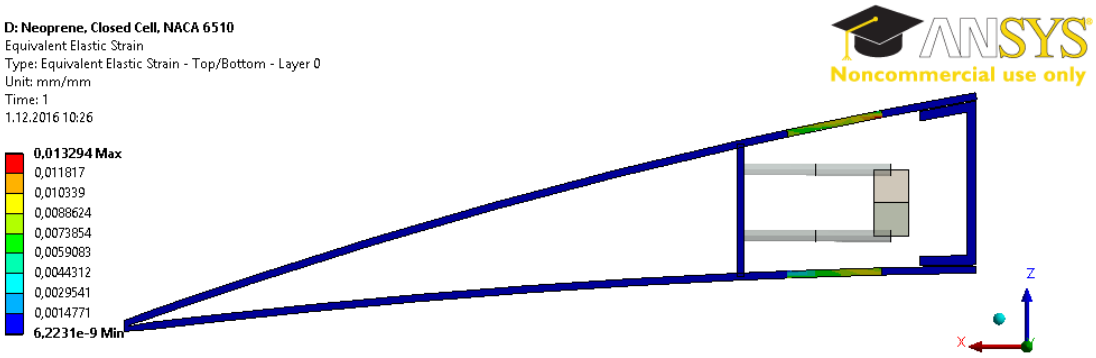

Figure 200: Equivalent Elastic Strain (von-Mises) Contour - Maintaining the NACA 6510 Profile under 2g Aerodynamic Loading (Max 0.01 [mm/mm], Closed Cell- Neoprene Rubber Design with 1.5 [mm] composite thickness)

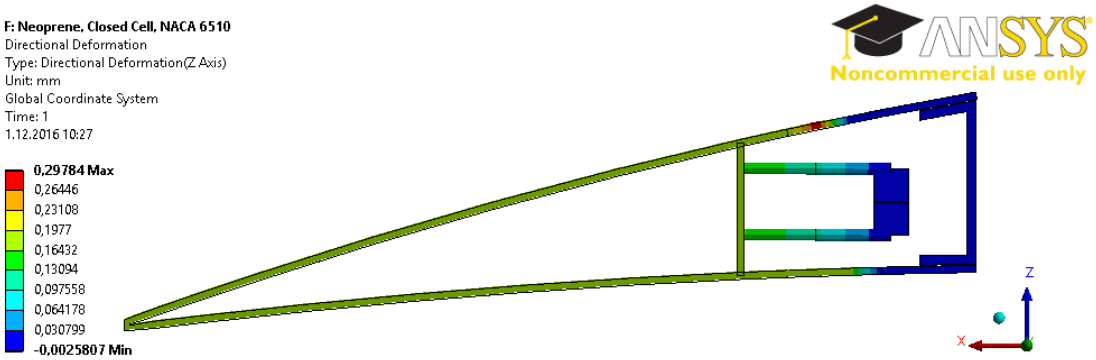

Figure 201: Displacement in z Direction Contour - Maintaining the NACA 6510 Profile under 3g Aerodynamic Loading (Max 0.30 [mm], Closed Cell- Neoprene Rubber Design with 1.5 [mm] composite thickness)

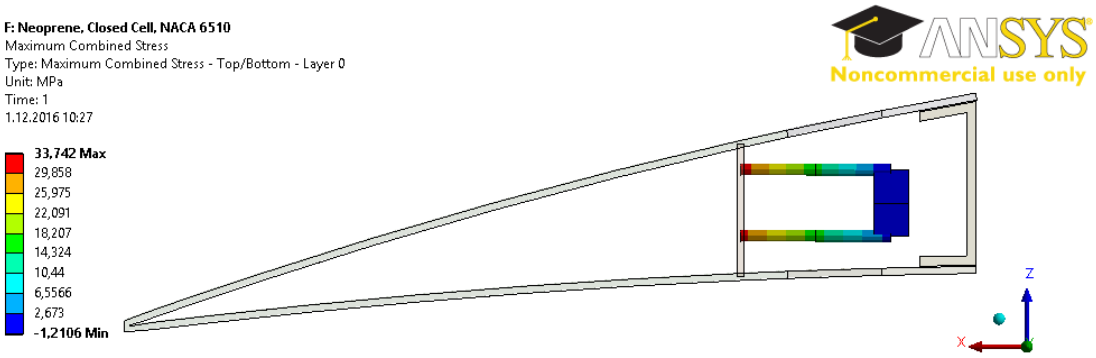

Figure 202: Maximum Beam Combined Stress Contour - Maintaining the NACA 6510 Profile under 3g Aerodynamic Loading (Max 33.74 [MPa], Closed Cell- Neoprene Rubber Design with 1.5 [mm] composite thickness)

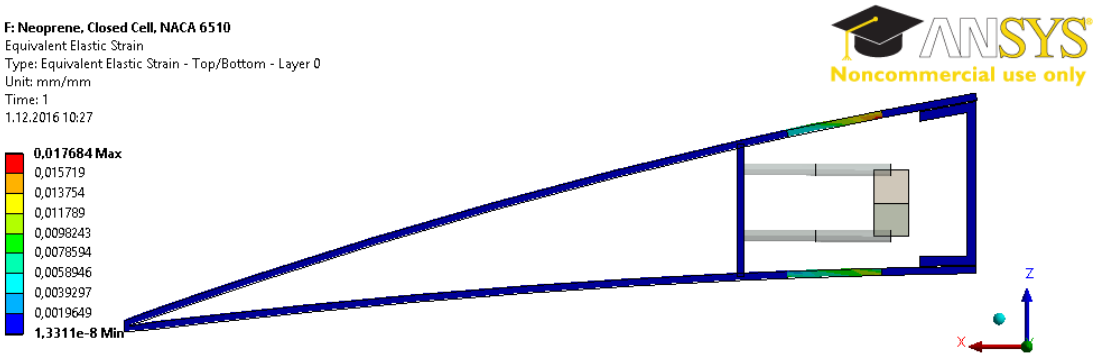

Figure 203: Equivalent Elastic Strain (von-Mises) Contour - Maintaining the NACA 6510 Profile under 3g Aerodynamic Loading (Max 0.01 [mm/mm], Closed Cell- Neoprene Rubber Design with 1.5 [mm] composite thickness)

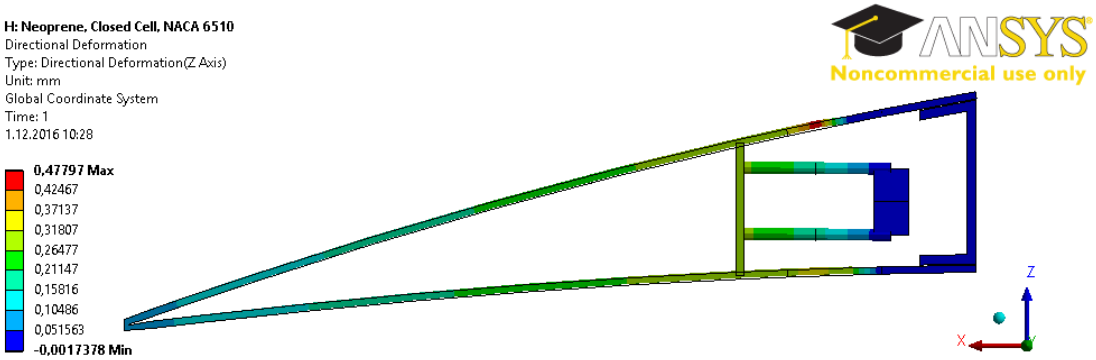

Figure 204: Displacement in z Direction Contour - Maintaining the NACA 6510 Profile under 4g Aerodynamic Loading (Max 0.48 [mm], Closed Cell- Neoprene Rubber Design with 1.5 [mm] composite thickness)

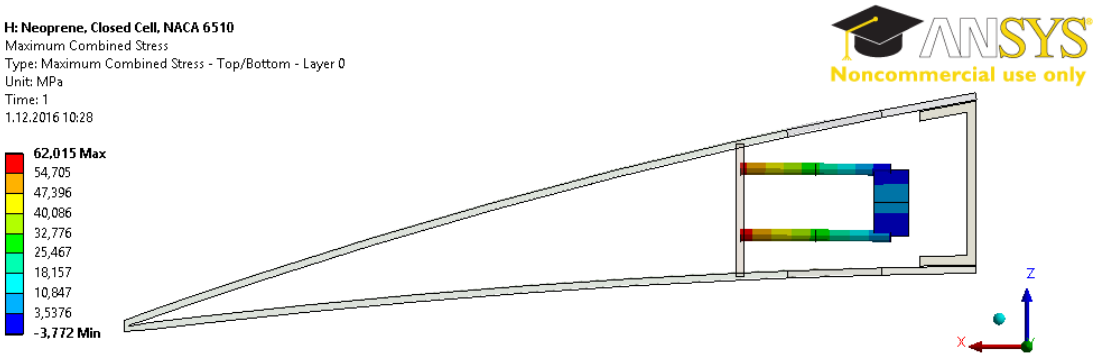

Figure 205: Maximum Beam Combined Stress Contour - Maintaining the NACA 6510 Profile under 4g Aerodynamic Loading (Max 62.02 [MPa], Closed Cell- Neoprene Rubber Design with 1.5 [mm] composite thickness)

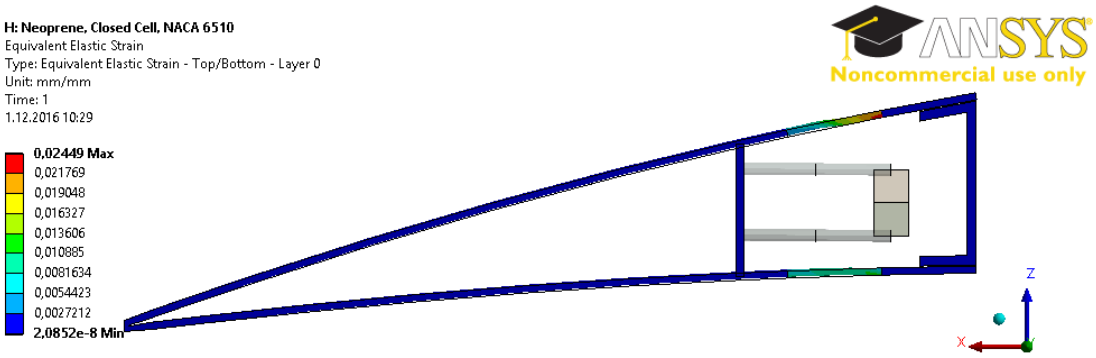

Figure 206: Equivalent Elastic Strain (von-Mises) Contour - Maintaining the NACA 6510 Profile under 4g Aerodynamic Loading (Max 0.03 [mm/mm], Closed Cell- Neoprene Rubber Design with 1.5 [mm] composite thickness)

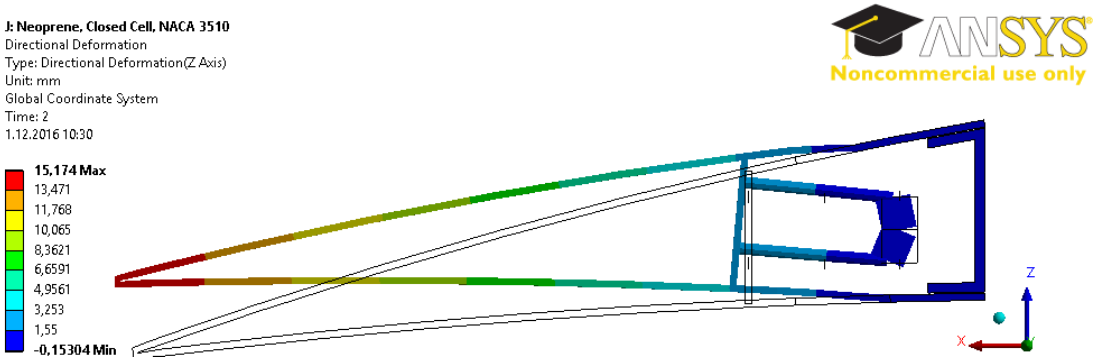

Figure 207: Displacement in z Direction Contour - Morphing from NACA 6510 to NACA 3510 Profile under 1g Aerodynamic Loading (Max 15.17 [mm], Closed Cell-Neoprene Rubber Design with 1.5 [mm] composite thickness)

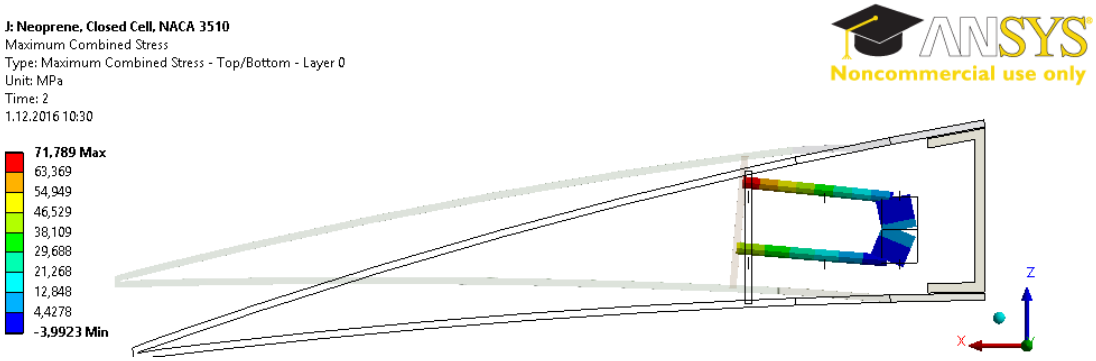

Figure 208: Maximum Beam Combined Stress Contour - Morphing from NACA 6510 to NACA 3510 Profile under 1g Aerodynamic Loading (Max 71.79 [MPa], Closed Cell-Neoprene Rubber Design with 1.5 [mm] composite thickness)

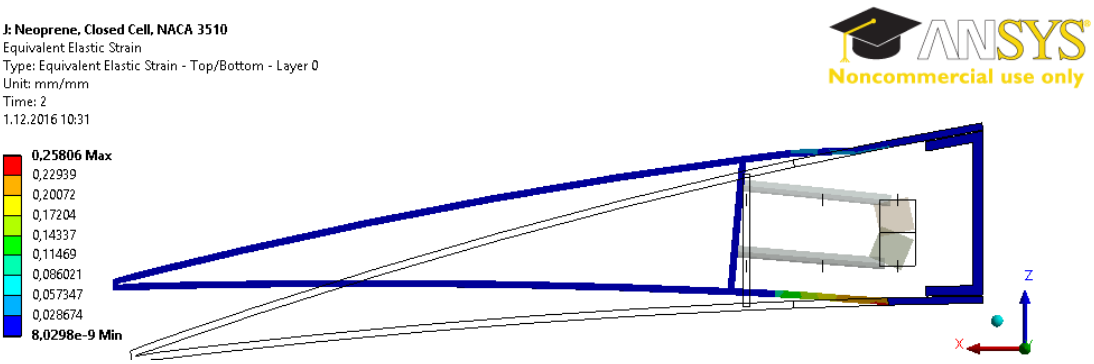

Figure 209: Equivalent Elastic Strain (von-Mises) Contour - Morphing from NACA 6510 to NACA 3510 Profile under 1g Aerodynamic Loading (Max 0.26 [mm/mm], Closed Cell-Neoprene Rubber Design with 1.5 [mm] composite thickness)

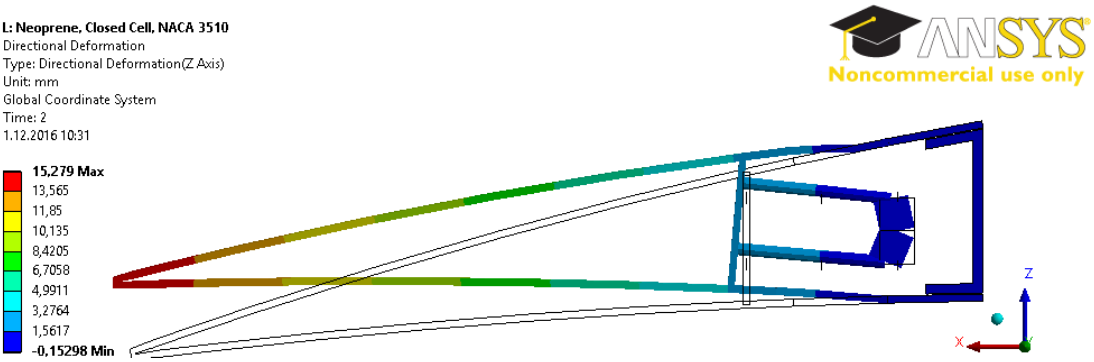

Figure 210: Displacement in z Direction Contour - Morphing from NACA 6510 to NACA 3510 Profile under 2g Aerodynamic Loading (Max 15.28 [mm], Closed Cell-Neoprene Rubber Design with 1.5 [mm] composite thickness)

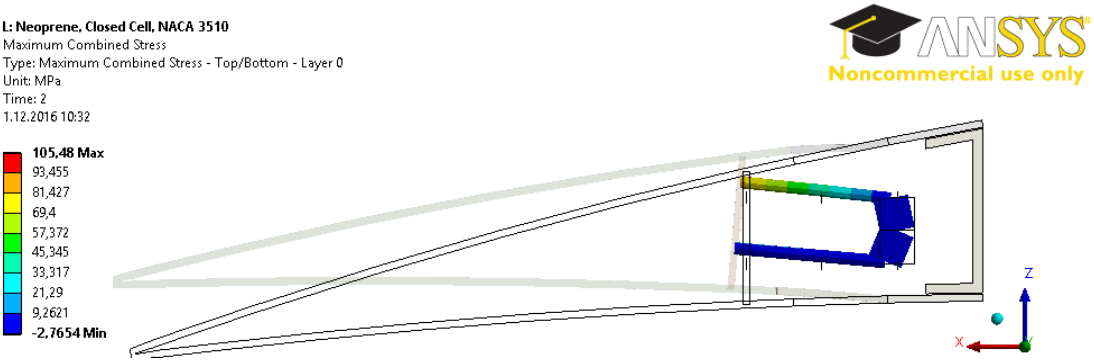

Figure 211: Maximum Beam Combined Stress Contour - Morphing from NACA 6510 to NACA 3510 Profile under 2g Aerodynamic Loading (Max 105.48 [MPa], Closed Cell-Neoprene Rubber Design with 1.5 [mm] composite thickness)

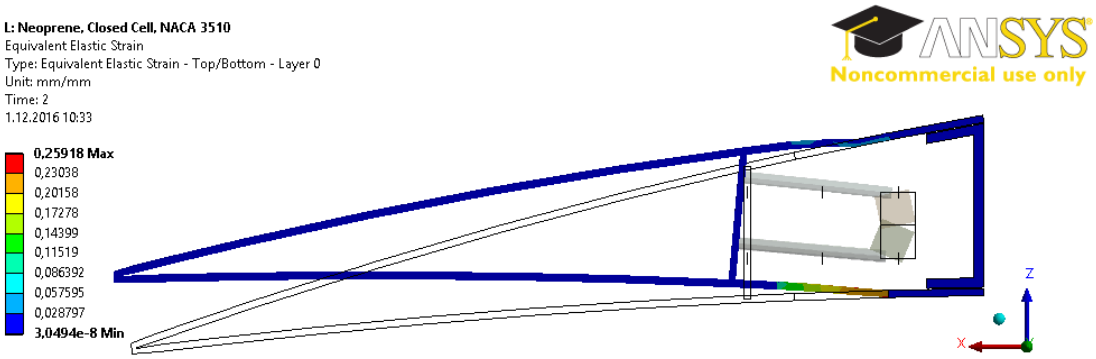

Figure 212: Equivalent Elastic Strain (von-Mises) Contour - Morphing from NACA 6510 to NACA 3510 Profile under 2g Aerodynamic Loading (Max 0.26 [mm/mm], Closed Cell-Neoprene Rubber Design with 1.5 [mm] composite thickness)

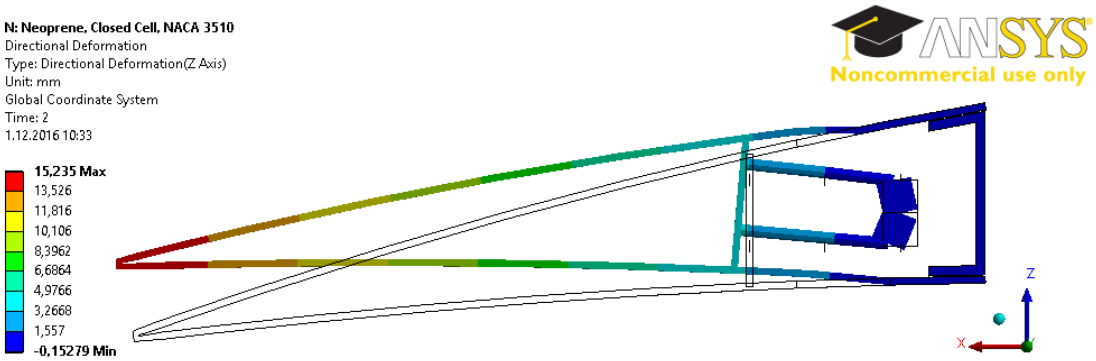

Figure 213: Displacement in z Direction Contour - Morphing from NACA 6510 to NACA 3510 Profile under 3g Aerodynamic Loading (Max 15.24 [mm], Closed Cell-Neoprene Rubber Design with 1.5 [mm] composite thickness)

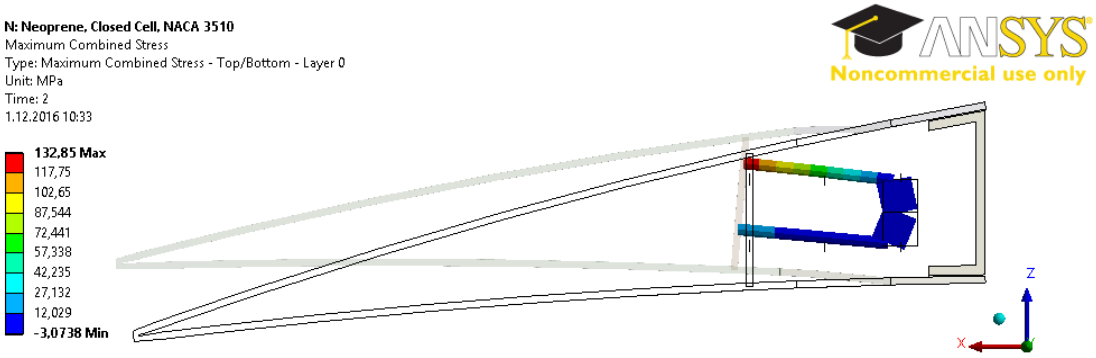

Figure 214: Maximum Beam Combined Stress Contour - Morphing from NACA 6510 to NACA 3510 Profile under 3g Aerodynamic Loading (Max 132.85 [MPa], Closed Cell-Neoprene Rubber Design with 1.5 [mm] composite thickness)

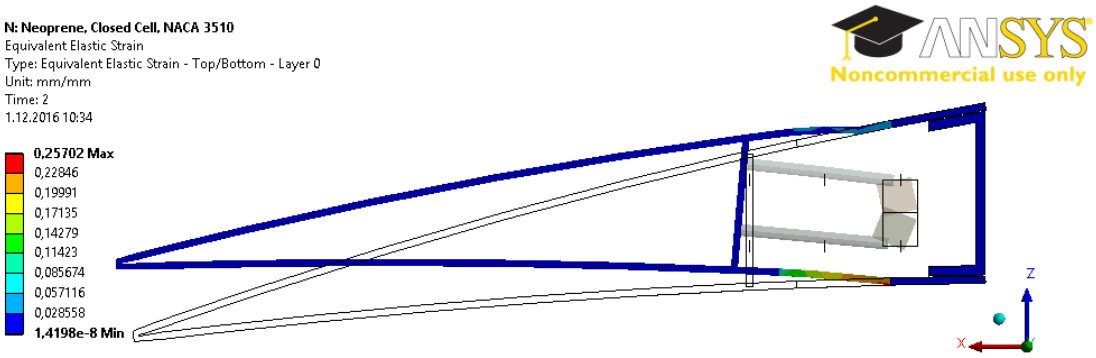

Figure 215: Equivalent Elastic Strain (von-Mises) Contour - Morphing from NACA 6510 to NACA 3510 Profile under 3g Aerodynamic Loading (Max 0.26 [mm/mm], Closed Cell-Neoprene Rubber Design with 1.5 [mm] composite thickness)

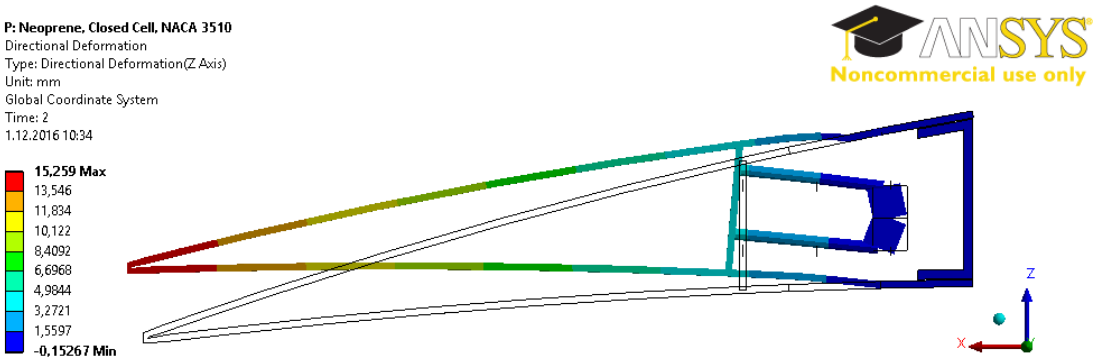

Figure 216: Displacement in z Direction Contour - Morphing from NACA 6510 to NACA 3510 Profile under 4g Aerodynamic Loading (Max 15.26 [mm], Closed Cell-Neoprene Rubber Design with 1.5 [mm] composite thickness)

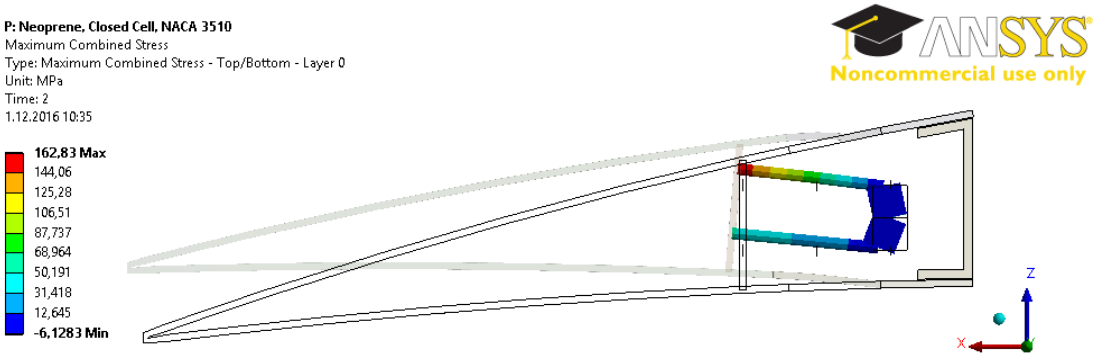

Figure 217: Maximum Beam Combined Stress Contour - Morphing from NACA 6510 to NACA 3510 Profile under 4g Aerodynamic Loading (Max 162.83 [MPa], Closed Cell-Neoprene Rubber Design with 1.5 [mm] composite thickness)

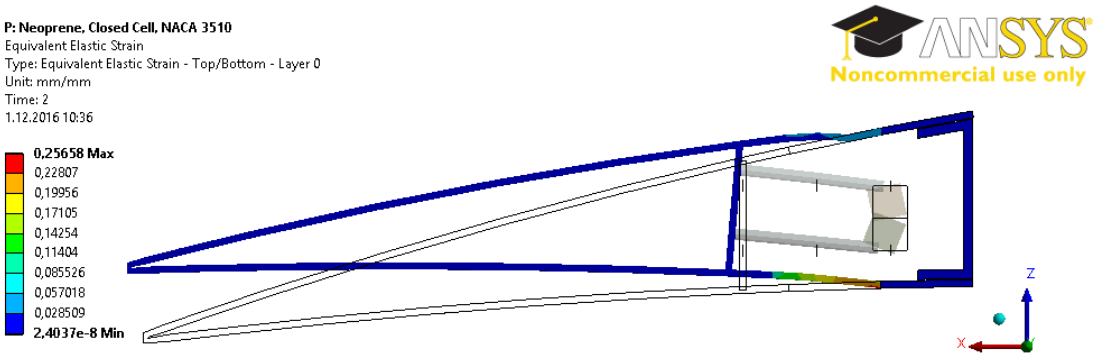

Figure 218: Equivalent Elastic Strain (von-Mises) Contour - Morphing from NACA 6510 to NACA 3510 Profile under 4g Aerodynamic Loading (Max 0.26 [mm/mm], Closed Cell-Neoprene Rubber Design with 1.5 [mm] composite thickness)

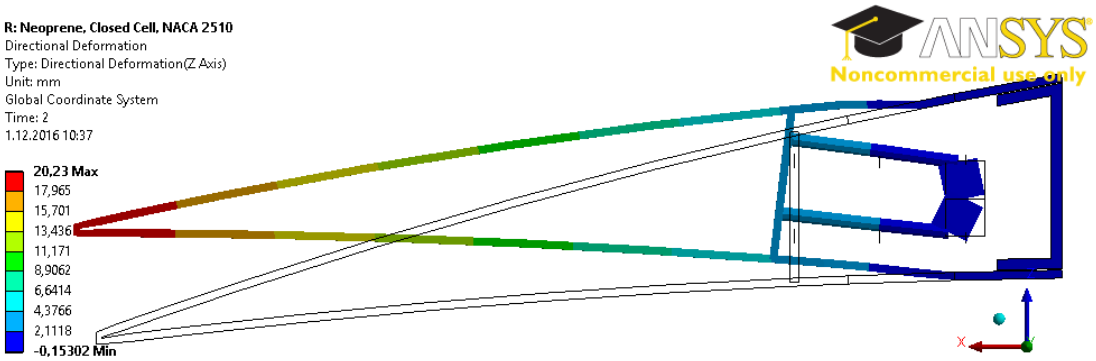

Figure 219: Displacement in z Direction Contour - Morphing from NACA 6510 to NACA 2510 Profile under 1g Aerodynamic Loading (Max 20.23 [mm], Closed Cell-Neoprene Rubber Design with 1.5 [mm] composite thickness)

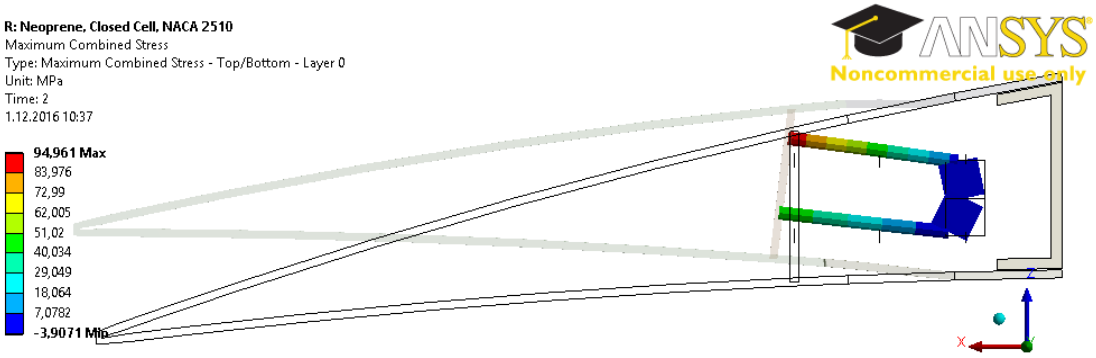

Figure 220: Maximum Beam Combined Stress Contour - Morphing from NACA 6510 to NACA 2510 Profile under 1g Aerodynamic Loading (Max 94.96 [MPa], Closed Cell-Neoprene Rubber Design with 1.5 [mm] composite thickness)

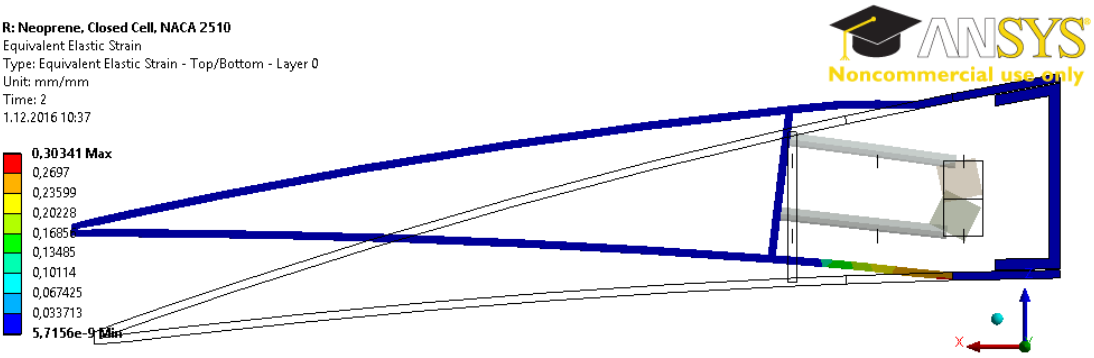

Figure 221: Equivalent Elastic Strain (von-Mises) Contour - Morphing from NACA 6510 to NACA 2510 Profile under 1g Aerodynamic Loading (Max 0.30 [mm/mm], Closed Cell-Neoprene Rubber Design with 1.5 [mm] composite thickness)

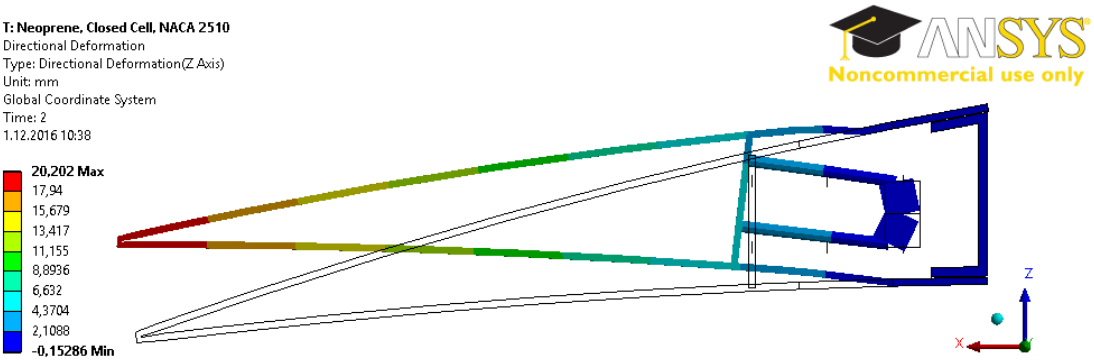

Figure 222: Displacement in z Direction Contour - Morphing from NACA 6510 to NACA 2510 Profile under 2g Aerodynamic Loading (Max 20.20 [mm], Closed Cell-Neoprene Rubber Design with 1.5 [mm] composite thickness)

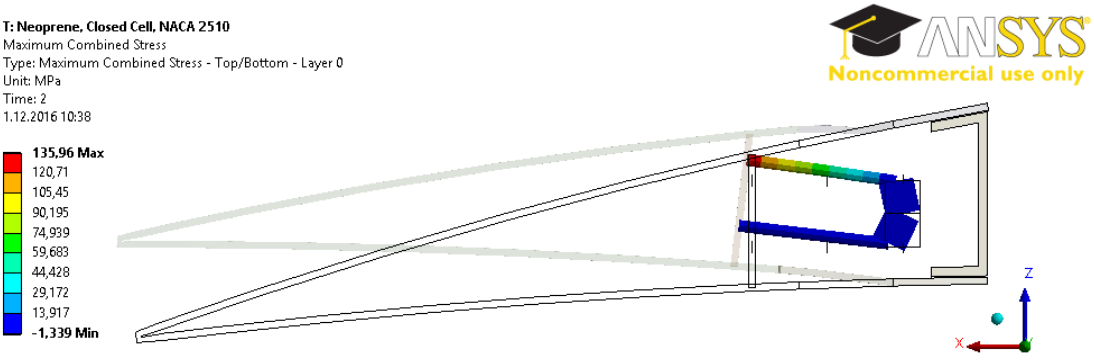

Figure 223: Maximum Beam Combined Stress Contour - Morphing from NACA 6510 to NACA 2510 Profile under 2g Aerodynamic Loading (Max 135.96 [MPa], Closed Cell-Neoprene Rubber Design with 1.5 [mm] composite thickness)

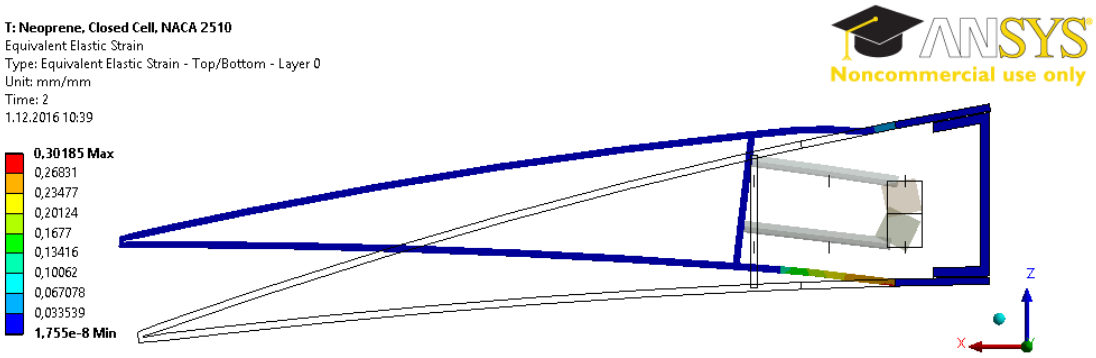

Figure 224: Equivalent Elastic Strain (von-Mises) Contour - Morphing from NACA 6510 to NACA 2510 Profile under 2g Aerodynamic Loading (Max 0.30 [mm/mm], Closed Cell-Neoprene Rubber Design with 1.5 [mm] composite thickness)

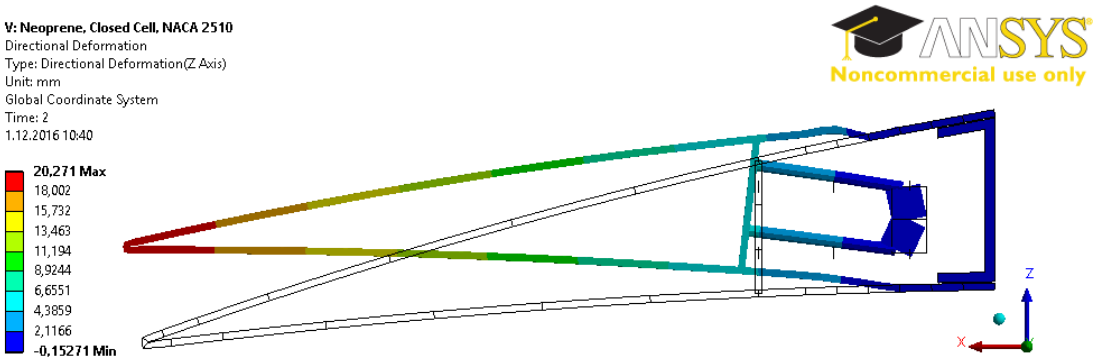

Figure 225: Displacement in z Direction Contour - Morphing from NACA 6510 to NACA 2510 Profile under 3g Aerodynamic Loading (Max 20.27 [mm], Closed Cell-Neoprene Rubber Design with 1.5 [mm] composite thickness)

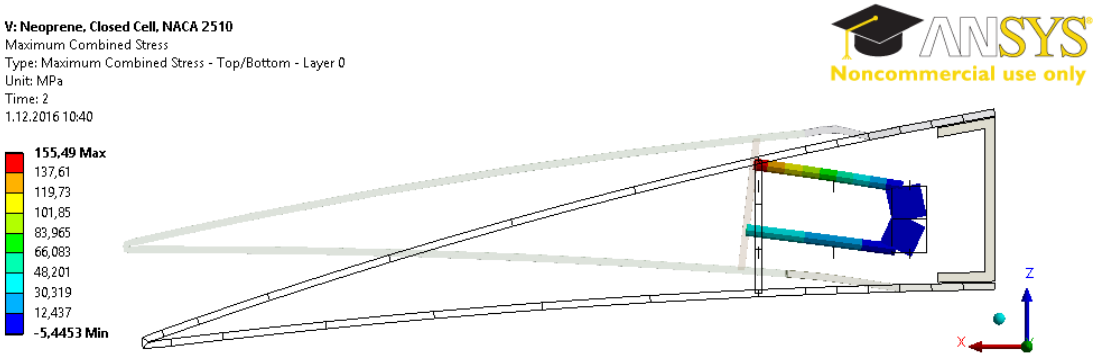

Figure 226: Maximum Beam Combined Stress Contour - Morphing from NACA 6510 to NACA 2510 Profile under 3g Aerodynamic Loading (Max 155.49 [MPa], Closed Cell-Neoprene Rubber Design with 1.5 [mm] composite thickness)

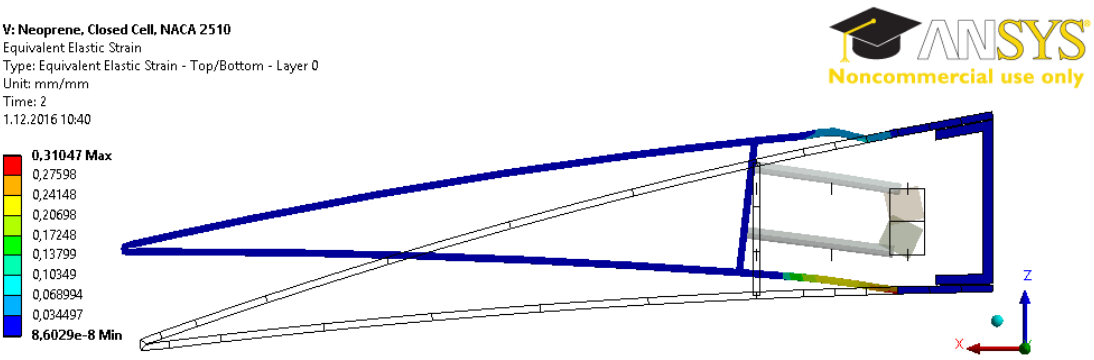

Figure 227: Equivalent Elastic Strain (von-Mises) Contour - Morphing from NACA 6510 to NACA 2510 Profile under 3g Aerodynamic Loading (Max 0.31 [mm/mm], Closed Cell-Neoprene Rubber Design with 1.5 [mm] composite thickness)

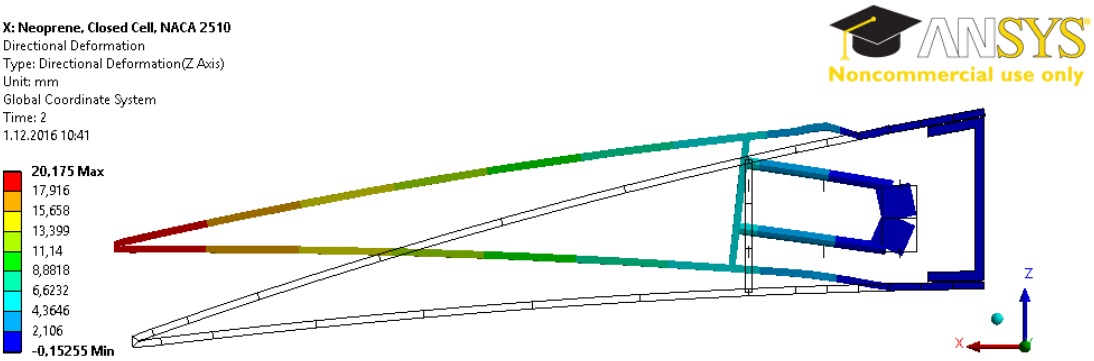

Figure 228: Displacement in z Direction Contour - Morphing from NACA 6510 to NACA 2510 Profile under 4g Aerodynamic Loading (Max 20.18 [mm], Closed Cell-Neoprene Rubber Design with 1.5 [mm] composite thickness)

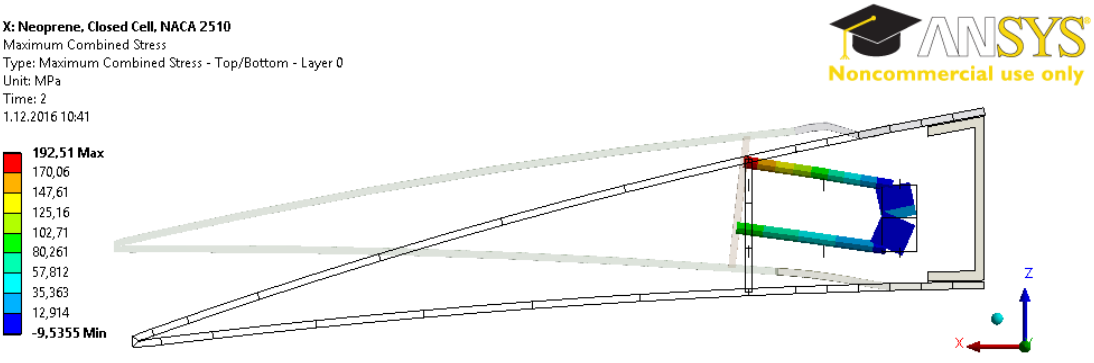

Figure 229: Maximum Beam Combined Stress Contour - Morphing from NACA 6510 to NACA 2510 Profile under 4g Aerodynamic Loading (Max 192.51 [MPa], Closed Cell-Neoprene Rubber Design with 1.5 [mm] composite thickness)

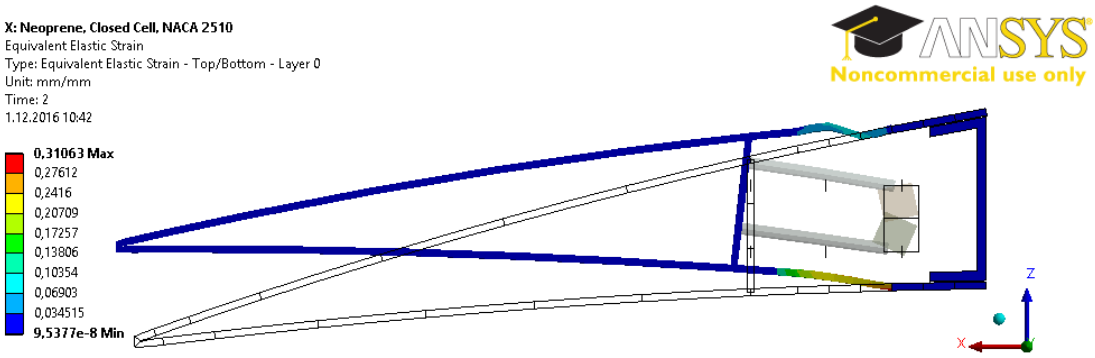

Figure 230: Equivalent Elastic Strain (von-Mises) Contour - Morphing from NACA 6510 to NACA 2510 Profile under 4g Aerodynamic Loading (Max 0.31 [mm/mm], Closed Cell-Neoprene Rubber Design with 1.5 [mm] composite thickness)

APPENDIX B3

Closed Cell – Neoprene Rubber with 1.0 [mm] Composite Thickness Design Results

In this part, Closed Cell – Neoprene Rubber design analysis results under aerodynamic loads are presented for 1.0 [mm] composite thickness.

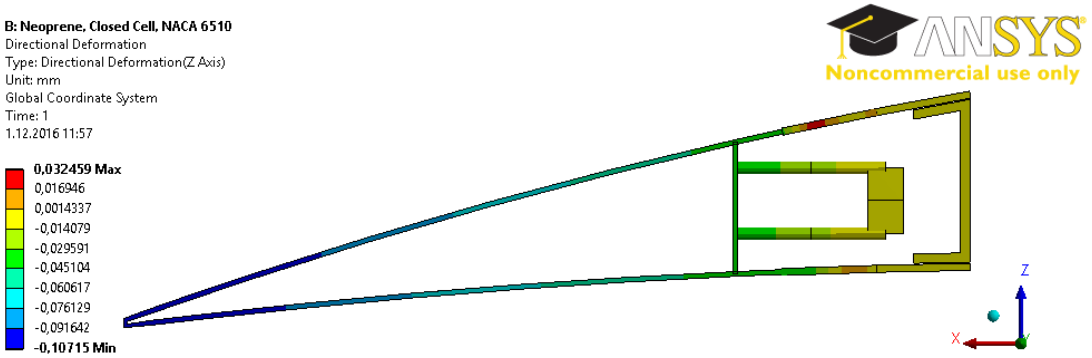

Figure 231: Displacement in z Direction Contour - Maintaining the NACA 6510 Profile under 1g Aerodynamic Loading (Max 0.03 [mm], Closed Cell-Neoprene Rubber Design with 1.0 [mm] composite thickness)

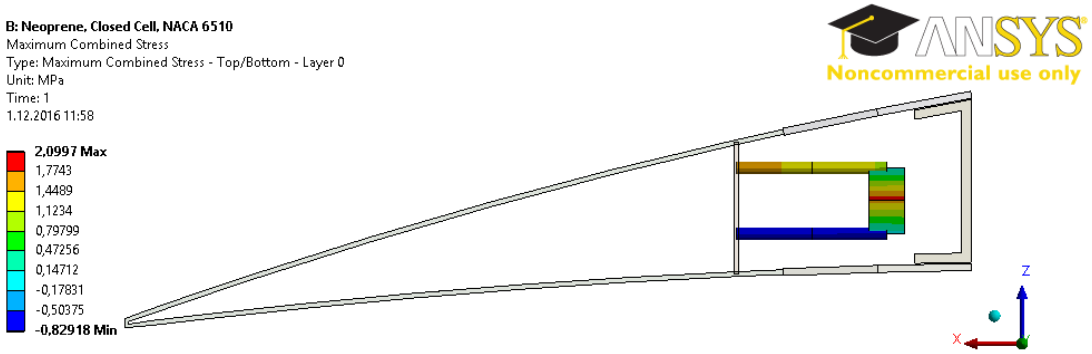

Figure 232: Maximum Beam Combined Stress Contour - Maintaining the NACA 6510 Profile under 1g Aerodynamic Loading (Max 2.10 [MPa], Closed Cell-Neoprene Rubber Design with 1.0 [mm] composite thickness)

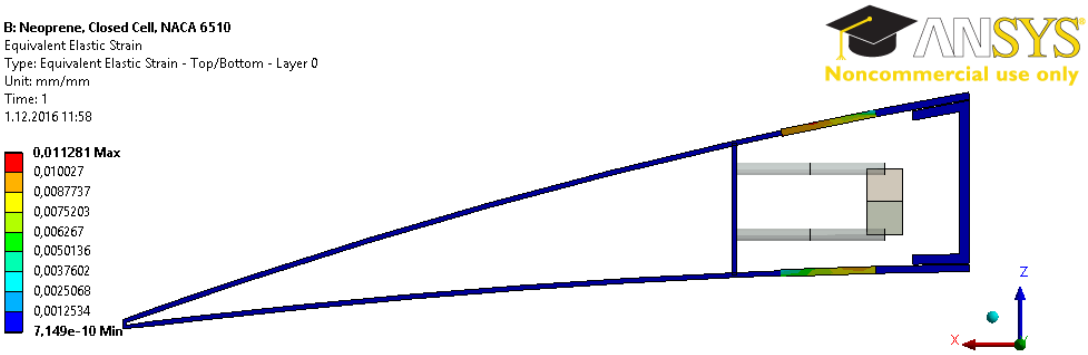

Figure 233: Equivalent Elastic Strain (von-Mises) Contour - Maintaining the NACA 6510 Profile under 1g Aerodynamic Loading (Max 0.01 [mm/mm], Closed Cell- Neoprene Rubber Design with 1.0 [mm] composite thickness)

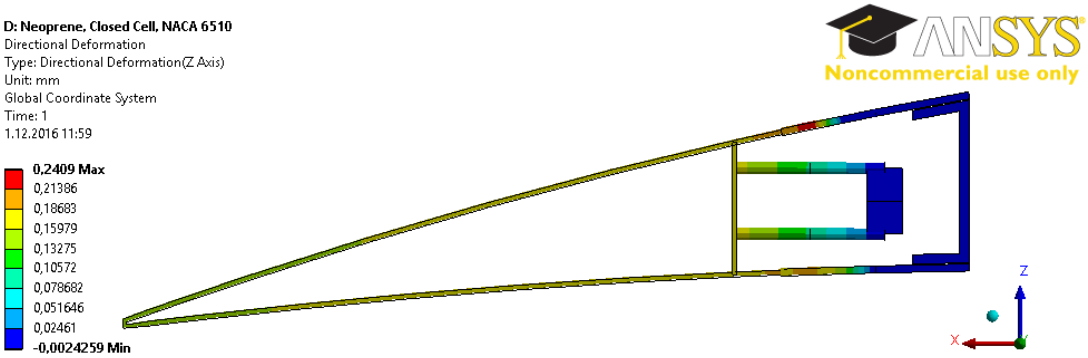

Figure 234: Displacement in z Direction Contour - Maintaining the NACA 6510 Profile under 2g Aerodynamic Loading (Max 0.24 [mm], Closed Cell- Neoprene Rubber Design with 1.0 [mm] composite thickness)

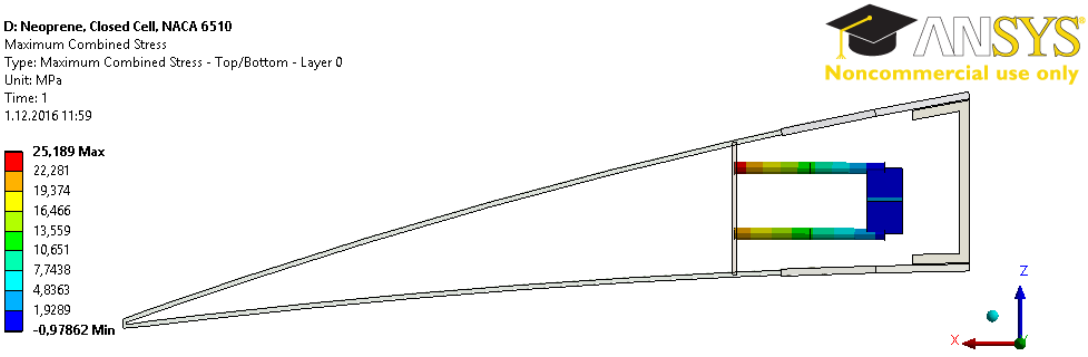

Figure 235: Maximum Beam Combined Stress Contour - Maintaining the NACA 6510 Profile under 2g Aerodynamic Loading (Max 25.19 [MPa], Closed Cell- Neoprene Rubber Design with 1.0 [mm] composite thickness)

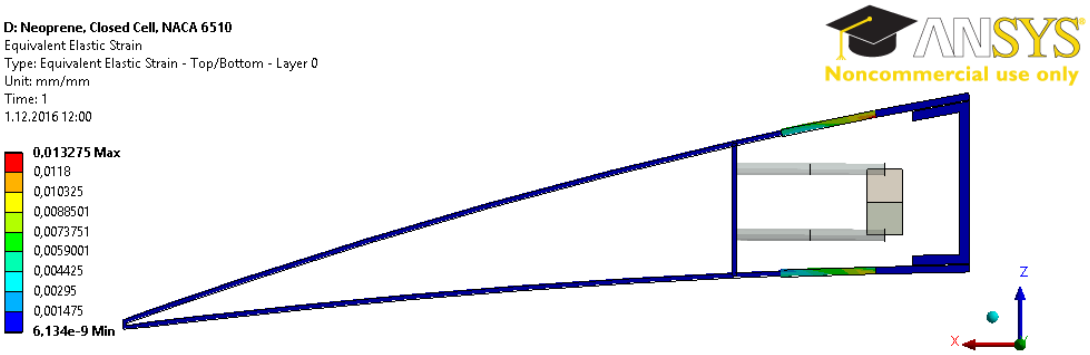

Figure 236: Equivalent Elastic Strain (von-Mises) Contour - Maintaining the NACA 6510 Profile under 2g Aerodynamic Loading (Max 0.01 [mm/mm], Closed Cell- Neoprene Rubber Design with 1.0 [mm] composite thickness)

Figure 237: Displacement in z Direction Contour - Maintaining the NACA 6510 Profile under 3g Aerodynamic Loading (Max 0.41 [mm], Closed Cell- Neoprene Rubber Design with 1.0 [mm] composite thickness)

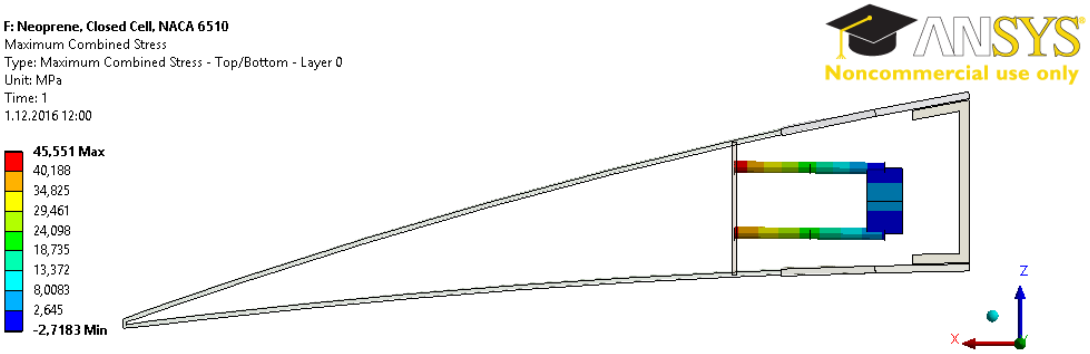

Figure 238: Maximum Beam Combined Stress Contour - Maintaining the NACA 6510 Profile under 3g Aerodynamic Loading (Max 45.55 [MPa], Closed Cell- Neoprene Rubber Design with 1.0 [mm] composite thickness)

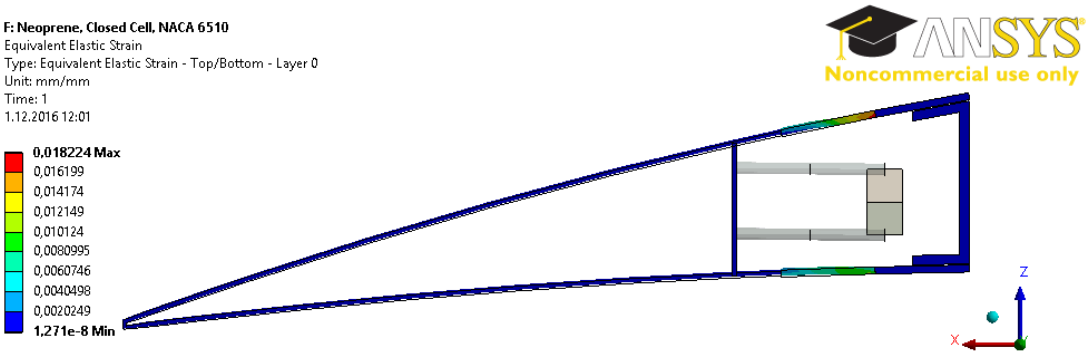

Figure 239: Equivalent Elastic Strain (von-Mises) Contour - Maintaining the NACA 6510 Profile under 3g Aerodynamic Loading (Max 0.02 [mm/mm], Closed Cell- Neoprene Rubber Design with 1.0 [mm] composite thickness)

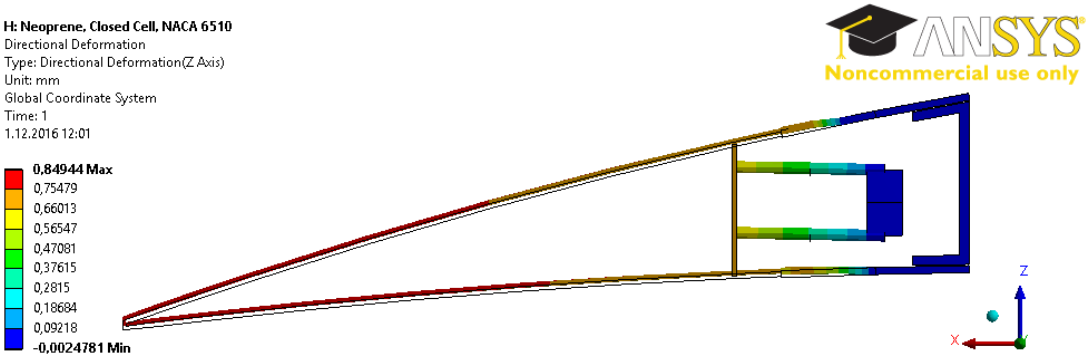

Figure 240: Displacement in z Direction Contour - Maintaining the NACA 6510 Profile under 4g Aerodynamic Loading (Max 0.85 [mm], Closed Cell- Neoprene Rubber Design with 1.0 [mm] composite thickness)

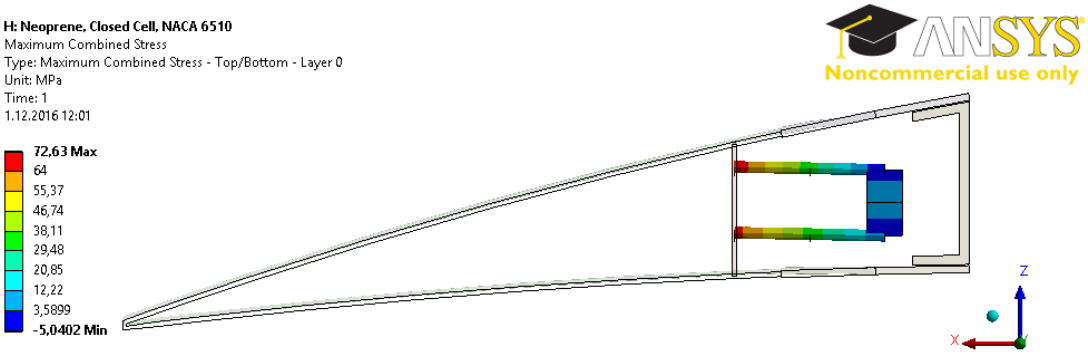

Figure 241: Maximum Beam Combined Stress Contour - Maintaining the NACA 6510 Profile under 4g Aerodynamic Loading (Max 72.63 [MPa], Closed Cell- Neoprene Rubber Design with 1.0 [mm] composite thickness)

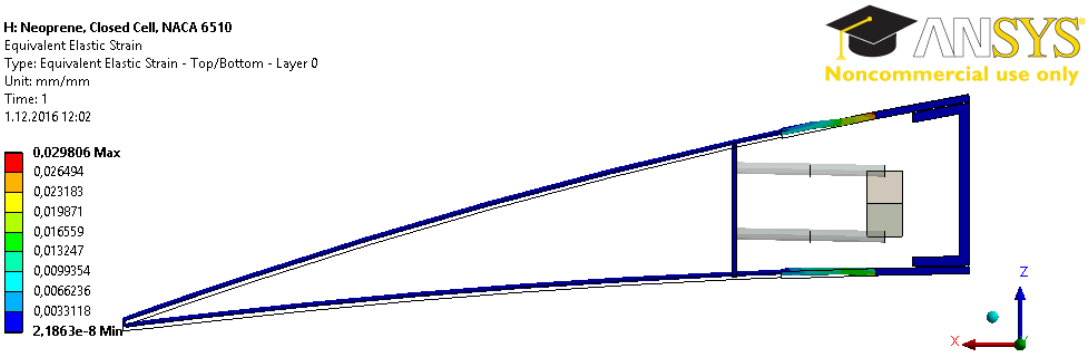

Figure 242: Equivalent Elastic Strain (von-Mises) Contour - Maintaining the NACA 6510 Profile under 4g Aerodynamic Loading (Max 0.03 [mm/mm], Closed Cell- Neoprene Rubber Design with 1.0 [mm] composite thickness)

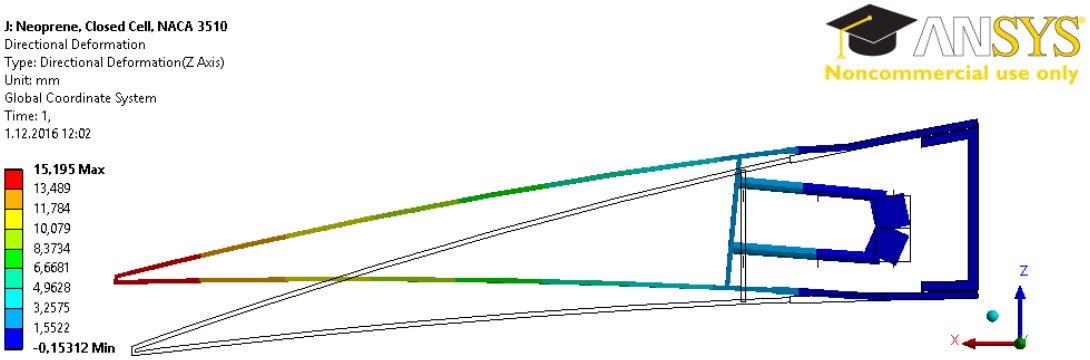

Figure 243: Displacement in z Direction Contour - Morphing from NACA 6510 to NACA 3510 Profile under 1g Aerodynamic Loading (Max 15.20 [mm], Closed Cell-Neoprene Rubber Design with 1.0 [mm] composite thickness)

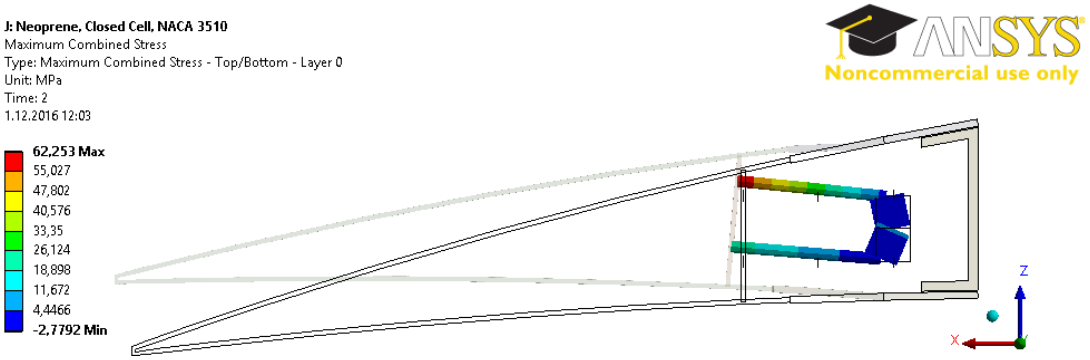

Figure 244: Maximum Beam Combined Stress Contour - Morphing from NACA 6510 to NACA 3510 Profile under 1g Aerodynamic Loading (Max 62.25 [MPa], Closed Cell-Neoprene Rubber Design with 1.0 [mm] composite thickness)

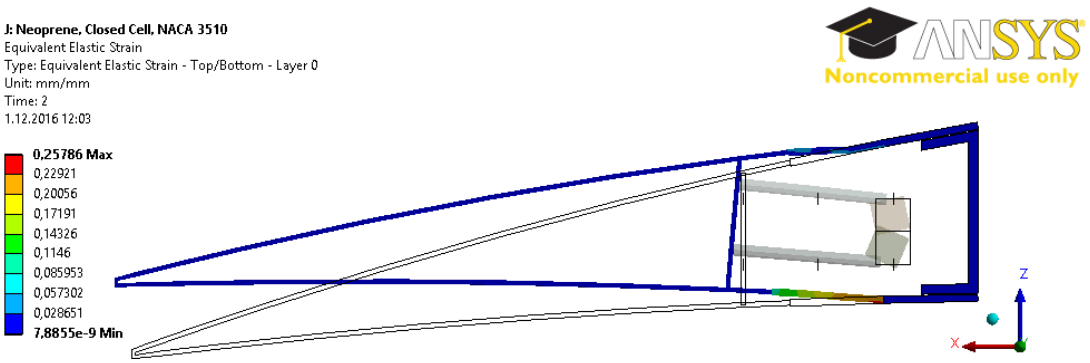

Figure 245: Equivalent Elastic Strain (von-Mises) Contour - Morphing from NACA 6510 to NACA 3510 Profile under 1g Aerodynamic Loading (Max 0.26 [mm/mm], Closed Cell-Neoprene Rubber Design with 1.0 [mm] composite thickness)

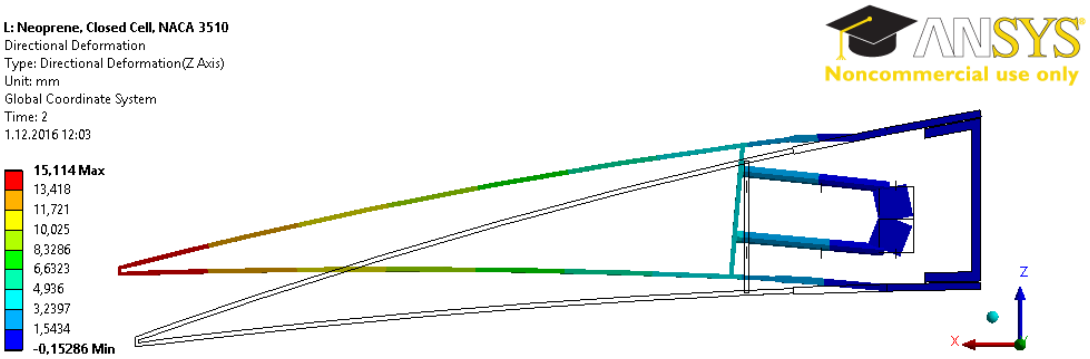

Figure 246: Displacement in z Direction Contour - Morphing from NACA 6510 to NACA 3510 Profile under 2g Aerodynamic Loading (Max 15.11 [mm], Closed Cell-Neoprene Rubber Design with 1.0 [mm] composite thickness)

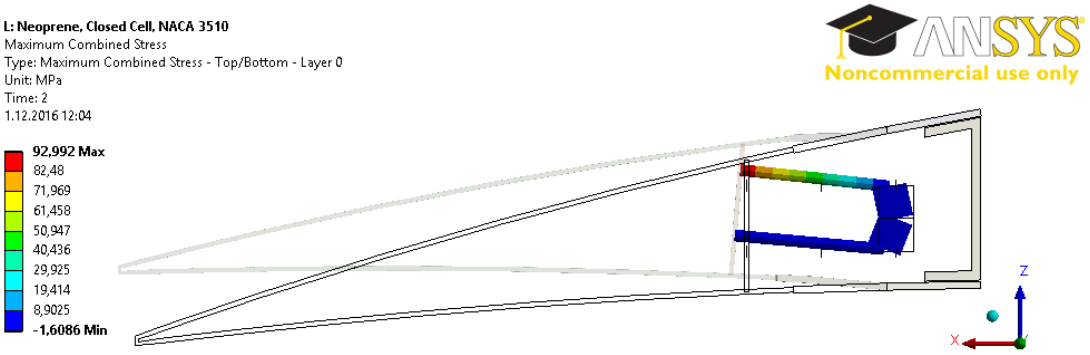

Figure 247: Maximum Beam Combined Stress Contour - Morphing from NACA 6510 to NACA 3510 Profile under 2g Aerodynamic Loading (Max 92.99 [MPa], Closed Cell-Neoprene Rubber Design with 1.0 [mm] composite thickness)

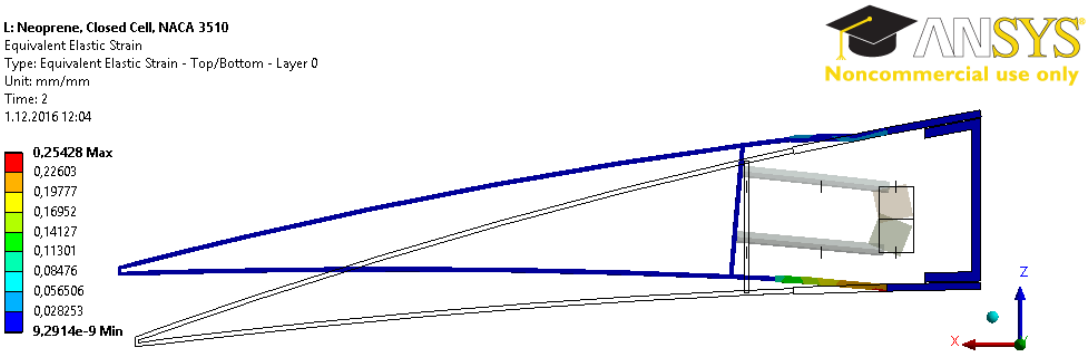

Figure 248: Equivalent Elastic Strain (von-Mises) Contour - Morphing from NACA 6510 to NACA 3510 Profile under 2g Aerodynamic Loading (Max 0.26 [mm/mm], Closed Cell-Neoprene Rubber Design with 1.0 [mm] composite thickness)

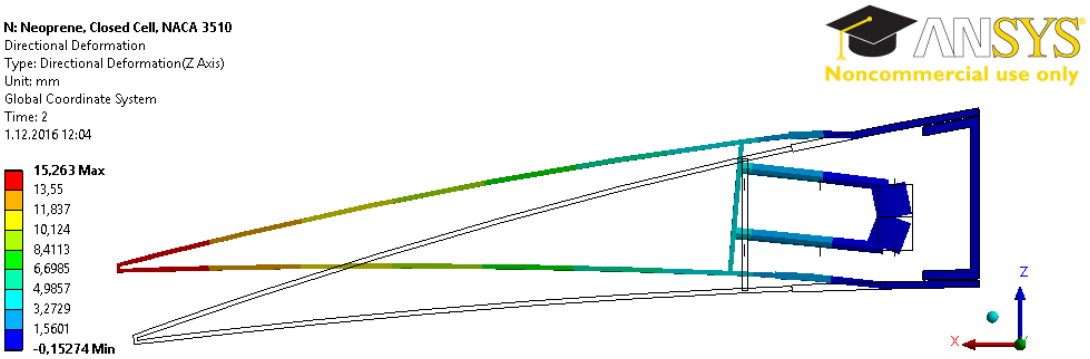

Figure 249: Displacement in z Direction Contour - Morphing from NACA 6510 to NACA 3510 Profile under 3g Aerodynamic Loading (Max 15.26 [mm], Closed Cell-Neoprene Rubber Design with 1.0 [mm] composite thickness)

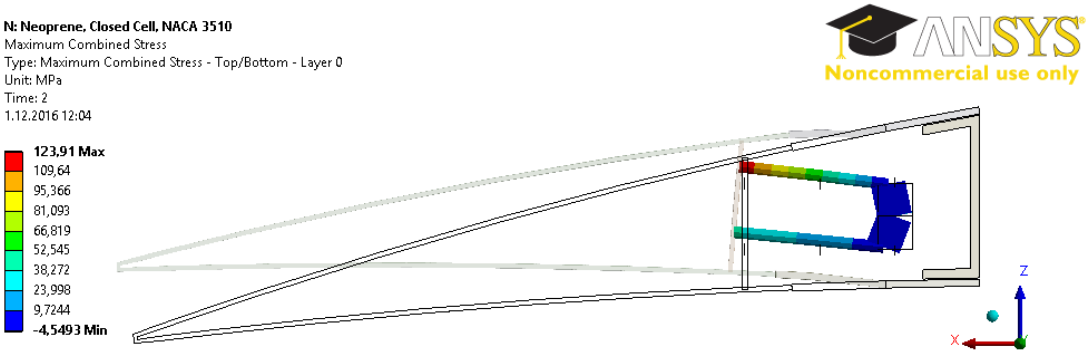

Figure 250: Maximum Beam Combined Stress Contour - Morphing from NACA 6510 to NACA 3510 Profile under 3g Aerodynamic Loading (Max 123.91 [MPa], Closed Cell-Neoprene Rubber Design with 1.0 [mm] composite thickness)

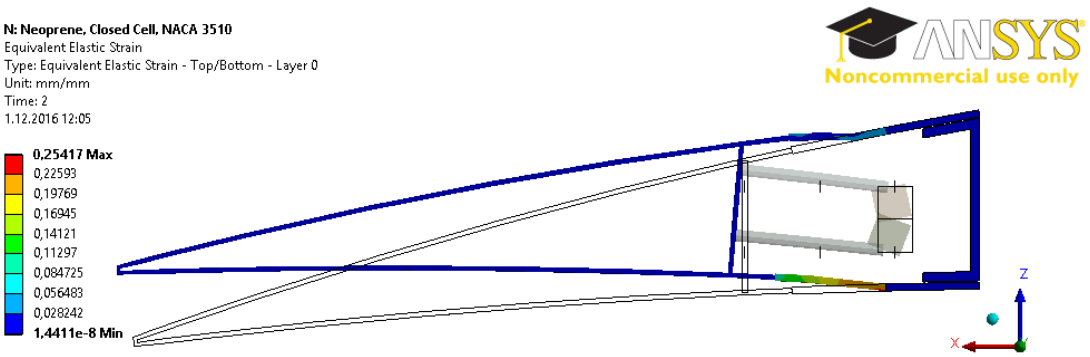

Figure 251: Equivalent Elastic Strain (von-Mises) Contour - Morphing from NACA 6510 to NACA 3510 Profile under 3g Aerodynamic Loading (Max 0.25 [mm/mm], Closed Cell-Neoprene Rubber Design with 1.0 [mm] composite thickness)

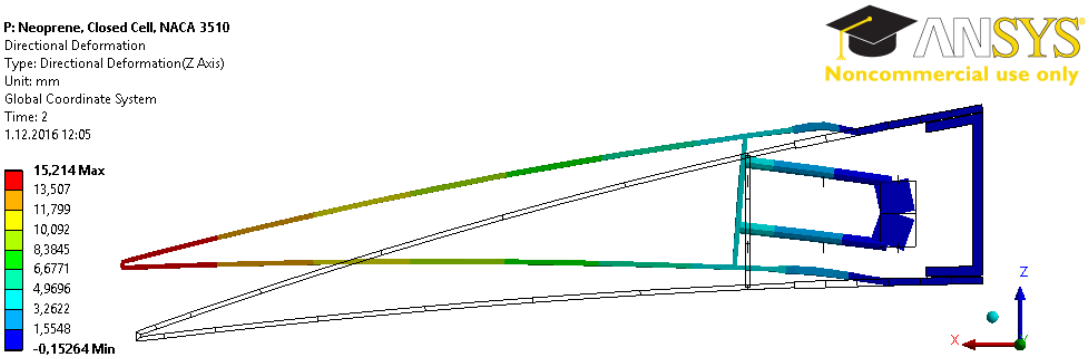

Figure 252: Displacement in z Direction Contour - Morphing from NACA 6510 to NACA 3510 Profile under 4g Aerodynamic Loading (Max 15.21 [mm], Closed Cell-Neoprene Rubber Design with 1.0 [mm] composite thickness)

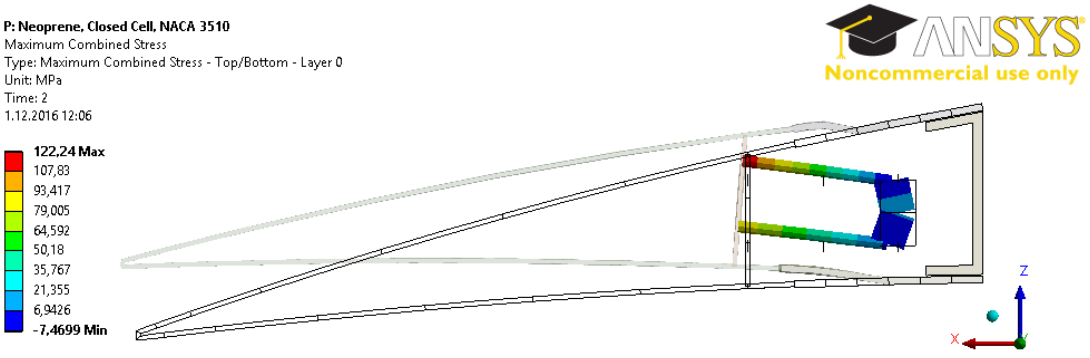

Figure 253: Maximum Beam Combined Stress Contour - Morphing from NACA 6510 to NACA 3510 Profile under 4g Aerodynamic Loading (Max 122.24 [MPa], Closed Cell-Neoprene Rubber Design with 1.0 [mm] composite thickness)

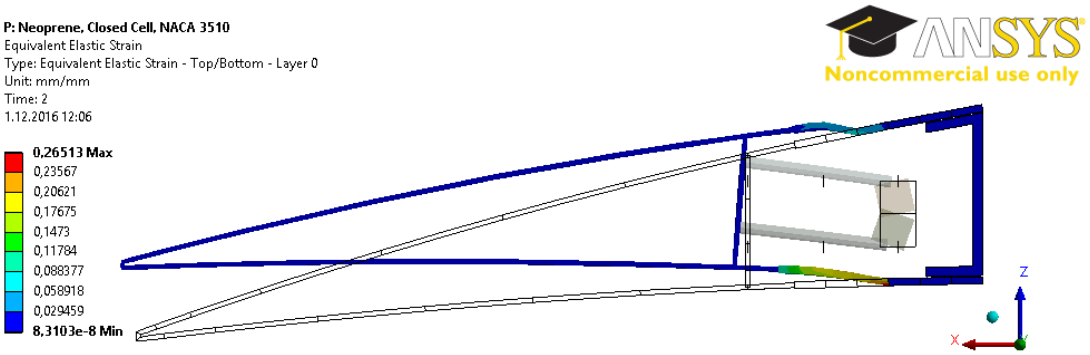

Figure 254: Equivalent Elastic Strain (von-Mises) Contour - Morphing from NACA 6510 to NACA 3510 Profile under 4g Aerodynamic Loading (Max 0.26 [mm/mm], Closed Cell-Neoprene Rubber Design with 1.0 [mm] composite thickness)

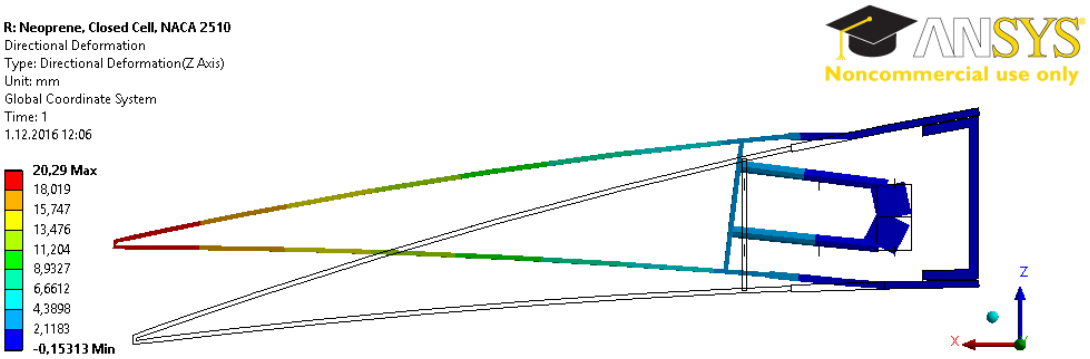

Figure 255: Displacement in z Direction Contour - Morphing from NACA 6510 to NACA 2510 Profile under 1g Aerodynamic Loading (Max 20.29 [mm], Closed Cell-Neoprene Rubber Design with 1.0 [mm] composite thickness)

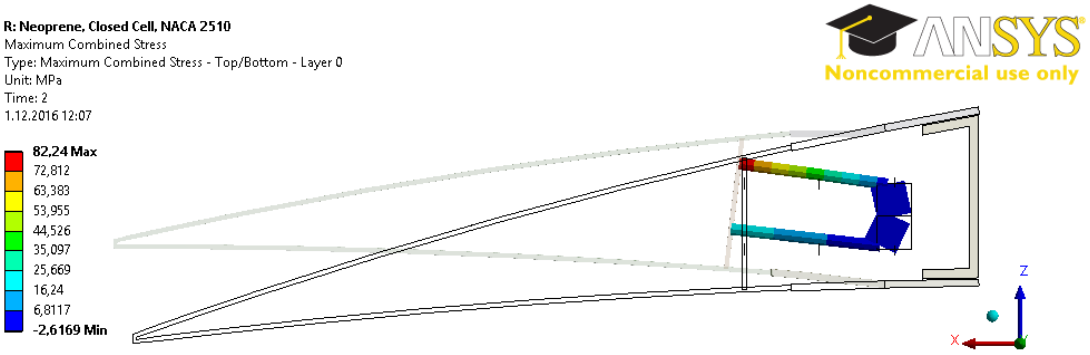

Figure 256: Maximum Beam Combined Stress Contour - Morphing from NACA 6510 to NACA 2510 Profile under 1g Aerodynamic Loading (Max 82.24 [MPa], Closed Cell-Neoprene Rubber Design with 1.0 [mm] composite thickness)

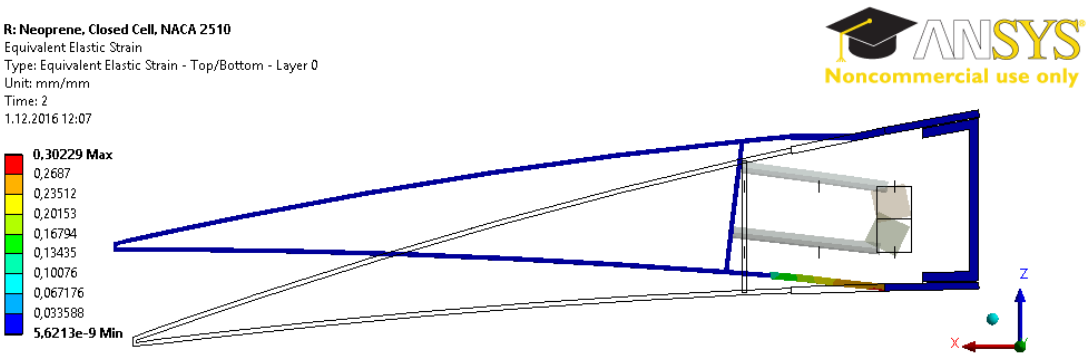

Figure 257: Equivalent Elastic Strain (von-Mises) Contour - Morphing from NACA 6510 to NACA 2510 Profile under 1g Aerodynamic Loading (Max 0.30 [mm/mm], Closed Cell-Neoprene Rubber Design with 1.0 [mm] composite thickness)

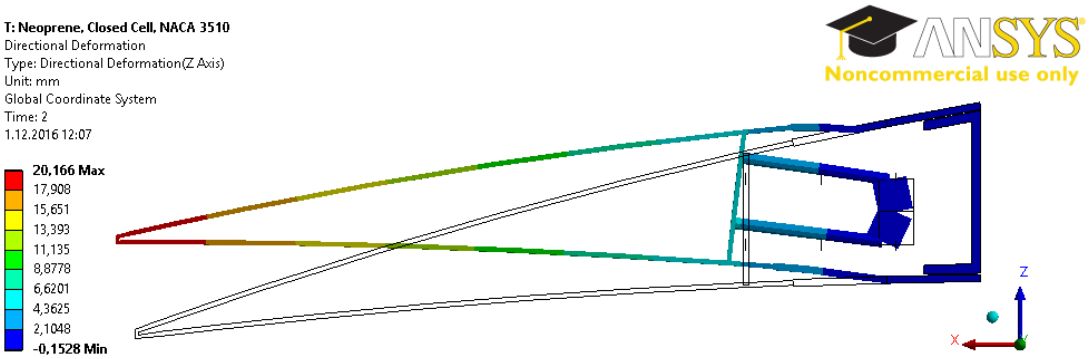

Figure 258: Displacement in z Direction Contour - Morphing from NACA 6510 to NACA 2510 Profile under 2g Aerodynamic Loading (Max 20.17 [mm], Closed Cell-Neoprene Rubber Design with 1.0 [mm] composite thickness)

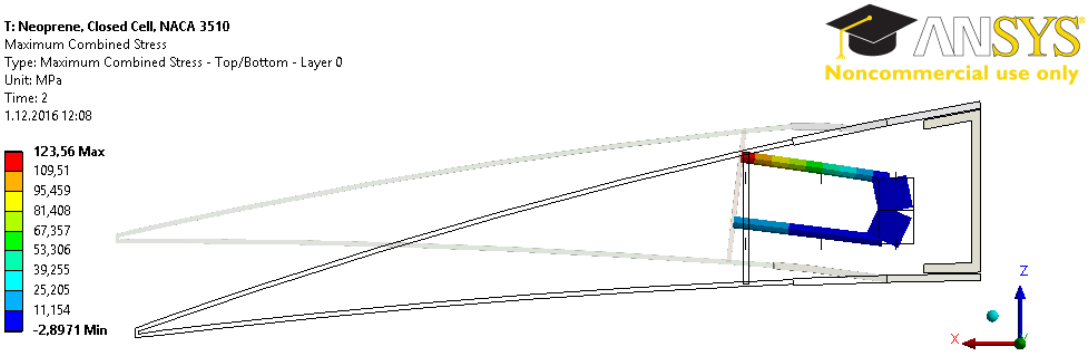

Figure 259: Maximum Beam Combined Stress Contour - Morphing from NACA 6510 to NACA 2510 Profile under 2g Aerodynamic Loading (Max 123.56 [MPa], Closed Cell-Neoprene Rubber Design with 1.0 [mm] composite thickness)

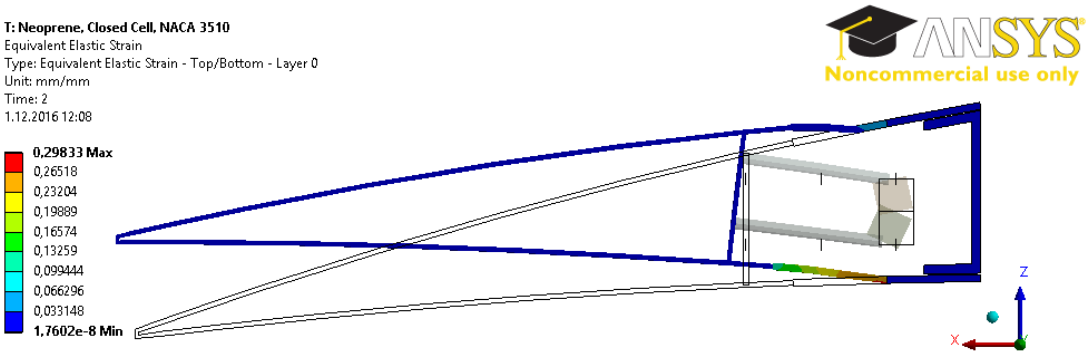

Figure 260: Equivalent Elastic Strain (von-Mises) Contour - Morphing from NACA 6510 to NACA 2510 Profile under 2g Aerodynamic Loading (Max 0.30 [mm/mm], Closed Cell-Neoprene Rubber Design with 1.0 [mm] composite thickness)

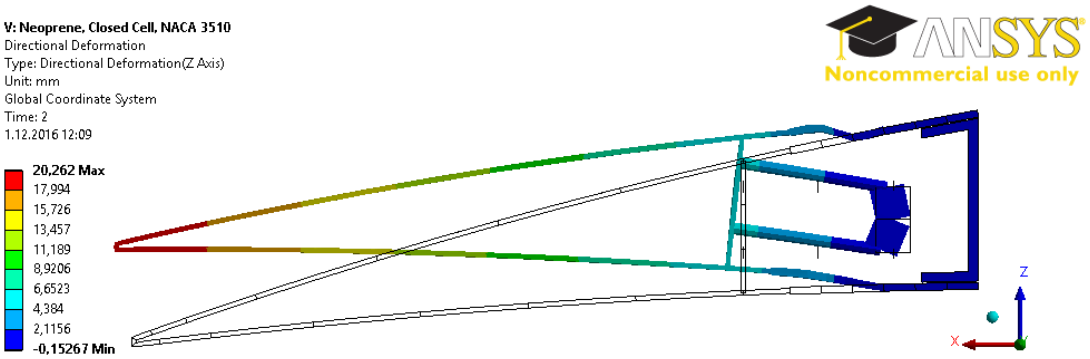

Figure 261: Displacement in z Direction Contour - Morphing from NACA 6510 to NACA 2510 Profile under 3g Aerodynamic Loading (Max 20.26 [mm], Closed Cell-Neoprene Rubber Design with 1.0 [mm] composite thickness)

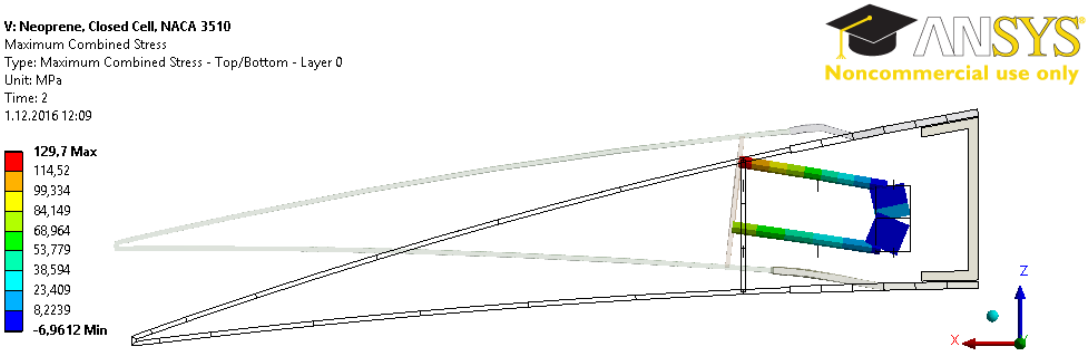

Figure 262: Maximum Beam Combined Stress Contour - Morphing from NACA 6510 to NACA 2510 Profile under 3g Aerodynamic Loading (Max 129.70 [MPa], Closed Cell-Neoprene Rubber Design with 1.0 [mm] composite thickness)

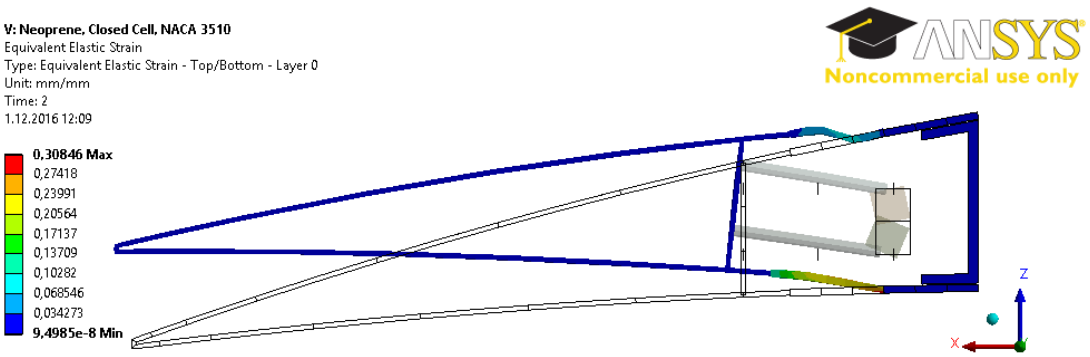

Figure 263: Equivalent Elastic Strain (von-Mises) Contour - Morphing from NACA 6510 to NACA 2510 Profile under 3g Aerodynamic Loading (Max 0.30 [mm/mm], Closed Cell-Neoprene Rubber Design with 1.0 [mm] composite thickness)

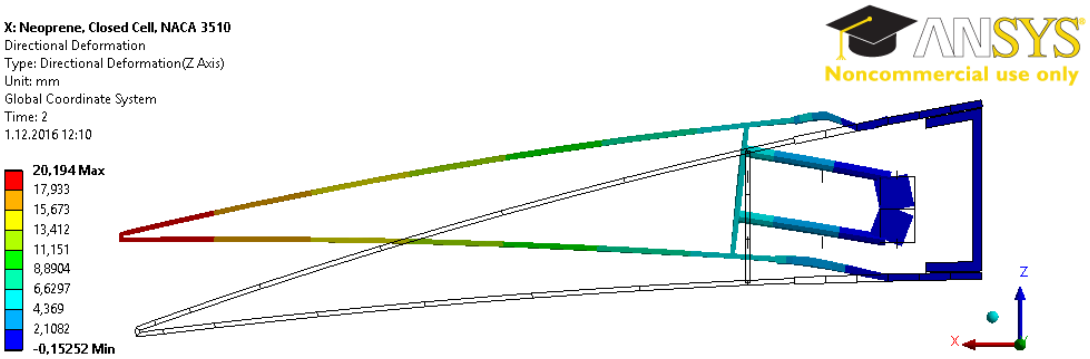

Figure 264: Displacement in z Direction Contour - Morphing from NACA 6510 to NACA 2510 Profile under 4g Aerodynamic Loading (Max 20.19 [mm], Closed Cell-Neoprene Rubber Design with 1.0 [mm] composite thickness)

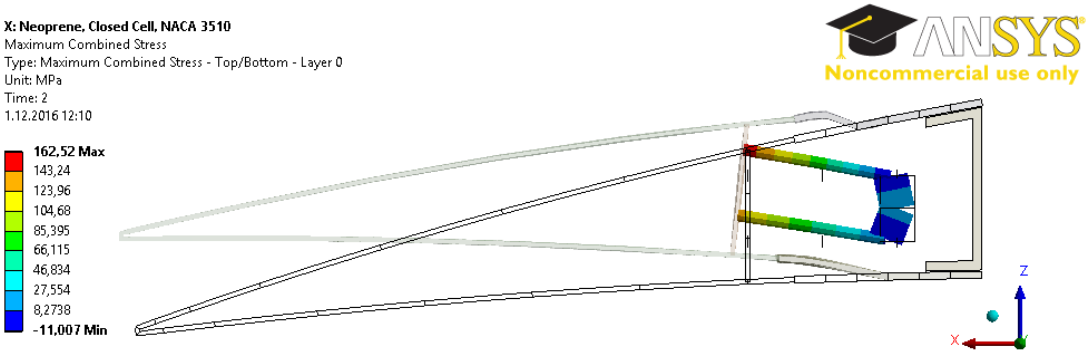

Figure 265: Maximum Beam Combined Stress Contour - Morphing from NACA 6510 to NACA 2510 Profile under 4g Aerodynamic Loading (Max 162.52 [MPa], Closed Cell-Neoprene Rubber Design with 1.0 [mm] composite thickness)

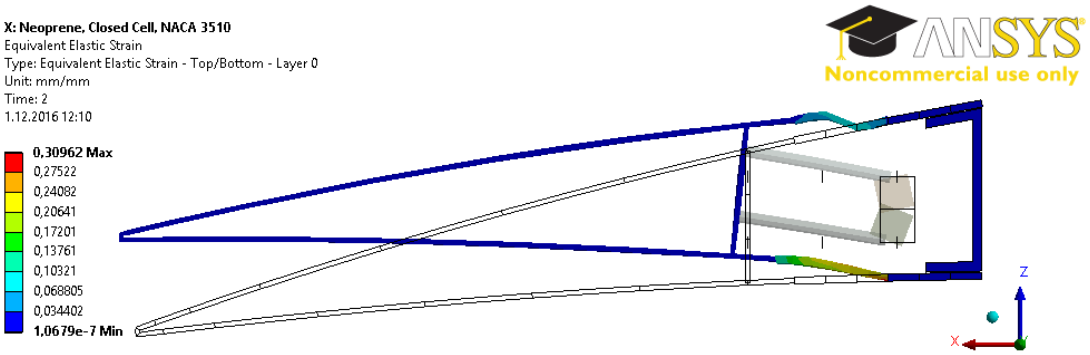

Figure 266: Equivalent Elastic Strain (von-Mises) Contour - Morphing from NACA 6510 to NACA 2510 Profile under 4g Aerodynamic Loading (Max 0.31 [mm/mm], Closed Cell-Neoprene Rubber Design with 1.0 [mm] composite thickness)